MULTIPLE ARRAY PROCESSOR
FINAL REPORT

by

James P. Edwards III

Richard G. Baldwin, Project Manager
FL 7-5411, Ext. 441

George Burrell

Brooks Fowler

Contract AF 33(657)-13904
Beginning 1 October 1964
Terminating 31 August 1965

TEXAS INSTRUMENTS INCORPORATED
Science Services Division
P. O. Box 5621
Dallas, Texas 75222

Prepared for:

AIR FORCE TECHNICAL APPLICATIONS CENTER
VELA SEISMOLOGICAL CENTER
Washington, D. C. 20333

Code 1

Sponsored by

ADVANCED RESEARCH PROJECT AGENCY
NUCLEAR TEST DETECTION OFFICE
ARPA Order 104 Project Code 8100

29 October 1965

DISCLAIMER NOTICE

THIS DOCUMENT IS THE BEST QUALITY AVAILABLE.

COPY FURNISHED CONTAINED A SIGNIFICANT NUMBER OF PAGES WHICH DO NOT REPRODUCE LEGIBLY.

ABSTRACT

This report describes the synthesis and evaluation of multichannel filters for the Uinta Basin Seismological Observatory. The filters were designed for use in two on-line multiple array processors (MAP).

A 19-channel and a 10-channel multiple array processor were designed, fabricated and installed at the Uinta Basin Seismological Observatory.

The 19-channel processor was equipped with 7 multichannel filters and 6 beam-steer outputs. These filters were designed for operation on various configurations of the subsurface 3-dimensional 16-element array.

The 10-channel processor was equipped with 3 multichannel filters and 6 beam-steer outputs. All were designed for operation on the 10-element subsurface planar array.

BLANK PAGE

TABLE OF CONTENTS

TABLE OF CONTENTS (CONTD)

LIST OF APPENDICES

LIST OF ILLUSTRATIONS

LIST OF ILLUSTRATIONS (CONTD)

LIST OF ILLUSTRATIONS (CONTD)

LIST OF ILLUSTRATIONS (CONTD)

LIST OF ILLUSTRATIONS (CONTD)

SECTION I

INTRODUCTION

Contract AF33(657)-13904 has been directed toward the development and installation of two on-line Multiple Array Processors (MAP's) for the Uinta Basin Seismological Observatory (UBO) located in Vernal, Utah.

This report contains results obtained from the synthesis and evaluation of the optimum multichannel filter systems designed for installation in the MAP's.

Two on-line processors have been installed at the UBO location. These processors are a 10-channel system which operates on the surface Z1-10 planar array and a 19-channel system which operates on both the subsurface (buried 200 ft) SZ1-10 planar array and the 6-element deep-hole vertical array. Figure I-1 presents the UBO array complex.

Fold-out pages have been provided in Appendix E which outline in tabular form the systems under discussion. The appendix will provide easy reference to the systems during the reading of this report and are designed particularly for use by station personnel in interpreting MAP output results.

A. BRIEF DESCRIPTION OF THE 10-CHANNEL PROCESSOR SYSTEMS

The following paragraphs present a description of the 10-channel MAP systems. Other optimum multichannel filter systems developed under this contract, but not installed in the MAP, will be discussed in Section V and Appendix D.

1. UBO MCF-1

This filter was synthesized in the time domain and was designed for use with the surface Z1-10 planar array. The noise matrix used for designing this filter was formed from an ensemble of measured noise correlations which were averaged over 12 ambient noise samples recorded during a 1-month period. The signal was defined to propagate with infinite apparent horizontal velocity. The noise spectrum was approximately whitened and the signal spectrum was weighted the same as that of the noise. A signal-to-noise ratio of 4 was used in the filter development.

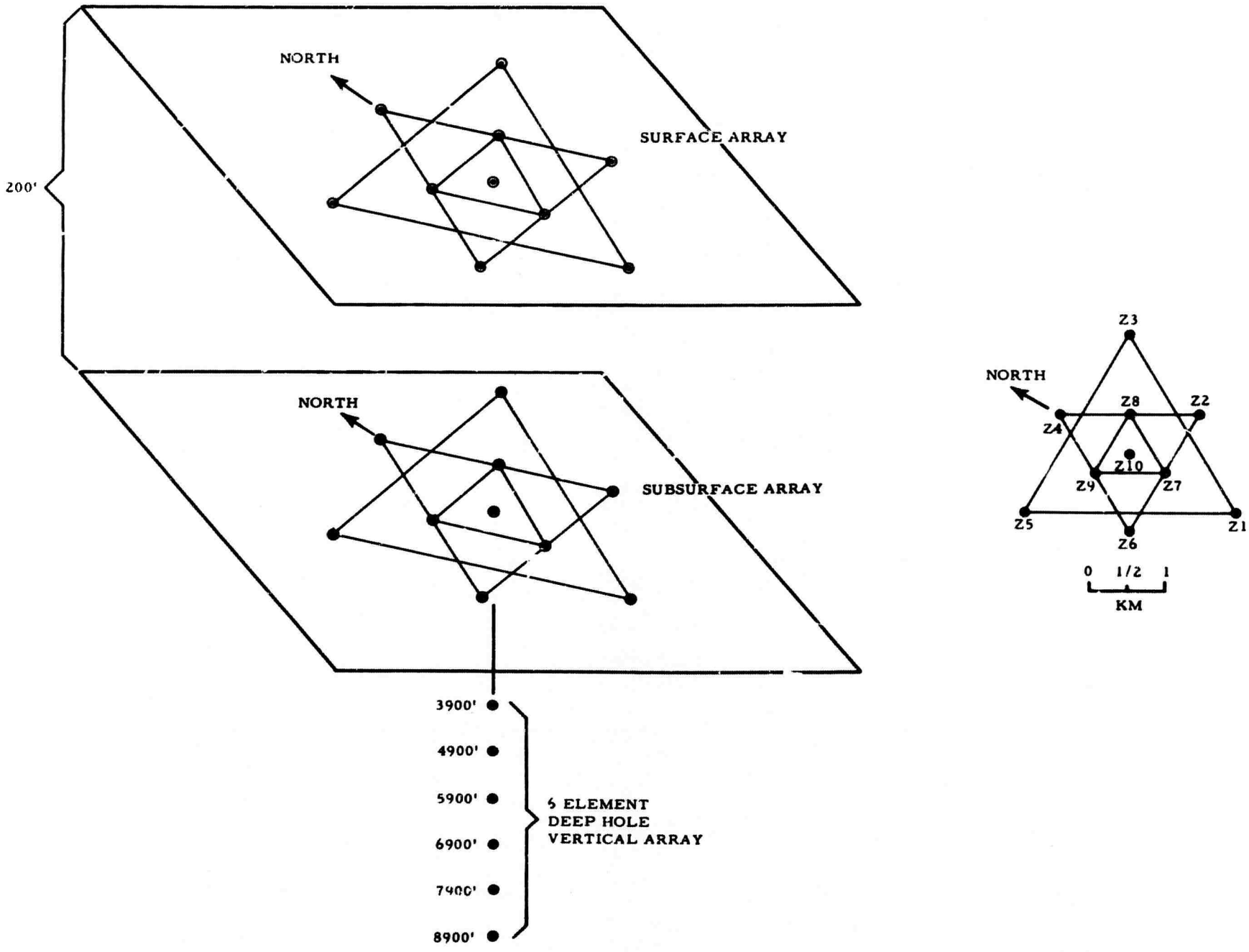

Figure I-1. Artist's Concept of UBO Array Complex

2. UBO MCF-2

This filter was synthesized in the time domain by using the same noise matrix as that used in the UBO MCF-1. The signal model was defined to be one of infinite apparent horizontal velocity and its spectrum was weighted the same as that of the noise spectrum above 1.0 cps. Below 1.0 cps, the signal spectrum was shaped such that the resulting optimum filter possessed an 18-db/octave low-cut frequency filter. The filter was synthesized using a 2.75 signal-to-noise ratio above 1.0 cps.

3. UBO MCF-3

This filter was synthesized in the time domain by using the same measured noise matrix as that used in the UBO MCF-1. The signal area was defined to be from 8.1 km/sec to infinite, apparent horizontal velocity. The signal and noise spectra were weighted equally and a signal-to-noise ratio of 4 was used in the filter synthesis.

4. UBO 10-Channel Beam-Steer Outputs

Six beam-steer outputs have been provided on the 10-channel MAP which are designed to enhance signal energy propagating with an apparent horizontal velocity of 8.1 km/sec. The following directions have been provided:

BS-1:	0 degrees from N
BS-2:	60 degrees E from N
BS-3:	120 degrees E from N
BS-4:	180 degrees E from N
BS-5:	240 degrees E from N
BS-6:	300 degrees E from N

5. UBO 10-Channel Straight-Summation Output

A simple-summation output also has been provided on the 10-channel MAP which will enhance signals propagating with infinite apparent horizontal velocity.

B. BRIEF DESCRIPTION OF THE 19-CHANNEL PROCESSOR SYSTEMS

The following paragraphs present a description of the 19-channel MAP systems.

1. UBO MCF-8

This filter was synthesized in the time domain and was designed for use with the subsurface SZ1-10 planar array. A measured ambient noise matrix was used in the filter development. This noise matrix was approximately whitened and averaged over 3 ambient noise samples taken from a 2-day period. The signal model was defined to be a single point in wavenumber space at $\vec{k} = 0$ (i.e. signals propagating with infinite apparent horizontal velocity). The noise and signal spectra were weighted equally and a signal-to-noise ratio of 4 was used in the filter synthesis.

2. UBO IP-1

This filter was synthesized in the time domain and was designed to operate on the UBO 3-dimensional array consisting of the subsurface SZ1-10 elements summed on 4 rings (the center element considered to be 1 ring) and the 6-element deep-hole vertical array. The signal and noise models were theoretical isotropic models consisting of a white frequency spectrum. The noise model was defined for the first 3 modes of surface-propagating energy and was developed from theoretical dispersion data. An infinite, apparent horizontal velocity signal model was specified. A signal-to-noise ratio of 4 was used in synthesis of the filter.

3. UBO IP-2

This filter was synthesized in the time domain and uses the 6-element deep-hole vertical array as input. The signal and noise models consisted of a white frequency spectrum; a signal-to-noise ratio of 4 was used in synthesis of the filter. The signal model was defined for infinite apparent horizontal velocity energy and the noise model consisted of surface-mode noise which would appear to the vertical array as infinite velocity energy.

4. UBO Deghosting Filters

Four deghosting filters were developed for use in the 19-channel processor. These filters are designed to operate on the 6-element deep-hole vertical array using 3 inputs for each filter. White signal and noise spectra and a signal-to-noise ratio of 4 were used in synthesis of the filters. In each filter, the noise model was defined for surface-mode (horizontally propagating) energy plus either down-traveling or up-traveling infinite apparent horizontal velocity signal, depending on whether the filter was designed to extract up-traveling or down-traveling signals, respectively. The following is an outline of the filters by signal model:

a. UBO DG-1

The signal is defined to be up-traveling infinite apparent

horizontal velocity energy. The 4900-, 6900- and 8900-ft elements are used as input.

b. UBO DG-2

The signal is defined to be down-traveling infinite apparent horizontal velocity energy. The 4900-, 6900- and 8900-ft elements are used as input.

c. UBO DG-3

The signal is defined to be up-traveling infinite apparent horizontal velocity energy. The 3900-, 5900- and 7900-ft elements are used as input.

d. UBO DG-4

The signal is defined to be down-traveling infinite apparent horizontal velocity energy. The 3900-, 5900- and 7900-ft elements are used as input.

5. UBO 19-Channel Beam-Steer Outputs

The following beam-steer (i.e., time-shift and summation) outputs have been provided on the 19-channel MAP for the 6-element deep-hole vertical array. The signal for each beam-steer is defined as follows:

a. BS - 7

Up-traveling infinite apparent horizontal velocity P-waves.

b. BS - 8

Up-traveling apparent 8-km/sec horizontal velocity P-waves.

c. BS - 9

Up-traveling apparent 8-km/sec horizontal velocity S-waves.

d. BS - 10

Down-traveling infinite apparent horizontal velocity P-waves.

e. BS - 11

Down-traveling apparent 8-km/sec horizontal velocity P-waves.

f. BS - 12

Down-traveling apparent 8-km/sec horizontal velocity S-waves.

6. UBO 19-Channel Straight-Summation Output

The straight-summation output of the 6-element deep-hole vertical array has been provided on the 19-channel MAP.

SECTION II

SUMMARY AND CONCLUSIONS

The purpose of this contract was to construct, equip and install 2 operational multiple array processors at the Uinta Basin Seismological Observatory in Vernal, Utah. A 10-channel processor and a 19-channel processor were constructed and installed at the array location. Each processor was provided with several optimum multichannel filters, a variety of beam-steer (i.e., time-shift and summation) outputs and a straight-summation output.

A. THE 10-CHANNEL PROCESSOR

The filters synthesized for the 10-channel processor were designed for operation on the surface 10-element planar array. Three filters (UBO MCF-1, -2 and -3), based on measured noise, were installed in the processor and 6 beam-steer outputs for 8.1-km/sec energy were provided, together with a straight-summation output.

An evaluation of the 3 multichannel filters was conducted with the following conclusions.

The multichannel filters, in general, demonstrated a 6- to 15-db signal-to-noise improvement relative to the Z 10 output, at frequencies below 0.75 cps while the straight summation demonstrated only 0-to-3-db improvement, relative to the same reference. Between frequencies of 0.75 and 5.0 cps, the filters demonstrated signal-to-noise improvement approximately equal to that obtained through straight-summation processing, in spite of the fact that the UBO noise field contained significant amounts of low-velocity organized energy which should have been rejected by the filters on the basis of wavenumber structure. Analysis of the apparent discrepancy indicated that the UBO array had an ideal configuration for rejecting the known low-velocity organized noise contributors by straight summation. The process of straight summation, therefore, yielded approximately equivalent results in the 0.75- to 5.0-cps frequency band with the filters installed in the MAP.

Analysis of the UBO noise field indicated a non-time and space-stationary* noise source present in the 1.75- to 3.0-cps frequency band. Optimum processing with the 3 multichannel filters of noise samples which were shown to contain this high-frequency organized, low-velocity

*Space-stationary means that the crosscorrelations between equal vector pairs, as measured at any point in correlation space, are the same. It should be noted that the noise field need be organized only and not necessarily space- or time-stationary, in order to reject the noise on the basis of multichannel processing.

energy, indicated that the filters were unable to reject this energy. The reason for this failure in the filters was due to the choice of noise samples used to construct the measured-noise model. These noise samples did not contain measureable amounts of the noise source in the model.

Application of the filters to measured teleseismic signals indicated that two of the filters which were designed for infinite velocity signals (UBO MCF-1 and -2) slightly attenuated signal energy by approximately 2- to 3 db. This attenuation is natural for an infinite velocity filter which is designed to pass only a single point in wavenumber space and normally will reject all other points to a varying degree. A third multichannel filter (UBO MCF-3) which consisted of a disc signal model enclosing velocities of 8.1 km/sec and greater, did not attenuate noticeably the teleseismic signal energy.

In spite of the conclusions that the multichannel filters do not show significant improvement above a straight summation in the 0.75- to 5.0-cps frequency band, multichannel filtering of the UBO sensor outputs is justified because of the large signal-to-noise improvement obtained at low frequencies and because of the signal preservation which can be accomplished by specifying other than a point-signal model.

Additional work should be conducted for the UBO array to develop filters which will reject the non-time and space-stationary low-velocity organized energy in the 1.75- to 3.0-cps frequency band.

B. THE 19-CHANNEL PROCESSOR

The filters provided in the 19-channel processor were designed for operation on the 16-channel subsurface (buried) UBO array which consists of the 10-element planar array and the 6-element deep-hole vertical array. A total of 7 optimum filters were installed in the processor and 6 beam-steer outputs and a straight-summation output of the 6-element deep-hole vertical array were provided.

Evaluation of UBO MCF-8, which was designed on measured noise correlation statistics for operation on the 10-element buried planar array, indicated that this filter produced slightly greater signal-to-noise improvement than did the comparable filter developed for application to the surface array data (UBO MCF-1). The improvement above that of UBO MCF-1 probably was a misrepresentation and due to the time span from which the noise matrix and evaluation data were taken. The subsurface noise ensemble covered 10 percent of the time span of the surface ensemble, indicating UBO MCF-8 was more highly tuned to the ensemble; but on a long term basis this filter probably will show results comparable to that of

UBO MCF-1, with the exception of improvement in the 2.0- to 3.0 cps frequency band.

Evaluation of UBO MCF-8 indicated that a possible noise source in the 2.0- to 3.0-cps frequency band which was organized but did not appear in the noise ensemble collected for the development of filters for the 10-channel processor. The noise source is non-time stationary and is not the same source as that referred to in the evaluation and analysis of surface data.

Comparison of the theoretical and measured response for UBO MCF-8 indicated a phase and amplitude distortion when this filter was installed in the MAP. These distortions occurred whenever the amplitude response of the filter showed greater than a 40-db variation between frequencies of 0 and 6.94 cps and were due to the approximation of filter weights by 1-percent resistors. Whenever amplitude variations of 40 db or greater occur, the MAP filter actually is working in the system noise level.

At present, UBO MCF-8 is being redesigned for compatibility with the MAP system. The redesigned filter probably will not be as effective in rejecting the organized noise, particularly at frequencies below 0.75 cps.

A partial evaluation of UBO IP-1, which was developed to operate on the 16-channel, 3-dimensional buried array, indicated that the theoretical signal and noise models used in the synthesis of this filter were accurate to 2.0 cps for the planar array. Results obtained through this partial analysis indicated improvement comparable to that of UBO MCF-8, which was developed from measured noise, with the exception of the high degree of improvement noted in the 0- to 0.75-cps region. This difference is due to the increased complexity of the noise model used in the synthesis of UBO IP-1.

Evaluation of the remaining 5 filter systems developed for the 19-channel processor was limited, due to the unavailability of deep-hole vertical array data. Thus, evaluation of UBO IP-1 was limited to a partial evaluation of that part of the filter system applicable to the 10-element planar array and evaluation of the UBO IP-2 was prohibited.

The remaining 4 filters were deghosting filters (UBO DG-1 through UBO DG-4) which were evaluated partially by using synthetic laboratory tests. The results indicated that the filters were capable of extracting the appropriate signal energy and rejecting the signal ghost, if the assumption is made that the signal travel-time data used in computing the signal models was accurate.

BLANK PAGE

SECTION III

ANALYSIS OF THE UBO AMBIENT NOISE FIELD

A. INTRODUCTION

The results of the UBO ambient noise field (as recorded by the 10-element surface and subsurface planar arrays) analysis conducted for this contract have been presented in a report titled "Noise Analysis for Uinta Basin Seismological Observatory" dated 15 October 1965. For continuity, a brief summary of these results will be presented in this section with particular emphasis on the following points pertinent to the multichannel filter problem.

- Spatial organization of the ambient noise field
- Time stationarity of the ambient noise field
- Spatial wavenumber structure of the ambient noise field

B. AMBIENT NOISE POWER-DENSITY SPECTRA

Analysis of the single power-density spectra for the UBO ambient noise field indicates a noise level at 1.0 cps comparable to other arrays placed on sediment. For example, the Angela subarray of LASA averages approximately -4 db relative to 1 $m\mu^2$ of ground motion/cps at 1.0 cps; the UBO averages -2 db to -6 db relative to the same reference. For further comparison with other array stations, CPO average 0 db and TFO averages -15 db relative to 1 $m\mu^2$ of ground motion/cps at 1.0 cps.

If the assumption of a universal mantle P-wave level is made, the UBO ambient noise power-density spectra indicate that the noise field is not mantle P-wave limited in the 0.5 to 2.0-cps frequency band. For example, at 0.5 cps, UBO is approximately 5 db above the assumed universal mantle P-wave level, 12 db at 1.0 cps and 17 db at 1.5 cps. These results indicate that the noise field contains a significant amount of energy attributable to either random noise or organized surface-mode energy.

C. THE MULTIDIMENSIONAL AMBIENT NOISE FIELD

A previous investigation made of the spatial organization (spatial predictability) of the UBO ambient noise field indicated that the noise field is spatially organized in the 0- to 2.0-cps frequency band.

Narrowband displays in the 0.2- to 0.33-cps frequency band indicate the noise field is composed partially of low-velocity (approximately

3 km/sec) 3- and 5-sec period microseisms which principally originate from a generally northern direction.

In the 0.33 to 0.75-cps frequency band, the analysis could not demonstrate the presence of low-velocity energy, because of the increased complexity of the noise field and the predominate mantle P-wave contribution. It was concluded, however, that the noise field did consist of some low-velocity components in this frequency range, but principally was composed of high-velocity mantle P-wave energy.

In the 0.75- to 2.0-cps frequency range, wavenumber analysis of the noise field demonstrated that the mantle P-wave noise level falls off rapidly with frequency, in agreement with the anticipated universal mantle P-wave level. The wavenumber analysis indicated that there was low-velocity organized energy (i.e., surface-mode) present in the noise field in the 0.75- to 2.0-cps range. Three organized noise lobes appeared relatively time-stationary during the 1-month period of the analysis and 1 of these 3 has been shown to be present in the noise field over as great as a 2-year period. These 3 lobes of organized energy originate from the North, the East-South-East and the West.

Analysis of the Z1-10 single-channel power density spectra for 2 noise samples indicated that a non-time and space-stationary organized noise source was contributing to the noise field between frequencies of 1.75 and 3.0 cps. This energy probably originated from a nearby highway (East-West U.S. Highway 40).

The points to be derived from this noise analysis are:

1. The organized noise field is composed of some low-velocity components which are separated in wavenumber space from the signal regions of interest (i.e., teleseismic signals) which indicates that a multichannel filter could be designed to reject this organized energy on the basis of wavenumber component.

2. The low-velocity organized noise field appears relatively time stationary over the period that the analysis was conducted. Time stationarity of the organized noise field is necessary when designing multichannel filters on measured noise samples which must be optimum on a long-time basis.

SECTION IV

MULTICHANNEL FILTER DEVELOPMENT

A. INTRODUCTION

This section reviews briefly the multichannel filter techniques used in synthesizing the filters developed for this contract. Additionally, the topics of signal-to-noise ratio and signal and noise spectral weighting are covered relative to their importance in multichannel filter development.

B. TIME VS FREQUENCY DOMAIN SOLUTION

The synthesis of multichannel filters can be accomplished in either the time or frequency domain. The filters developed for this contract were synthesized in the time domain.

The advantage of solving multichannel filters in the time domain as opposed to the frequency domain is that the resulting time-domain operators are an exact solution to the multichannel filter equations, whereas, the frequency-domain operators are only an approximation. This approximation results first from transforming time to frequency the specified noise and signal models and, thus, introducing a spectral estimate error and second from inverse-transforming the frequency-domain operators obtained from the multichannel filter solution to obtain the time-domain operators. The true inverse transform yields an infinitely long function which must be truncated in order to be compatible with the MAP, therefore, introducing an additional error.

The first error may be avoided sometimes if both the noise and signal models are developed theoretically, since such development may be accomplished in the frequency domain. The second error due to truncation never can be avoided.

C. WIENER LINEAR MULTICHANNEL FILTER DEVELOPMENT

The derivation of the multichannel time-domain filter equations is a straight-forward extension to N-channels of the derivation given by Norman Levinson* for the solution of the single-channel Wiener equation and results in the following linear equations:

*Wiener, Norbert, 1964, Extrapolation, Interpolation, and Smoothing of Stationary Time Series: Appendix B, MIT Press.

$$\sum_{i=1}^{n} \sum_{j=-m}^{m} a_i(j)\, \varphi_{ik}(j-\ell) = \varphi_{is}(\ell)$$

$$(k=1,2,\ldots.n, \ell = -m, \ldots., -1, 0, 1, \ldots.m)$$

where a is the desired filter weight

φ_{ik} is the crosscorrelation of channel i and k and represents the sum of the signal and noise matrix

j and ℓ are lag values of the sampled correlation functions

φ_{is} is a crosscorrelation of the signal matrix

The solution to the multichannel time-domain equations is developed on the basis of minimizing the mean-square-error I which is given by

$$I = \varphi_{ss}(o) - \sum_{i=1}^{n} \sum_{j=-m}^{m} a_i(j)\, \varphi_{is}(j)$$

In other words, the best least-squares estimate of the signal is obtained.

D. SIGNAL-TO-NOISE RATIO

The signal-to-noise ratio as a function of frequency is important in multichannel filter development, because the solution to the equation is weighted in frequency by this ratio.

There are two cases to be considered in discussing signal-to-noise ratio. The first case is where this ratio is constant and the second case is where the ratio is variable from 0 to f_n when f_n is the folding or Nyquist frequency of the sampled data

1. Constant Signal-to-Noise Ratio

In solving the multichannel filter equation, if

$$\frac{\Phi_{ij}^{s}(f)}{\Phi_{ij}^{n}(f)} = c$$

where c is a constant, the resulting multichannel filter solution will be weighted by this constant. In other words, it may be considered that the signal is assigned importance of c and the noise is assigned importance of 1.

In the identification problem, where signal preservation is important, a signal-to-noise ratio of 4 will, in most cases, insure that the signal area in wavenumber space will lie between 0 and 3 db for other than a point model and usually will be 0 db for this model.

2. Variable Signal-to-Noise Ratio

The solution to the multichannel filter equation in the case of

$$\frac{\Phi_{ij}^{s}(f)}{\Phi_{ij}^{n}(f)} = \delta\,(f)$$

where δ is variable function of frequency, will result in a filter which will not have a flat response for the specified class of signal, but will be zero phase.*

In this case, the resulting filter may be considered as a multichannel filter possessing flat, approximately zero phase response and a single-channel nonflat zero phase frequency filter to be applied to the multichannel filter output.

As an example, consider the case where:

*As used in this report, zero phase will be referred to as absolutely zero phase and approximately zero phase. If the signal and noise models used in the filter synthesis are theoretical and isotropic, the resulting filter will be absolutely zero phase (i.e., symmetric convolution operator for specified signal). If either the signal or noise model, or both, used in the filter synthesis are nonisotropic (i.e., include measured noise), the resulting filter probably will be only approximately zero phase. A small phase error results from the mean-square-error technique of filter solution.

$$\Phi_{ij}^{s}(f) = 4 \qquad 0 \le f \le 3.0$$

$$= 4y(f) \qquad 3.0 < f \le 6.94$$

$$\Phi_{ij}^{n}(f) = 1 \qquad 0 \le f \le 6.94$$

The resulting filter then is considered as a multichannel filter designed with a signal-to-noise ratio of 4, combined with a frequency filter having an amplitude response for the specified signal given by

$$A(f) = 1.0 \qquad 0 \le f \le 3.0$$

$$= \frac{y(f)}{1+y(f)} \qquad 3.0 < f \le 6.94$$

In other words, the filter response for the specified signal is no longer flat, but is given by A(f). The filter will be zero phase.

UBO MCF-2 which is presented in Section V was designed on this principle so that it would possess a 1.0-cps, low-cut, 18-db/octave frequency filter.

SECTION V

DEVELOPMENT AND EVALUATION OF THE MULTICHANNEL FILTER SYSTEMS FOR THE 10-CHANNEL PROCESSOR

A. INTRODUCTION

This section contains the results of the synthesis and evaluation of the multichannel filters (MCF-1, -2 and -3) installed in the 10-channel MAP which is to be operated on the surface planar array (Figure I-1).

Seven multichannel filters (MCF -1 through -7) were developed for the 10-channel processor using as a noise matrix the average-measured correlation statistics. Appendix A describes in detail the formulation of this noise matrix. The 4 multichannel filters (MCF -4, -5, -6, and -7) which were not used in the MAP are discussed in detail in Appendix D.

The analysis of MCF -4 through -7 as compared with MCF -1 through -3 resulted in the following conclusions in MCF development for the surface planar array, where average correlation statistics were used for a noise matrix:

1. Superdirectivity vs. Gain Equalization

The multichannel filters developed, using as a noise matrix the average-noise correlation matrix described in Appendix A and a theoretical signal model, exhibited high signal-to-noise improvement between frequencies of 0 to 0.75 cps. This improvement was due to a superdirectivity configuration and not to a gain-equalization problem.

Briefly, the gain-equalization problem results from using measured correlation statistics which exhibit channel-to-channel gain differences and a theoretical, perfectly equalized signal model. It has been shown that, under these circumstances, a filter can result which will use gain unequalization as a criteria for signal-to-noise improvement (i.e., noise rejection). The disadvantage, is that when this type of filter is applied to measured signal (unequalized), the filter could reject the signal on the basis of the unequalized gain.

However, analysis determined that for the correlation set used in the synthesis of these multichannel filters, the gain equalization problem did not exist. The filters actually were exhibiting a superdirectivity effect, which yielded a high-resolution filter for low frequencies at the expense of large sidelobes. Since these large sidelobes appeared at wavenumber values greater than an existing organized noise or signal component, superdirectivity

did not affect the signal-to-noise improvement capabilities of the system (particularly at low frequencies where the random noise level was small).

2. Array Resolution Problem

Initially, MCF -4 and -5 were developed so that a velocity-partitioning type of filter could be installed in the on-line processor. These filters were designed for an isotropic signal area in wavenumber space that extended from 15 to 8.1 km/sec and 8.1 to 6.0 km/sec, respectively.

Due to the limited diameter (approximately 3 km) of the UBO array and the small number of sensors, the filters developed from these signal models were ineffective in rejecting noise (i.e., the mantle P-wave noise) within the inner specified signal range from 0.5 to 2.0 cps.

On the basis of these results, only simple signal models (i.e., infinite velocity and infinite-to-8.1-km/sec models) could be used in developing effective MCF's designed for signal-enhancement.

B. DEVELOPMENT OF THE 10-CHANNEL MCF'S

1. UBO MCF-1

UBO MCF-1 was developed in the time domain by using as a noise model the average-noise correlation matrix discussed in Appendix A. The signal model was defined to be a single point in wavenumber space at $\vec{k} = 0$ (i.e., corresponding to energy propagating with infinite apparent horizontal velocity). A signal-to-noise ratio of 4 was specified in developing the filter.

The signal and noise spectra were shaped identically so that the resulting multichannel filter would exhibit a flat, approximately zero phase response for the specified class of signal.

2. UBO MCF-2

In developing UBO MCF-2, the signal region was defined to be a single point in wavenumber space at $\vec{k} = 0$ (corresponding to energy propagating with infinite apparent horizontal velocity). The average-noise correlation matrix presented in Appendix A was used as the noise model.

This multichannel filter was designed for detection usage, not for identification purposes. The signal and noise spectra were shaped such that the response of the filter for the specified signal class would be flat in the 1.0- to 6.94-cps frequency band, but would decrease in power at an 18 db/octave rate below 1.0 cps. In other words, the MCF possessed a

built-in, low-cut frequency filter and would not exhibit a flat response for infinite velocity signals.

In order to design the low-cut frequency filter into the multichannel filter, the signal spectrum was shaped by the following equation:

$$\frac{\Phi^{s}_{ij}(f)}{\Phi^{s}_{ij}(f) + \Phi^{n}_{ij}(f)} = \frac{1}{2} \qquad 1.0 \leq f \leq 6.94$$

$$= \psi(f) \qquad 0 \leq f < 1.0$$

where $\psi(f)$ represents a line of 18-db/octave slope having the value $\Phi^{n}_{ij}(1.0)$ at 1.0 cps. Figure V-1 shows the signal and noise spectra used in developing this filter. As will be shown in subsection D, the resulting multichannel filter exhibits the appropriate low-cut frequency filter.

The signal-to-noise ratio used in developing this detection filter was approximately the same as the signal-to-noise ratio for a magnitude 4 event. This ratio was determined to be approximately 2.75 from the study of several approximate magnitude 4 events.

3. UBO MCF-3

UBO MCF-3 was developed in the time domain by using as a noise matrix the average-noise correlation matrix for the surface array as presented in Appendix A. The signal region was specified to be isotropic in wavenumber space and extended from 8.1 km/sec to infinite apparent horizontal velocity. A signal-to-noise ratio of 4 was used in design of this filter.

The signal and noise spectra were weighted equally so that the resulting filter would exhibit a flat, approximately zero phase response for the specified class of signals.

Due to the increased area coverage in wavenumber space of the signal model, compared with an infinite velocity model, this filter can be expected to demonstrate less actual noise rejection than MCF-1. However, the majority of teleseismic signals filtered with MCF-3 will be less attenuated than those processed through UBO MCF-1.

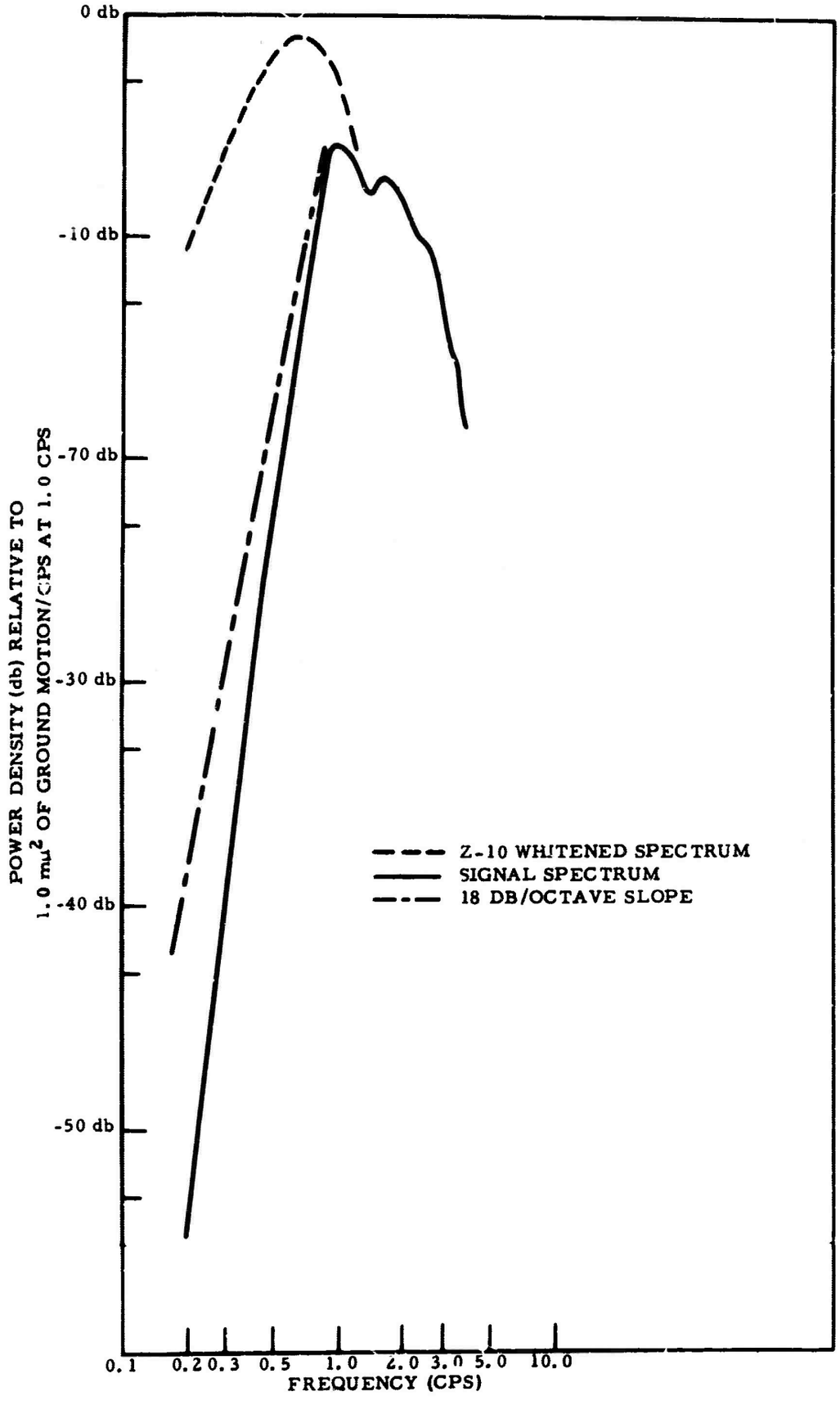

Figure V-1. Noise and Signal Spectrum Used in Development of UBO MCF-2

C. TIME-DOMAIN OPERATORS AND SIGNAL RESPONSE

Time-domain operators for each channel of MCF-1, -2 and -3 and the signal response of the 10-channel stacks are shown in Figures V-2 through V-4. The single curve labeled impulse response is the summation or stack of the convolution operators for individual filters and represents infinite velocity signal response characteristics of the multichannel filter. The ordinate in each case is a dimensionless quantity corresponding to the amplitude of the filter weights, as labeled. The abscissa is 2 sec in length with zero time at the center or 21st filter point.

D. THEORETICAL AND ACTUAL FREQUENCY RESPONSE COMPARED

In Figures V-5 through V-7, theoretical frequency responses are compared with actual measured responses of the MAP installation determined by taking the ratios of the transforms of the input and output wavelets from each MCF set. The method used to calculate these actual responses is explained in Appendix C.

E. EVALUATION OF THE 10-CHANNEL MULTICHANNEL FILTER SYSTEMS

1. Introduction

The evaluation of the multichannel filters designated UBO MCF-1, -2 and -3 designed for the 10-channel MAP basically consisted of:

- Computation of the filter wavenumber response
- Application of the filter to measured noise and measured signal
- Determination of the signal-to-noise improvement ratio using the results of filtering

The signal-to-noise ratio improvement as a functio of frequency is defined as the spectral ratios:

$$\frac{\dfrac{\text{Signal After Processing}}{\text{Noise After Processing}}}{\dfrac{\text{Signal Before Processing}}{\text{Noise Before Processing}}}$$

The noise before processing is the reference trace (generally chosen to be Z10), the noise after processing is the MCF output and the signal is an in-phase spike corresponding to an infinite velocity white signal. The

Text cont'd page V-10

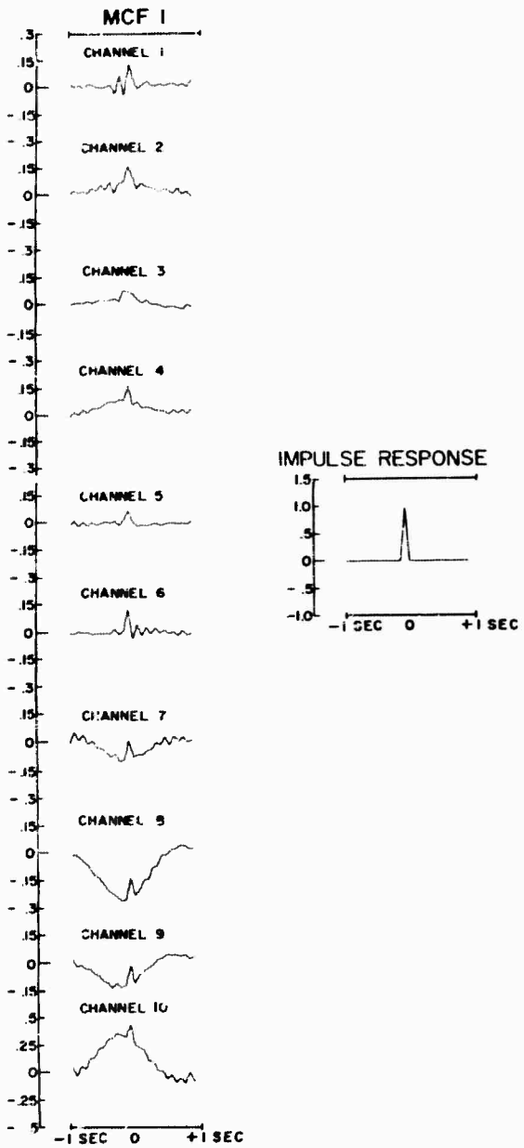

Figure V-2. Time Domain Operators and Signal Response for 10-Channel UBO Processor MCF-1

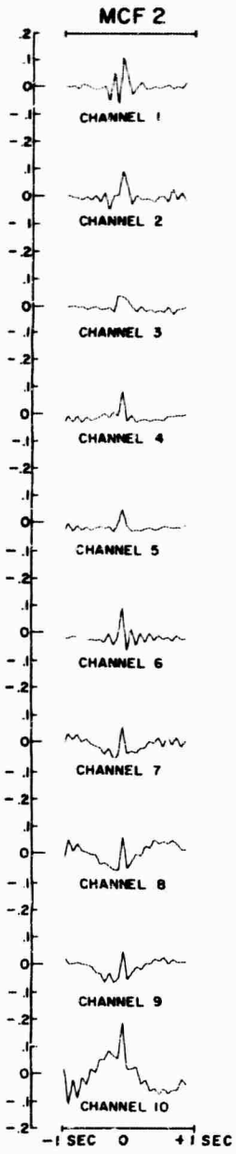

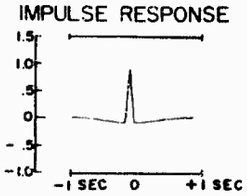

Figure V-3. Time Domain Operators and Signal Response for 10-Channel UBO Processor MCF-2

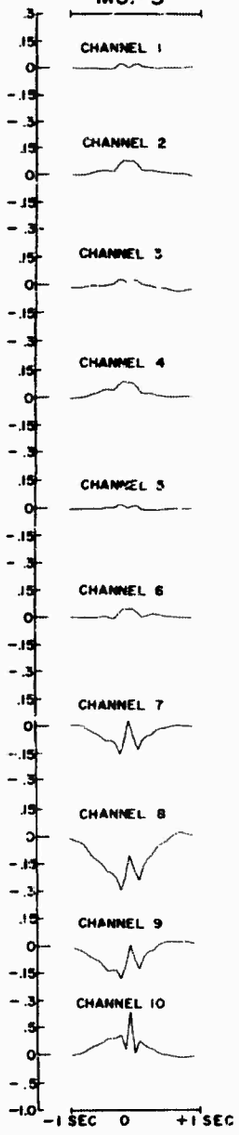

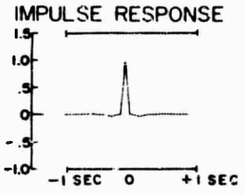

Figure V-4. Time Domain Operators and Signal Response for 10-Channel UBO Processor MCF-3

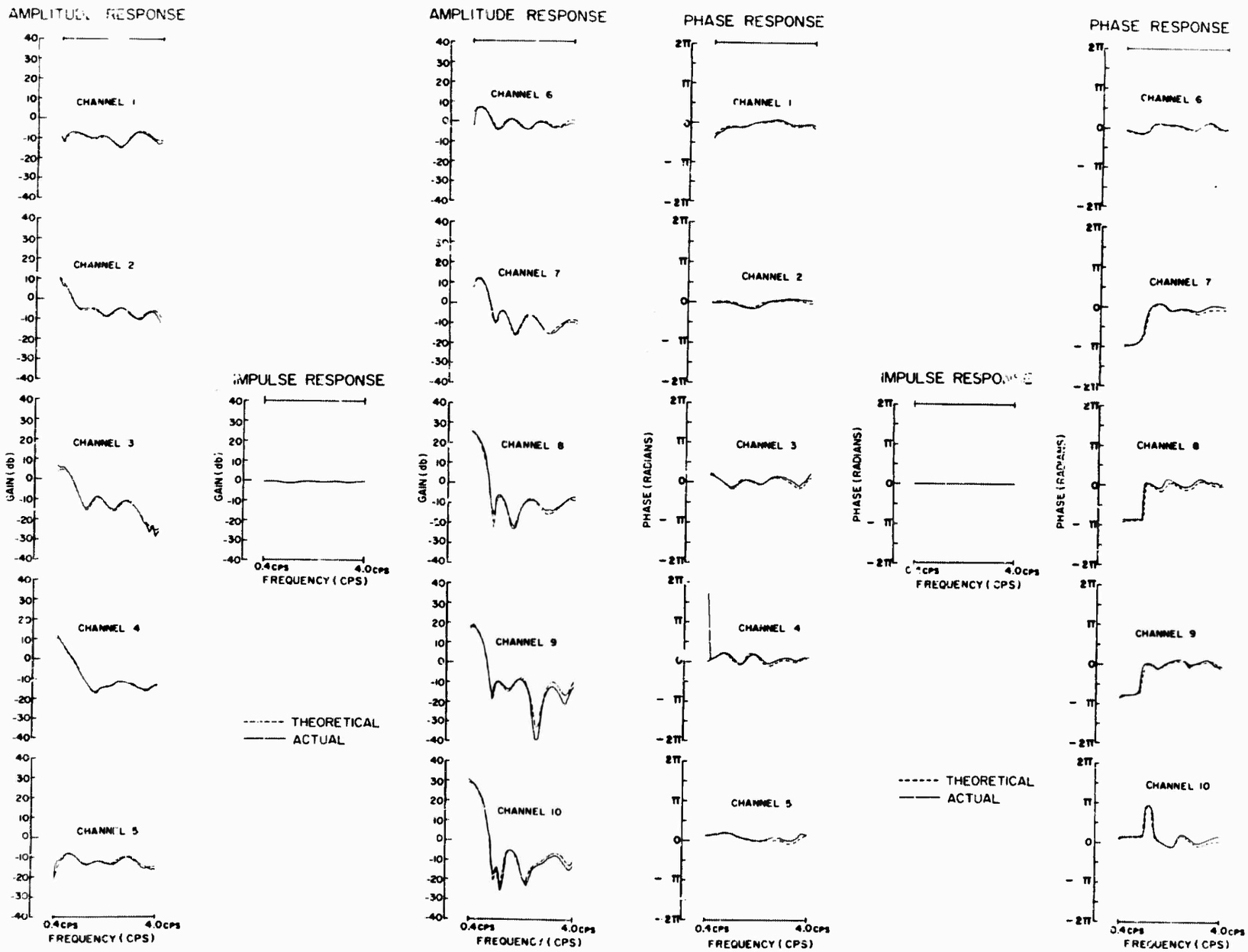

Figure V-5. Theoretical Transfer Functions Compared with Actual Filter Responses in the Frequency Domain (UBO MCF-1)

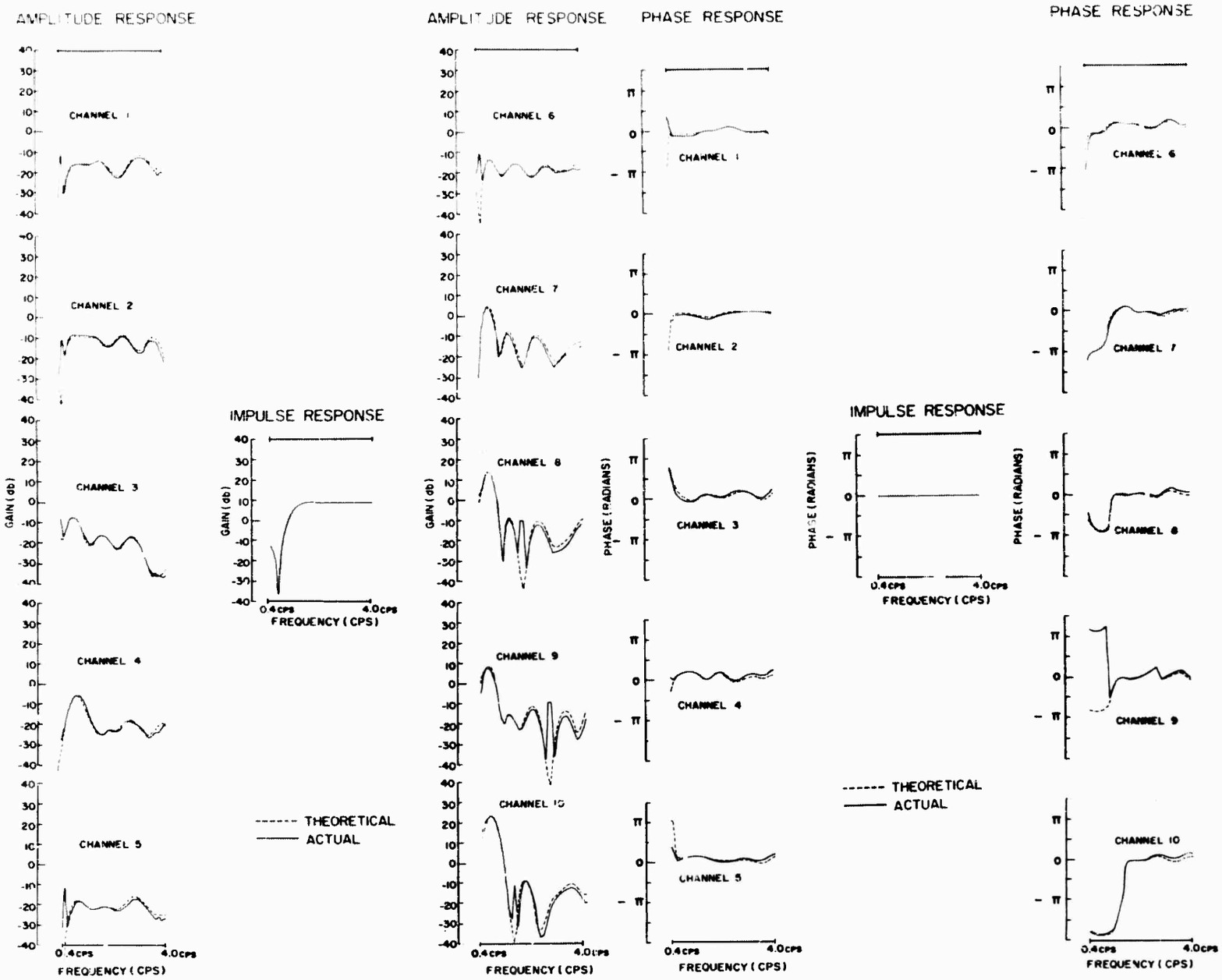

Figure V-6. Theoretical Transfer Functions Compared with Actual Filter Responses in the Frequency Domain (UBO MCF-2)

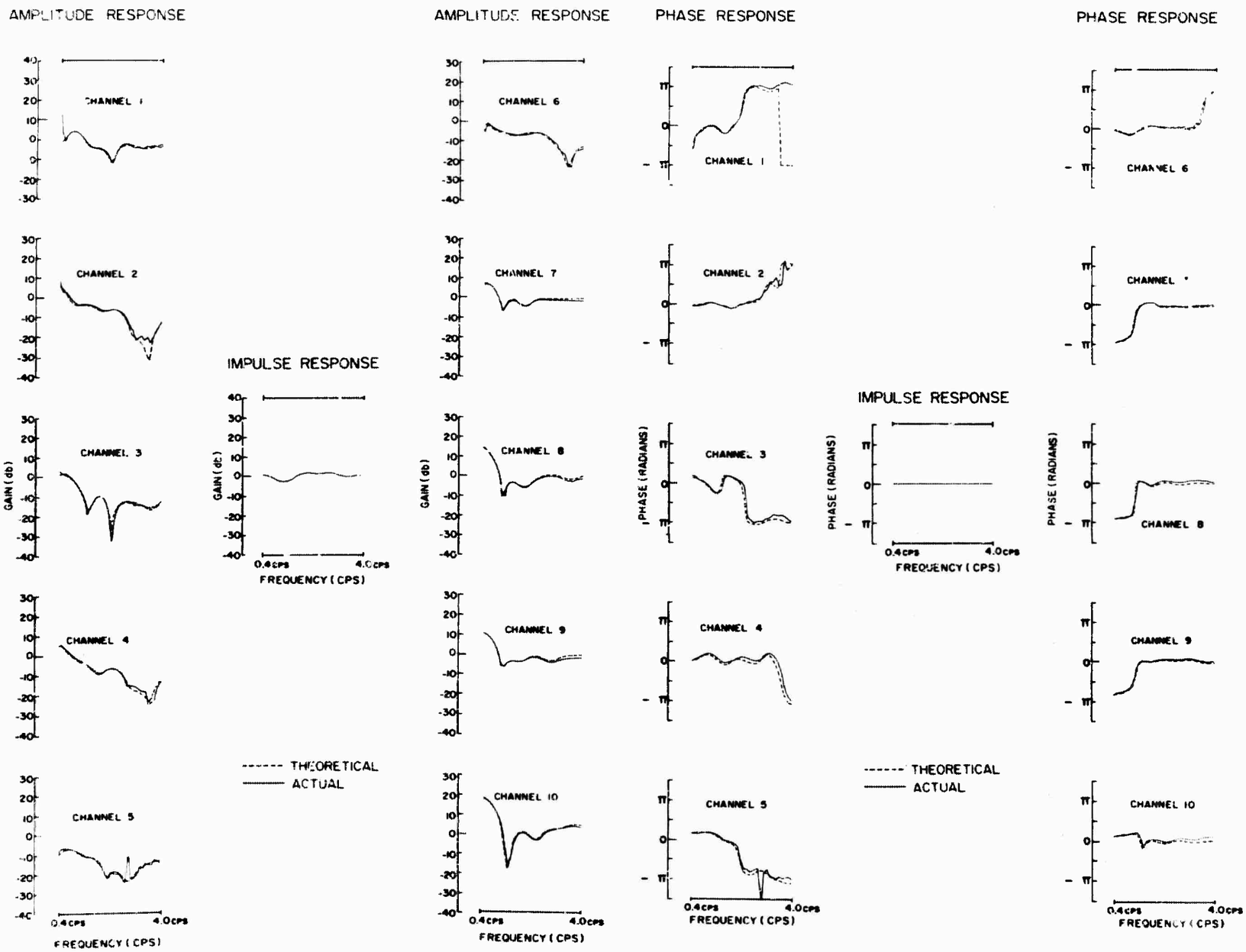

Figure V-7. Theoretical Transfer Functions Compared with Actual Filter Responses in the Frequency Domain (UBO MCF-3)

signal-to-noise ratio is, therefore, evaluated only for signals being of infinite velocity; and, in the case of UBO MCF-3, does not consider signals in the 8.1-km/sec to infinite velocity signal region. However, analysis of the wavenumber response of the filter basically will indicate the signal response to other than infinite velocity signals.

2. Measured Signal and Noise

The evaluation of filter application to 3 noise samples and 2 signal samples is presented. Figures V-8, -9 and -10 are a short portion of the 3 noise samples before and after processing. Figures V-11 and -12 are the results of applying the 3 multichannel filter to 2 signals. Figures V-13 and -14 are the single-channel power density spectra of the 2 signals before and after processing.

3. Evaluation of UBO MCF-1

a. Wavenumber Response

The wavenumber response of UBO MCF-1 at frequencies of 0.25, 0.75, 1.0, and 1.5 cps is shown in Figures V-15 through -18, respectively.

Each of these figures shows that the specified signal area ($\vec{k}$=0) is being passed with 0 db attenuation, consistent with the results presented in Figure V-5, which indicates a flat, approximately zero phase response for infinite velocity signals. At 0.25 cps (Figure V-15), the filter rejects organized energy in the 1- to 2-km/sec region propagating from S-SE and N-NW, thus, indicating a superdirectivity configuration, as discussed in sub-section A and Appendix D. Briefly, this means the filter is rejecting inside the resolution area of the array at the expense of large sidelobes (as great as +18 db). It should be noted, however, that these sidelobes lie outside the area of organized signal and noise (i.e., less than 1 km/sec), and the random noise level at 0.25 cps is only 1.5 percent of the total noise power.

At 0.75, 1.0 and 1.5 cps, the filter is seen to reject strongly the 3 organized noise lobes, which were mentioned in the noise analysis, propagating from the E-SE, W and N.

An important point to be derived from the wavenumber analysis of the filter response is that some rejection (on the basis of wavenumber component) of teleseismic energy can be expected since the signal model was specified to be that of only a single point at $\vec{k}$ = 0. For example, in Figure V-17, signal energy originating north of the array at an epicentral distance of 40 to 80 degrees will be rejected 3 to 6 db.

Text cont'd page V-22

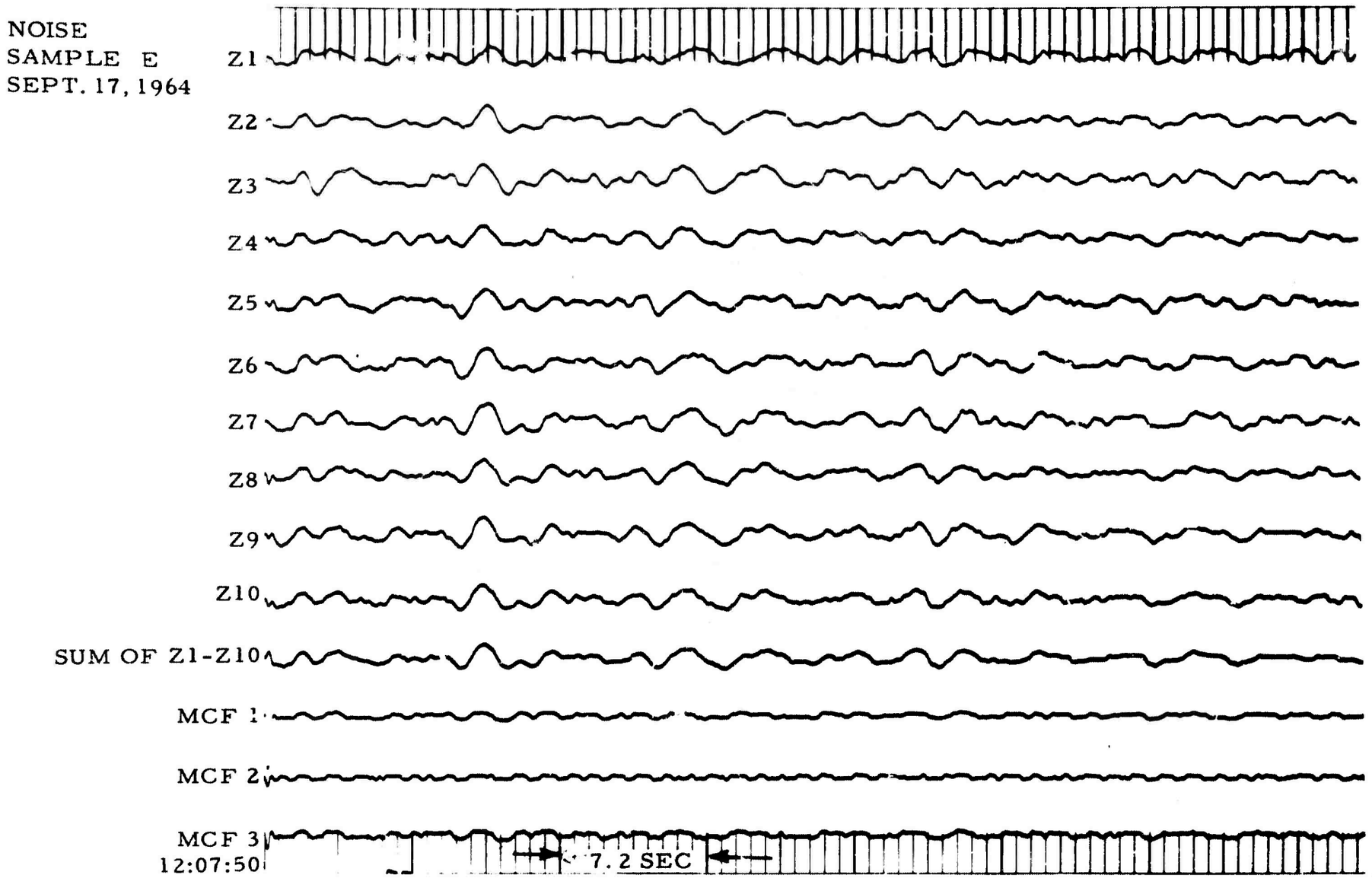

Figure V-8. A Short Portion of UBO Noise Sample-E (Surface) Results of MCF

Figure V-9. A Short Portion of UBO Noise Sample-M (Surface) Results of MCF

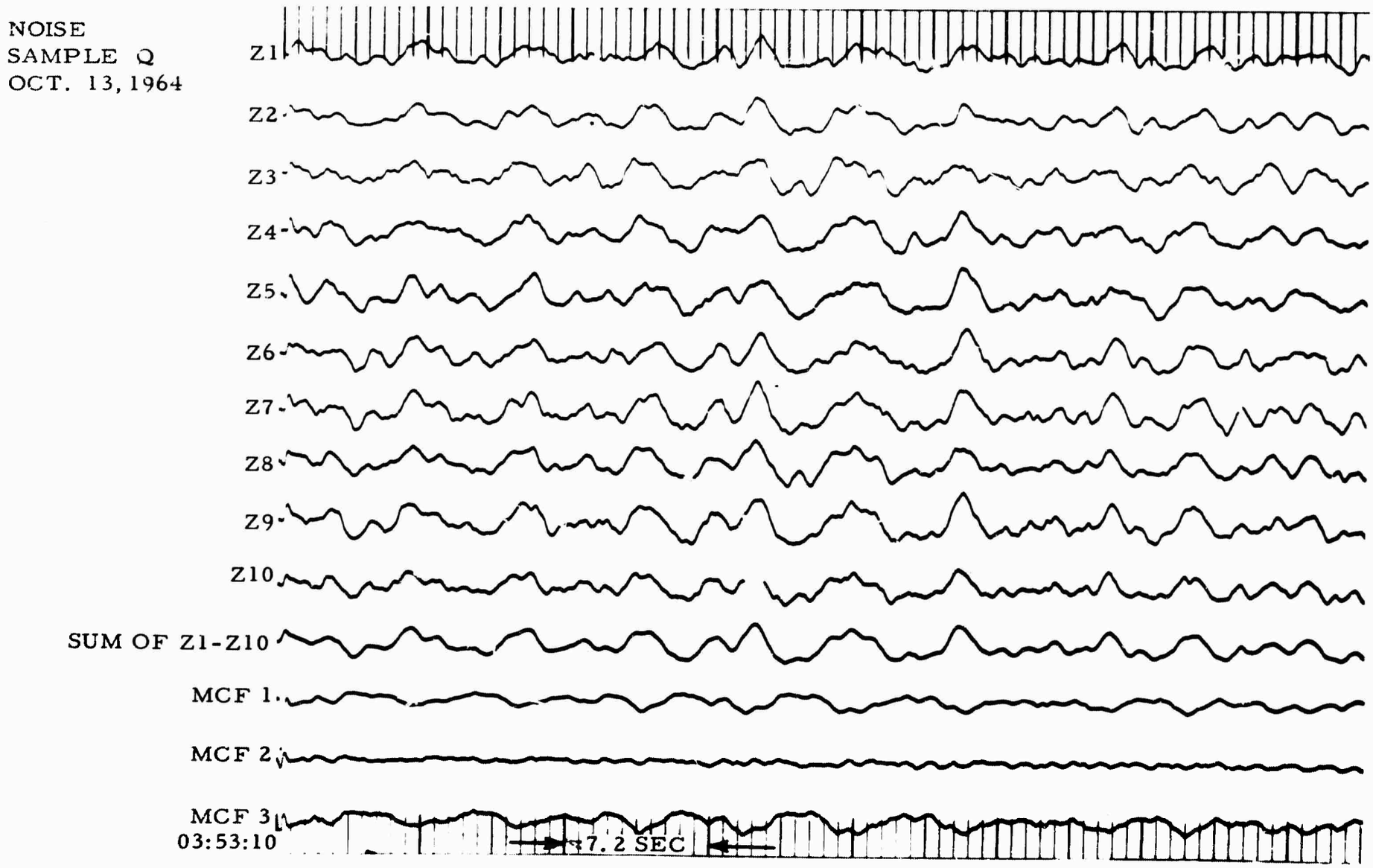

Figure V-10. A Short Portion of Noise Sample-Q (Surface) Results of MCF

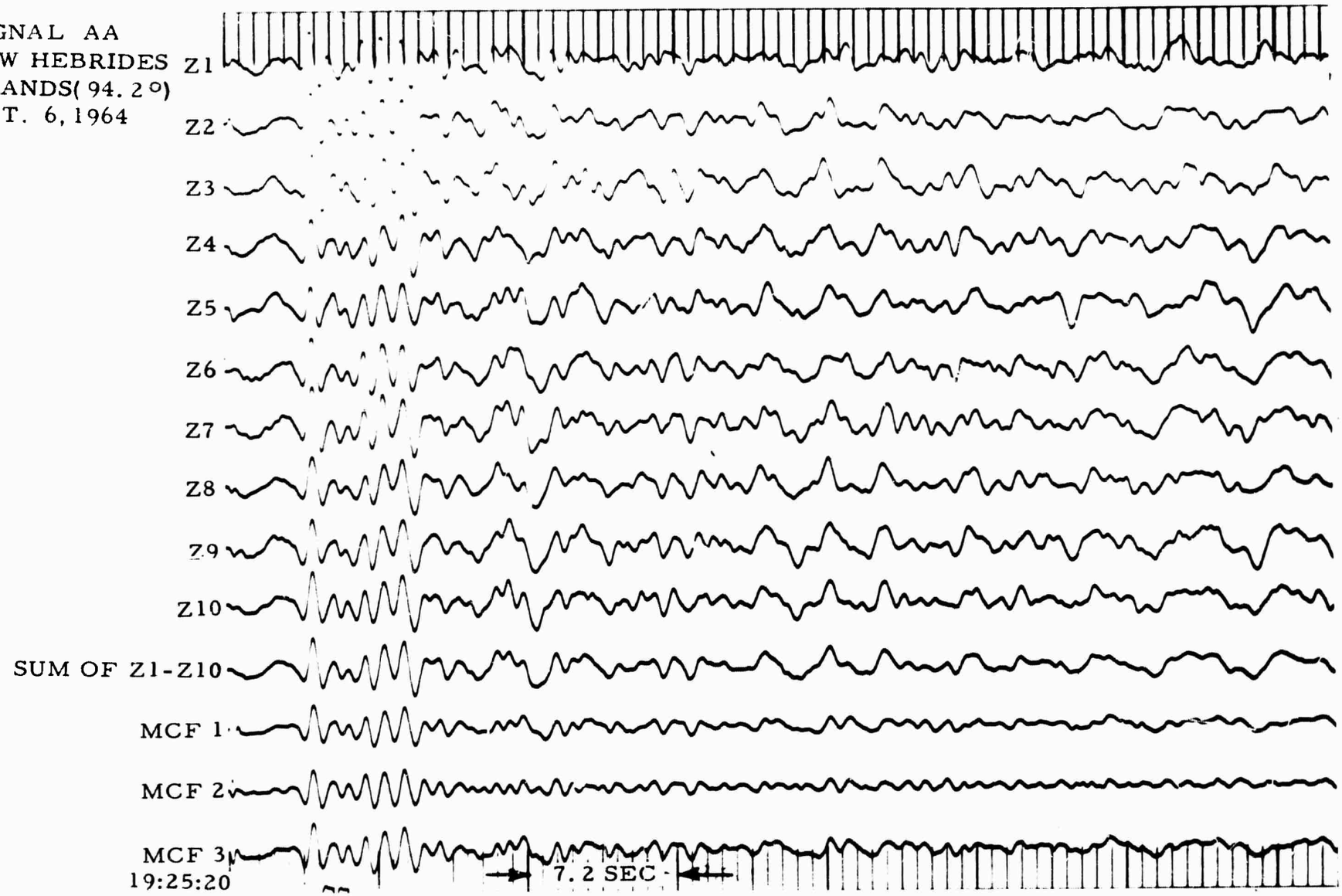

Figure V-11. A Short Portion of UBO Signal AA(Surface) Results of MCF

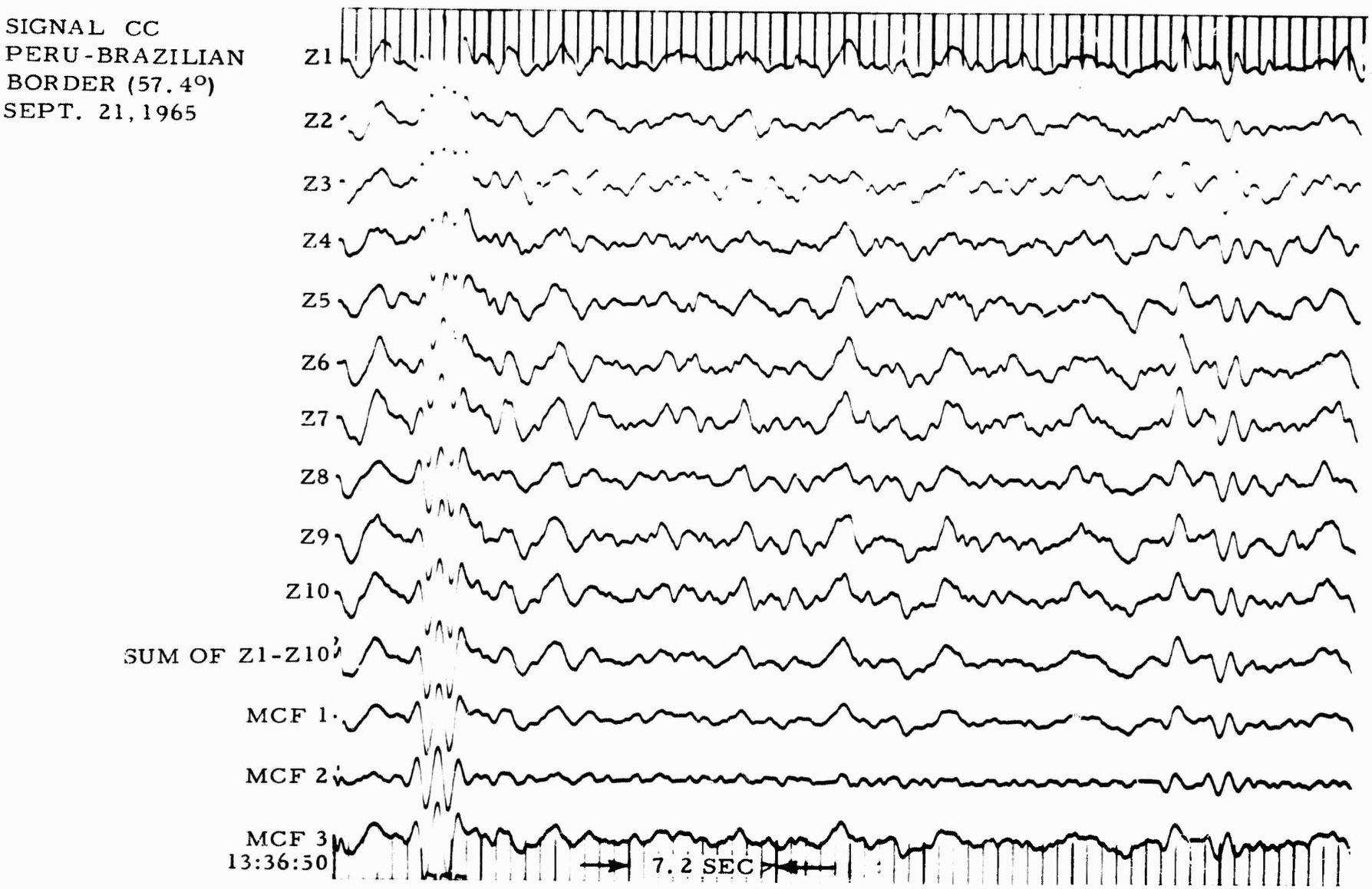

Figure V-12. A Short Portion of UBO Signal CC (Surface) Results of MCF

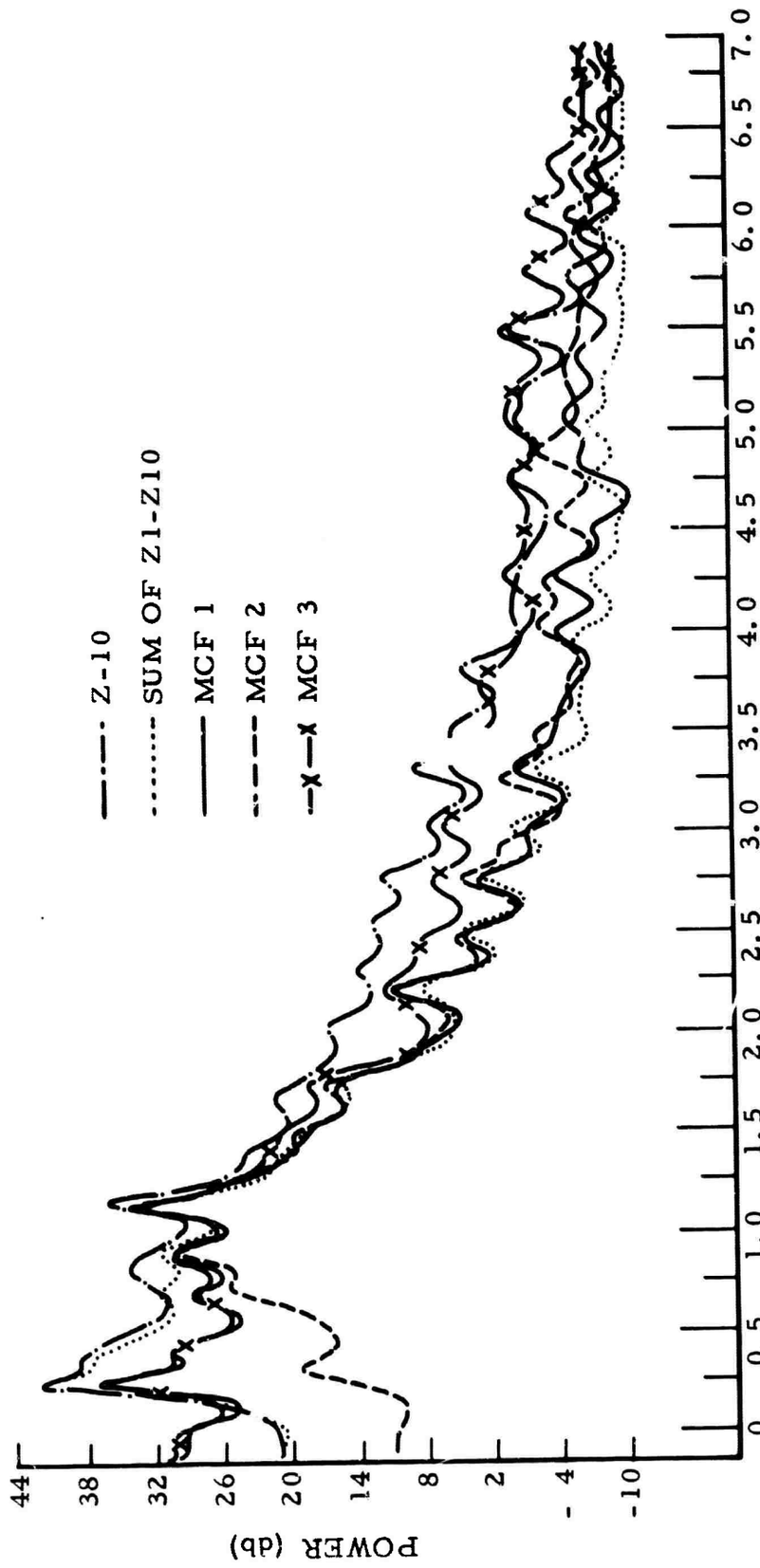

Figure V-13. Single-Channel Power Density Spectra for UBO Signal -AA Results of MCF

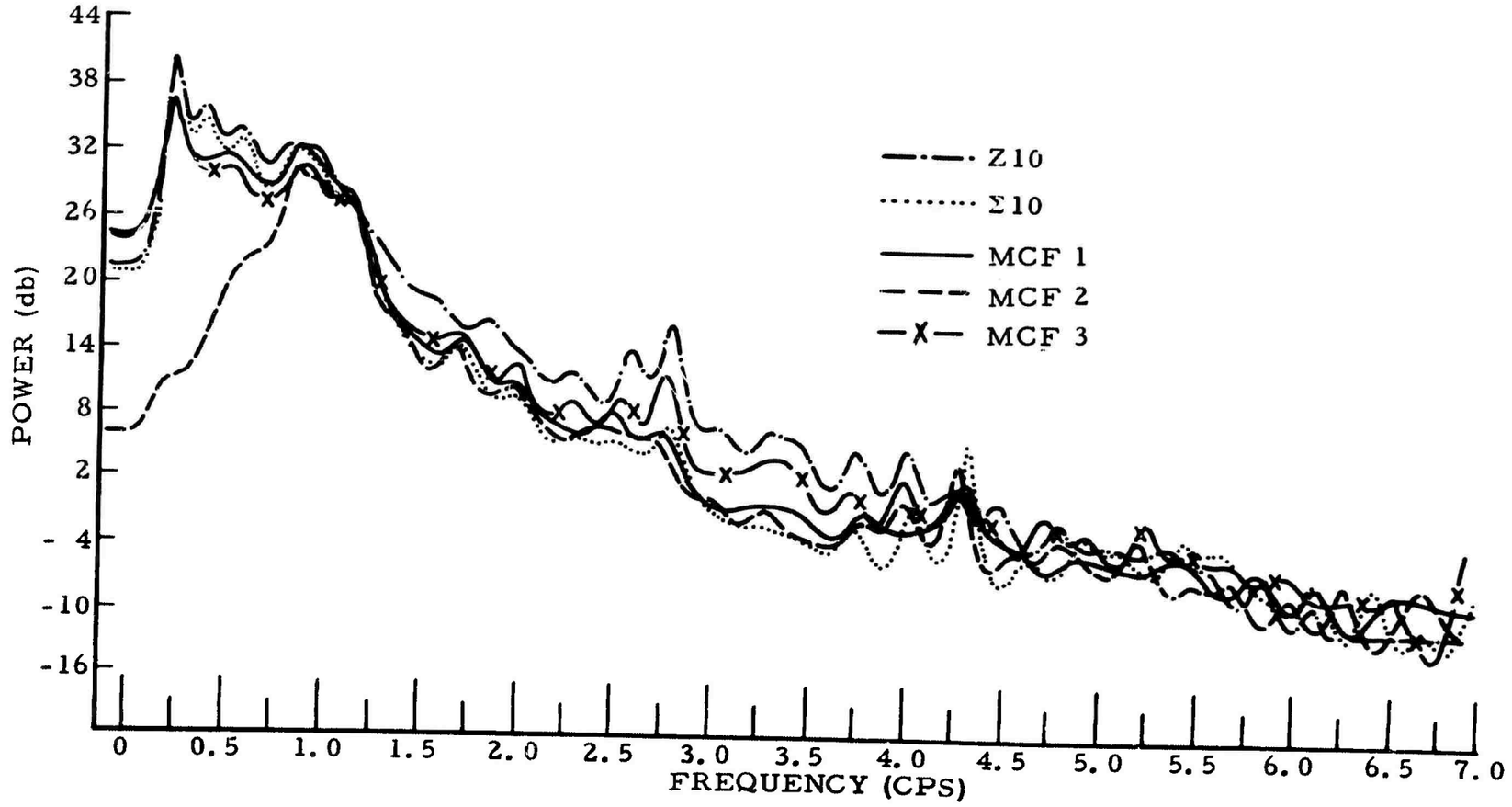

Figure V-14. Single-Channel Power Density Spectra for UBO Signal-CC Results of MCF

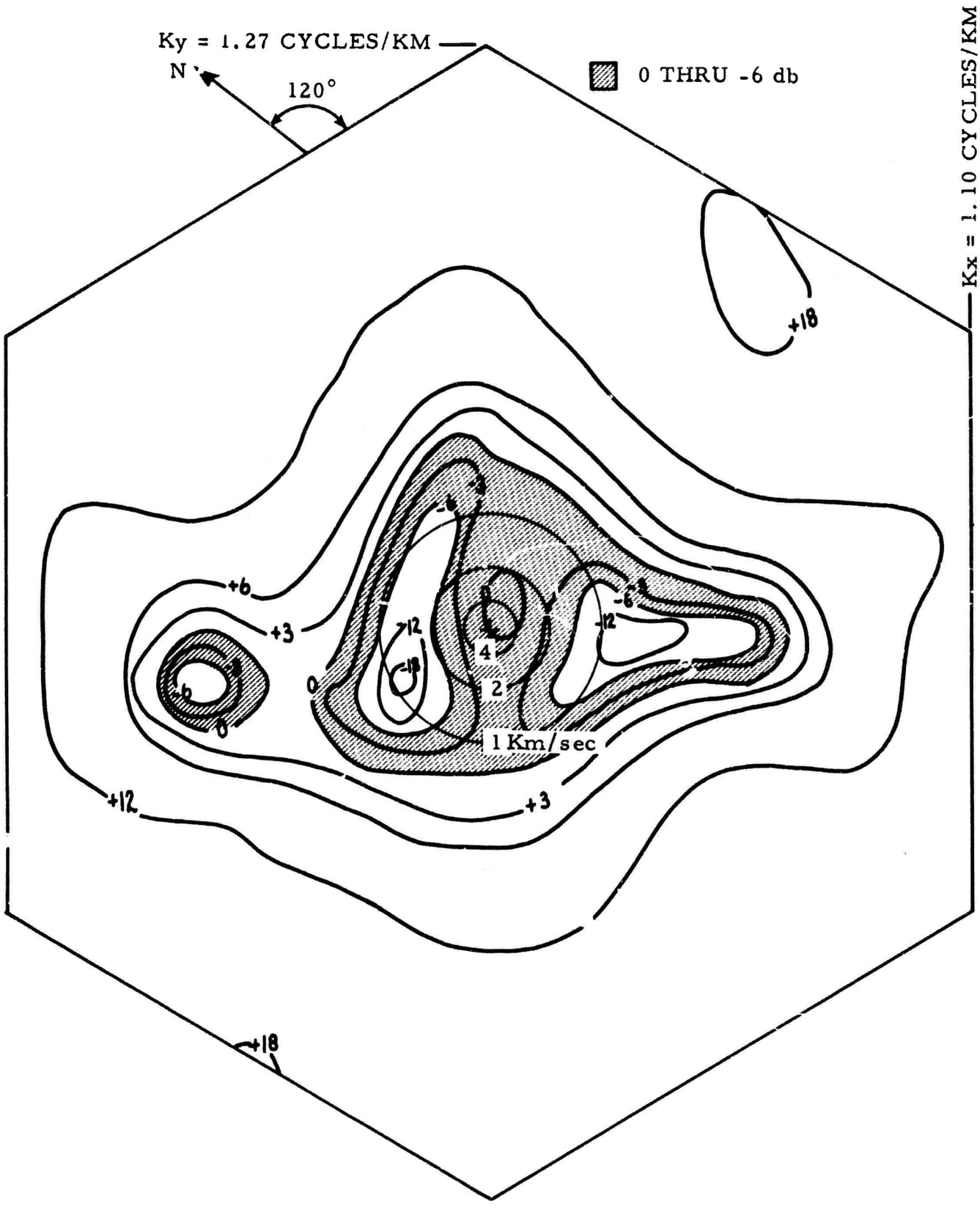

Figure V-15. Two-Dimensional Wavenumber Response UBO MCF-1, f = 0.25 CPS

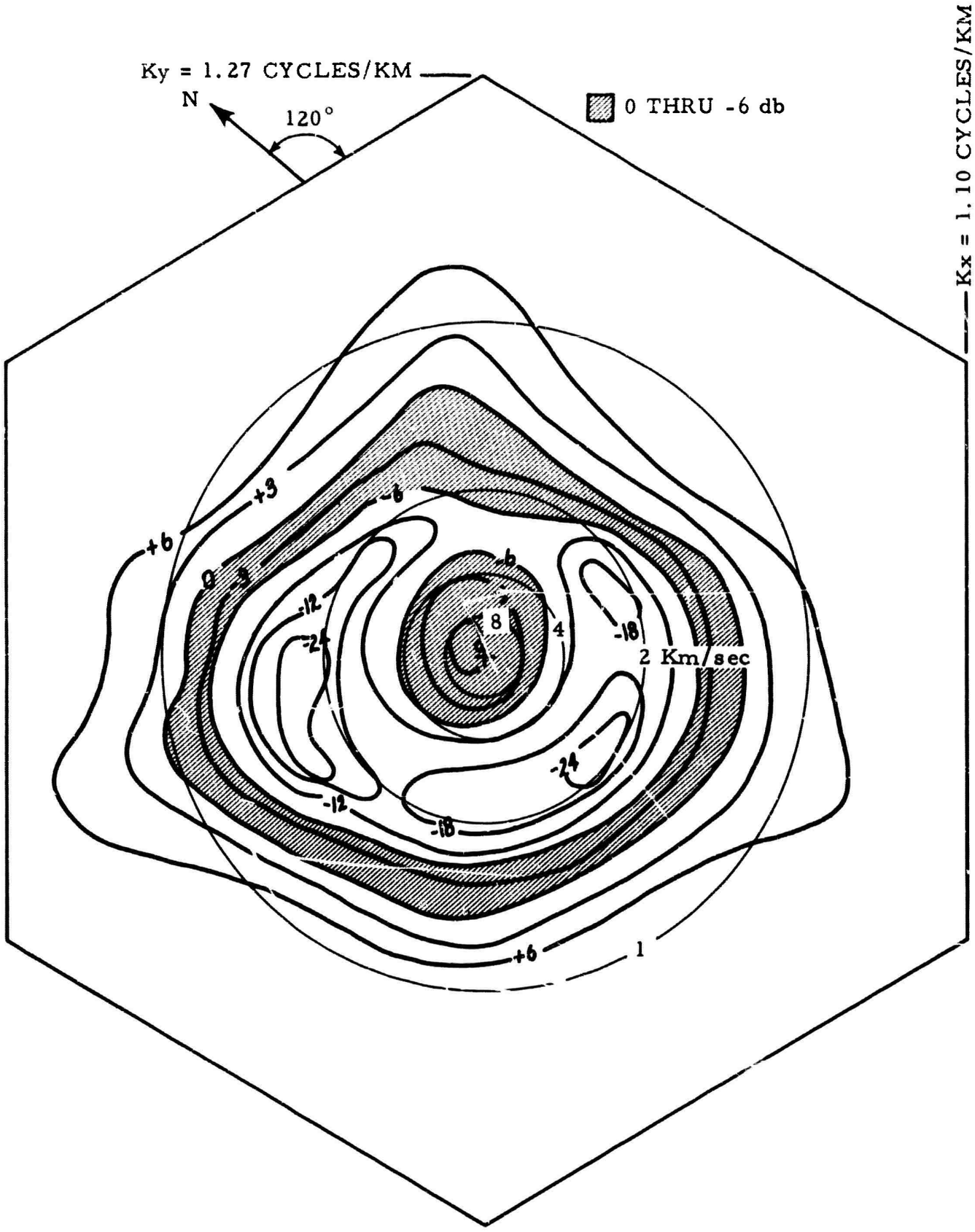

Figure V-16. Two-Dimensional Wavenumber Response UBO MCF -1, f=0.75 CPS

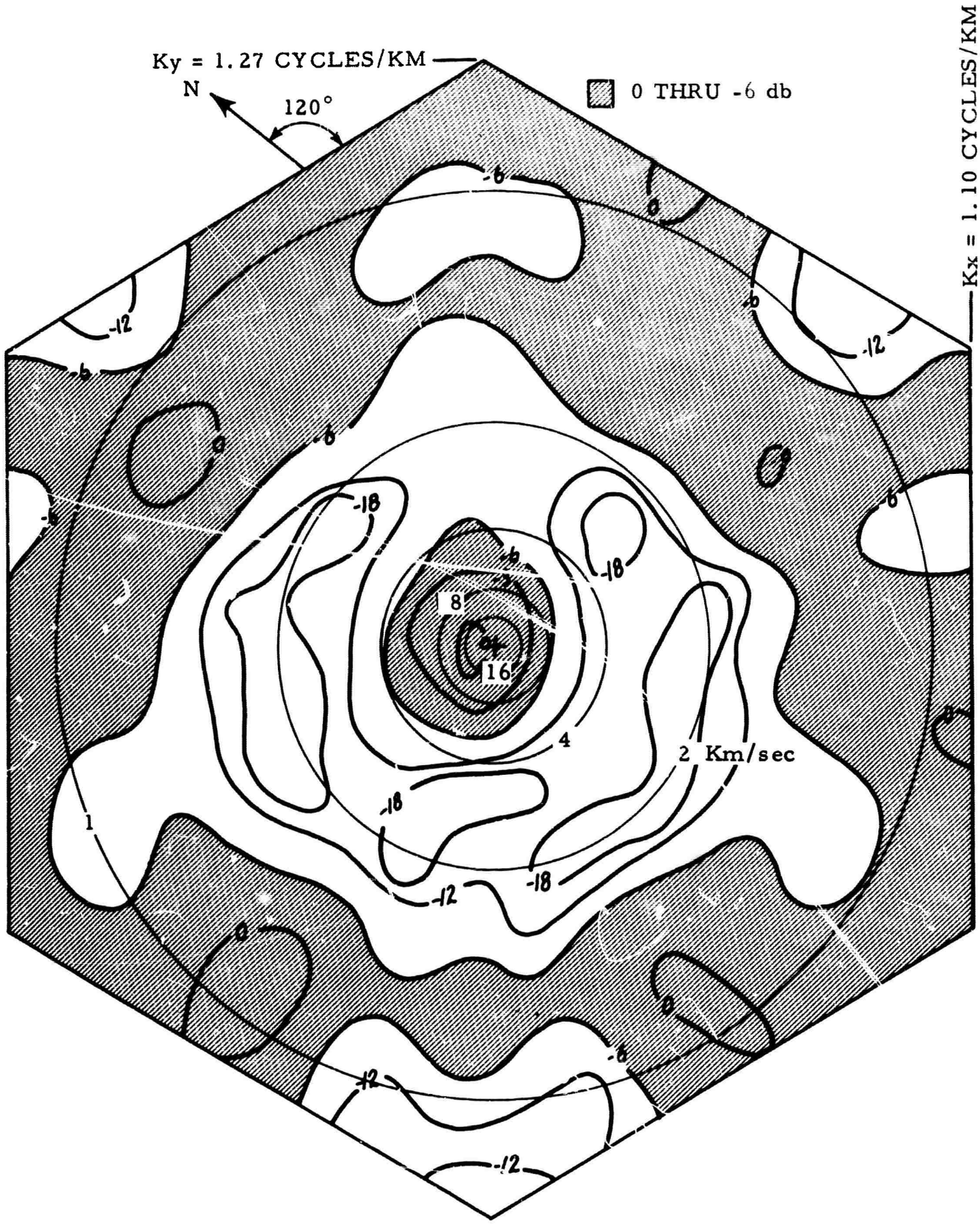

Figure V-17. Two-Dimensional Wavenumber Response UBO MCF -1, f=1.0 CPS

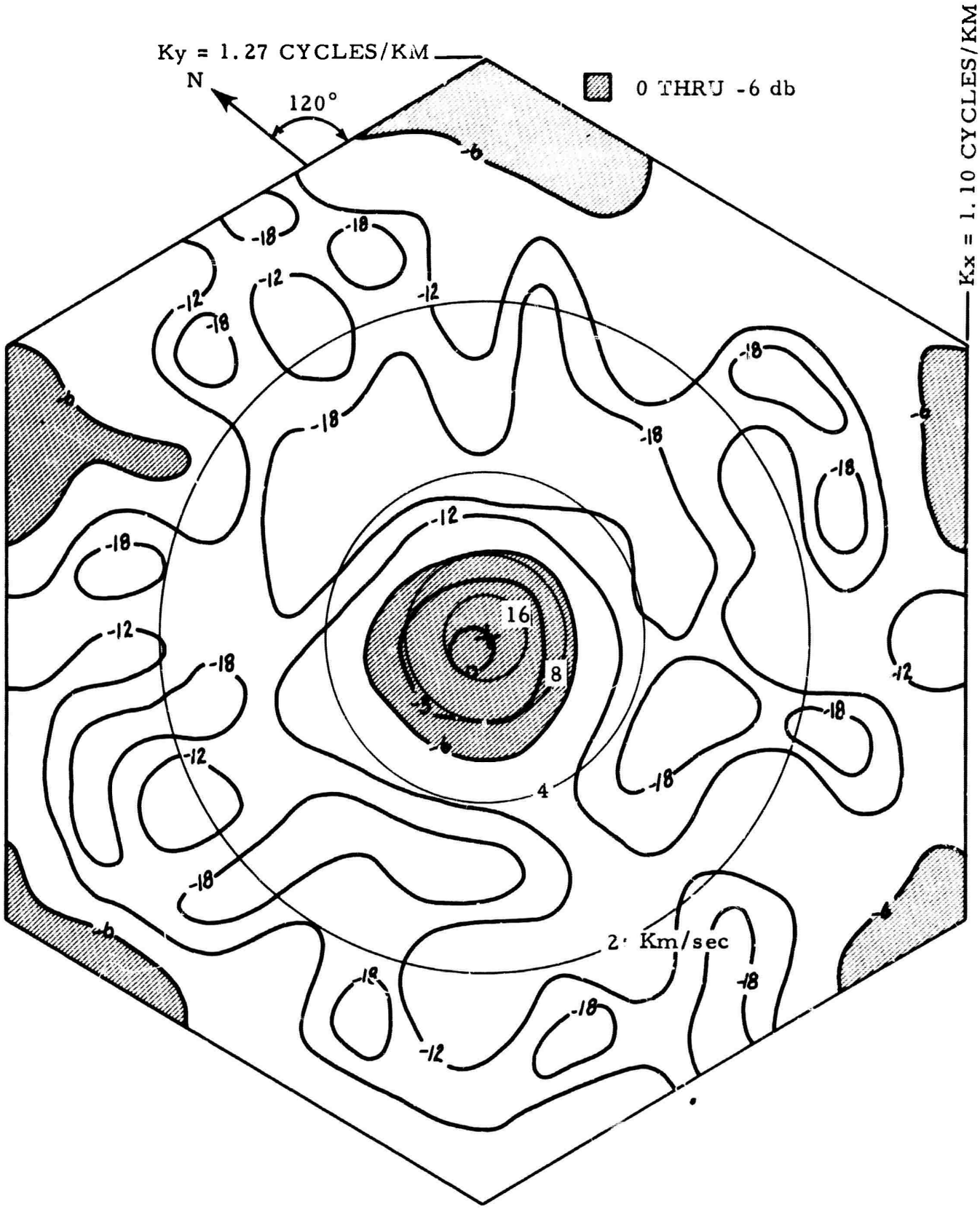

Figure V-18. Two-Dimensional Wavenumber Response UBO MCF -1, f=1.5 CPS

b. Signal-to-Noise Improvement

The signal-to-noise improvement for an infinite velocity white signal has been computed using the noise samples presented in Figures V-8, -9 and -10 for the MCF-1 output and the straight summation output both relative to a single data channel (the Z-10 center seismometer) and is presented in Figures V-19, -20 and -21.

In each of these figures, at most frequencies the multichannel filter is seen to do at least as good as the straight sum, and at frequencies below 0.75 cps, considerably better. In Figures V-19 and -20 the multichannel filter indicates a 6 to 15 db signal-to-noise improvement whereas the straight sum can show little improvement due to the limitations of the array resolution.

Noise sample Q in Figure V-21 does not indicate this significant an improvement below 0.75 cps. This is attributable to either of two reasons which are: (1) a reduction in the microseismic energy level and (2) a change of direction of the microseismic energy. Investigation of the Z-10 single-channel power density spectrum in Figure V-21 indicates that both reasons are probably applicable. The power density spectra indicates a reduced noise level in the 0.25 to 0.75 cps band, but not sufficient to explain the reduced improvement which would indicate a probable change of direction for this energy.

On the basis of the ambient noise studies, which indicated surface mode energy present in the 0.75 to 2.0 cps region (specifically 3 noise lobes), a significant signal-to-noise improvement would be expected relative to the straight sum. However, the improvement is approximately 6 to 10 db in these noise samples, but does not indicate significant improvement relative to the straight sum. This fact is explainable on the basis of the straight sum response for the UBO 10-element planar array shown in Figure V-22. Analysis of the straight summation response in view of the known low-velocity organized noise field indicates that the UBO array is suited ideally for rejecting the 3 noise lobes between frequencies of 0.75 to 2.0 cps. The normal rejection pattern in wavenumber space is 9 to 18 db on these noise lobes.

The significant point to be derived from this analysis is that comparison of the signal-to-noise improvement for MCF processing and straight summation processing is actually the comparison of 2 processing techniques. For the UBO noise field and array configuration, the array straight summation processing is approximately optimum in the 0.75 to 2.0-cps frequency range for infinite velocity signal preservation.

Text cont'd page V-27

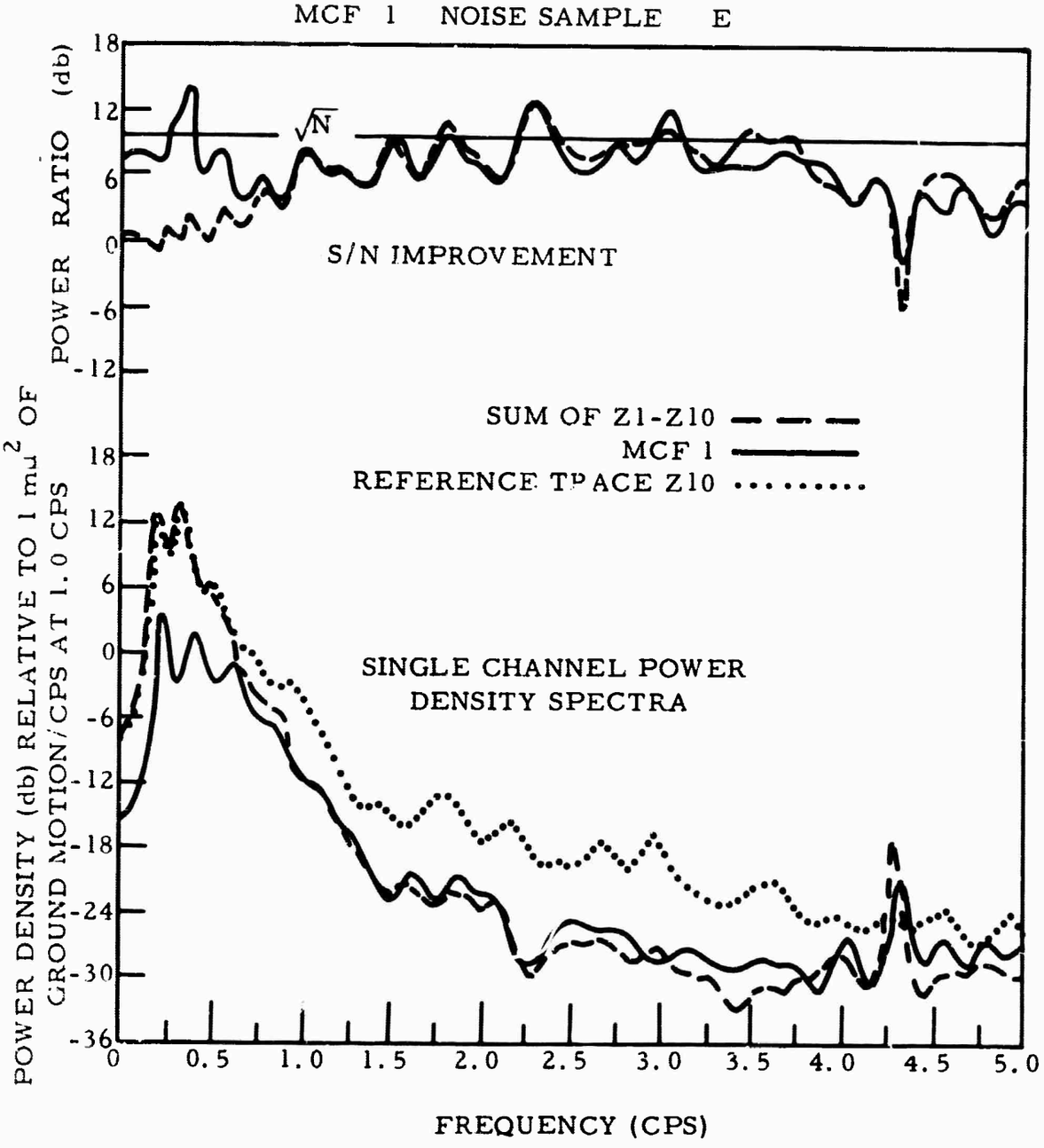

Figure V-19. S/N Improvement and Single-Channel Power Density Spectra for MCF-1 Noise Sample E

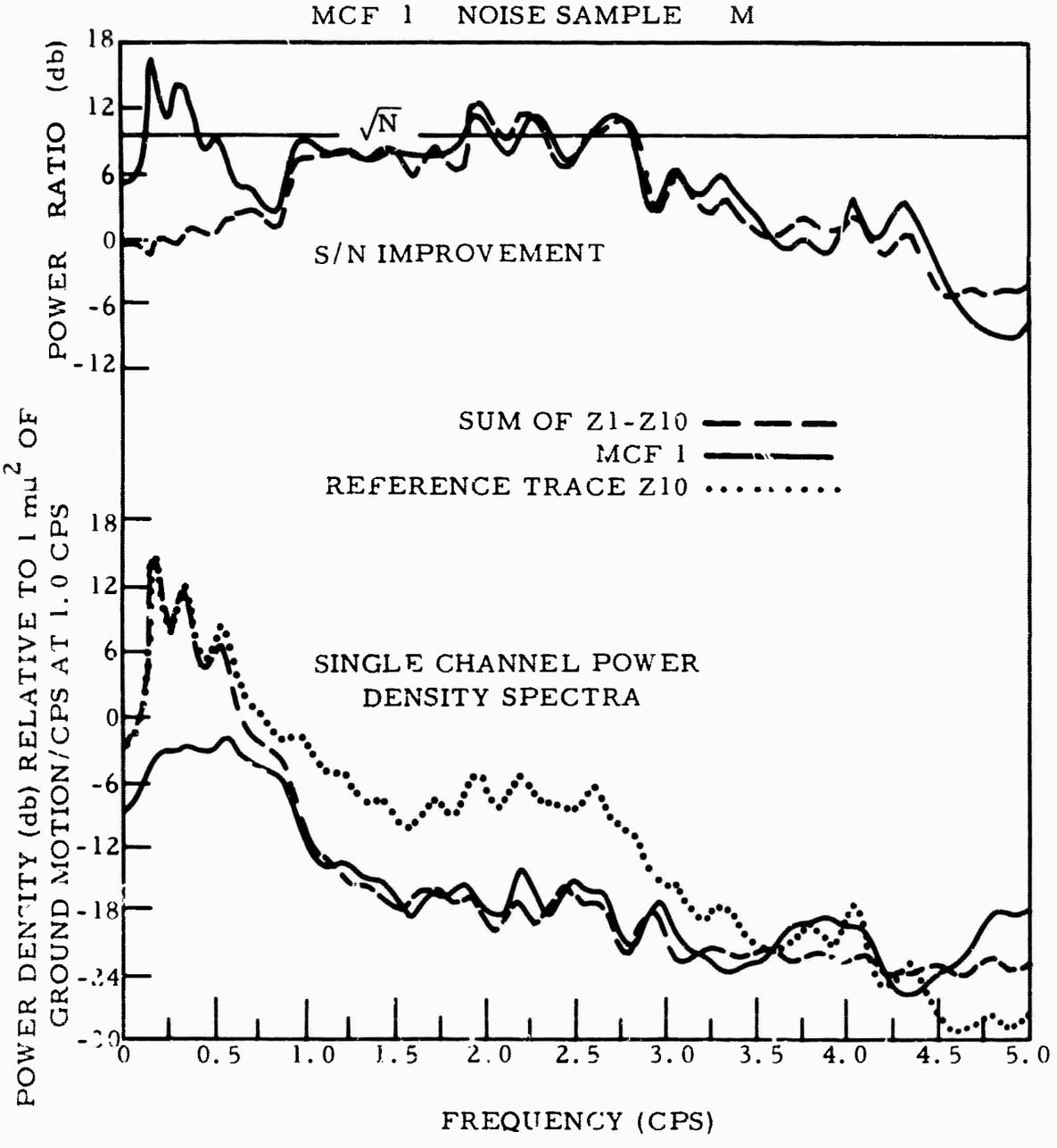

Figure V-20. S/N Improvement and Single-Channel Power Density Spectra for MCF-1 Noise Sample M

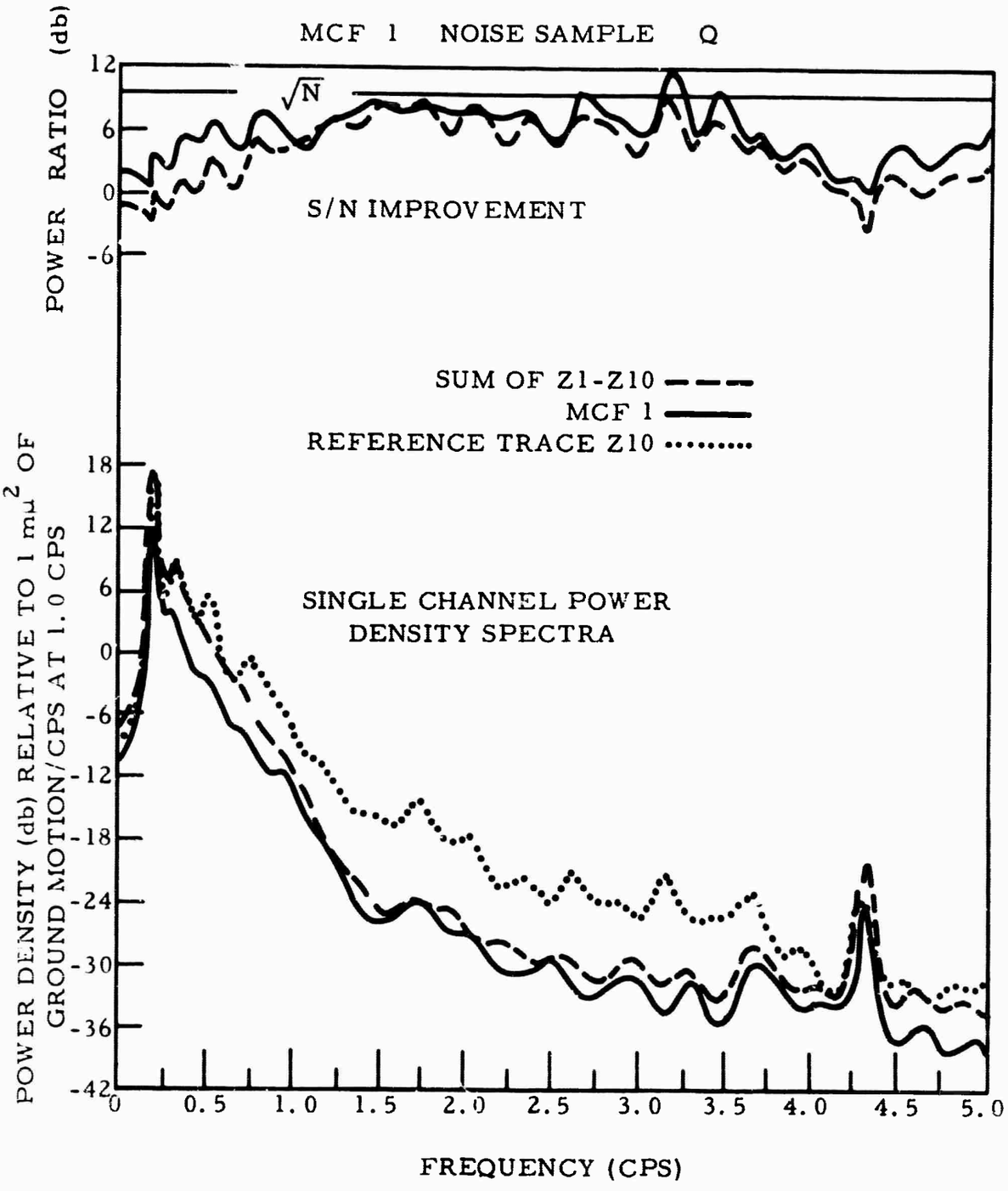

Figure V-21. S/N Improvement and Single-Channel Power Density Spectra for MCF-1 Noise Sample Q

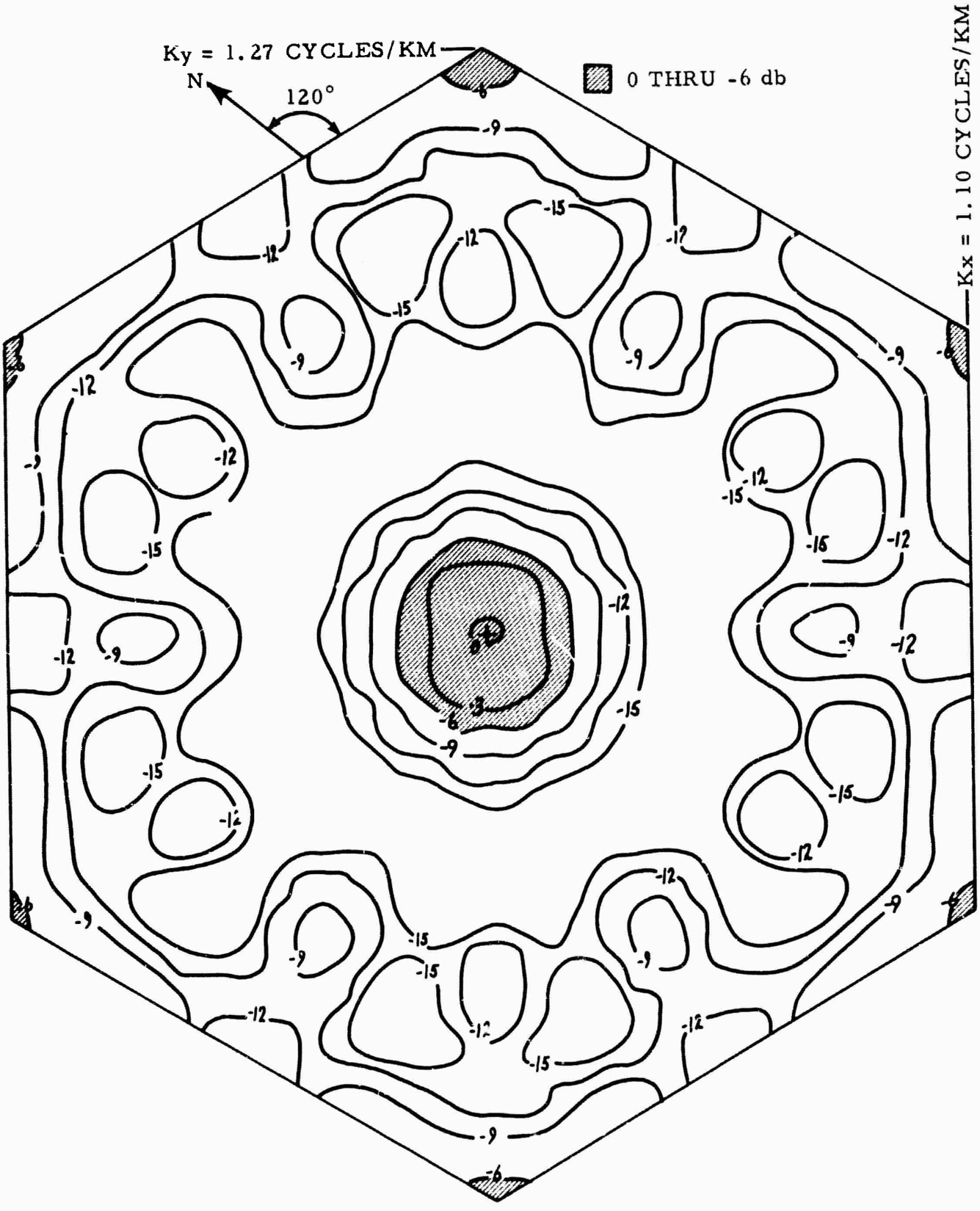

Figure V-22. Straight-Summation Response UBO 10-Element Planar Array

Above 2.0 cps, both the straight summation and multichannel filter results are comparable approximately in signal-to-noise improvement. This improvement generally is limited by $\sqrt{N}$ where N is the number of sensors if the noise field is random. This level is indicated in each of the signal-to-noise improvement curves.

As was pointed out in the ambient noise analysis (Section III), there appeared to be a non-time and space-stationary organized noise source in the 1.75-to 3.0-cps region. The filtering results in Figures V-19, -20 and -21 indicate that if this organized noise component is present, the filter is not rejecting it. Filtering 9 other noise samples (both ensemble and non-ensemble) indicated the same results. Two of the non-ensemble samples were presented in the noise analysis report* and were shown to contain a significant component of this energy.

The conclusion for this analysis is that the ensemble noise samples (Appendix A) did not contain this organized energy and, therefore, the filters (MCF-1, -2 and -3) will not reject it specifically.

In analyzing the improvement curves in Figures V-19, -20 and -21, it should be noted that the decrease in S/N improvement above 3.0 to 4.0 cps is not due to the inability of the filters to reject random noise, but is due to the small amount of noise power so that the filter process can indicate little noise rejection. In other words, the power at these frequencies probably is system noise only.

c. Application of UBO MCF-1 to Measured Signals

The application of MCF-1 to 2 measured signals is shown in Figures V-11 and -12. In the case of signal AA (Figure V-11), MCF-1 rejects the signal energy approximately 2 db when compared with the straight summation and MCF-3 output. This rejection, mentioned in paragraph 3a, is explainable on the basis of the filter wavenumber response (Figures V-15 through -18).

Signal CC (Figure V-12) also is rejected somewhat on the basis of wavenumber component.

4. Evaluation of UBO MCF-2

a. Wavenumber Response

This response at frequencies of 0.25, 0.75, 1.0, and 1.5 cps is shown in Figure V-23 through -26 respectively. Since MCF-2 has designed into the response a 1.0-cps, 18-db/octave low-cut frequency filter (Figure V-6), the wavenumber response at 0.25 and 0.75 cps (Figures V-23 and -24)

*Texas Instruments Incorporated, 1965: Noise Analysis for Uinta Basin Seismological Observatory, sponsored by AFTAC, Oct. 15, P. III-5/6, III-7/8.

Text cont'd page V-32

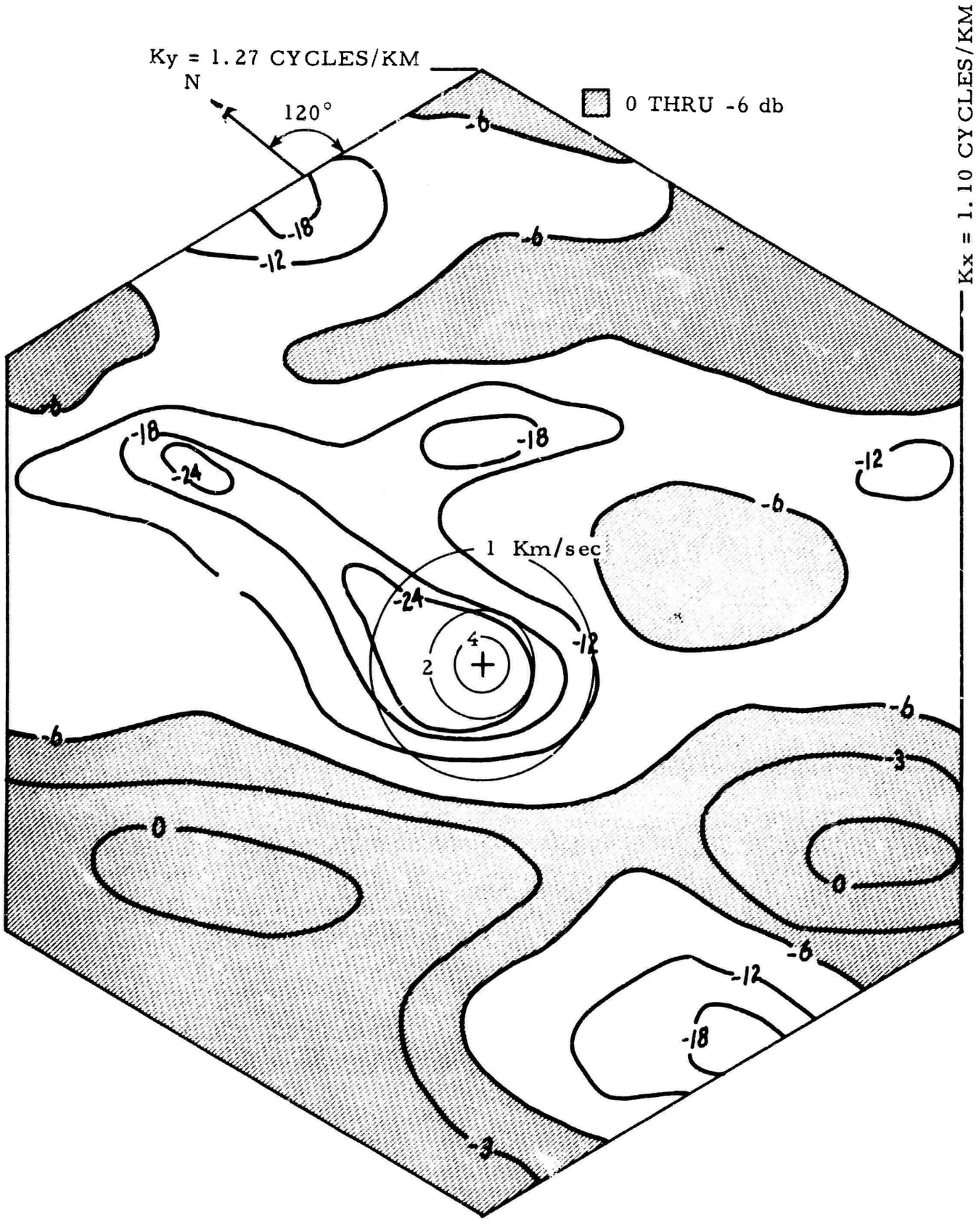

Figure V-23. Two-Dimensional Wavenumber Response UBO MCF-2, f = 0.25 cps

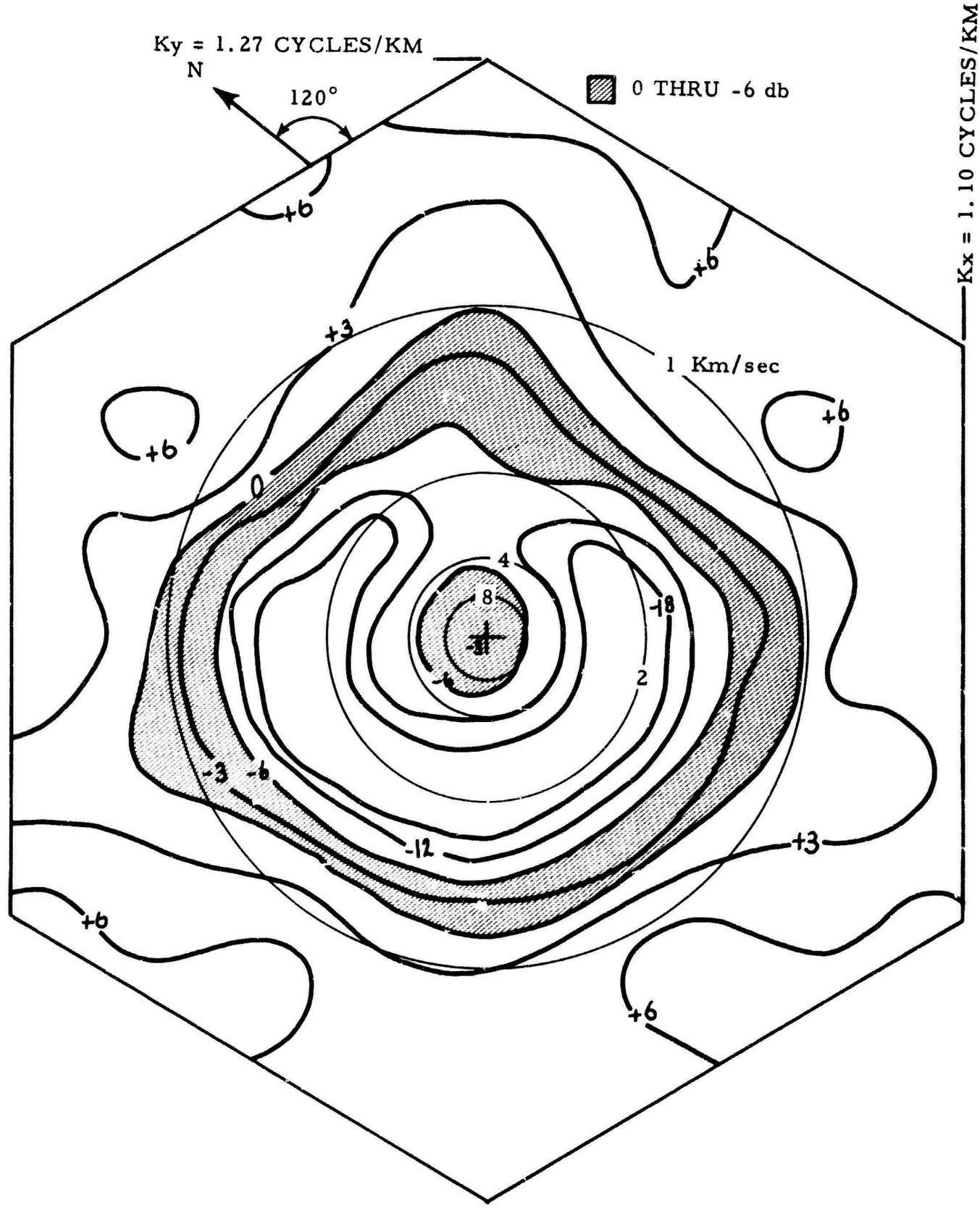

Figure V-24. Two-Dimensional Wavenumber Response UBO MCF-2, f=0.75 CPS

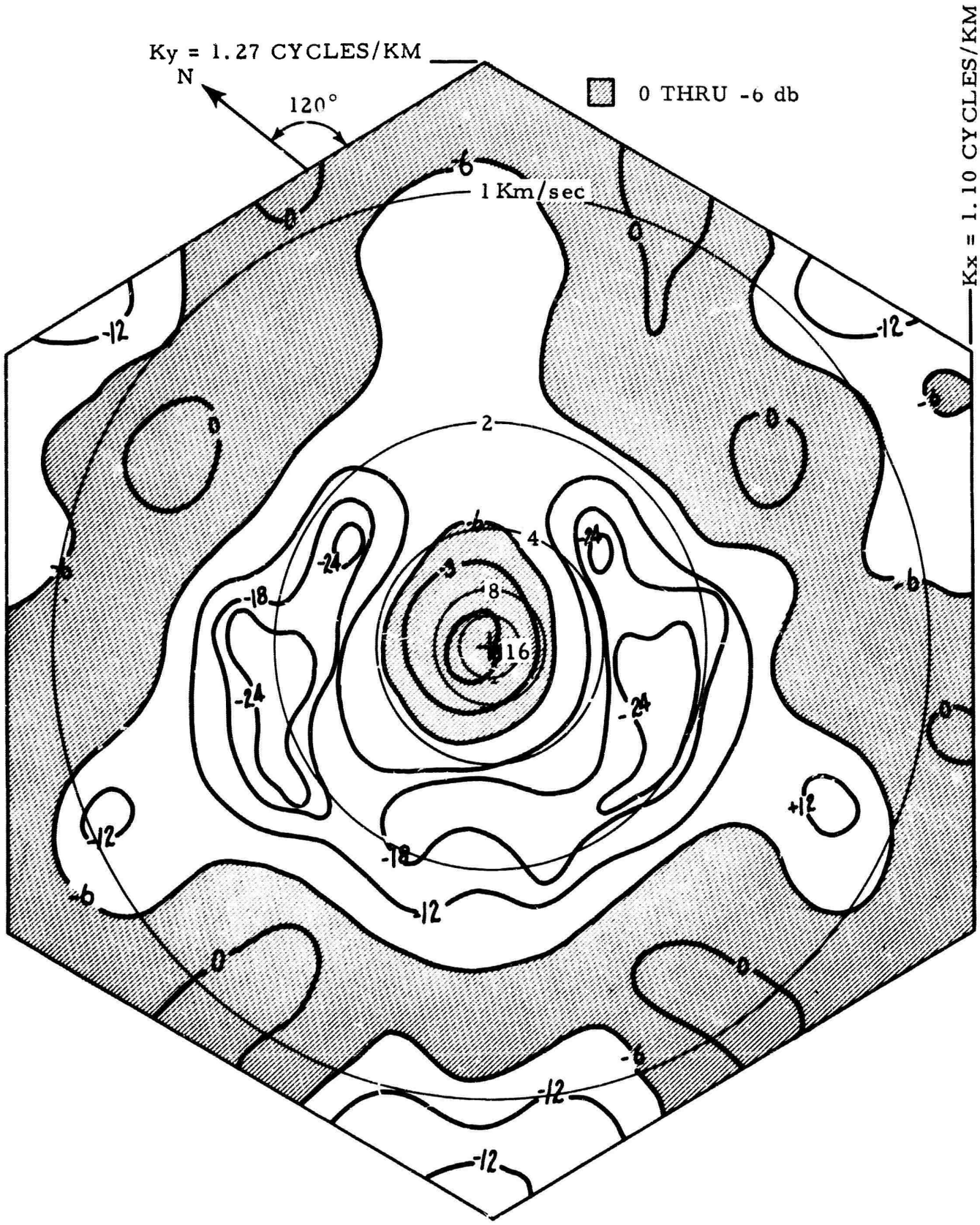

Figure V-25. Two-Dimensional Wavenumber Response UBO MCF-2, f=1.0 CPS

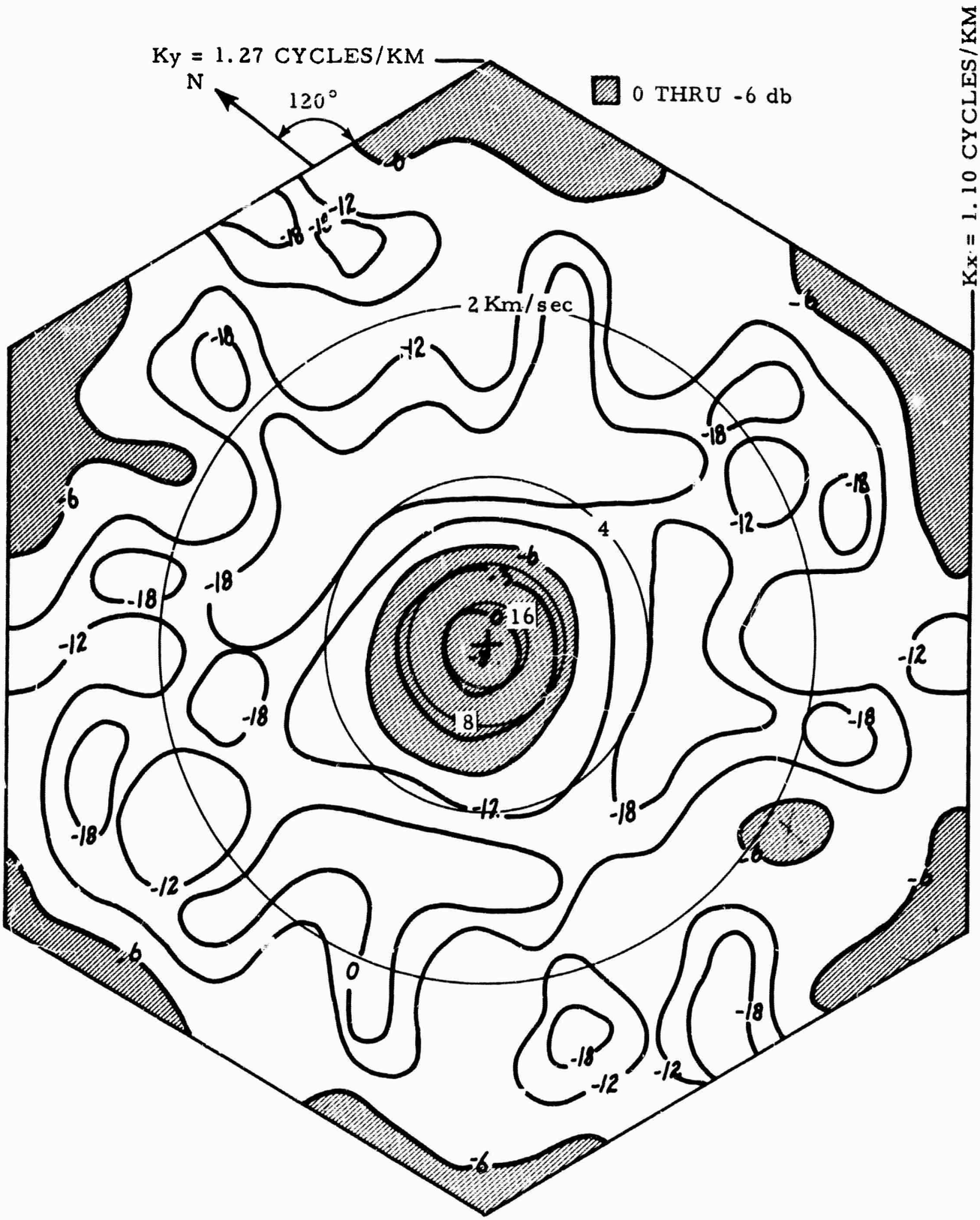

Figure V-26. Two-Dimensional Wavenumber Response UBO MCF-2, f=1.5 CPS

indicates rejection of both noise and infinite velocity energy of 12 to 26 db and 3 to 24 db, respectively.

At 1.0 and 1.5 cps the wavenumber response of the filter is almost identical to that of the MCF-1 (i.e., infinite velocity energy is passed with 0 db attenuation and the 3 organized noise lobes are rejected strongly).

The point to be derived from the wavenumber analysis of MCF-2 is that this multichannel filter can be expected to indicate results comparable to MCF-1 above 1.0 cps, and below 1.0 cps to reject both noise and signal on the basis of single-channel frequency filtering.

b. Signal-to-Noise Improvement

The signal-to-noise improvement for Noise Samples E, M and Q (Figures V-8, -9 and -10, respectively) are shown in Figures V-27, -28 and -29, respectively, for both MCF-2 and straight summation processing as referenced to Z-10.

Below 1.0 cps, the single-channel power density spectra of UBO MCF-2 output trace is considerably lower in power compared to that of the summation and reference trace due to the application of the effective low-cut frequency filter. In noise samples E and M (Figures V-27 and -28), as with MCF-1, some signal-to-noise improvement still is observed and is attributable to velocity filtering of low-velocity organized energy at these frequencies. As noted in MCF-1, noise sample Q evaluation shows little signal-to-noise improvement, due to the reduced level and direction change of the surface-mode energy.

The results obtained with MCF-2 are almost identical to those obtained with MCF-1 above 1.0 cps. (Refer to MCF-1 results for a thorough discussion of filter performance at these frequencies).

c. Application to Measured Signals

Figures V-11 and -12 display MCF-2 output for signals AA and CC, respectively. In both figures, some signal energy attenuation is noted which is attributable to wavenumber filtering of the signals above 1.0 cps and to frequency filtering of the signals below 1.0 cps. Comparison of these signals with the MCF-1 filtered signals indicates a slightly greater attenuation for MCF-2 signals. This difference is probably due to the frequency-filtering capability of MCF-2.

In analyzing the signals filtered by MCF-2, an important point to remember is that this filter will induce waveform distortion if signal energy is present below 1.0 cps, because of precursor effect of the filter.

Text cont'd page V-36

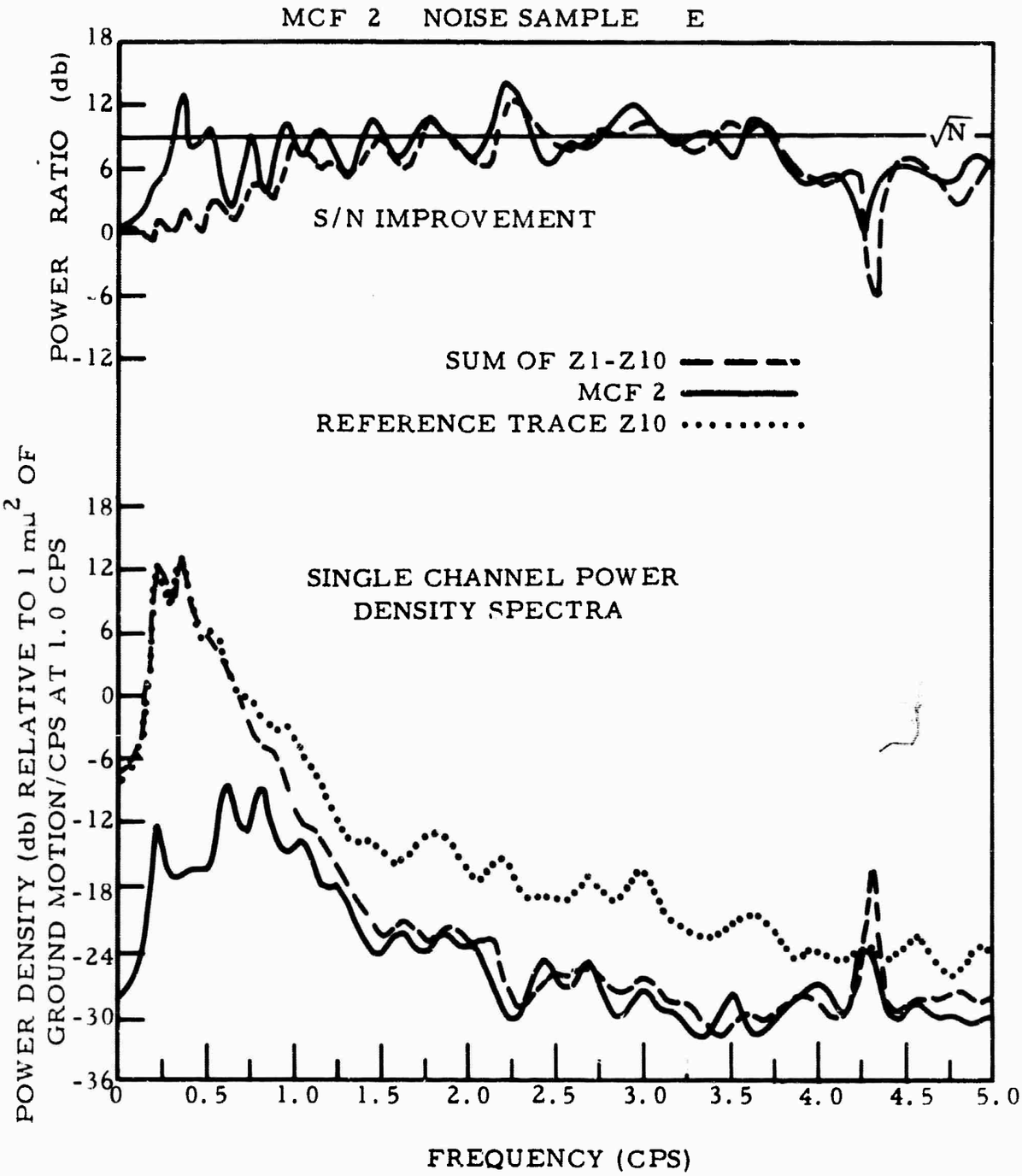

Figure V-27. S/N Improvement and Single-Channel Power Density Spectra for MCF-2 Noise Sample E

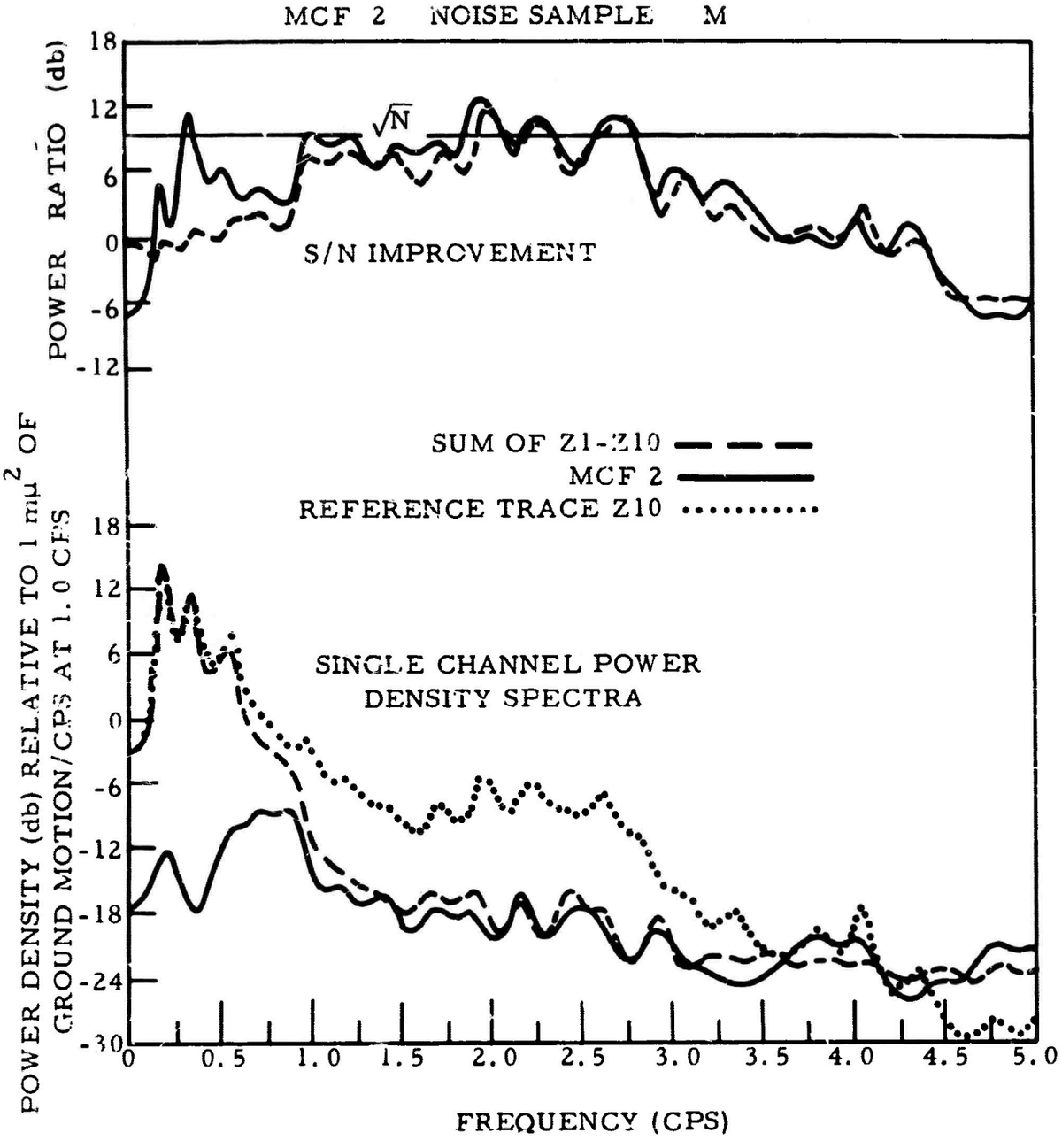

Figure V-28. S/N Improvement and Single-Channel Power Density Spectra for MCF-2 Noise Sample M

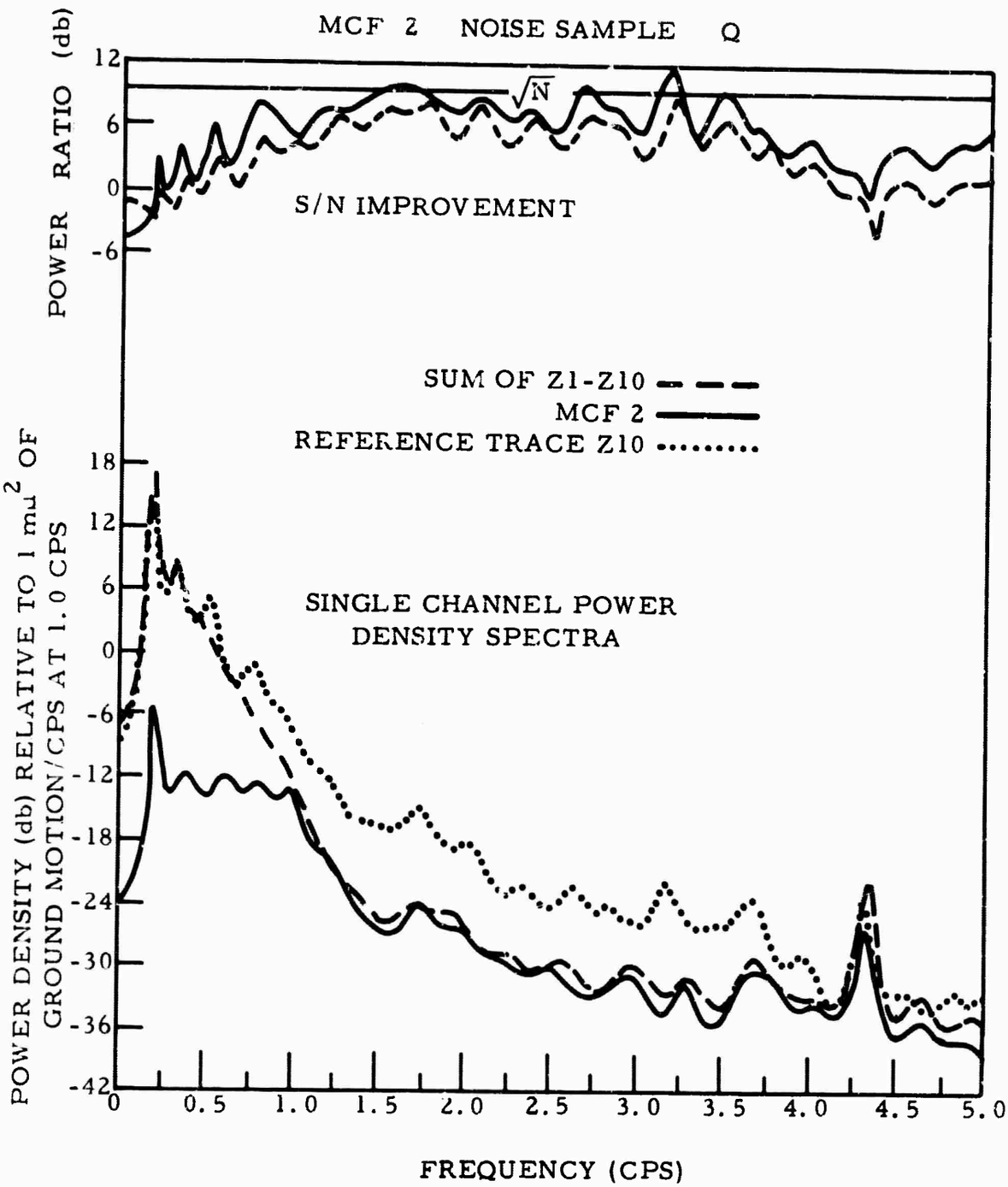

Figure V-29. S/N Improvement and Single-Channel Power Density Spectra for MCF-2 Noise Sample Q

5. Evaluation of UBO MCF-3

a. Wavenumber Responses of UBO MCF-3

This response a 0.25, 0.75, 1.0 and 1.5 cps is shown in Figures V-30 through V-33, respectively.

For frequencies of 0.25 to 1.0 cps, MCF-3 rejects the low-velocity organized surface-mode energy in a manner comparable to that of MCF-1. At 1.5 cps, there is some trade-off between signal preservation and noise rejection. When compared with the MCF-1 results (Figure V-18), MCF-3 does not indicate comparable noise rejection capability in the 1.7- to 4.0-km/sec velocity range. The filter does, however, preserve teleseismic signal energy (velocities greater than 8.1 km/sec).

b. Signal-to-Noise Improvement for UBO MCF-3

The signal-to-noise improvement and single-channel power density spectra for noise samples E, M and Q (Figures V-8, -9 and -10, respectively) are shown in Figures V-34, -35 and -36, respectively, for MCF-3 and straight-summation processing relative to Z-10.

These results indicate that MCF-3 demonstrates signal-to-noise improvement results comparable to MCF-1 below 1.5 cps, as was predicted in the wavenumber analysis of the filter. At frequencies less than 0.75 cps, the filter indicates improvement results comparable to that of MCF-1 by demonstrating a superdirectivity configuration. Above 1.5 cps, the filter improvement degenerates below that of a straight summation, which is consistent with the explanation in paragraph 5a. This is noticable particularly in Noise Samples E and M (Figures V-34 and -35, respectively).

This trade-off between signal preservation and noise rejection can be expected, since a more stringent condition is placed on an MCF when more than a single point in wavenumber space is to be passed (as with MCF-1 and -2).

An important consideration in the analysis of MCF-3 capabilities is that if a comparison of MCF-3 signal-to-noise improvement for white signals of other than infinite velocity (e.g., 8.1-km/sec signals) could be made with the signal-to-noise improvement of a straight summation (or MCF-1 or -2), MCF-3 probably would demonstrate comparable or possibly higher signal-to-noise improvement at frequencies above 1.0 cps, because MCF-3 is able to preserve teleseismic signals to 8.1 km/sec, whereas, the straight summation (or MCF-1 or -2) would reject this signal energy.

c. Application of MCF-3 to Measured Signals

The results of filtering signals AA and CC with MCF-3 are shown in Figures V-11 and -12, respectively.

Text cont'd page V-44

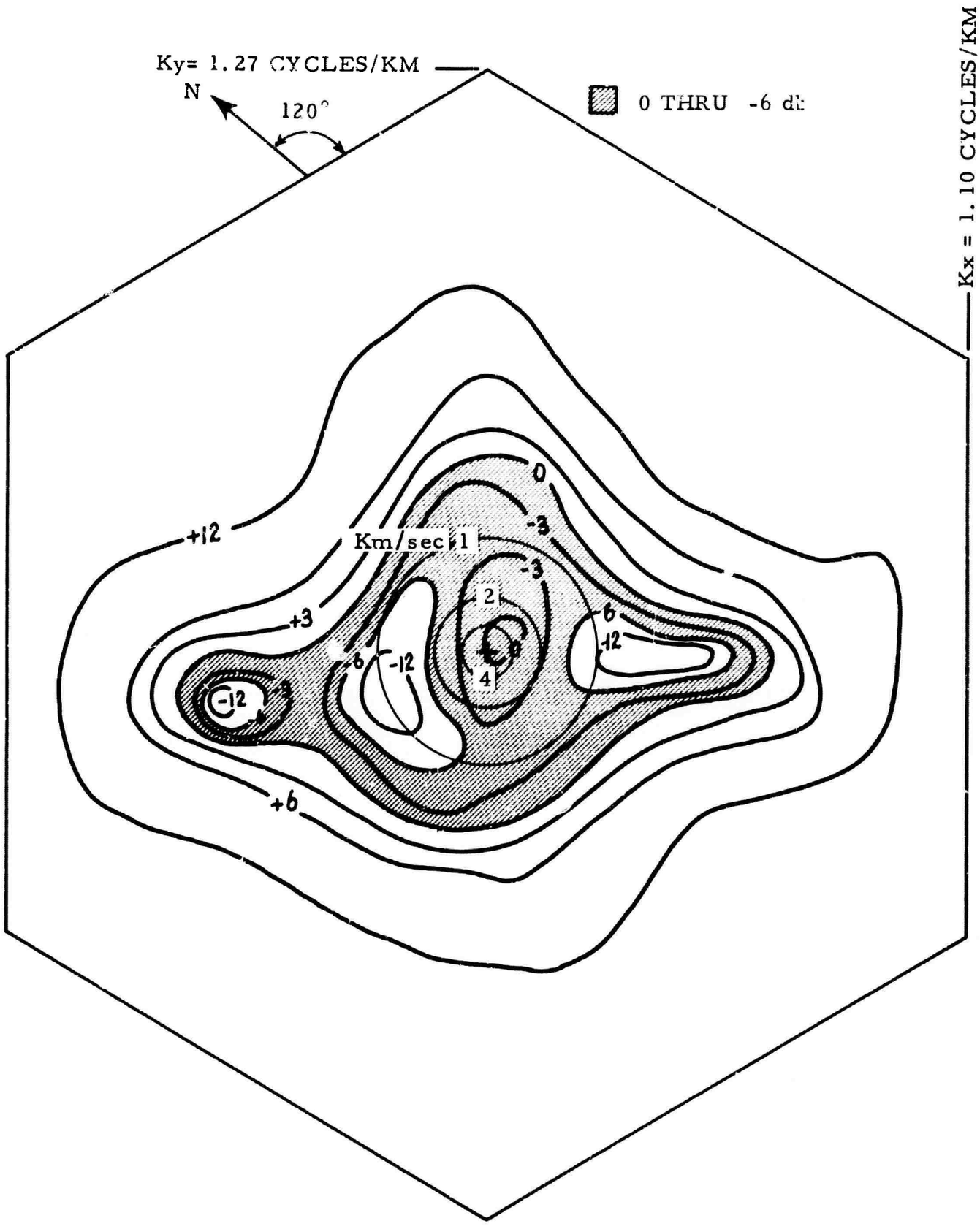

Figure V-30. Two-Dimensional Wavenumber Response UBO MCF-3, f=0.25 CPS

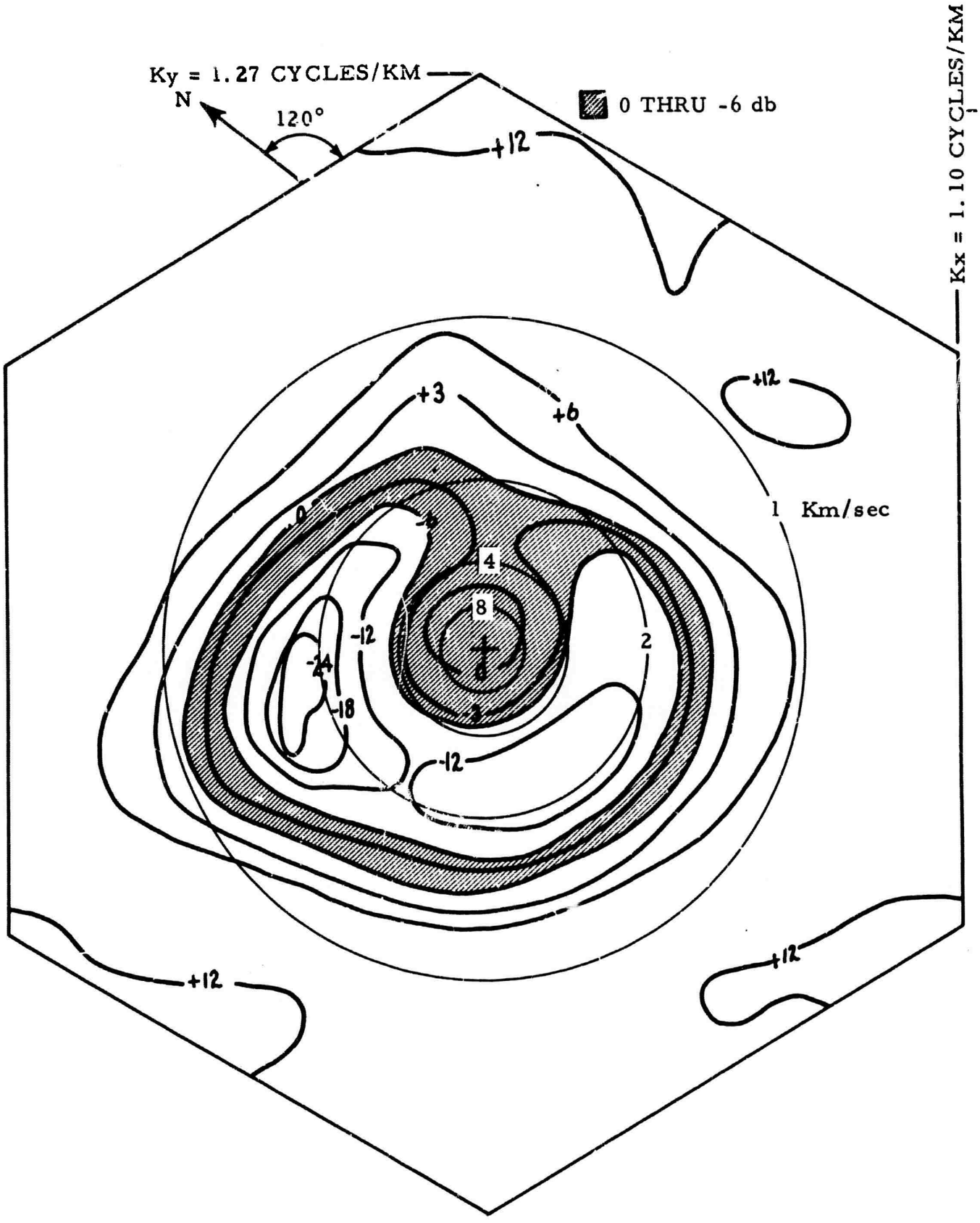

Figure V-31. Two-Dimensional Wavenumber Response UBO MCF-3, f=0.75 CPS

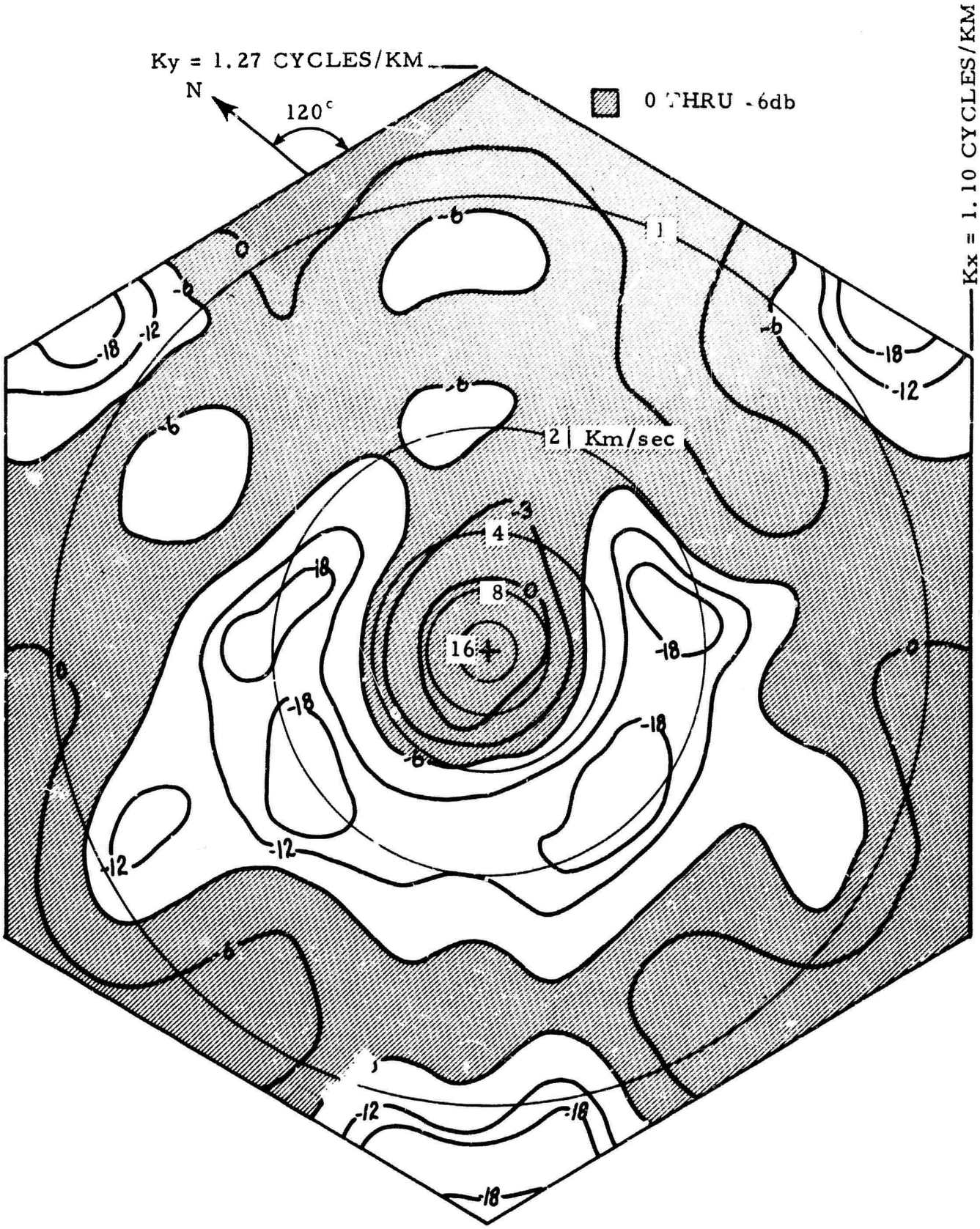

Figure V-32. Two-Dimensional Wavenumber Response UBO MCF-3, f=1.0 CPS

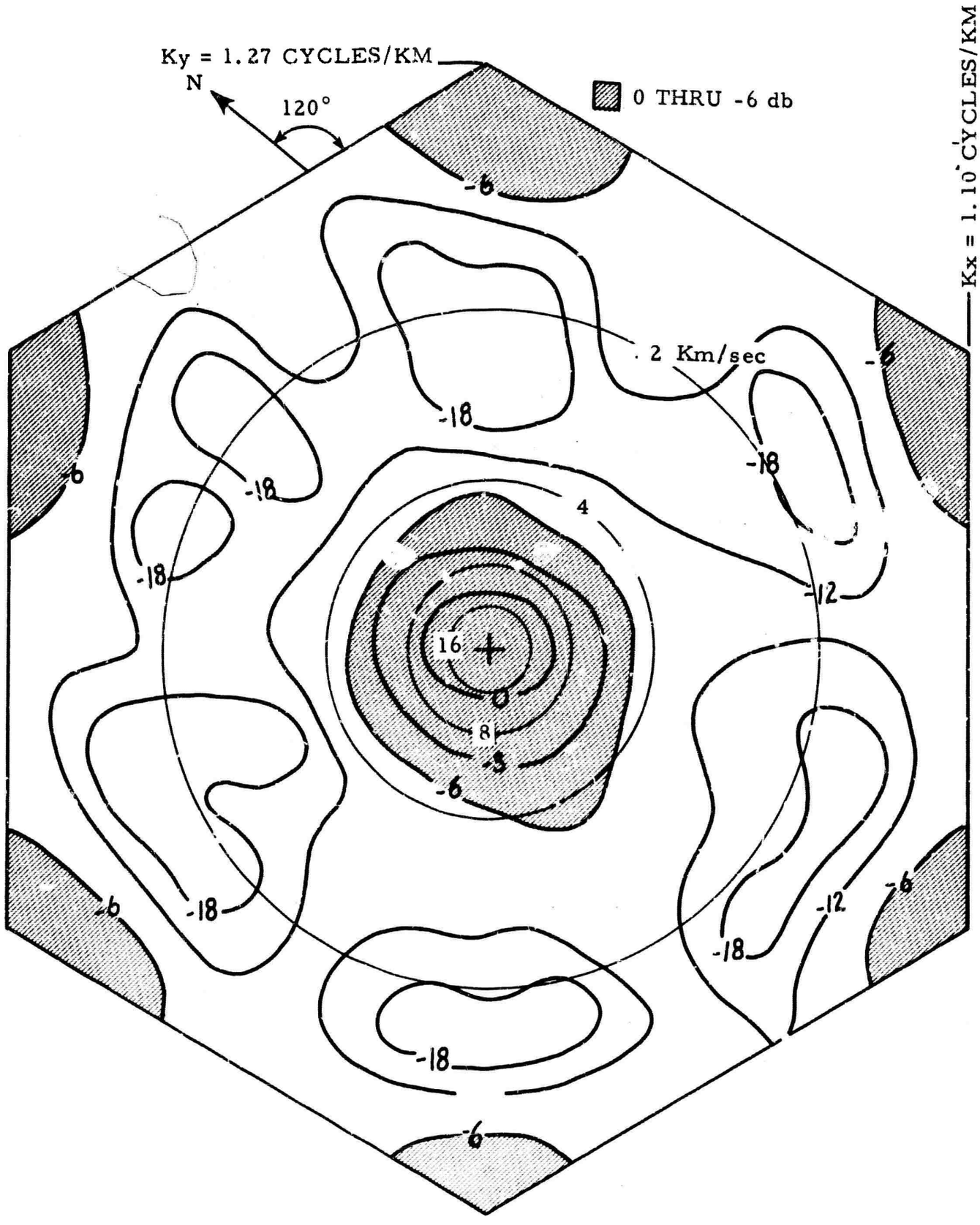

Figure V-33. Two-Dimensional Wavenumber Response UBO MCF-3, f=1.5 CPS

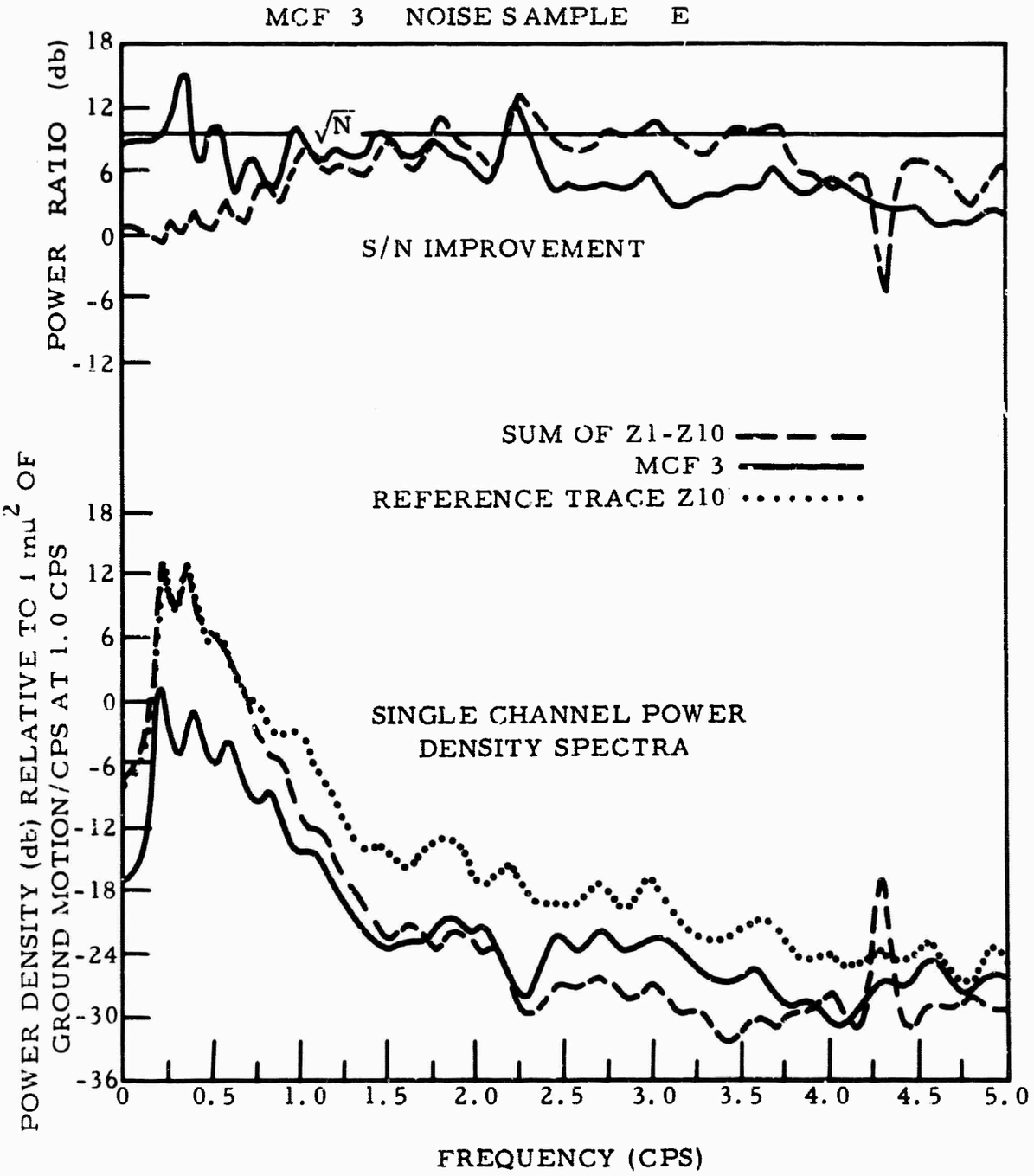

Figure V-34. S/N Improvement and Single-Channel Power Density Spectra for MCF-3 Noise Sample E

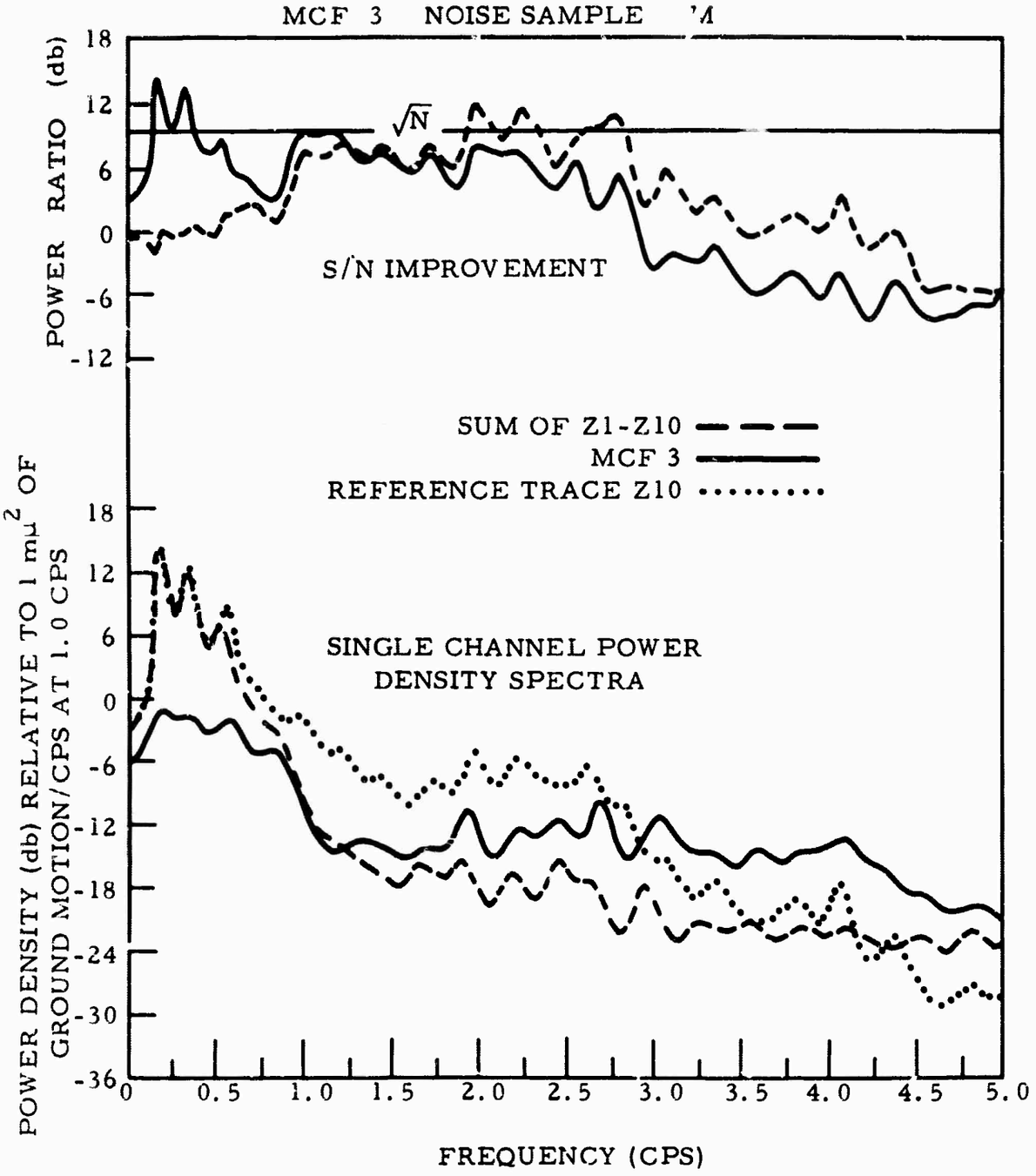

Figure V-35. S/N Improvement and Single-Channel Power Density Spectra for MCF-3 Noise Sample M

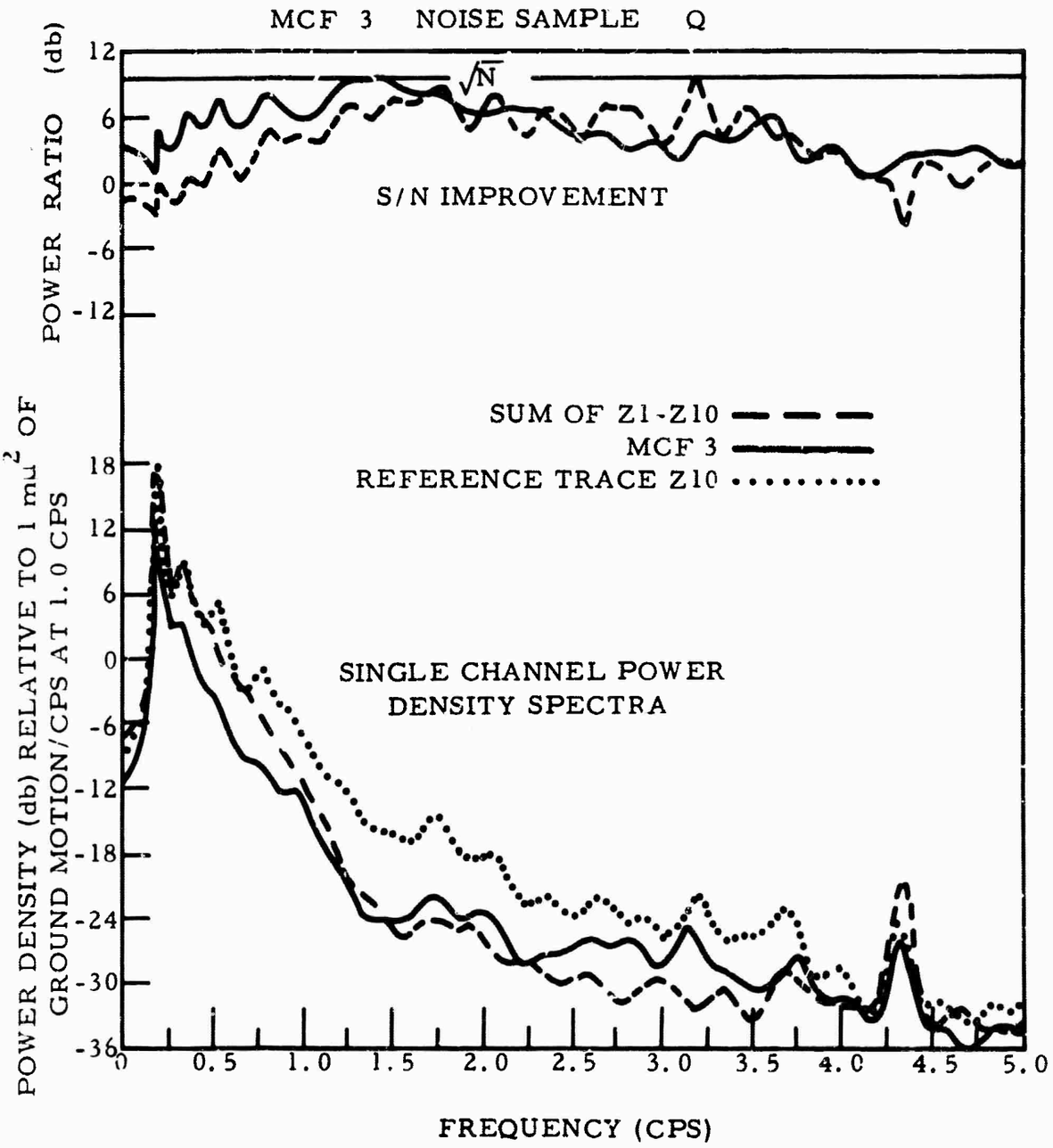

Figure V-36. S/N Improvement and Single-Channel Power Density Spectra for MCF-3 Noise Sample Q

In these figures, the MCF-3 output indicates a high degree of signal preservation when compared with the straight summation (or MCF-1 and MCF-2) outputs, consistent with the explanation in paragraph 5b.

From a comparison of the time-trace displays in Figures V-11 and -12, these two signals have less noise rejection above 2.0 cps. This fact is substantiated by Figures V-13 and -14 which are the single-channel power density spectra of the various output channels for signals AA and CC.

SECTION VI

DEVELOPMENT AND EVALUATION OF THE MULTICHANNEL FILTERS FOR THE 19-CHANNEL PROCESSOR

A. INTRODUCTION

This section contains the results of the synthesis and evaluation of the multichannel filters designed for the 19-channel MAP to operate on the 16-channel subsurface array which consists of the 200-ft, 10-element buried planar array and the 6-element deep-hole vertical array (Figure I-1).

A total of 7 multichannel filters were developed and installed in the 19-channel processor. Of these 7 filters, only UBO MCF-8 was developed using a noise model of measured correlation statistics. The remaining 6 filters were developed using theoretical noise and signal models. Due to the unavailability of measured signal and noise data for the 6-element vertical array, the multichannel filters designed for application to this system could not be evaluated properly. The deghosting filters were evaluated through laboratory tests using synthetic signal and noise data.

B. DEVELOPMENT OF THE MULTICHANNEL FILTERS FOR THE 19-CHANNEL PROCESSOR

1. UBO MCF-8

UBO MCF-8 was designed to filter the 10-element buried planar array data. The noise matrix used in synthesis of this filter was an average correlation matrix constructed from 3 measured ambient noise samples covering a 2-day period. Appendix A contains the details of the formulation of this noise model.

The signal model was defined to be a single point at $\vec{k} = 0$, corresponding to infinite apparent horizontal velocity energy. The signal and noise spectra were shaped identically in order that the multichannel filter would exhibit a flat, approximately zero phase response.

A signal-to-noise ratio of 4 was used in synthesis of the filter. Since it was indicated in the UBO ambient noise analysis that the surface and subsurface correlation matrices appeared approximately identical, this filter can be expected to show approximately comparable results to MCF-1, which also is an infinite velocity filter.

2. UBO IP-1

UBO Isotropic Processor-1 was designed to operate on the 10-channel, 3-dimensional array consisting of the 6-element vertical array and the buried planar array, summed on 4 rings (the center element is considered to be one ring).

The signal and noise models used in the synthesis of this multichannel filter were developed theoretically using isotropic models. Briefly, the signal model was designed to pass signals propagating with infinite apparent horizontal velocity. The noise model was constructed from theoretically developed dispersion data representing the fundamental and the first 2 higher-order modes of energy. Appendix B discusses in detail the formation of the signal and noise models.

The signal and noise spectra used in synthesis of this filter were white and consisted of energy only to 2.0 cps. A signal-to-noise ratio of 4 was specified.

3. UBO IP-2

The UBO Isotropic Processor-2 was designed to operate on the 6-element deep-hole vertical array and to use the same noise model as IP-1, with the exception of the deletion of the planar array. The signal model was defined for energy propagating with infinite apparent horizontal velocity. Appendix B discusses in detail the development of these signal and noise models.

The signal and noise spectra used in the synthesis of this filter were white and consisted of energy only to 2.0 cps. A signal-to-noise ratio of 4 was specified.

4. UBO DG-1, -2, -3, and -4

These 3-channel filters are deghosting filters designed to operate, 3 elements at a time, on the 6-element vertical array. For example, the 3900-, 5900-and 7900-ft elements or the 4900-, 6900-and 3900-ft elements are used as input.

Deghosting filters are designed to extract either up-traveling or down-traveling signal energy while rejecting either the down-traveling or up-traveling "ghost" signal.

The signal model used in the development of each of these filters was the appropriate up-traveling or down-traveling signal; the noise

model was the appropriate down-traveling or up-traveling signal; for both models, signal energy propagated with infinite apparent horizontal velocity. The development of the signal and noise models is described in detail in Appendix B.

The signal and noise spectra were white and consisted of energy only to 5.0 cps. A signal-to-noise ratio of 4 was specified.

Details of these 4 multichannel deghosting filters are as follows:

- UBO DG-1 filter was designed to extract up-traveling infinite apparent horizontal velocity signals using the 4900-, 6900- and 8900-ft instruments
- UBO DG-2 filter was designed to extract down-traveling infinite apparent horizontal velocity signals using the 4900-, 6900-and 8900-ft instruments
- UBO DG-3 filter was designed to extract up-traveling infinite apparent horizontal velocity signals using the 3900-, 5900-and 7900-ft instruments
- UBO DG-4 filter was designed to extract down-traveling infinite apparent horizontal velocity signals using the 3900-, 5900-and 7900-ft instruments

C. TIME-DOMAIN OPERATORS AND SIGNAL RESPONSE

The time-domain operators for MCF-8, IP-1 and -2, and DG-1 through -4, are shown in Figures VI-1 through -5.

D. THEORETICAL AND ACTUAL FREQUENCY RESPONSES COMPARED

Theoretical frequency responses are compared with actual measured frequency responses for MCF-8, IP-1 and -2, and DG-1 through -4 in Figures VI-6 through -10. The method used to obtain the measured responses is outlined in Appendix C.

Figure VI-6 indicates phase and amplitude discrepancies

Text cont'd page VI-15

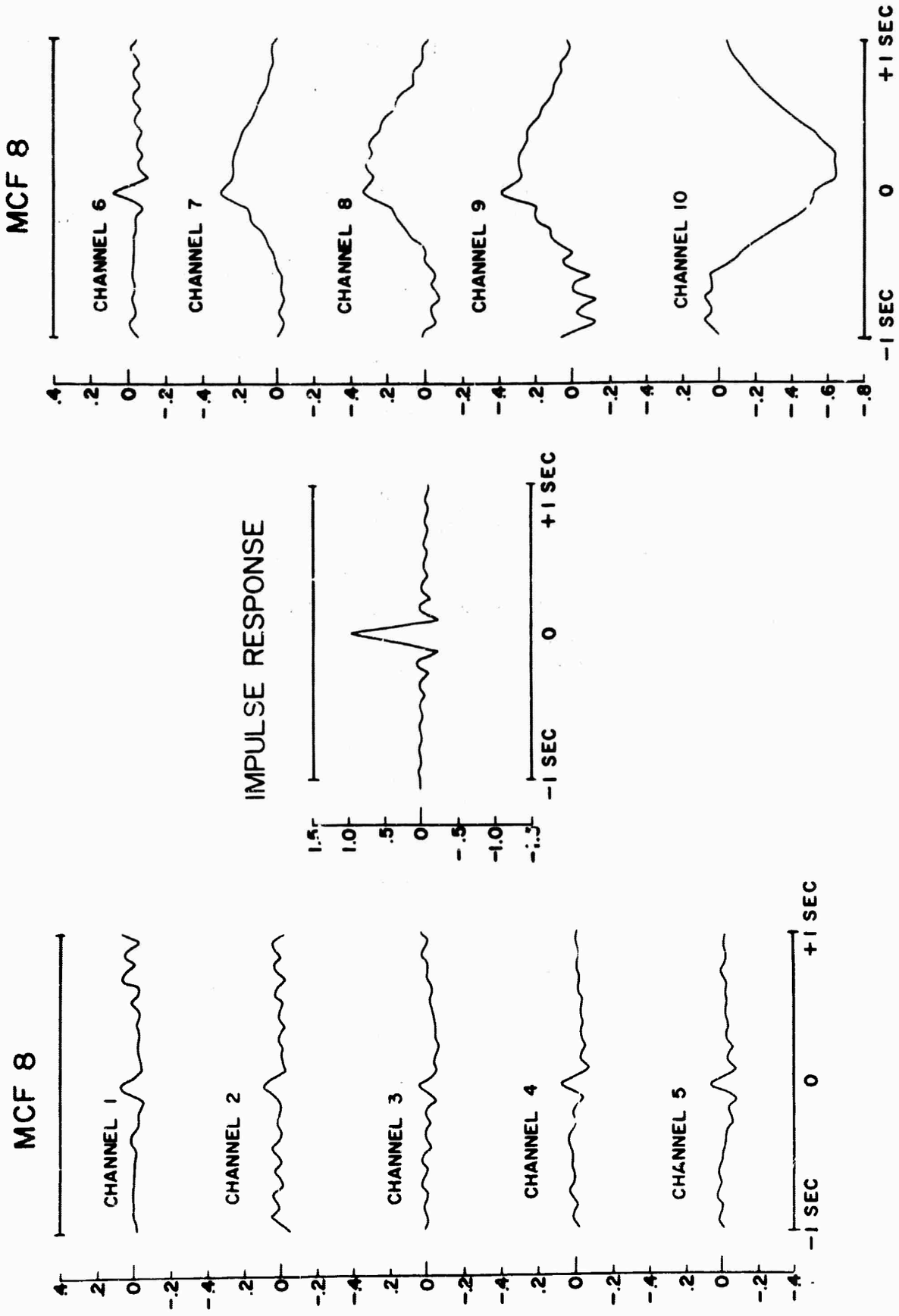

Figure VI-1. Time-Domain Operators and Signal Responses for 19-Channel UBO Processor (UBO MCF-8)

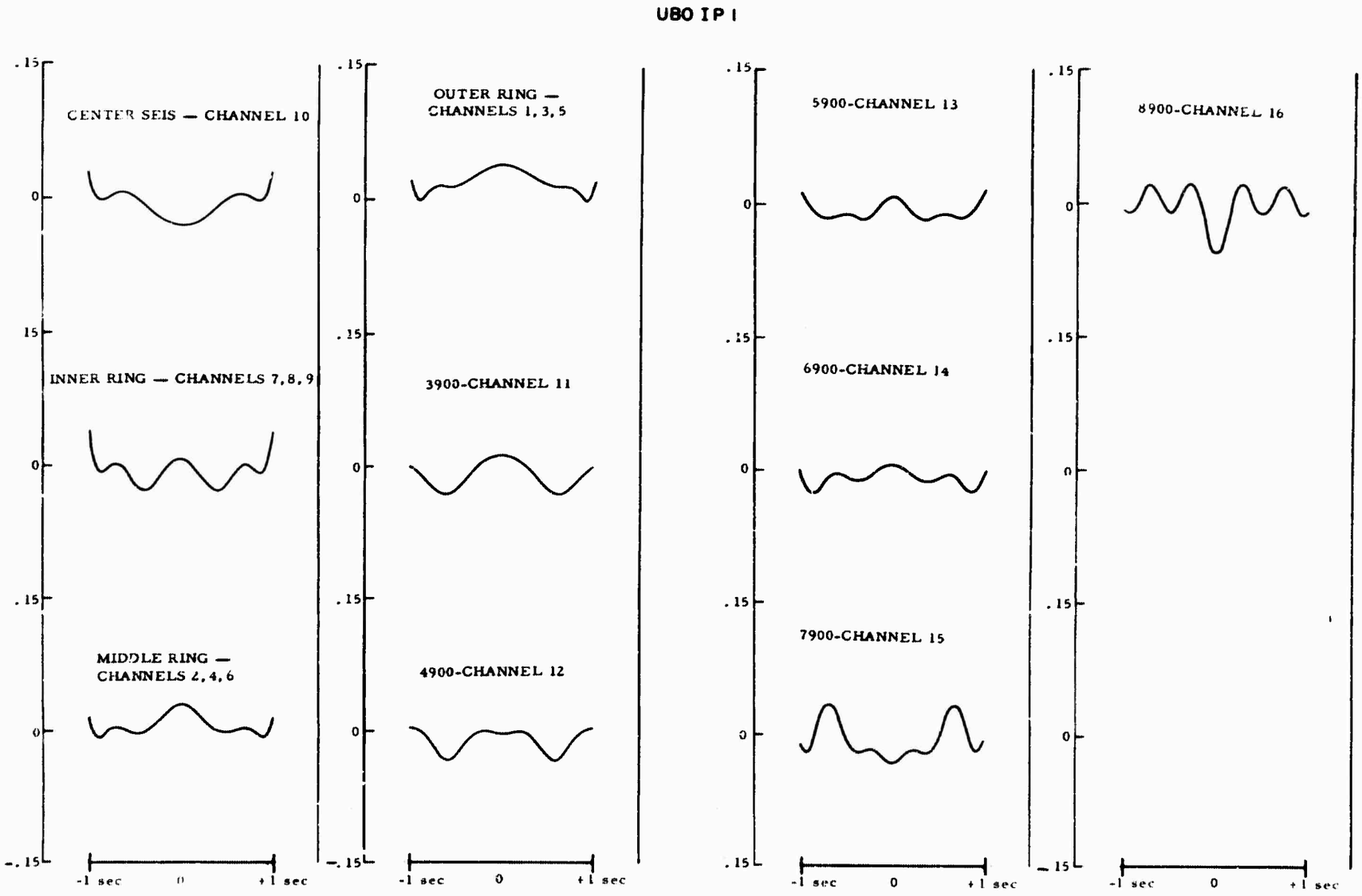

Figure VI-2. Time-Domain Operators for 19-Channel UBO Processor (UBO IP-1)

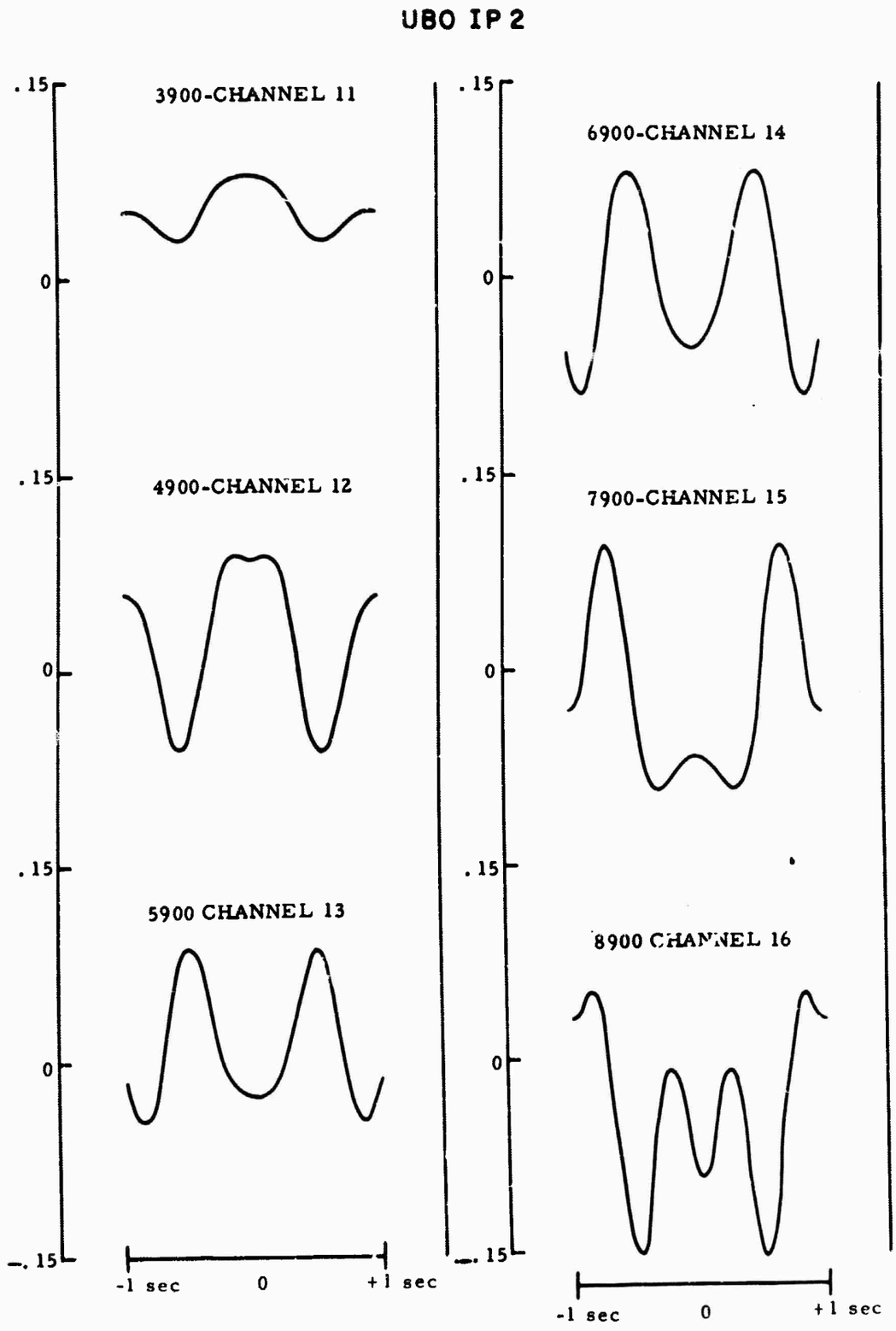

Figure VI-3. Time-Domain Operators for 19-Channel UBC Processor (UBO IP-2)

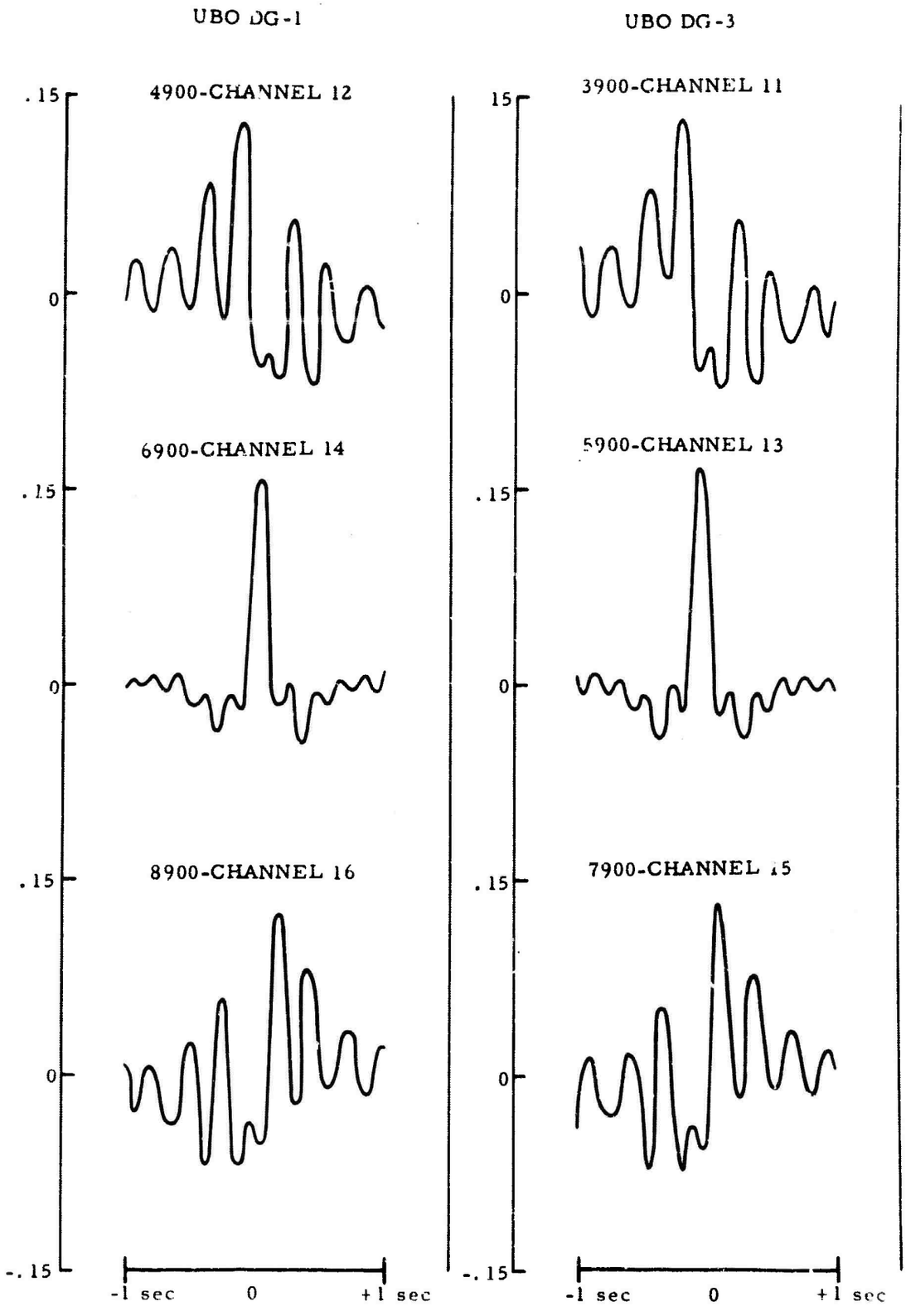

Figure VI-4. Time-Domain Operators for 19-Channel Processor (UBO DG-1, -3)

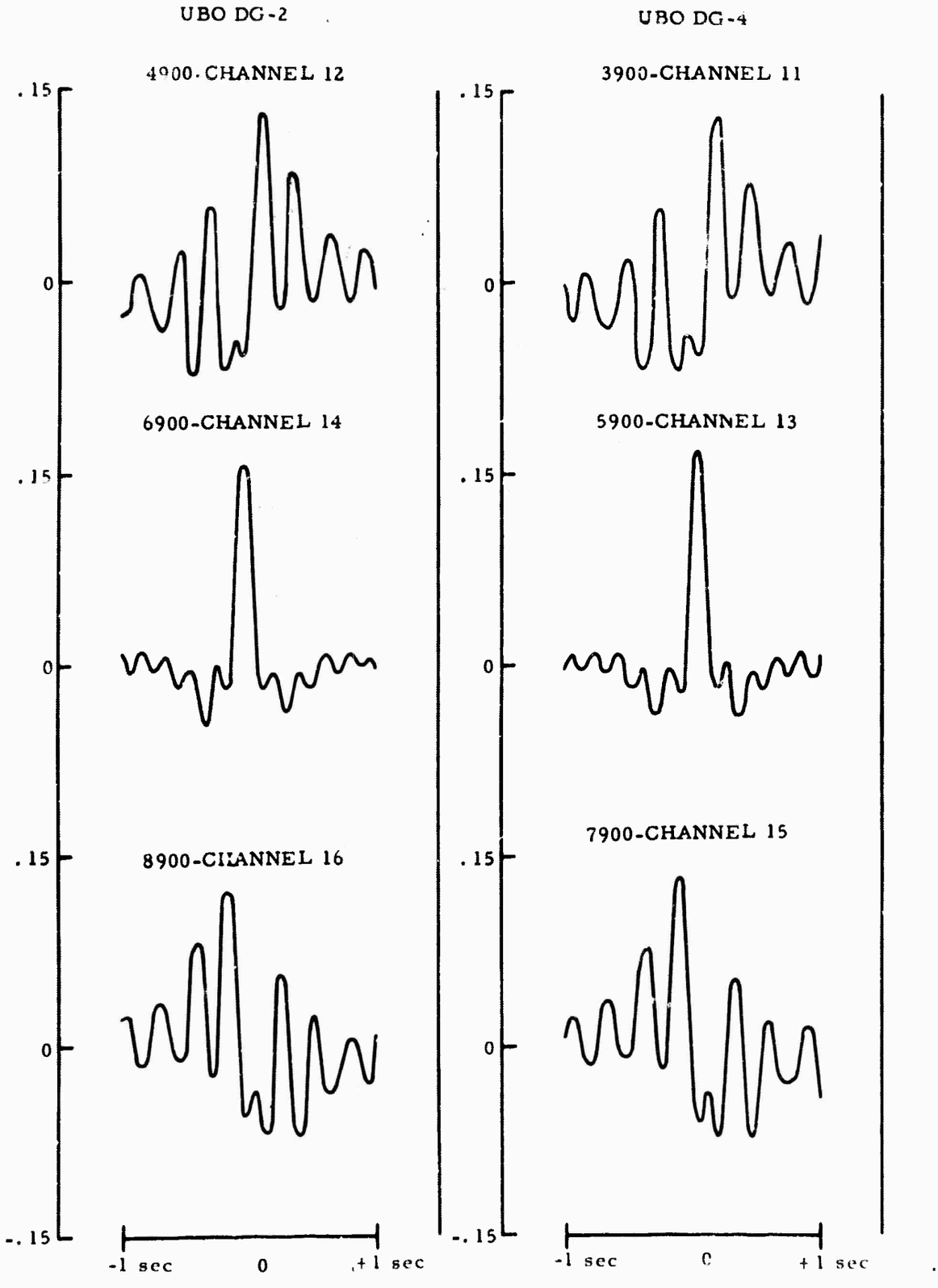

Figure VI-5. Time-Domain Operators for 19-Channel Processor (UBO DG-2, -4)

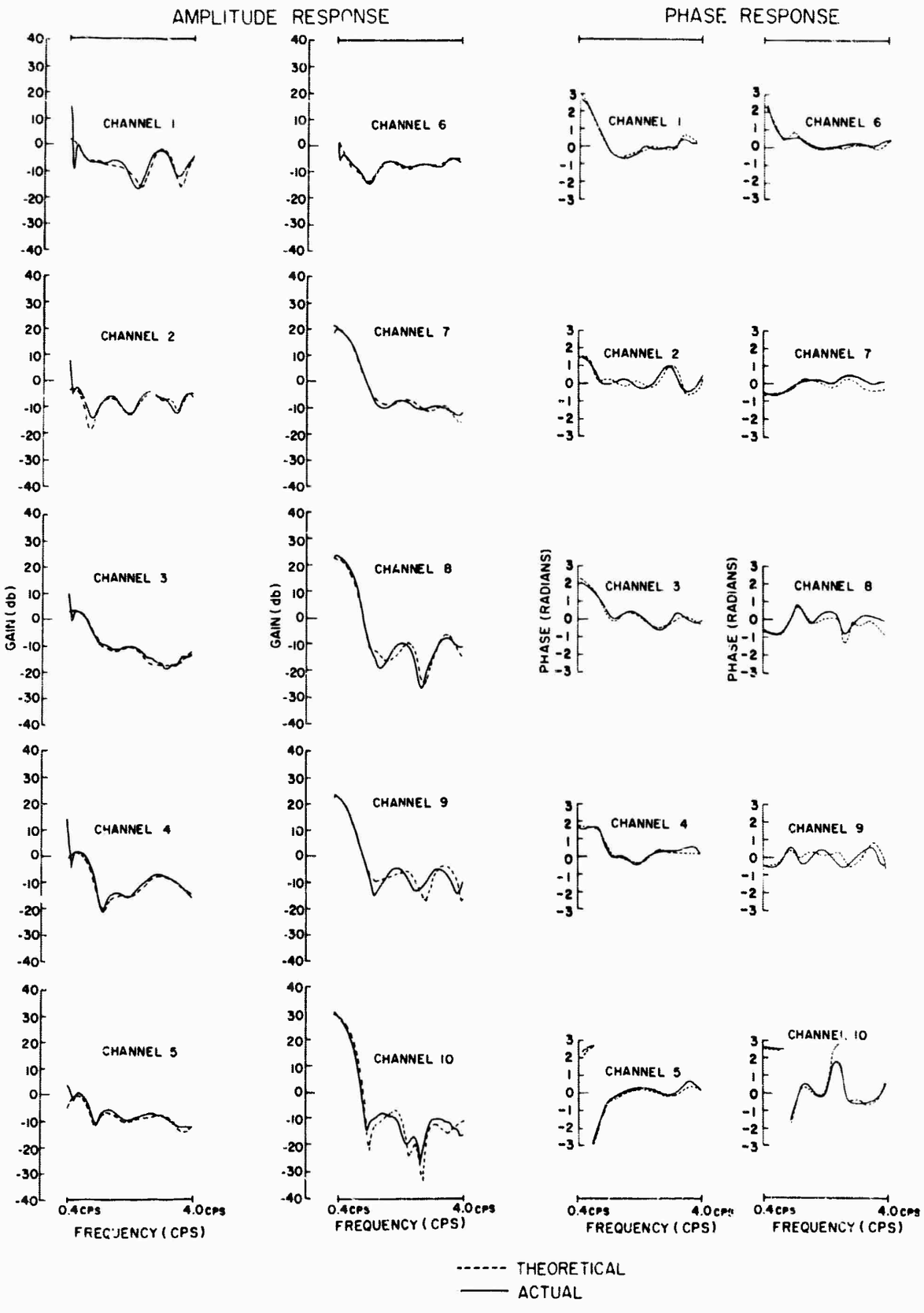

Figure VI-6. Theoretical Transfer Functions Compared With Actual Filter Responses in the Frequency Domain (UBO MCF-8)

AMPLITUDE RESPONSE

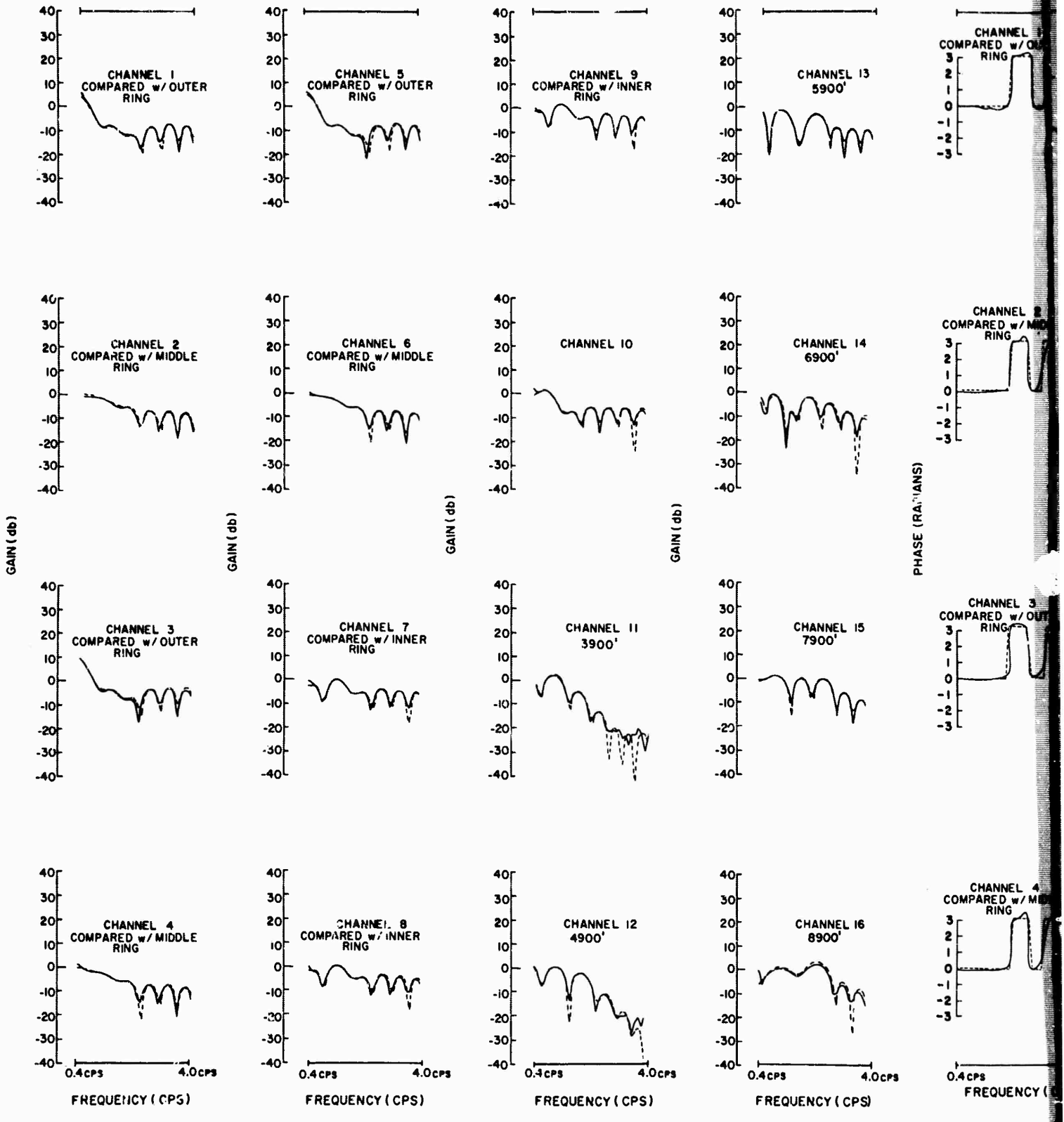

A

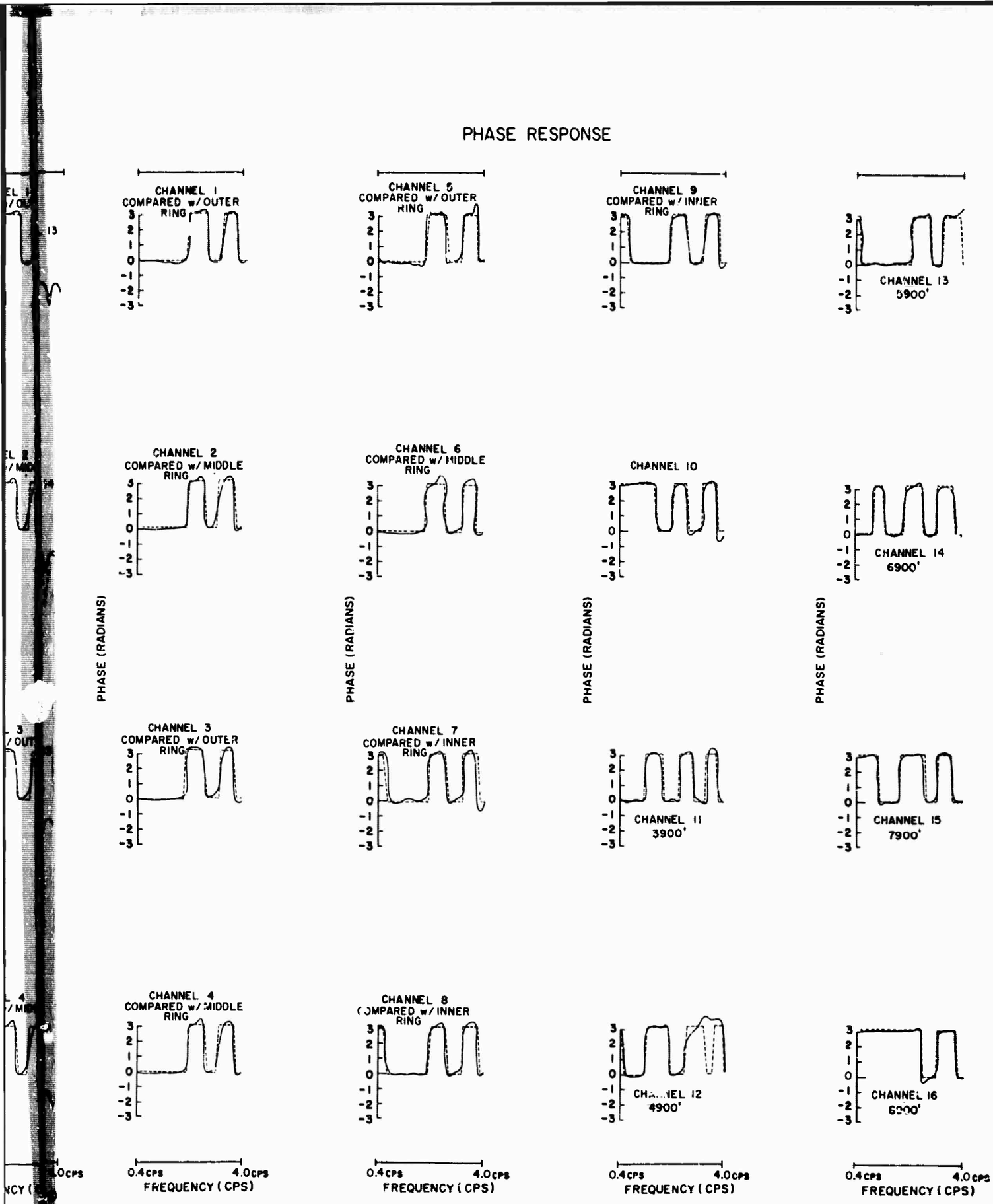

Figure VI-7. Theoretical Transfer Functions Compared With Actual Filter Responses in the Frequency Domain (UBO IP-1)

BLANK PAGE

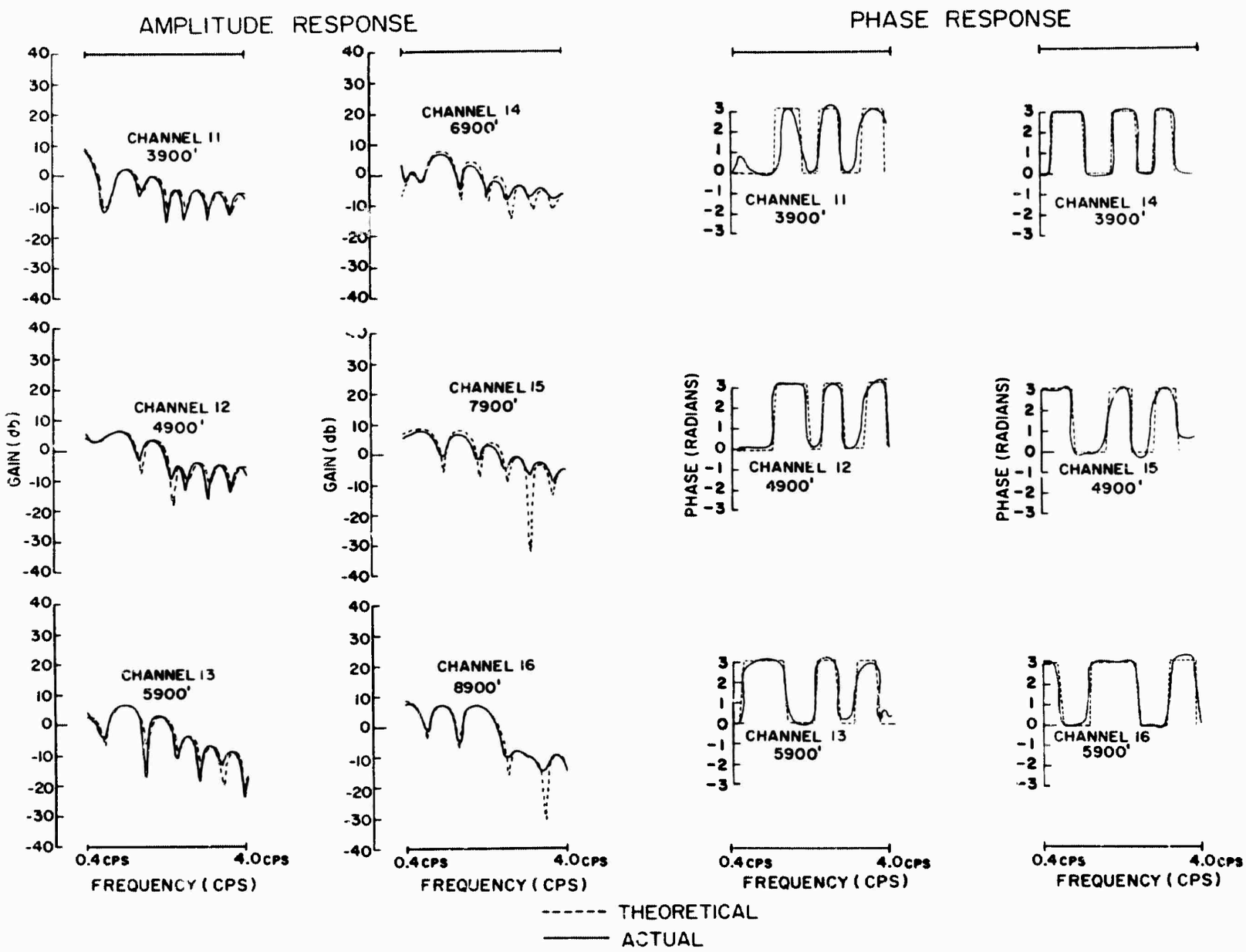

Figure VI-8. Theoretical Transfer Functions Compared With Actual Filter Responses in the Frequency Domain (UBO IP-2)

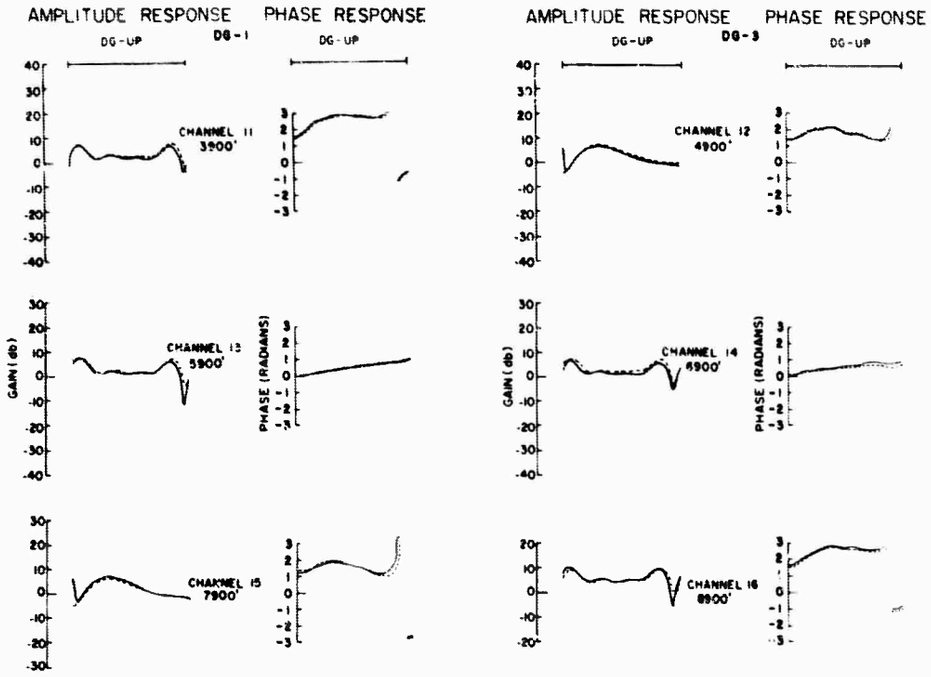

Figure VI-9. Theoretical Transfer Functions Compared With Actual Filter Responses in the Frequency Domain- (UBO DG-1, -3)

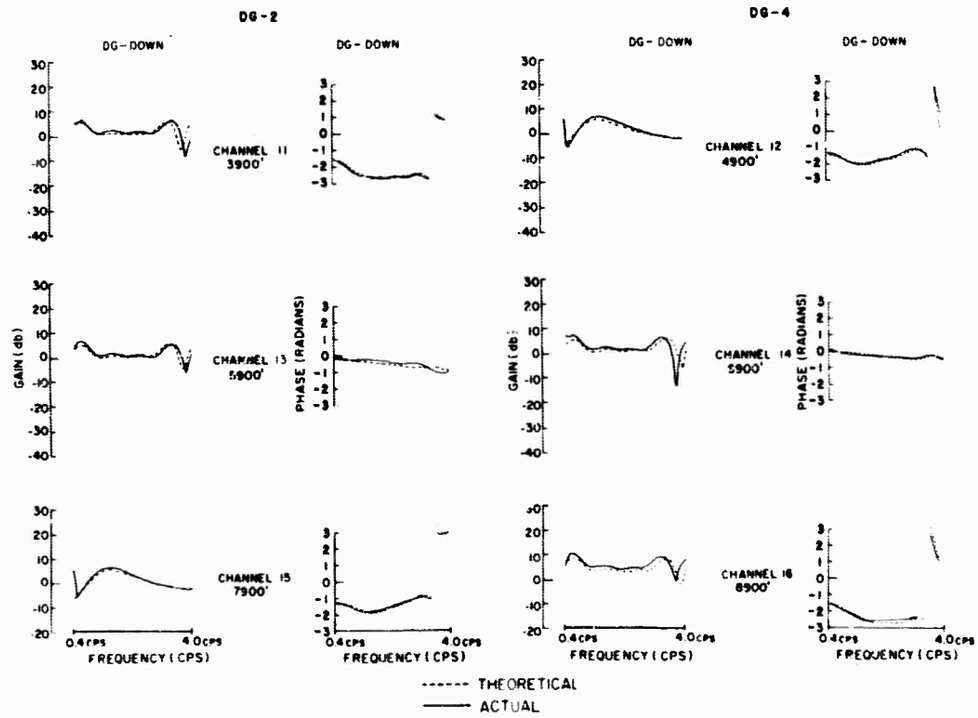

Figure VI-10. Theoretical Transfer Functions Compared With Actual Filter Responses in the Frequency Domain (UBO DG-2, -4)

between the theoretical and actual filter responses for MCF-8. These discrepancies occur primarily when the amplitude response curves have a dynamic range greater than 40 db. Since the actual filters were approximated (Appendix C) using 1-percent standard resistors, a 40-db gain fluctuation over a wide-frequency band permits the system noise resulting from this approximation to distort the response curves. Thus, the MCF-8 is limited because its amplitude range exceeds 40 db which may distort data over a wide band of frequencies.

A comparison of the MAP output at each frequency was made with the amplitudes of certain channels during a sine-wave calibration check. Good results generally were obtained. These ratios were supplied in Supplement 1 to the 10-Channel Multiple Array Processor and Supplement 1 to the 19-Channel Multiple Array Processor.

The point to be derived from the MCF-8 results is that the resistor approximation of the actual MCF has limited the performance capability of the filter over a wide-frequency band through phase and amplitude response distortion.

This filter (MCF-8) presently is being redesigned so that it will be compatible with the resistor approximation technique required of the analog MAP. The resulting filter probably will not be as effective as MCF-8, since the method which will be used to limit the filter amplitude range is the same as that discussed in Appendix D for MCF-6 and -7. Briefly, the method involves adding random noise in wavenumber space to the signal model, which constrains large sidelobes or effectively prevents the filter superdirectively configuration at low frequencies.

E. EVALUATION OF THE FILTERS DESIGNED FOR THE 19-CHANNEL PROCESSOR

1. Introduction

Since measured signal and noise data for the 6-element vertical array were not available during this analysis, complete evaluation of the filters designed for the deep-hole array could not be made.

This section contains the results of a complete evaluation of MCF-8. IP-1 was redesigned for application to the planar array only (4-channel) and was designated IP-1 A for which evaluation using measured noise and signal is presented.

An evaluation of deghosting filters (DG-1 through -4) is presented using theoretical signals.

2. UBO MCF-8

a. Wavenumber Response

The wavenumber response of UBO MCF-8 at frequencies of 0.25, 0.75, 1.0 and 1.5 cps is shown in Figures VI-11 through -14, respectively.

In each of these figures the filter is seen to pass the specified signal region (infinite apparent horizontal velocity) with 0 db attenuation and to reject low-velocity noise regions. At 0.25 cps the filter rejects energy traveling with an apparent horizontal velocity of approximately 0.5 to 1 km/sec propagating from the W-NW and E-SE. The filter at this low frequency is in a superdirectivity configuration (as discussed for MCF-1 and -3 in Section V). The large sidelobes (as large as +21 db) outside the 0.5-km/sec range are due to the superdirectivity configuration of the filter and are permissibie, since organized signal and noise energy will travel at velocities greater than 1 km/sec and the random noise level is only 1.5 percent of the total noise power, approximately.

Comparison of Figure VI-11 with Figure V-15 (wavenumber response of MCF-1) indicates an apparent change in direction of the 0.25-cps, low-velocity organized energy from N-NW to E-NW and S-SE to E-SE. As indicated in the UBO noise analysis, such change in direction for microseismic energy was observed. Additionally, the number of noise samples used in constructing the measured noise model for MCF-8 was 3 as compared with 12 samples for MCF-1 which implies a less complete statistical estimate of the time-varying noise field for MCF-8 resulted.

At 0.75 to 1.5 cps the filter rejects strongly the 3 organized noise lobes indicated in the analysis of the UBO noise field. The overall wavenumber response of the filter is quite similar to that of MCF-1 presented in Section V. This similarity is in agreement with results presented in the analysis of the UBO noise field which indicated that the surface and subsurface noise field correlations were highly similar.

b. Signal-to-Noise Improvement

Figures VI-15, -16 and -17 present 3 noise samples before and after processing with MCF-1. The signal-to-noise improvement explained in Section V, Subsection F-1) for these noise samples and the single-channel power density spectra of the filter output trace, the straight-summation output trace and the reference trace (SZ-10 center element) are shown in Figures VI-18 through -20.

Text cont'd page VI-27

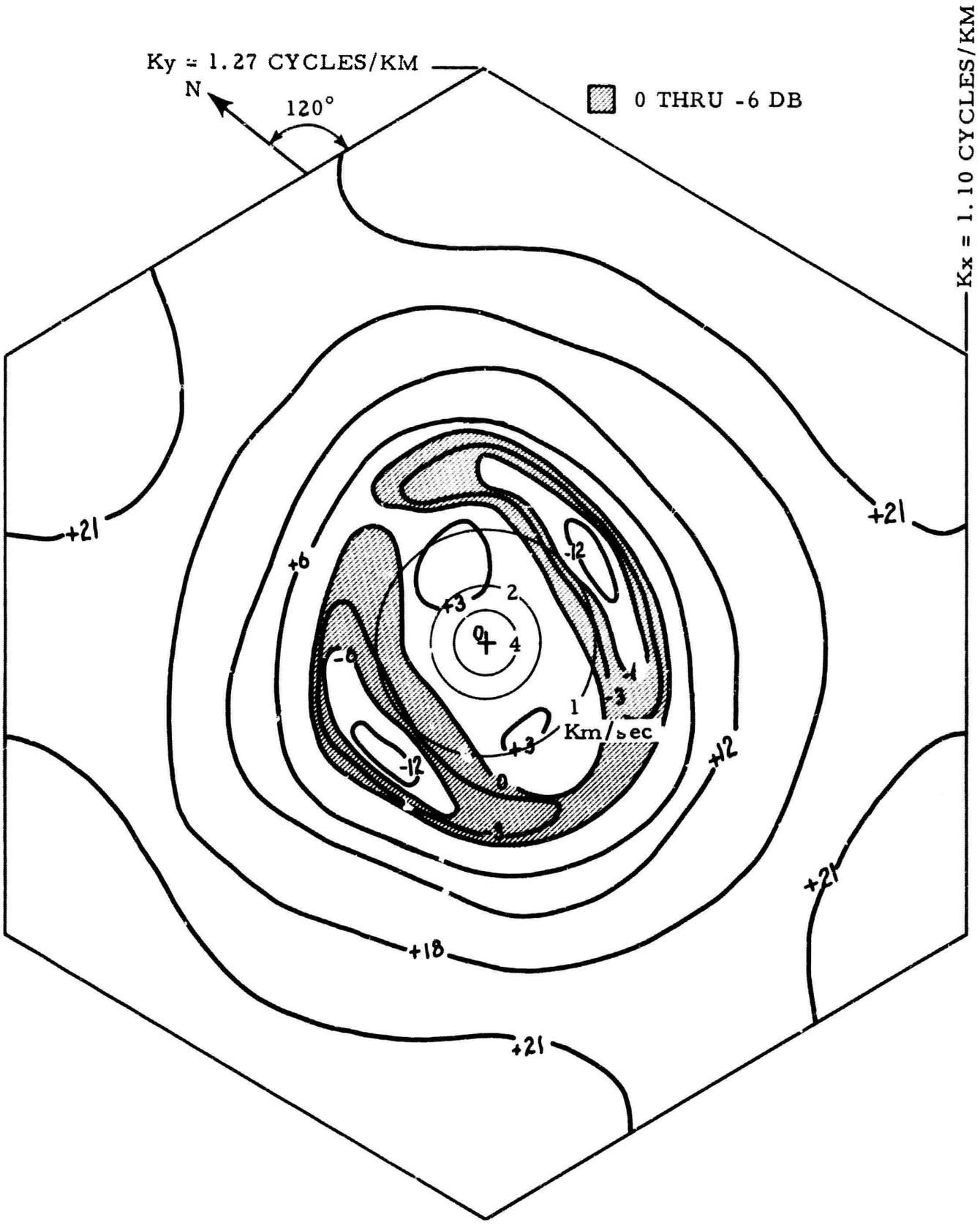

Figure VI-11. Two-Dimensional Wavenumber Response of UBO MCF-8, f = 0.25 CPS

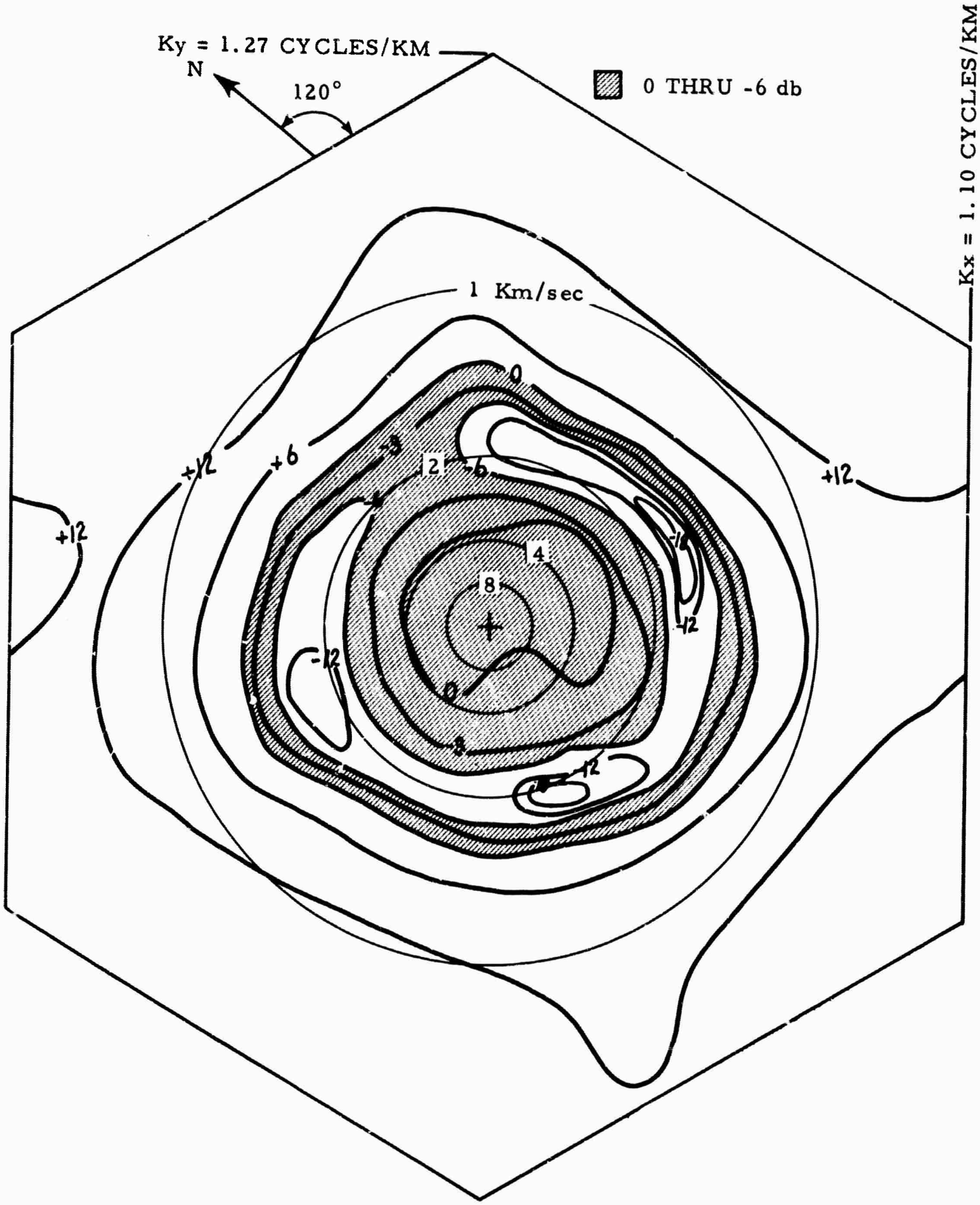

Figure V' 2. Two-Dimensional Wavenumber Response of UBO MCF-8, f = 0.75 CPS

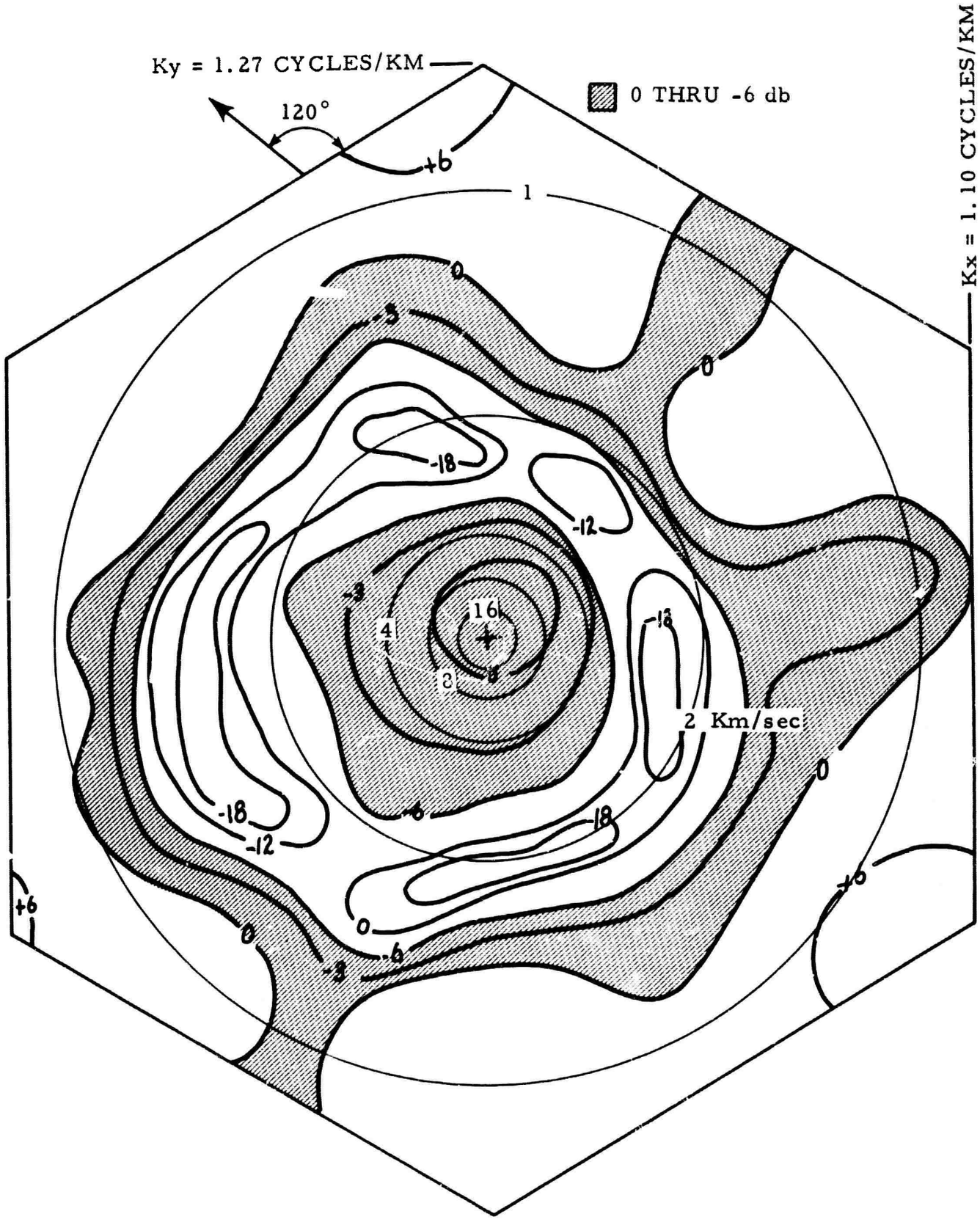

Figure VI-13. Two-Dimensional Wavenumber Response of UBO MCF-8, f = 1.0 CPS

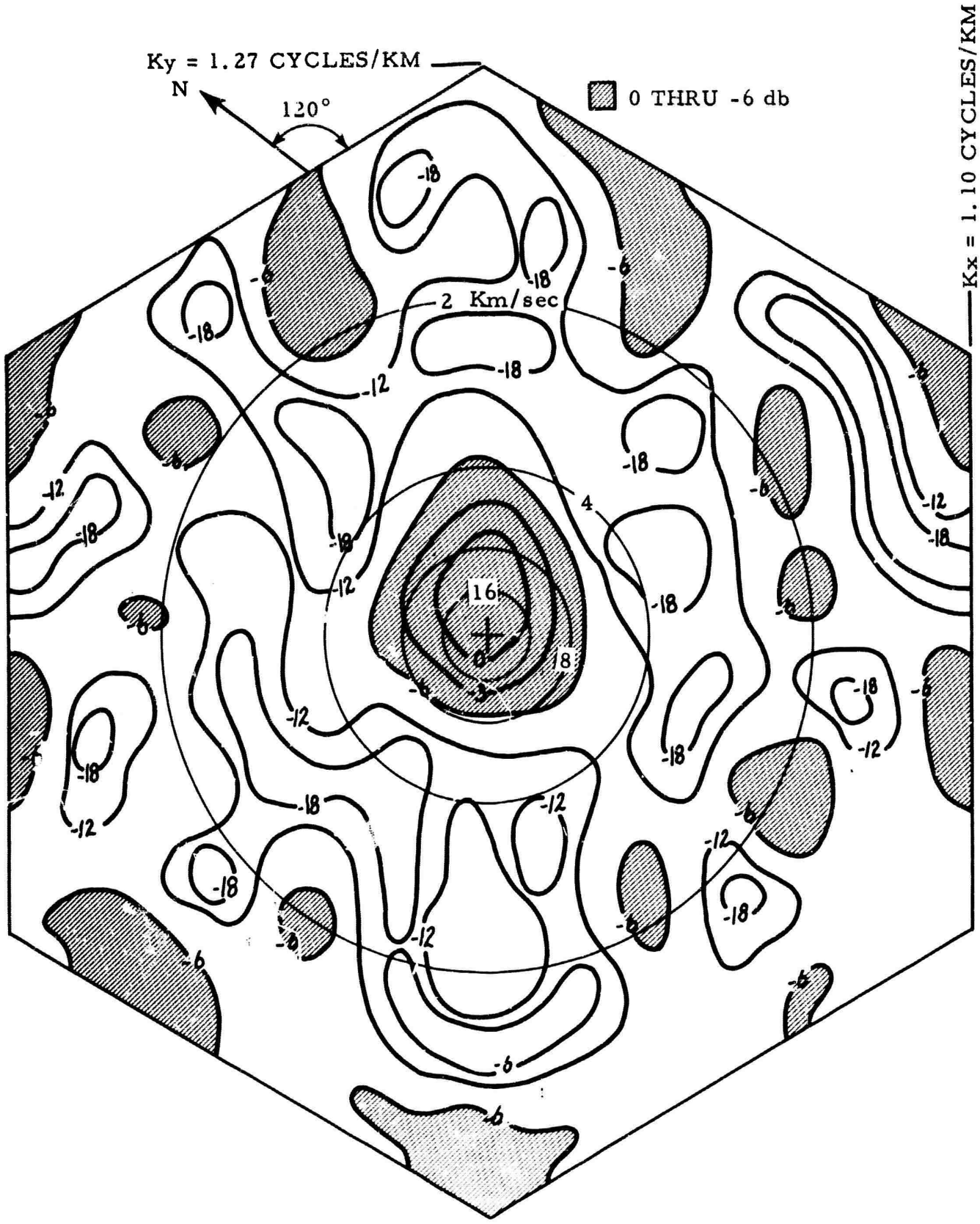

Figure VI-14. Two-Dimensional Wavenumber Response of UBO MCF-8, f = 1.5 CPS

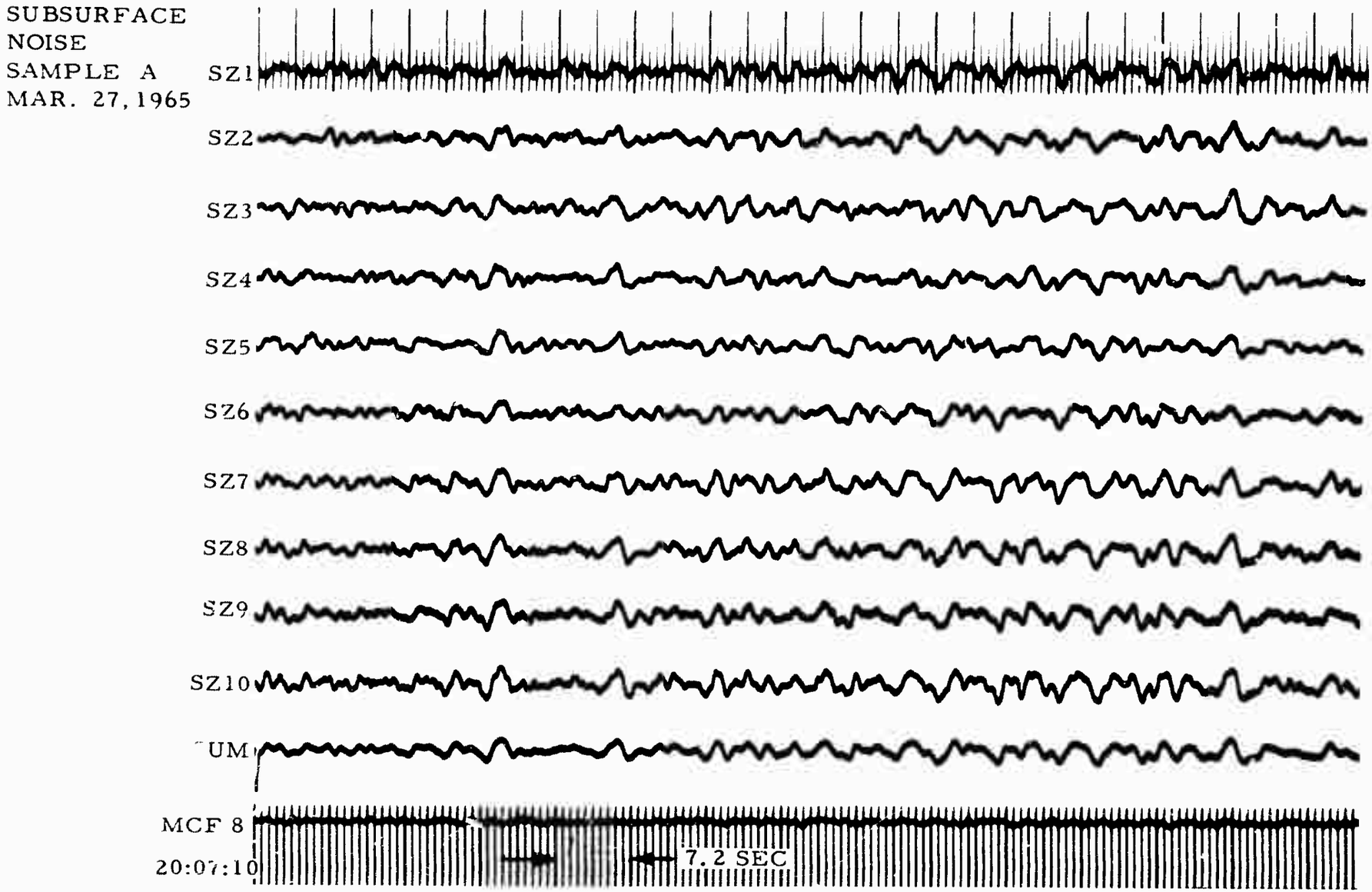

Figure VI-15. A Short Portion of UBO Noise Sample A (Subsurface) Results of MCF-8

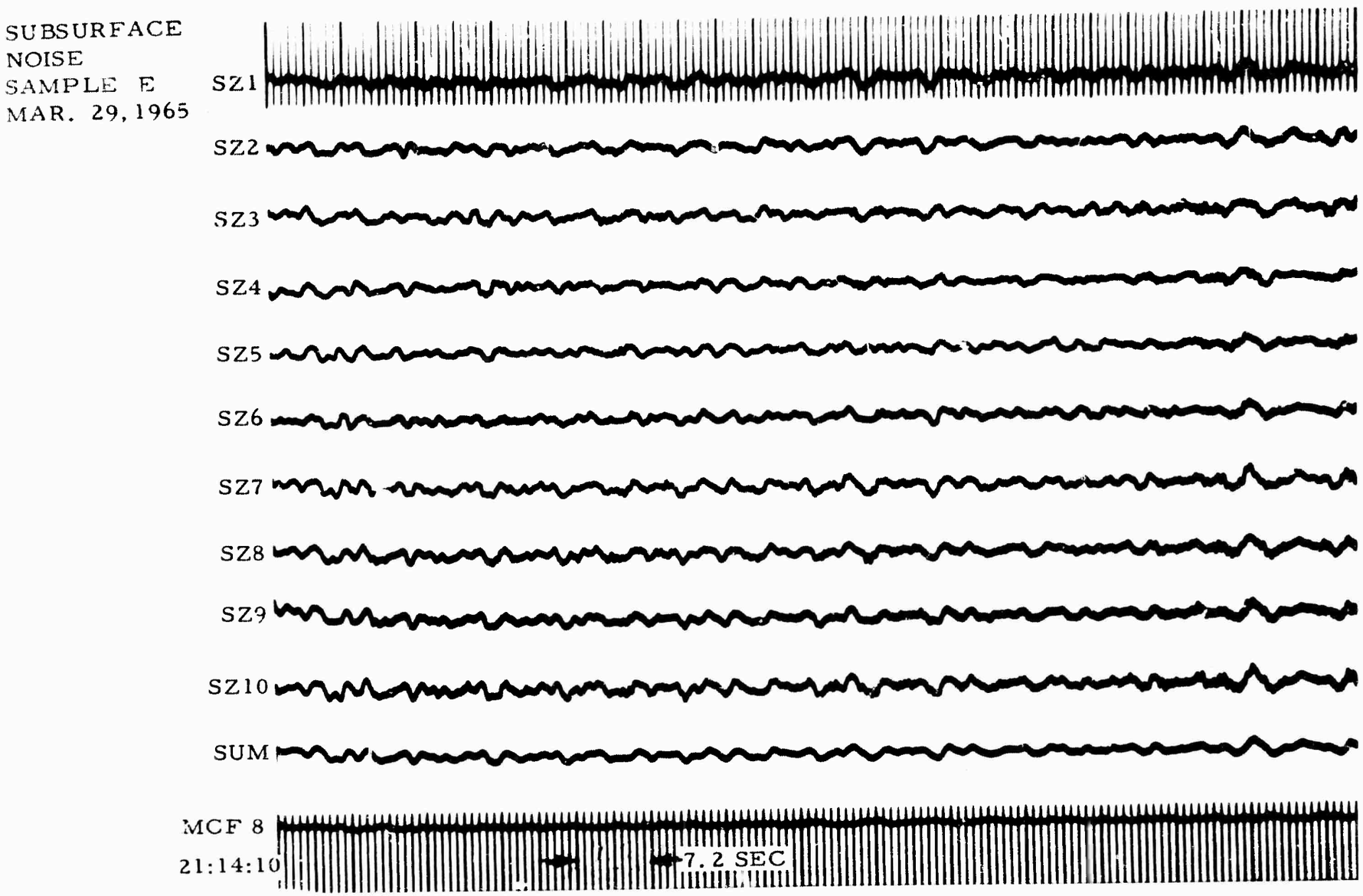

Figure VI-16. A Short Portion of UBO Noise Sample E (Subsurface) Results of MCF-8

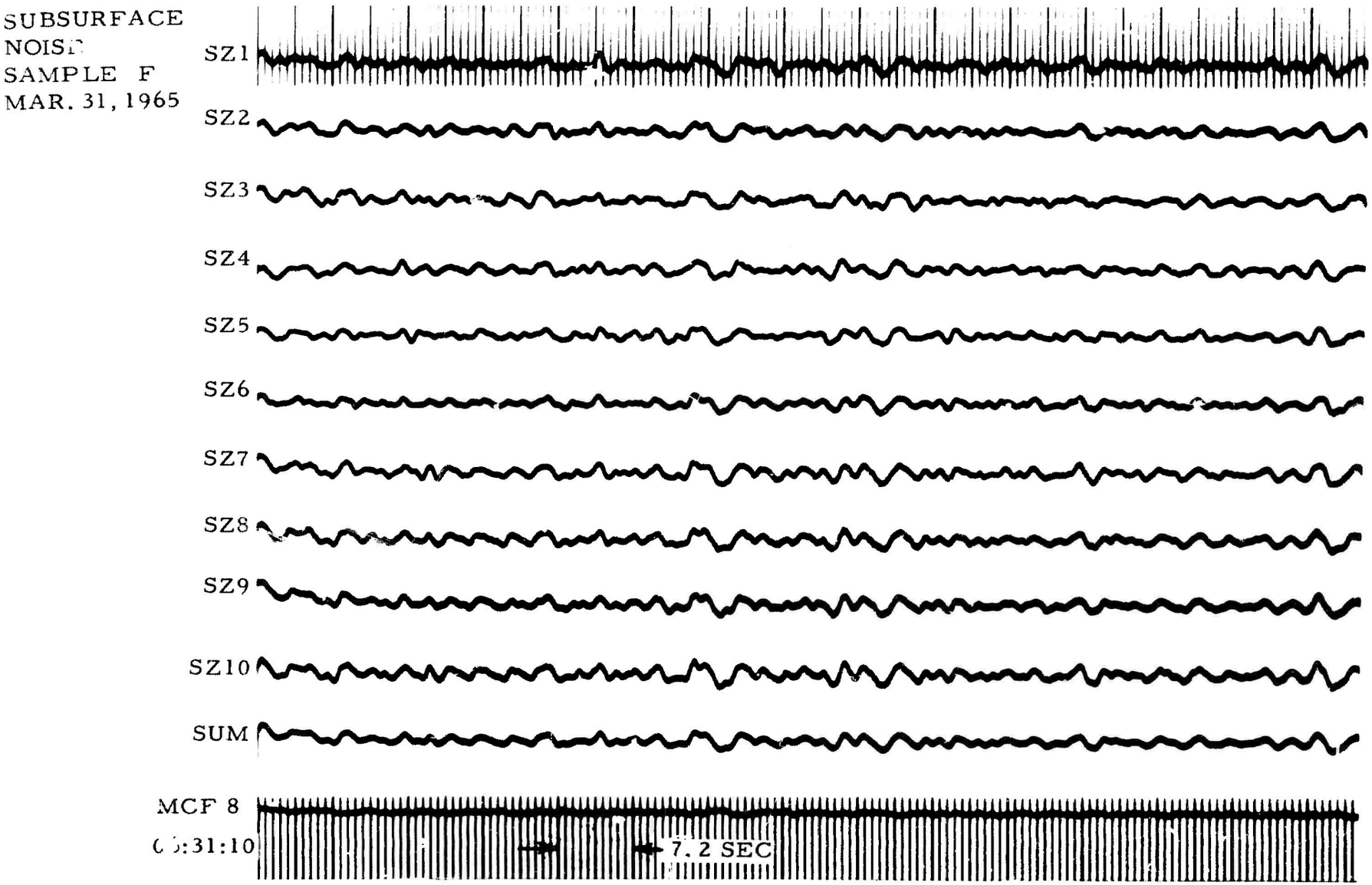

Figure VI-17. A Short Portion of UBO Noise Sample F (Subsurface) Results of MCF-8

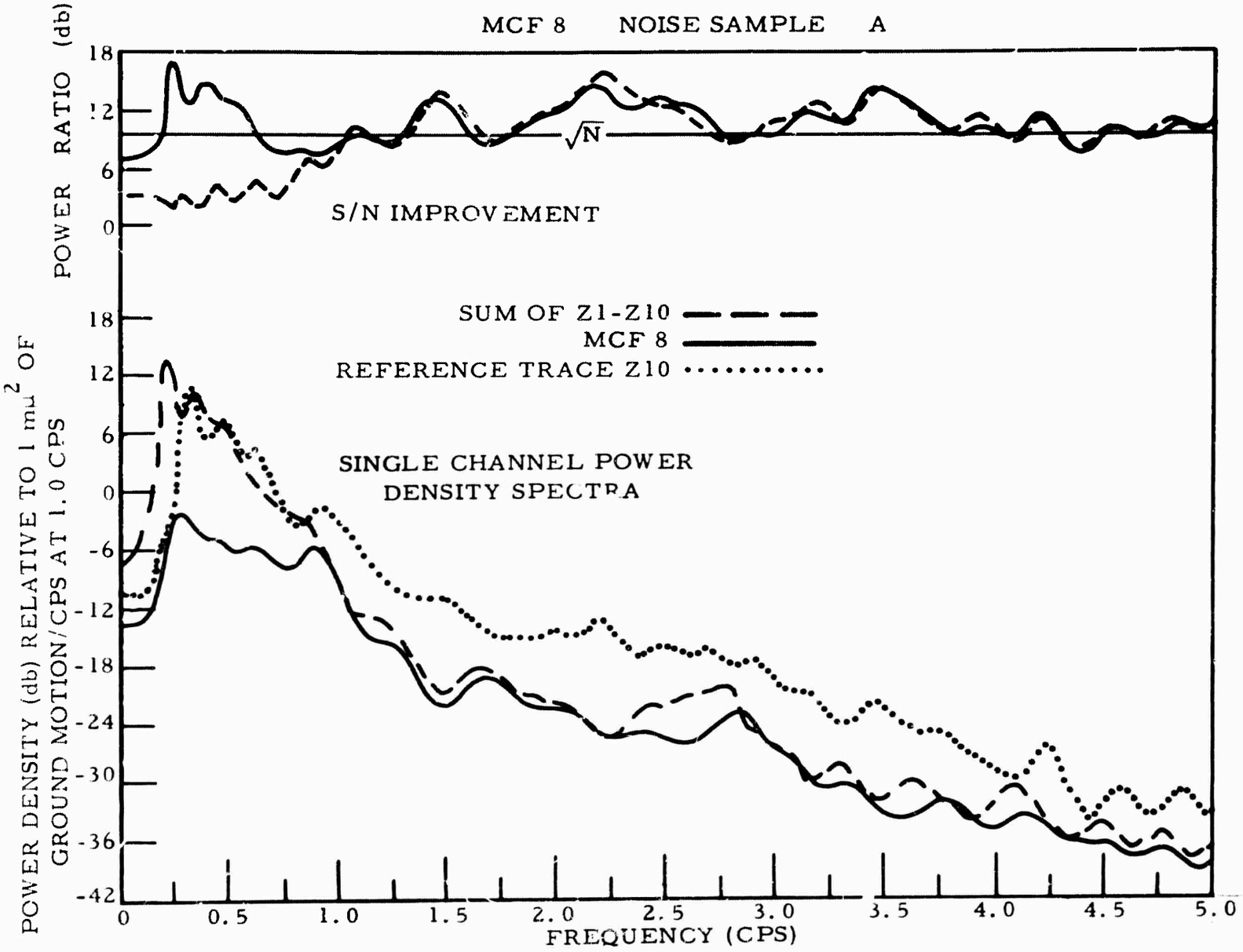

Figure VI-18. S/N Improvement and Single-Channel Power Density Spectra for MCF-8 Noise Sample A

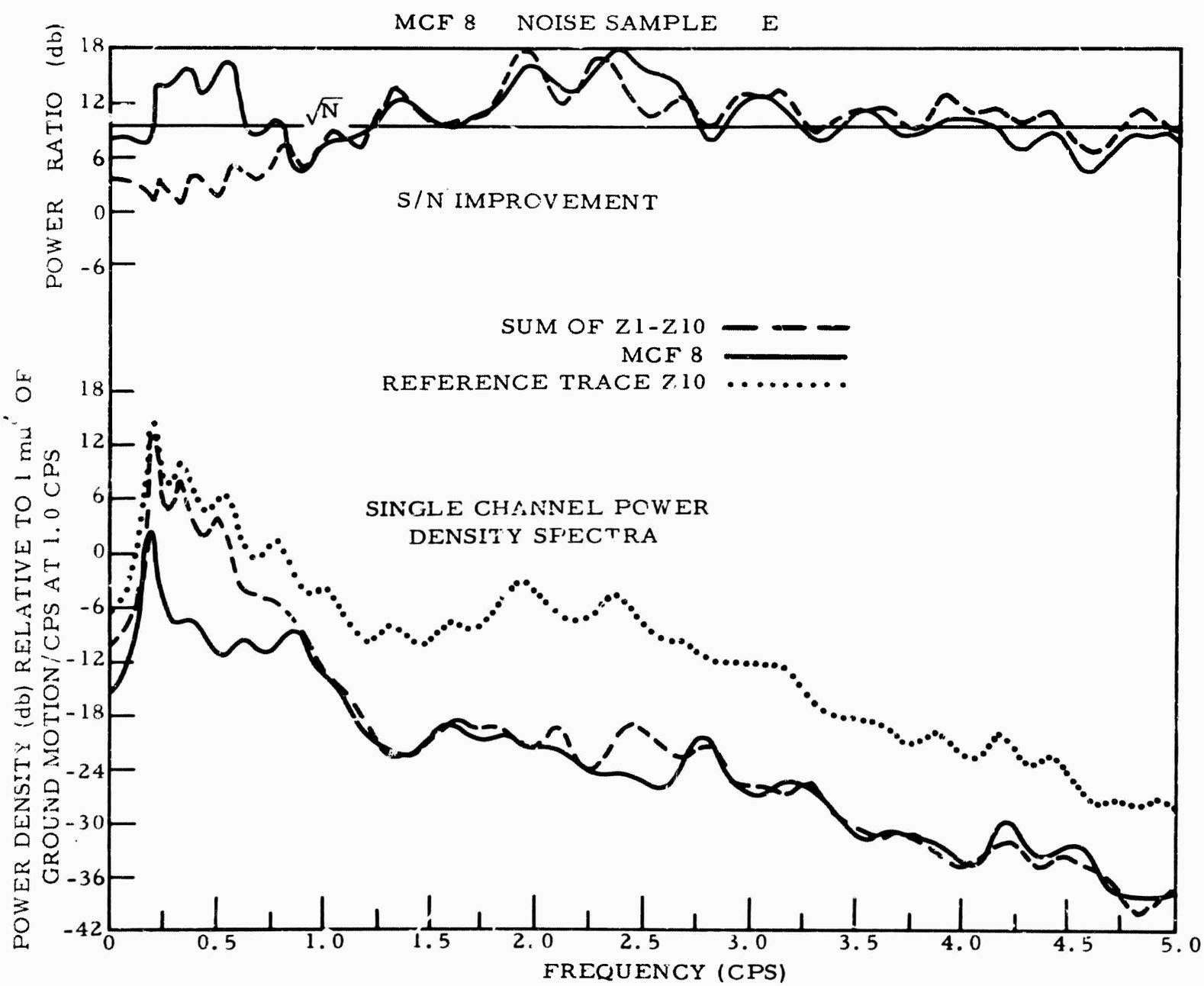

Figure VI-19. S/N Improvement and Single-Channel Power Density Spectra for MCF-8 Noise Sample E

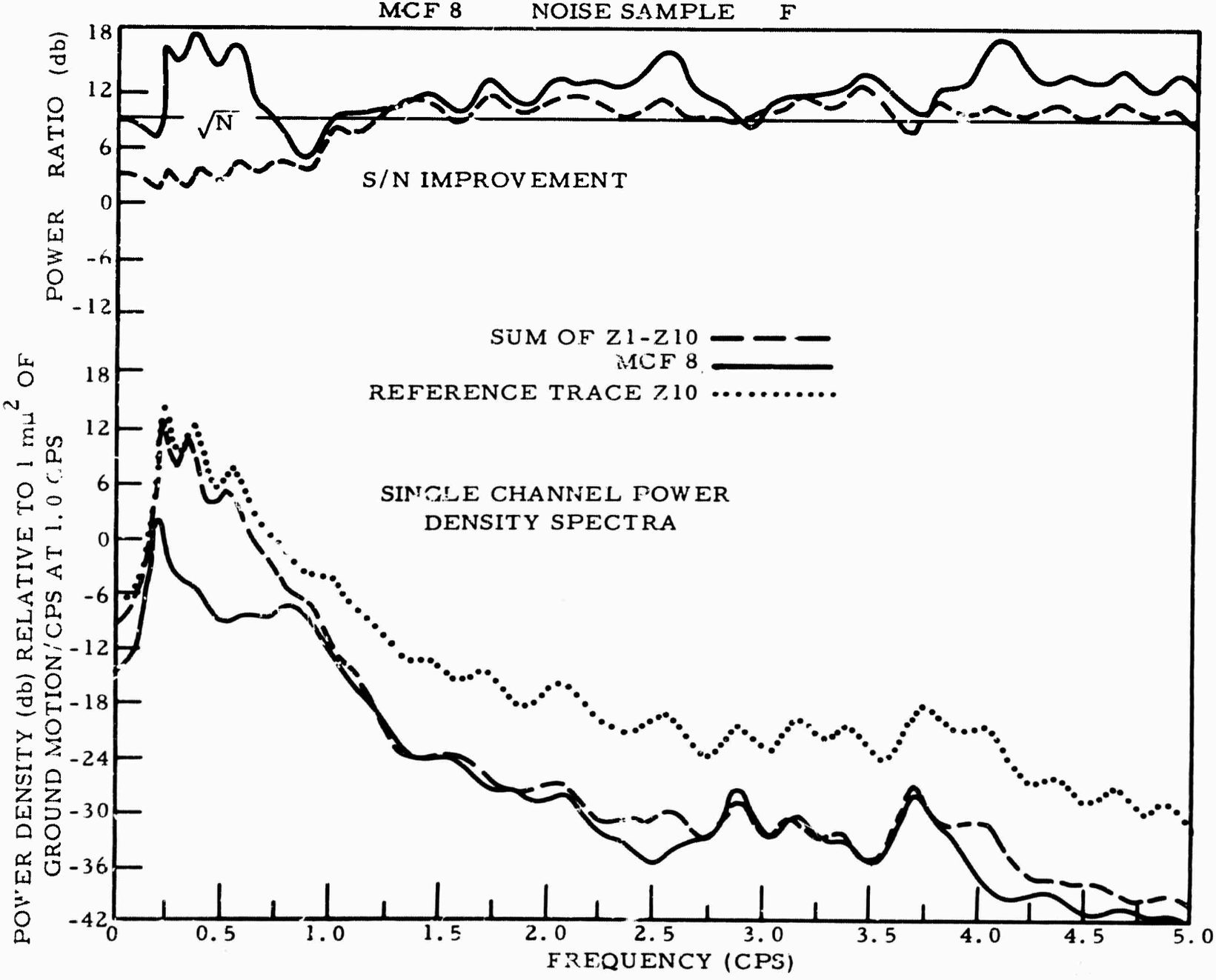

Figure VI-20. S/N Improvement and Single-Channel Power Density Spectra for MCF-8 Noise Sample F

Below 1.5 cps, the average signal-to-noise improvement for MCF-8 indicates 2- to 3-db improvement over MCF-1. In the 0.75 to 1.5-cps band, since signal-to-noise improvement for the straight summation also indicates comparable improvement (2 to 3 db), the conclusion is that a larger percentage of the noise field between 0.75 and 1.5 cps was organized for the time of year the subsurface data was collected. The increased improvement below 0.75 was probably due to MCF-8 being more highly tuned to a short time-span (3 days), whereas, MCF-1 was averaged over a month.

Between frequencies of 1.5 to 3.0 cps, both the straight summation and MCF-8 signal-to-noise improvements generally were greater than $\sqrt{N}$, indicating that both processing methods were rejecting organized energy on the basis of velocity and wavenumber component. Except for noise sample E (Figure VI-19) between 2.50 and 2.75 cps and noise sample F (Figure VI-20) between 2.00 and 2.75 cps, the straight summation and MCF-8 indicate comparable improvement in the 1.5-to 3.0-cps band. The noted differences probably occurred because the energy appeared in wavenumber space at points which the straight summation could not effectively reject.

As was indicated in the UBO noise analysis report, there appeared to be organized surface-mode energy in the 1.75-to 3.0-cps frequency band. Since it was shown in the MCF-1 evaluation that the straight summation was unable to reject this component, it is probable that the improvements noted above 2.0 cps were due to an addition in the organized noise field at these frequencies.

c. Application to Measured Signal

Only 3 very poor-quality signals were available for processing with the subsurface multichannel filters designed on the 10-channel planar array. Figure VI-21 shows signal BB that was processed by MCF-8.

The output from the multichannel filter process indicates that the signal has been attenuated slightly. This attenuation is explainable on the basis of the filter wavenumber response.

3. UBO IP-1A

a. General

UBO IP-1A is a 4-channel filter developed for use on the SZ1-10 array, summed on 4 rings. The signal and noise models were the same as those used in developing IP-1, except for the deletion of the deep-hole array elements.

MCF 8 NOISE SAMPLE F

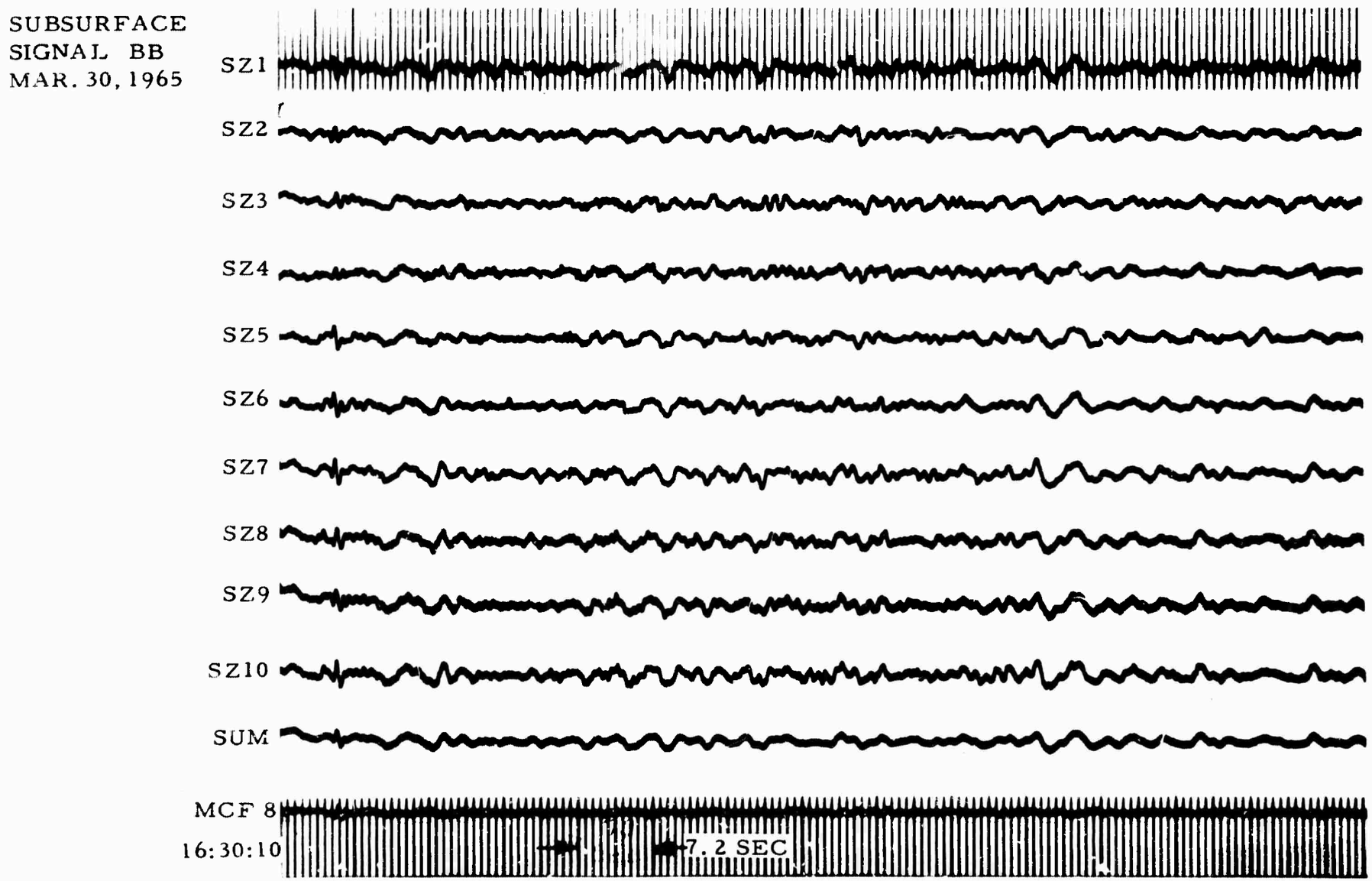

Figure VI-21. A Short Portion of UBO Signal BB (Subsurface) Results of MCF-8

The analysis of this filter will provide a partial measure of the IP-1 performance for measured signal and noise data.

b. Signal-to-Noise Improvement

Presented in Figures VI-22 through -24 are the results of filtering noise samples A, E and F with IP-1A.

The signal-to-noise improvement and single-channel power density spectra for the IP-1A output, for the straight summation output and for the reference trace are shown in Figures VI-25, -26 and -27 for noise samples A, E and F, respectively.

The signal-to-noise improvement of IP-1A in the 0.20 to 0.75-cps region indicates that the filter is rejecting some low-velocity energy (3- to 15-db improvement). However, the improvements shown were not as significant as those indicated for MCF-8, because of the increased noise model area requiring rejection with IP-1A.

Between frequencies of 0.75 to 2.0 cps, the signal-to-noise improvement results for IP-1A were similar to those of MCF-8, indicating that the theoretical model used for the noise was reasonable. Above 2.0 cps, the degeneration in signal-to-noise improvement for IP-1A is reasonable since energy above this frequency was not included, either in the signal or noise models.

c. Application to Measured Signal

Figure VI-28 presents a short portion of UBO signal BB processed by IP-1A. As with MCF-8, the signal is attenuated slightly and probably is explainable by the wavenumber response of the filter.

4. Evaluation of DG-1 through-4

Laboratory tests for DG-1 through -4 were conducted using band-limited signals comparable to up-traveling and down-traveling waves as input

Using the test setup shown in Figure VI-29, composite signals were generated by utilizing 6 available delay lines, each with its own summing amplifier. These composites were input to the deghosting filters 1, 2, 3, and 4 of the 19-channel system. The generated signals included two similar wavelets separated in time by an amount equal to the two-way travel time between each individual sensor and the surface.

Text cont'd page VI-39

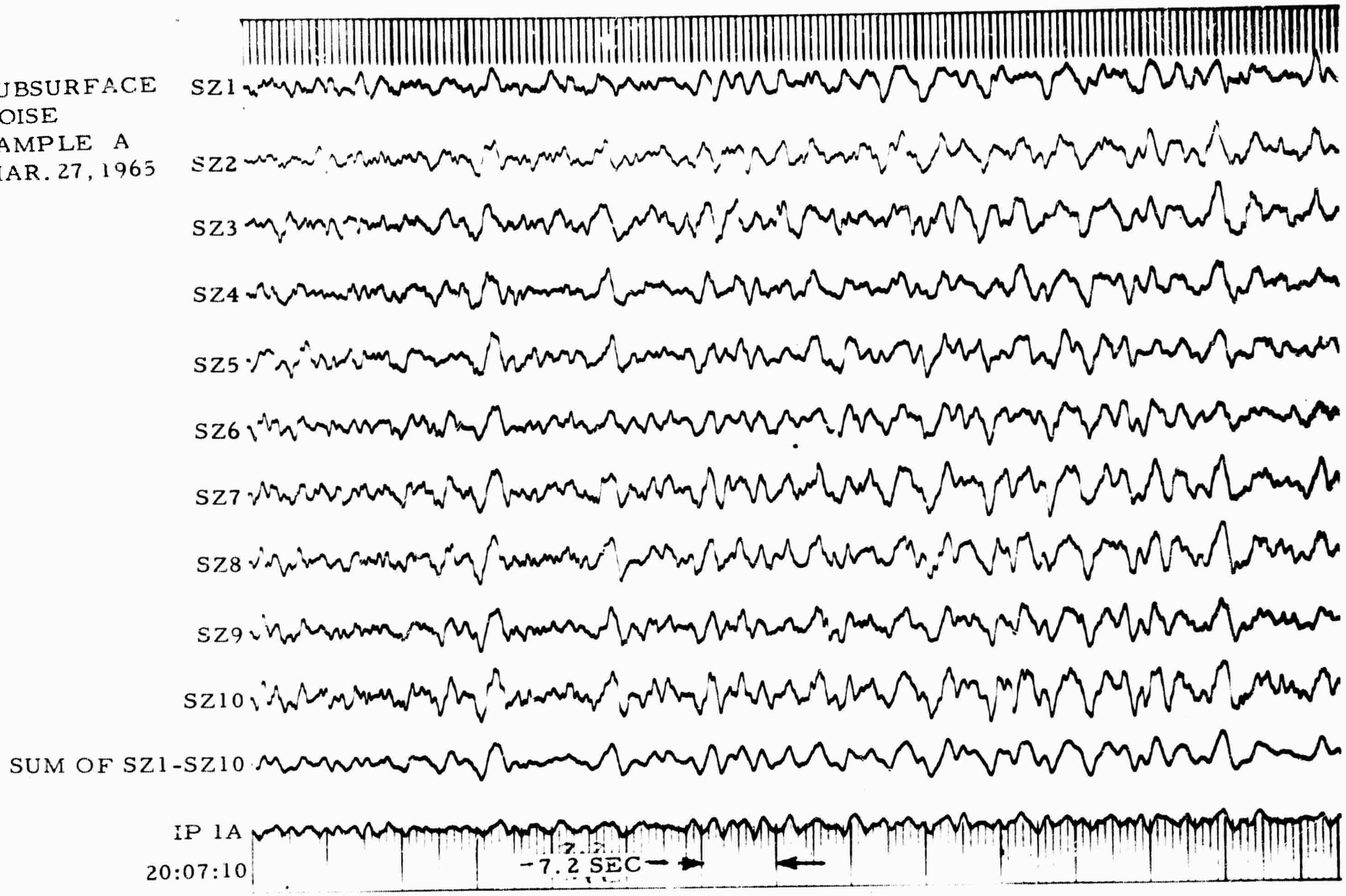

Figure VI-22. A Short Portion of UBO Noise Sample A (Subsurface) Results of IP-1A

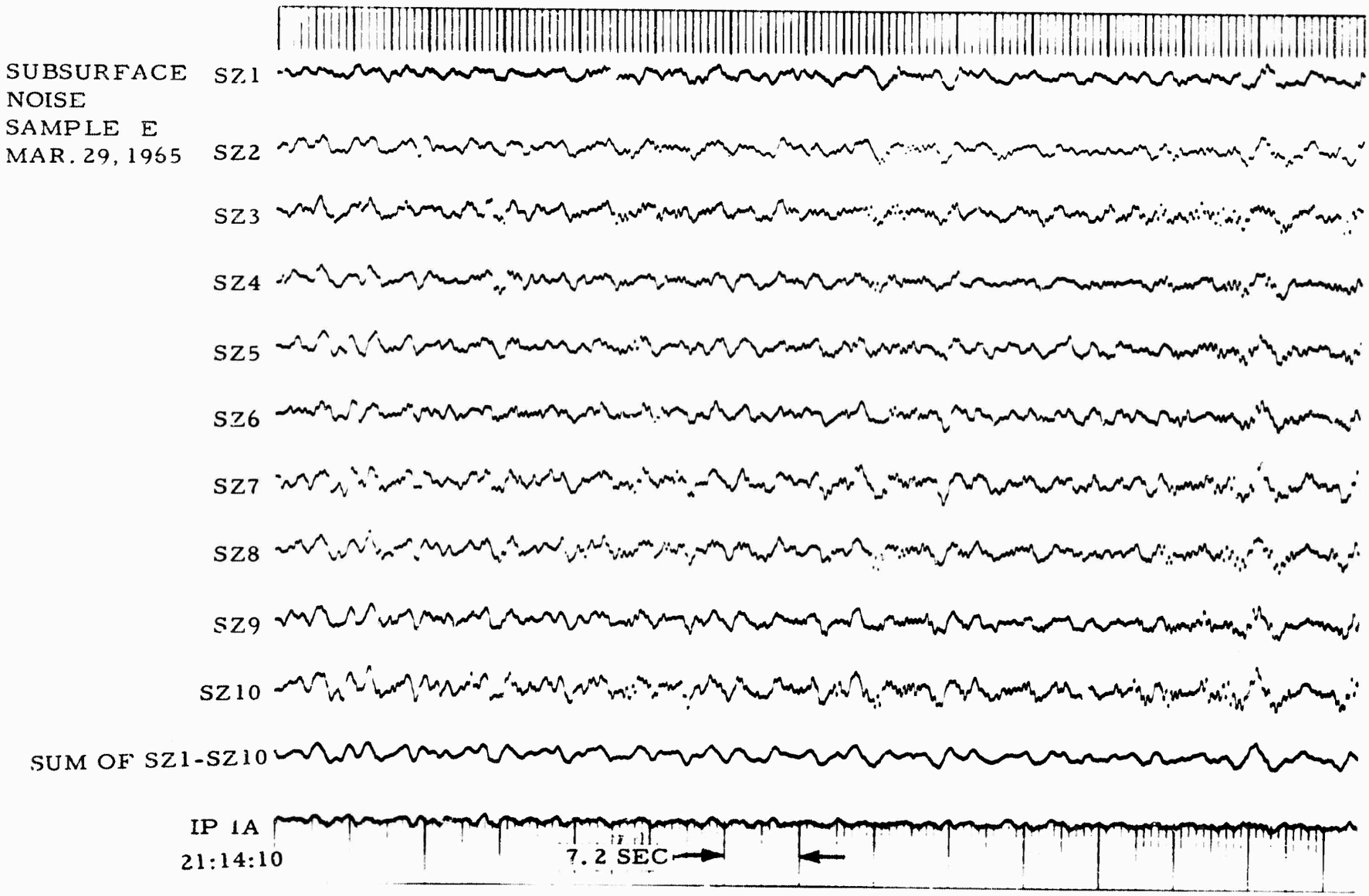

Figure VI-23. A Short Portion of UBO Noise Sample E (Subsurface) Results of IP-1A

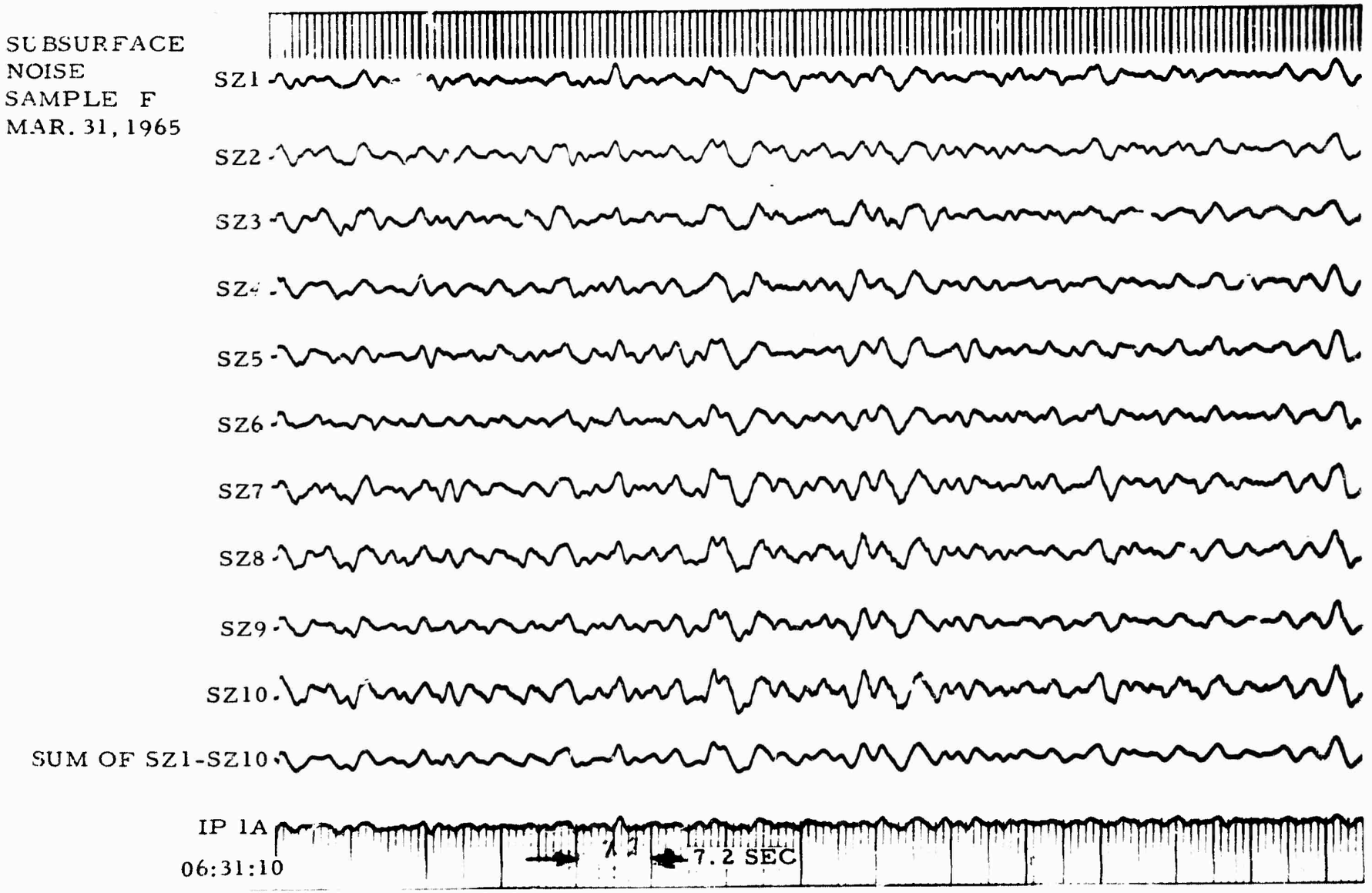

Figure VI-24. A Short Portion of UBO Noise Sample F (Subsurface) Results of IP-1A

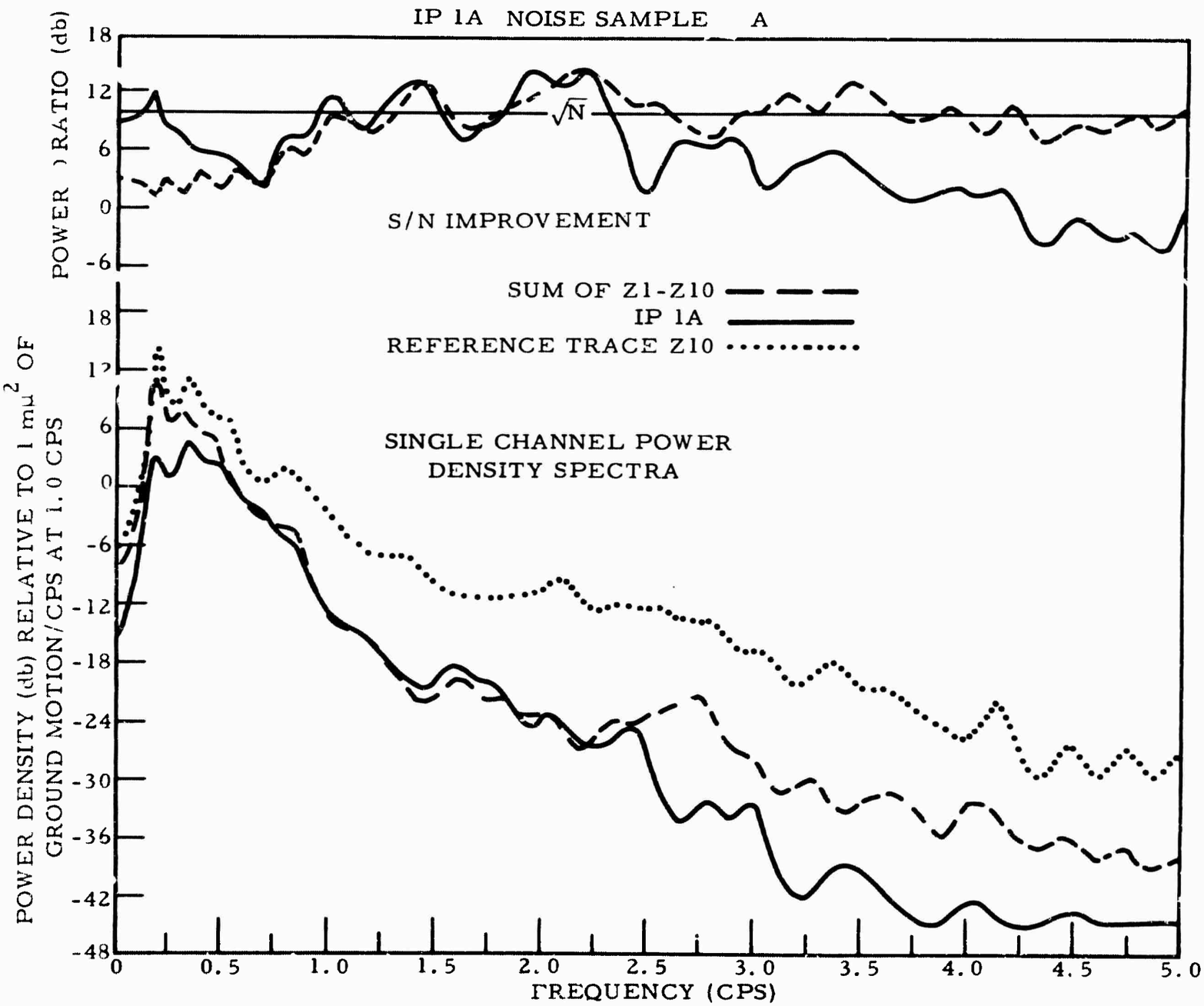

Figure VI-25. S/N Improvement and Single-Channel Power Density Spectra for IP-1A Noise Sample A

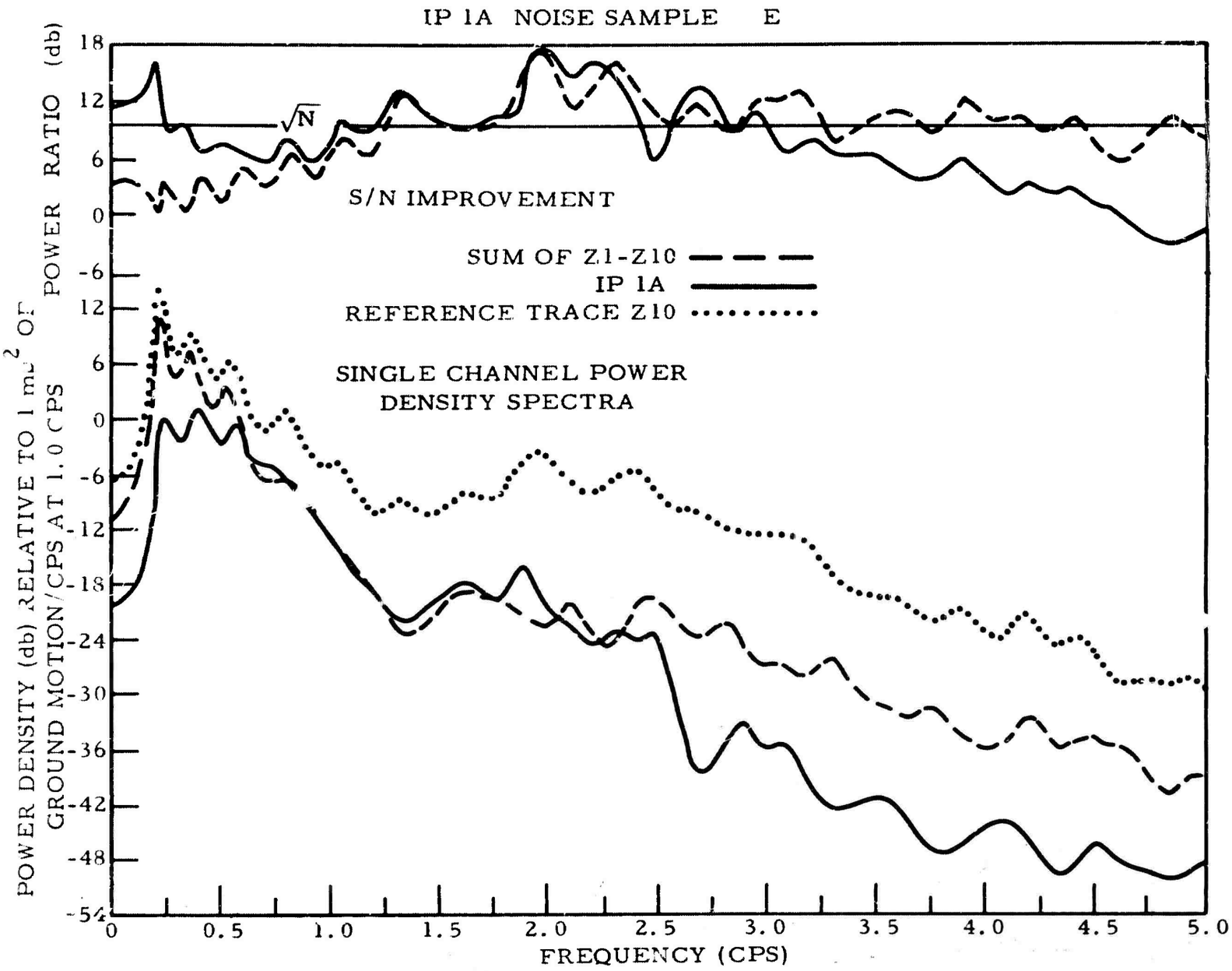

Figure VI-26. S/N Improvement and Single-Channel Power Density Spectra for IP-1A Noise Sample E

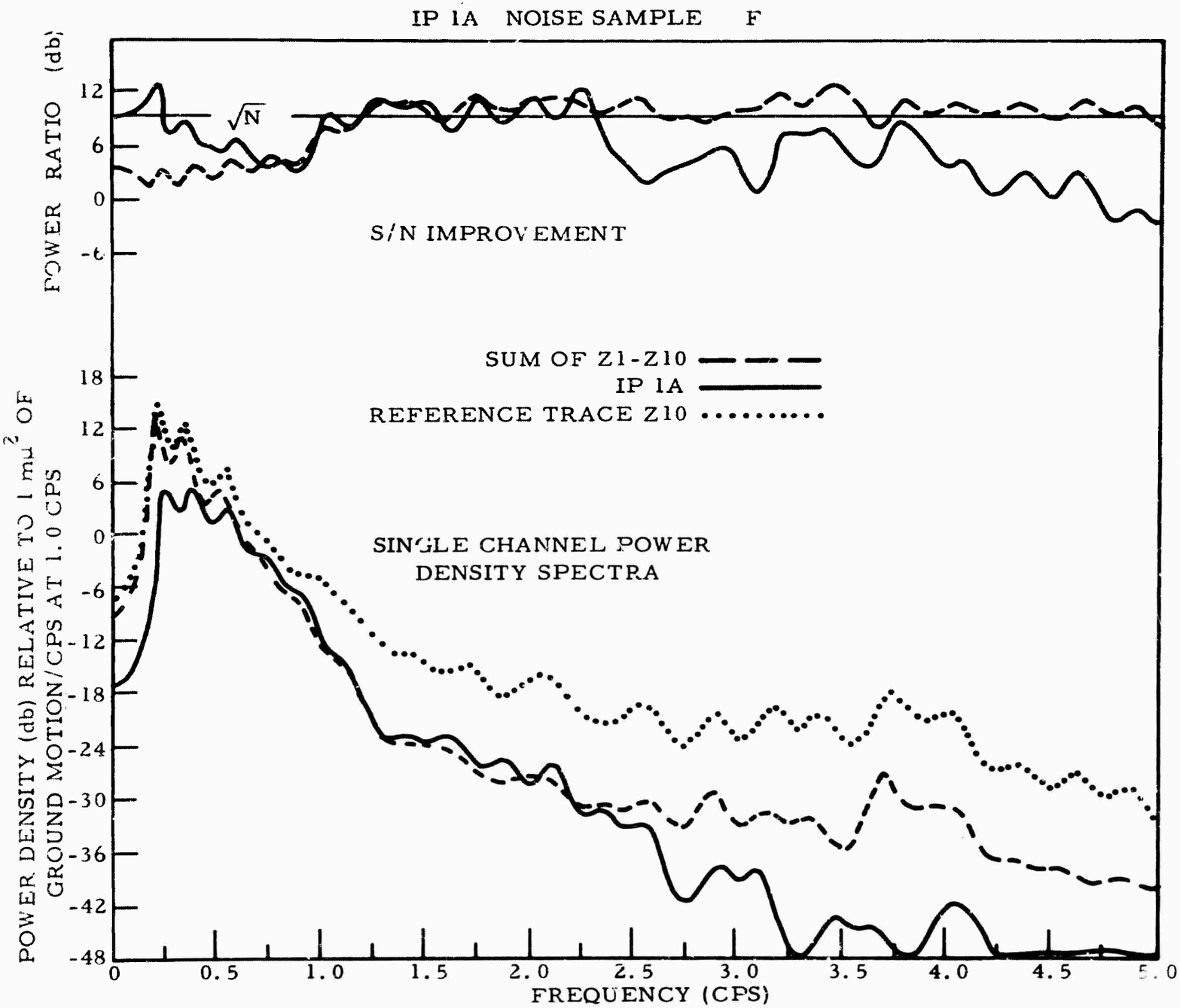

Figure VI-27. S/N Improvement and Single-Channel Power Density Spectra for IP-1A Noise Sample F

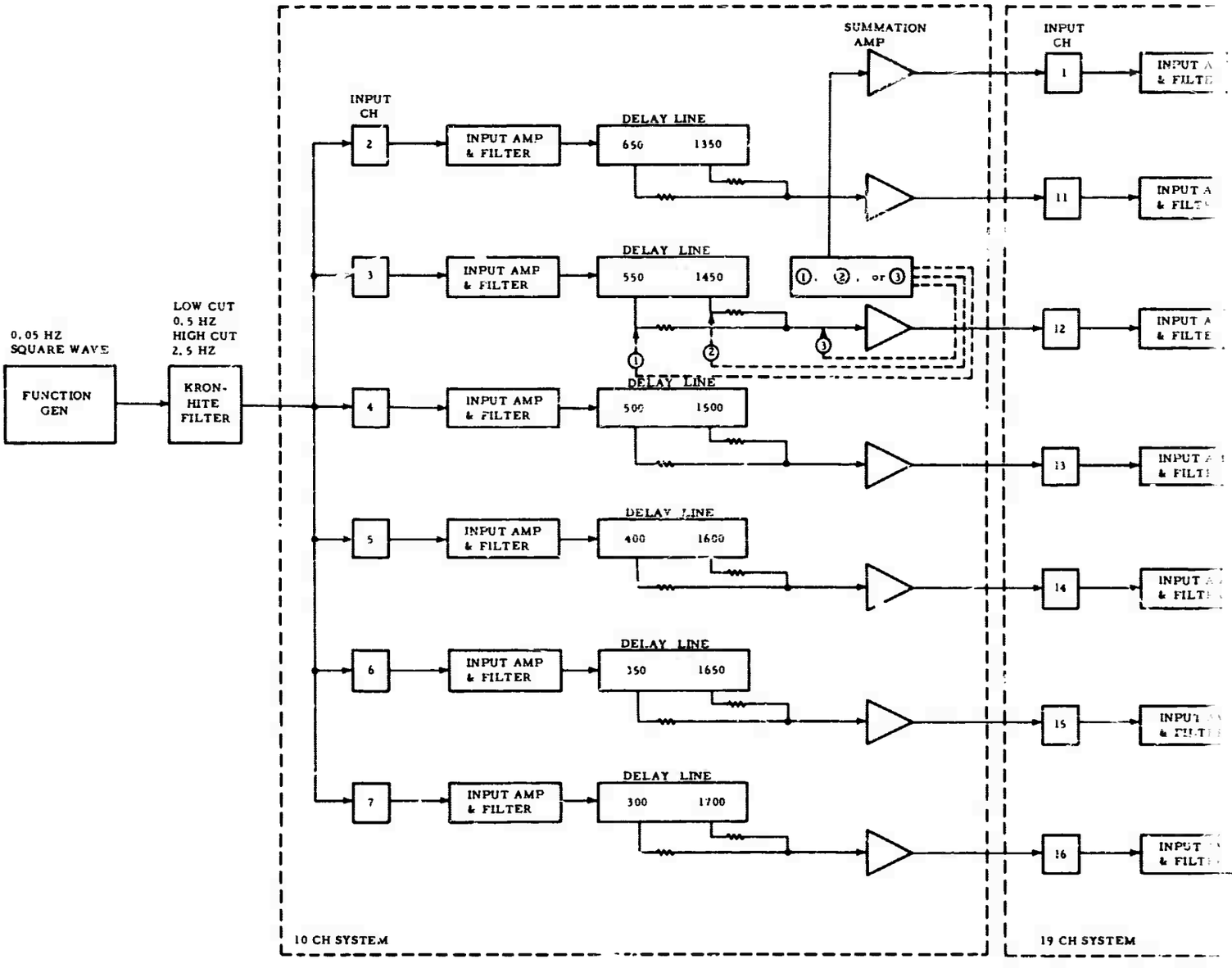

1) ALL WEIGHTING R' ISTORS IN 10 CH SYSTEM = 50 K
2) SIMULATED INPUT TO 19 CH SYSTEM ARE AS FOLLOWS

CH 1	- ORIGINAL OR COMPOSITE
CH 11	3900 FT SEIS
CH 12	4900 F T SEIS
CH 13	5900 FT SEIS
CH 14	690 : FT SEIS
CH 15	7900 FT SEIS
CH 16	8900 FT SEIS

A

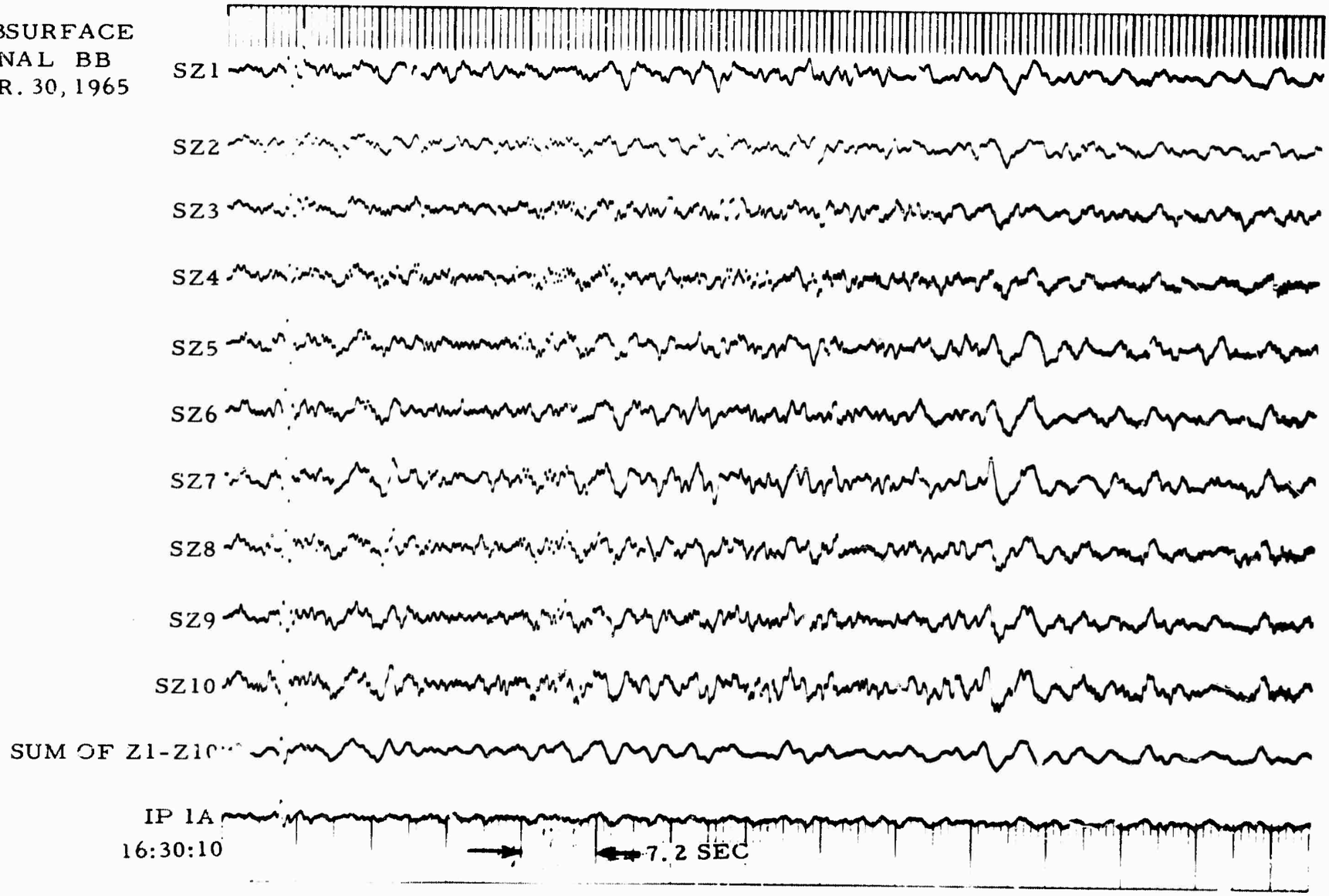

Figure VI-28. A Short Portion of UBO Signal BB (Subsurface) Results of IP-1A

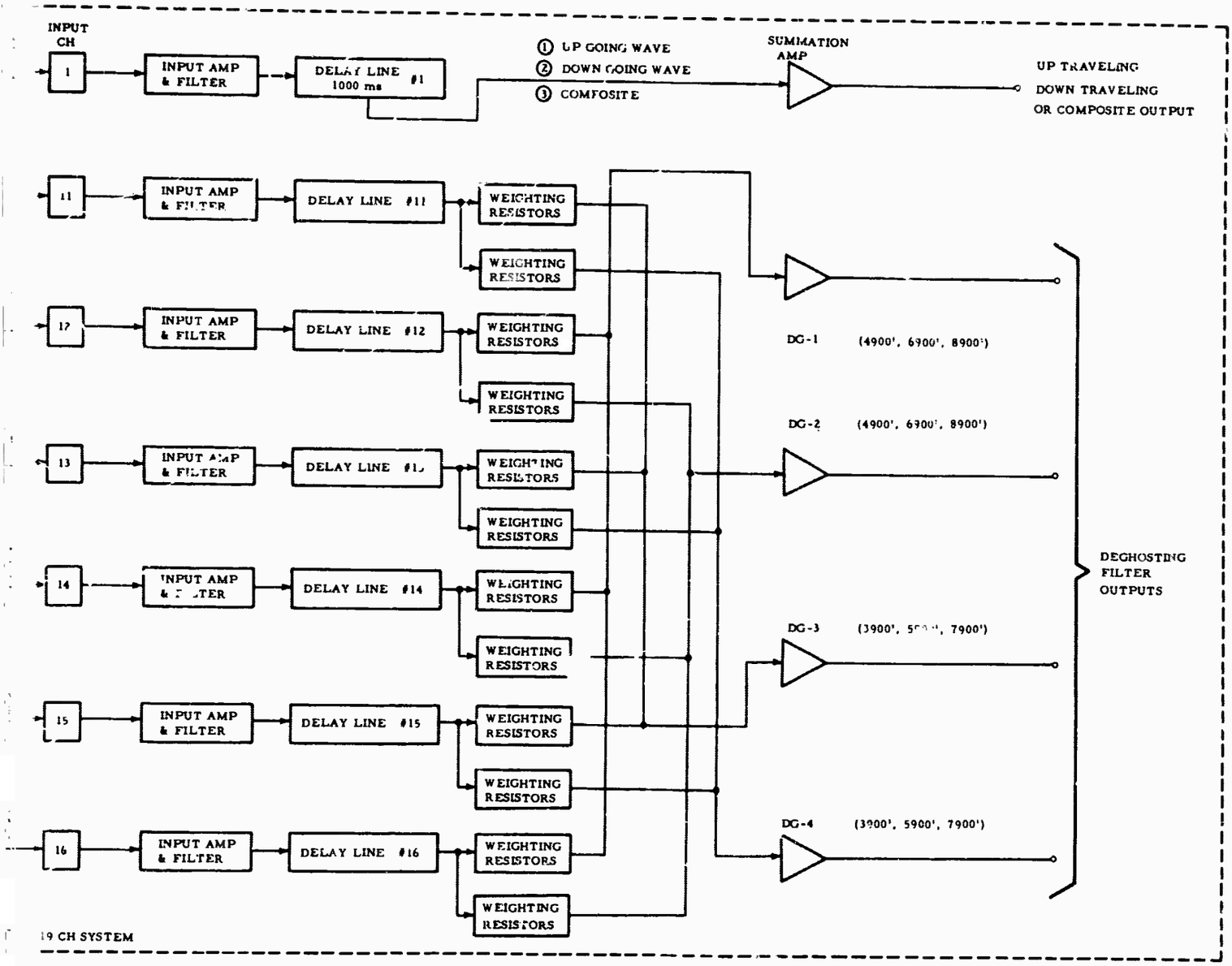

B

Figure VI-29. Test Setup for Deghost Filter Quality Check

The input to the 6 delay lines was a band-limited wavelet (0.5 to 2.0 cps and 0.5 to 4.2 cps) for 2 separate tests. Time functions for both these data sets were recorded in the following figures: Figure VI-30 which shows the true up- and down-traveling signals compared with respective filtered signal estimates (note the high level of rejection and the relatively undistorted signal); Figure VI-31 compares the up- and down-traveling estimates with the input signal composite as it appears at 4900 ft (again the rejection of unwanted signal is quite apparent as is the low level of signal distortion); Figure VI-32 compares the estimated up-traveling DG-1 signals with DG-3 signals and the down-traveling DG-2 estimates with DG-4 estimates; Figure VI-33 compares the true (unfiltered) up- and down-traveling signals with their respective composites (it must be stressed that the composite of the up- and down-traveling signals were input to this point in each case).

As a final comparison, only up- and down-traveling signals were input to the processor. In Figure VI-34, the outputs of DG-1, -2, -3, and -4 are compared with the true down-traveling signals. In Figure VI-35, the same outputs are compared with up-traveling signals only. Again, two different input bandwidths were used. These figures clearly show that the noise (unwanted signal) is rejected strongly and the desired signal is passed with very little distortion.

A precursor and some signal distortion can be seen on all filtered signal estimates. This can be explained partially by the fact that the actual reflected travel time between any sensor and the surface could be approximated only by using 50-msec delay-line taps available in the 6 delay lines. (In Table VI-1 the theoretical travel time differences are compared with the available approximate values.)

Evidence to substantiate this conclusion can be obtained if the outputs from DG-1 and -2 are compared with outputs for DG-3 and -4. Travel-time approximations for DG-3 and -4 are slightly better than those for DG-1 and -2, the resulting precursor and signal distortion are reduced accordingly.

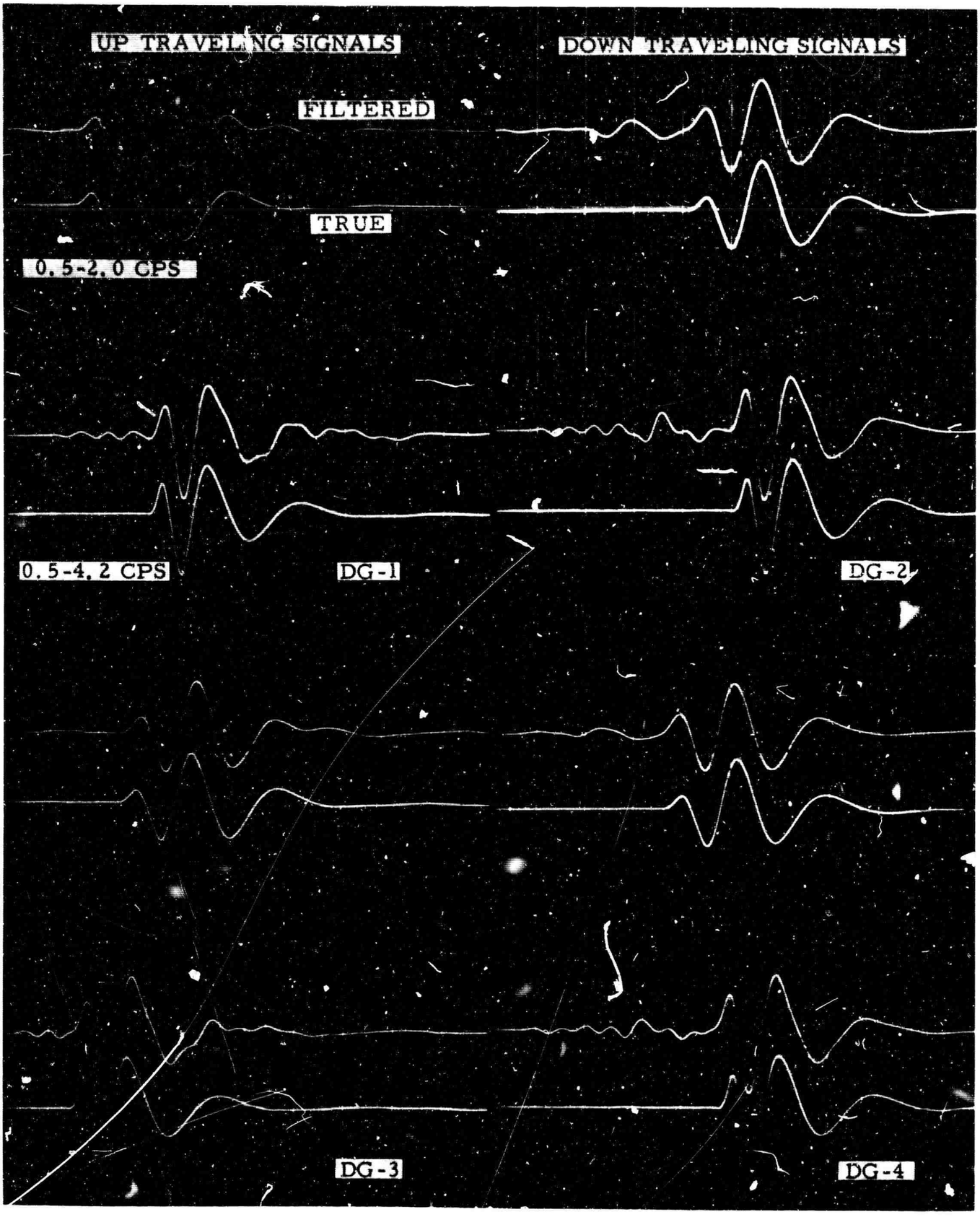

Figure VI-30 Comparison of Up- and Down-Traveling Signal Composite (only the relative part of the Composite is shown with the Corresponding Filtered Estimates)

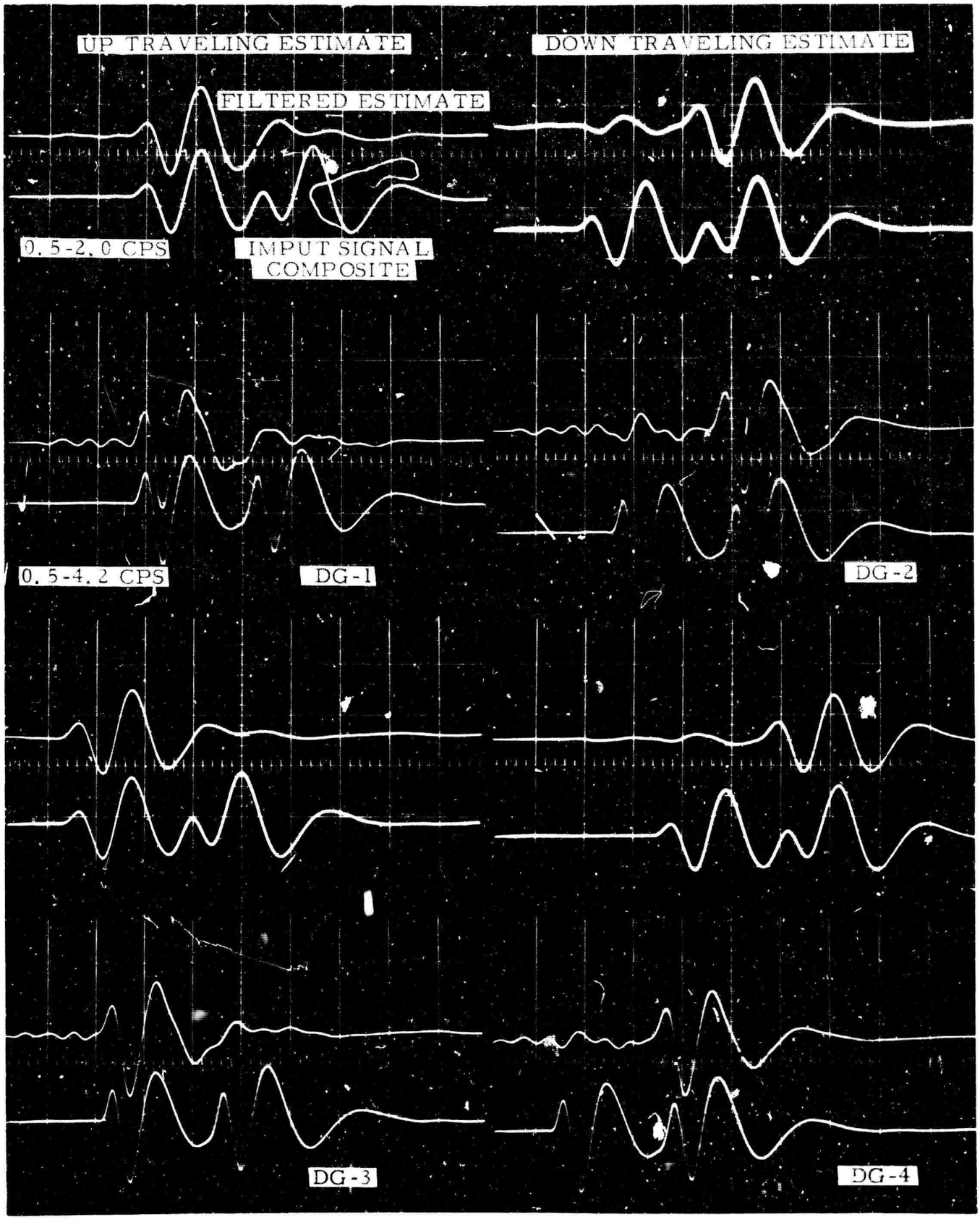

Figure VI-31. Comparison of Up- and Down-Traveling Signal Composite with the Corresponding Filtered Estimates

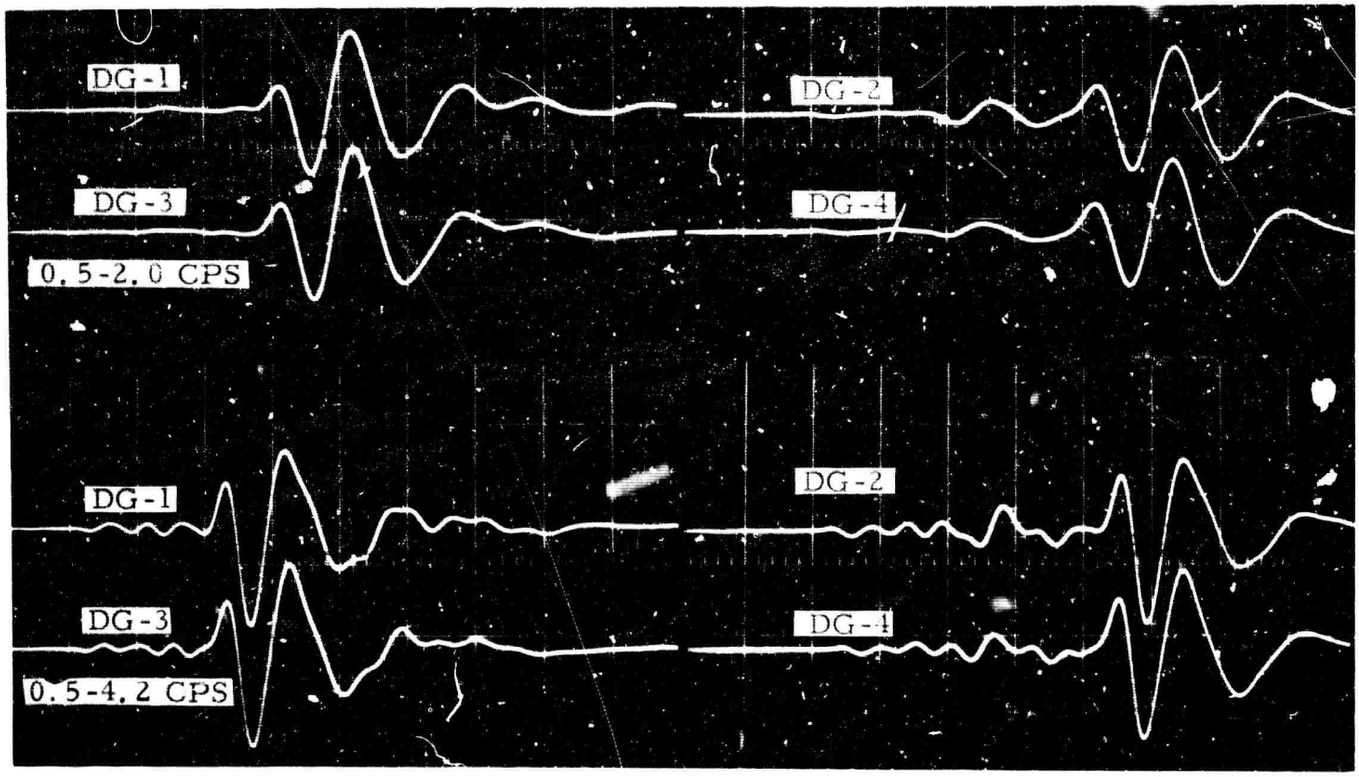

Figure VI-32. Comparison of Estimated Up-Traveling Signals (DG-1 Compared With DG-3) and Estimated Down-Traveling Signals (DG-2 Compared With DG-4)

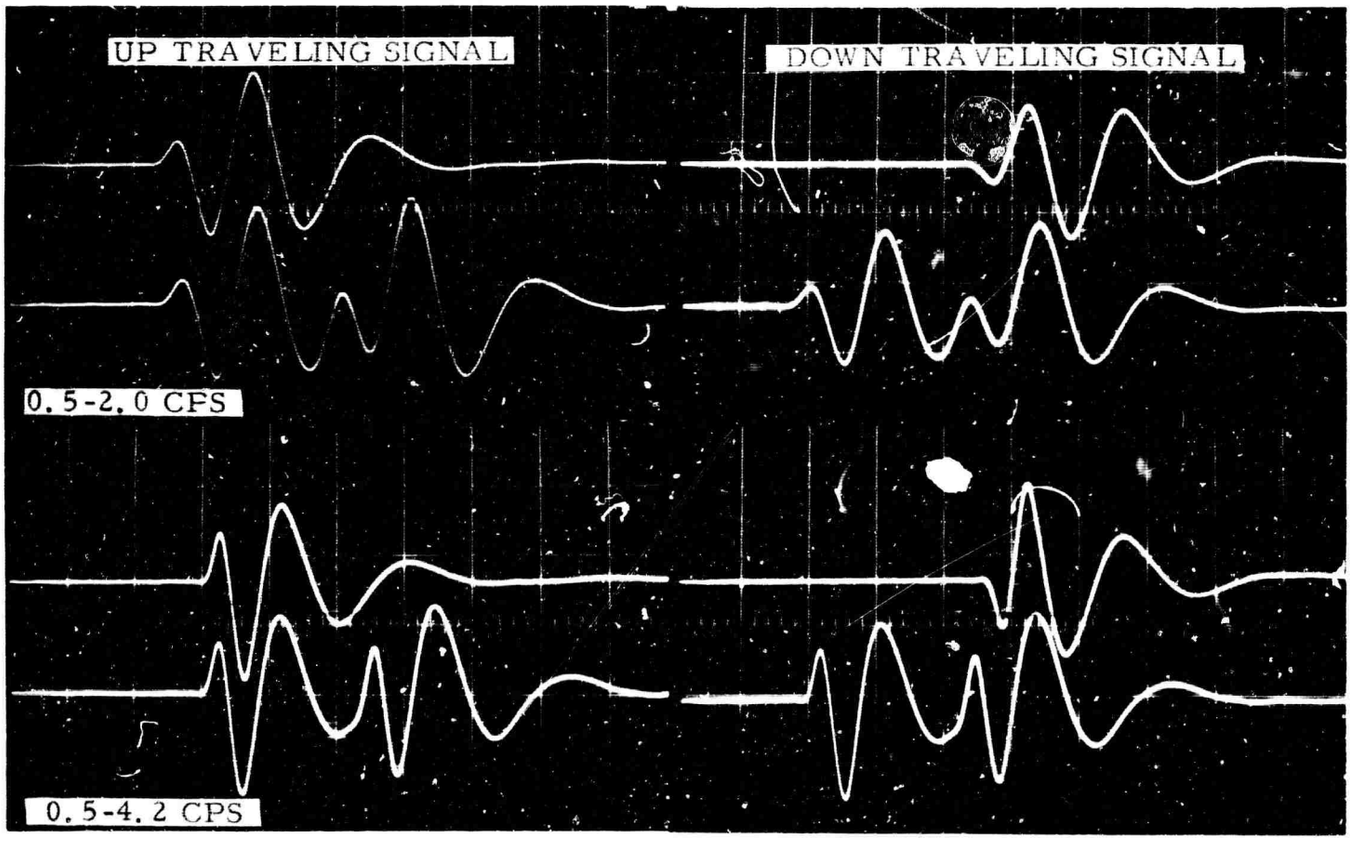

Figure VI-33. True Up-and Down-Traveling Signals Compared With Their Respective Composites

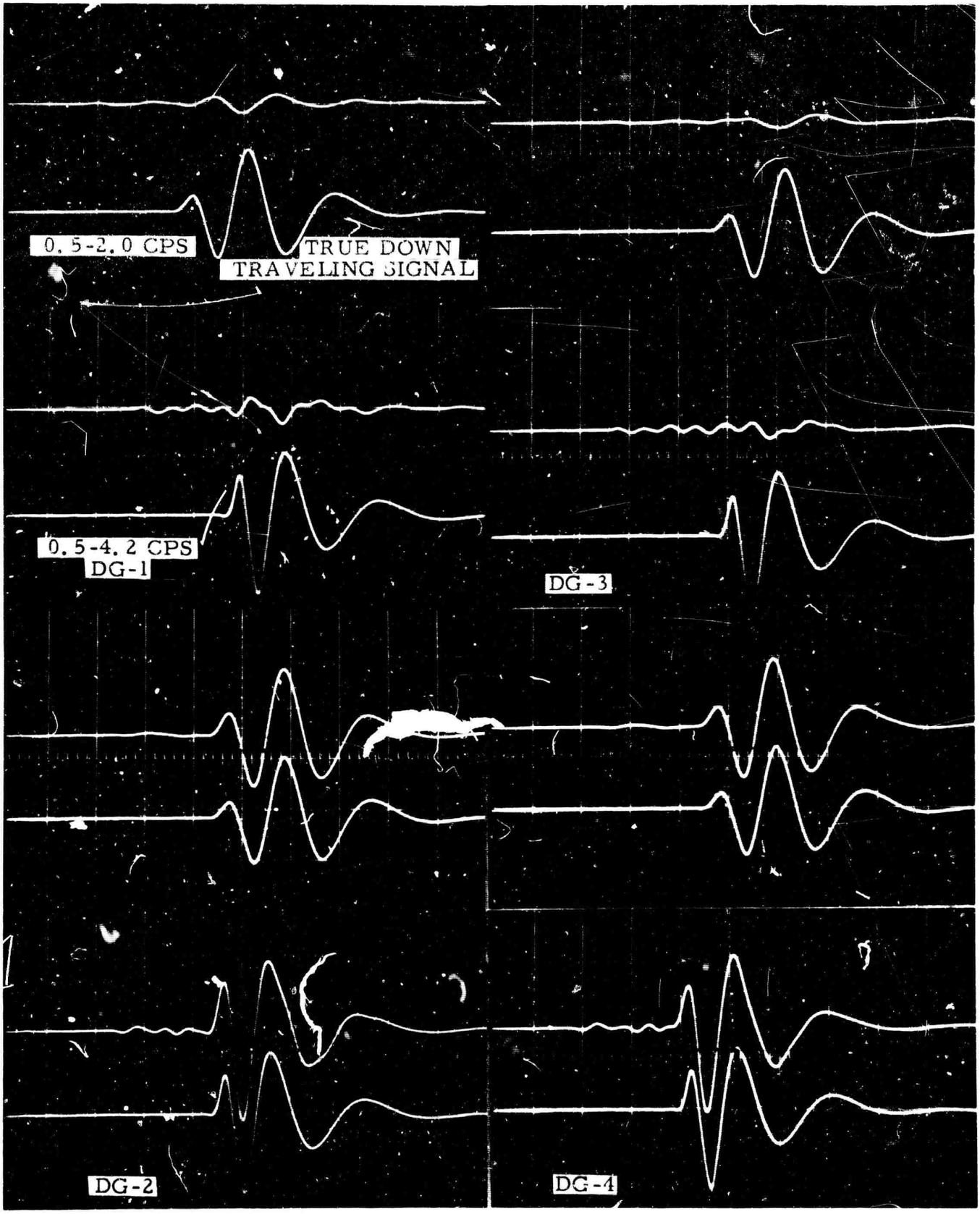

Figure VI-34. Outputs of DG-1, -2, -3 and -4 Compared With the True Down-Traveling Signal (Not a Composite Signal)

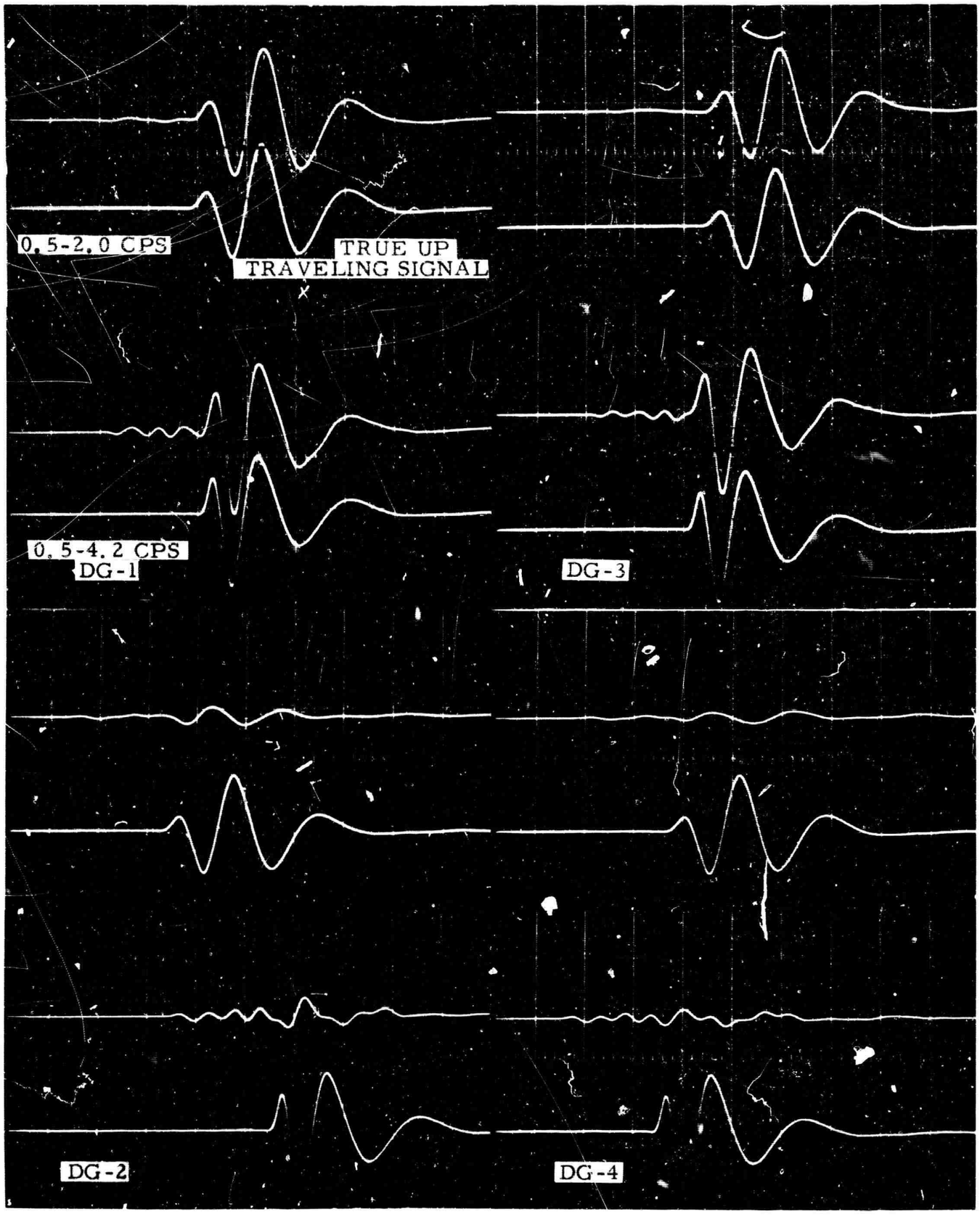

Figure VI-35. Outputs of DG-1, -2, -3 and -4 Compared With The True Up-Traveling Signal (Not a Composite)

TABLE VI-1

ACTUAL REFLECTION TRAVEL TIMES VS DELAY-LINE TAPS USED

DG Filter	Depth to Sensor (ft)	Actual Reflected Travel Time (ms)	Time Difference Between Taps on Delay Line (ms)
1-2	4900	890.6	900.0
	6900	1150.2	1200.0
	8900	1434.4	1400.0
3-4	3900	733.4	700.0
	5900	1020.4	1000.0
	7900	1299.2	1300.0

APPENDIX A

DEVELOPMENT OF UBO MEASURED NOISE CORRELATIONS

APPENDIX A

DEVELOPMENT OF UBO MEASURED NOISE CORRELATIONS

A. INTRODUCTION

This appendix presents the noise ensemble and data preparation accomplished in developing the average-measured noise correlation statistics for the surface and 200-ft-buried 10-element planar arrays at UBO.

B. THE NOISE ENSEMBLES

The data used in developing both the surface and subsurface average correlation sets were recorded on-site in digital format with a real-time sample interval of 0.024 sec using the Texas Instruments Digital Field System.

1. The Surface Noise Ensemble

The 10-channel (Z-1 through Z-10) noise used in developing the average correlation matrix for the surface noise field was collected during the period of 9 September 1964 through 13 October 1964.

Table A-1 lists information concerning the 12 noise samples which were selected for use in forming the average surface-measured noise correlation set.

Figure A-1 presents a short portion of noise sample C.

2. The Subsurface Noise Ensemble

The noise used in developing the subsurface verage correlation matrix was collected from the subsurface planar array (SZ-1 through SZ-10) during the period of 25 through 30 March 1965. It was initially intended that the recording period be longer than 6 days. However, occurrence of a high degree of seismic activity from the Aleutian Islands chain that began March 29 prevented recording of suitable noise samples and the recording period was terminated consequently.

A total of 3 noise samples were chosen from the subsurface noise ensemble for formulation of the average correlation set. A detailed description of these noise samples is outlined in Table A-2.

TABLE A-1

UBO Surface Ambient Measured Noise Used In Developing The Average Measured Noise Correlation Set

NOISE SAMPLE	DATE	TIME (GCT)	LENGTH
A	13 Sept. 1964	19:52:30	4.0 Min
B	21 Sept. 1964	13:20:10	"
C	5 Oct. 1964	02:08:10	"
D	15 Sept. 1964	13:48:50	"
E	17 Sept. 1964	12:07:50	"
F	20 Sept. 1964	20:00:10	"
G	27 Sept. 1964	20:47:10	"
H	29 Sept. 1964	22:16:20	"
I	30 Sept. 1964	22:07:00	"
J	2 Oct. 1964	20:28:50	"
K	8 Oct. 1964	19:16:10	"
L	12 Oct. 1964	18:58:10	"

TABLE A-2

UBO Subsurface Ambient Measured Noise Used In Developing The Average Measured Noise Correlation Set

NOISE SAMPLE	DATE	TIME (GCT)	LENGTH
A	27 Mar 1965	20:07:10	4.0 Min
B	28 Mar 1965	11:31:10	"
C	28 Mar 1965	20:32:20	"

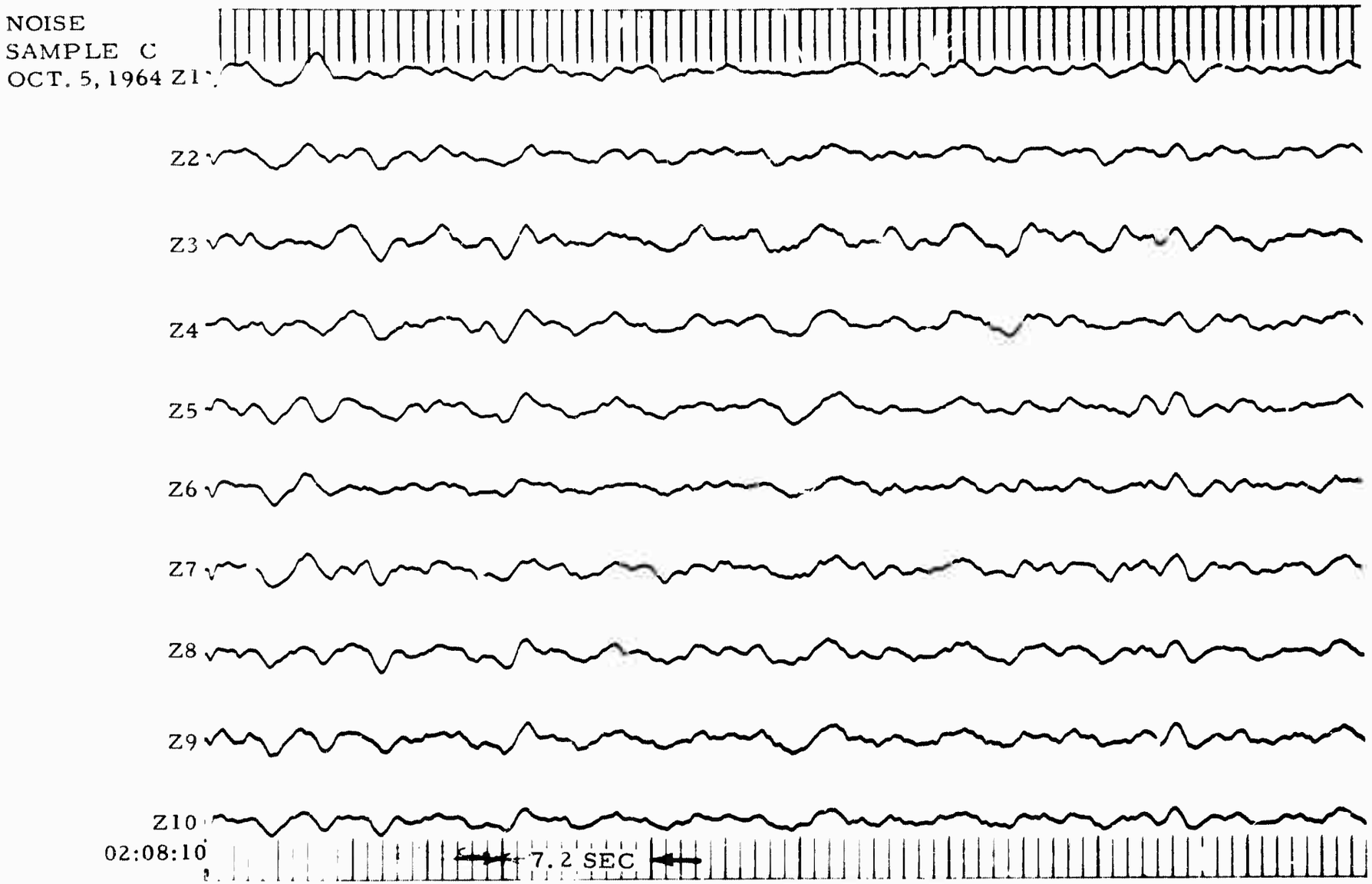

Figure A-1. A Short Portion of Surface Noise Sample C.

A short portion of noise sample B is shown in Figure A-2.

C. PROCESSING THE ENSEMBLE NOISE

Both surface and subsurface noise ensembles were processed in a similar manner. First, in order to reduce computation time, the data was decimated by a factor of 3 (converted from 0.024 to 0.072 sample interval data). Since the decimated data would have a Nyquist (folding) frequency of 6.94 cps, as opposed to 20.833 cps for the 0.024 data, it was first antialias-filtered to remove effectively energy above the Nyquist frequency prior to decimation and, thus, prevent energy above 6.94 cps from aliasing into the 0- to 6.94-cps band. Secondly, both noise ensembles were approximately whitened using a low-cut frequency filter. Whitening of the data produced approximate equal power at all frequencies and was necessary when the data was to have been used in filter development, since the time-domain filter solution was weighted as a function of frequency.

1. The Surface Noise Ensemble

The surface noise ensemble first was antialias filtered by using a zero-phase filter. The response of this filter is shown in Figure A-3. Then the noise data was resampled by 3 to yield a 0.072 sample interval and was whitened with a zero-phase, low-cut frequency filter, the response of which is shown in Figure A-4.

A short portion of the resampled and whitened noise sample C (original data shown in Figure A-1) is shown in Figure A-5.

The power density spectrum of the whitened and nonwhitened noise sample C for channel Z-10 is shown in Figure A-6.

2. The Subsurface Noise Ensemble

The subsurface noise ensemble was both antialias-filtered and whitened with a single zero-phase bandpass filter. The response of this filter is shown in Figure A-7.

A short portion of the resampled and whitened subsurface noise sample B (original data shown in Figure A-2) is shown in Figure A-8. The single-channel power density spectrum of both the whitened and nonwhitened data for channel Z-5, noise sample B, is shown in Figure A-9.

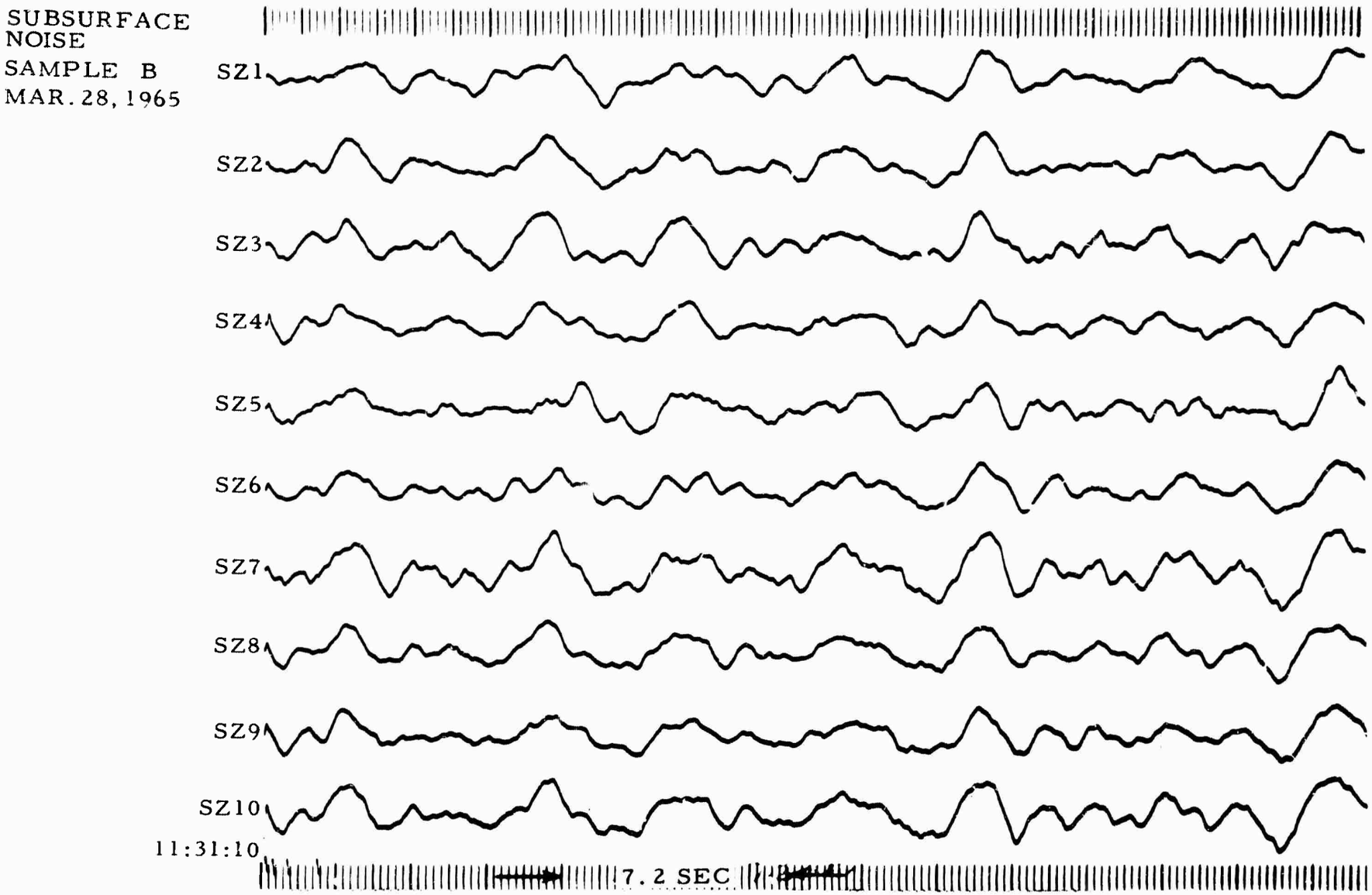

Figure A-2. A Short Portion of Subsurface Noise Sample B

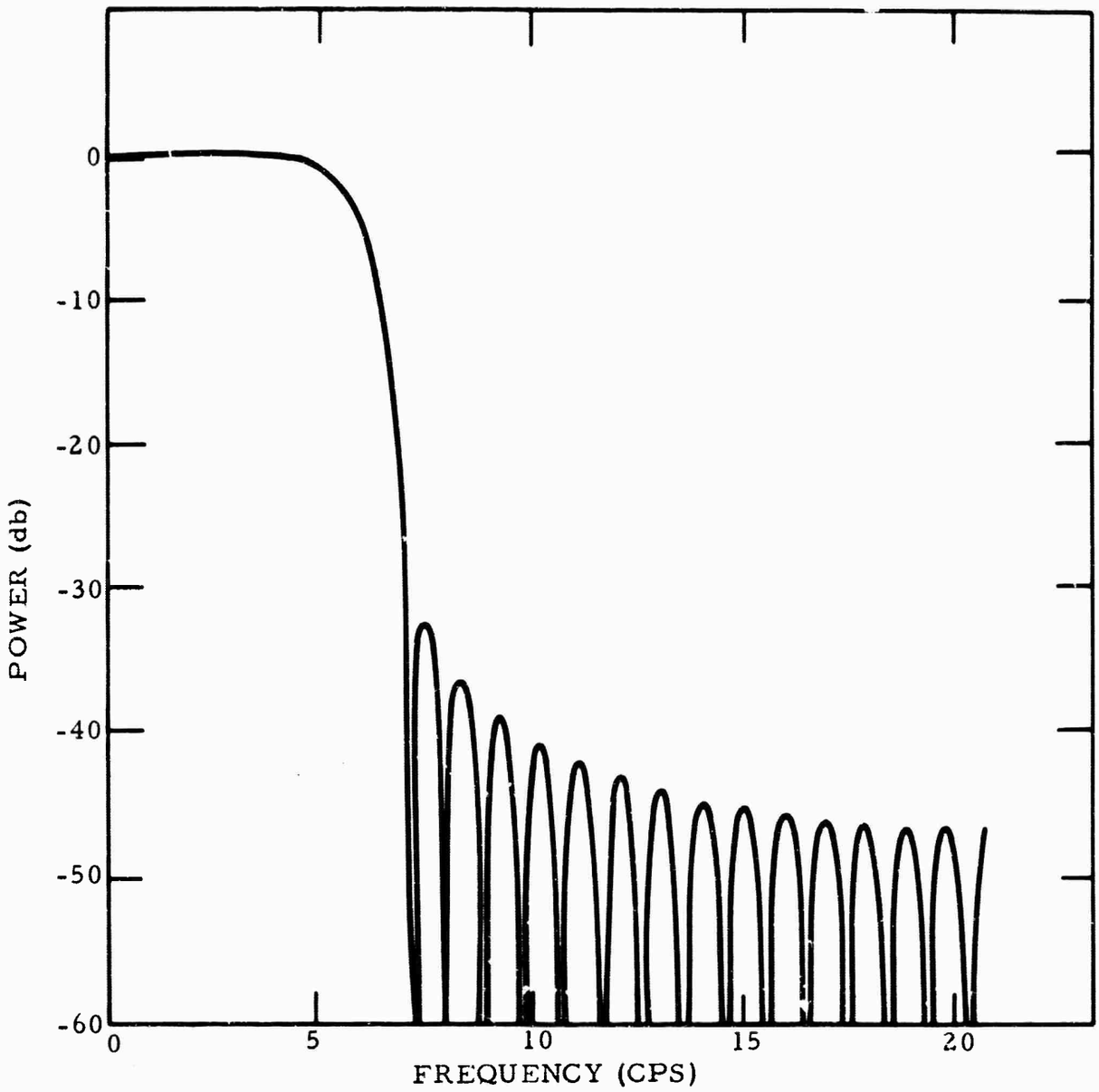

Figure A-3. Response of Antialiasing Filter Applied to Surface Data

D. FORMULATION OF THE ENSEMBLE CORRELATION MATRIX

The ensemble correlation matrix for both the surface and subsurface ensembles was formed by computing the correlation matrix for each of the resampled and whitened noise samples and then stacking correlation sets (i. e., point-by-point addition of respective correlations of the noise ensemble) to yield the ensemble correlation matrix.

Text contd page A-12

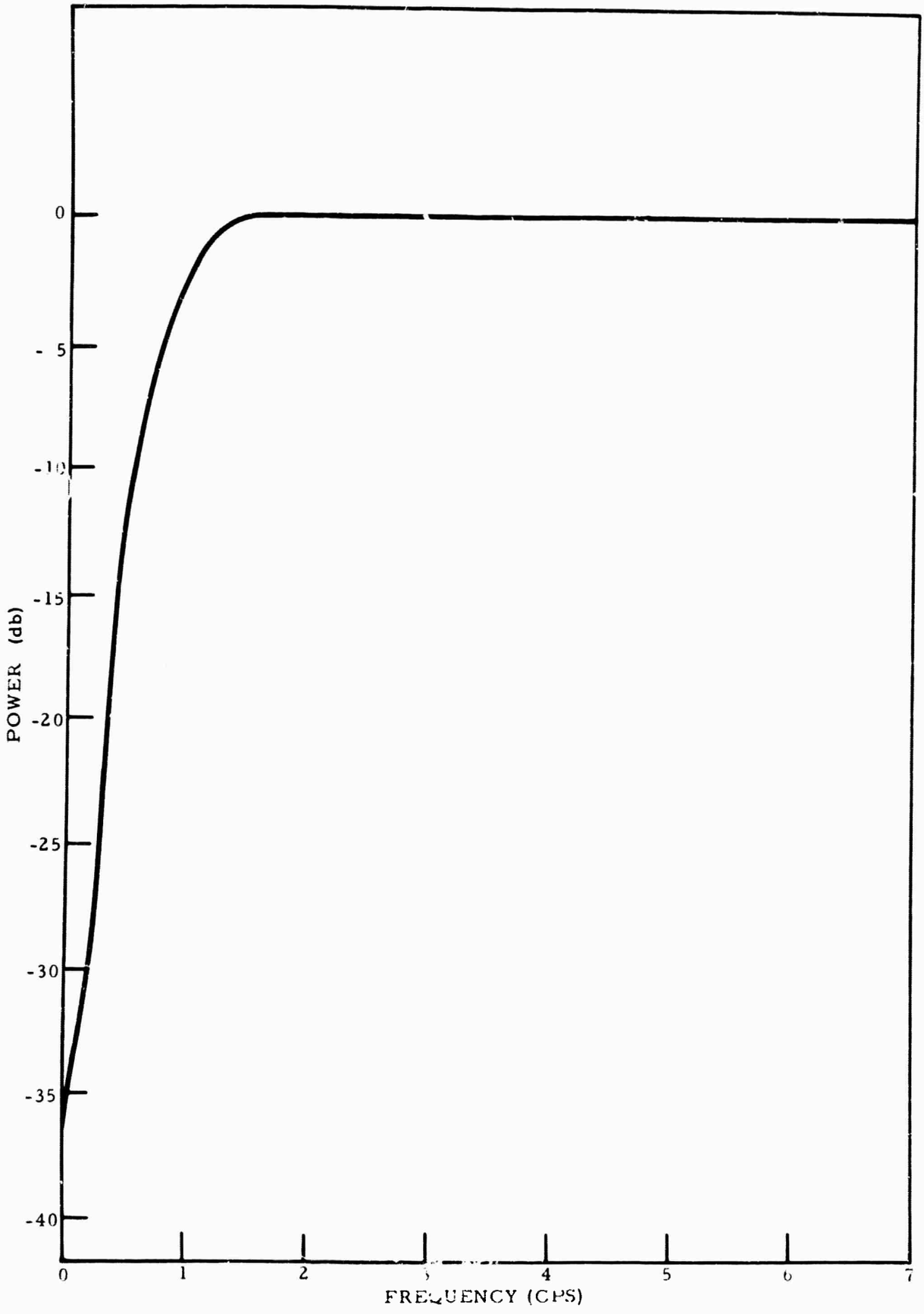

Figure A-4. Response of UBO Whitening Filter Applied to Surface Data

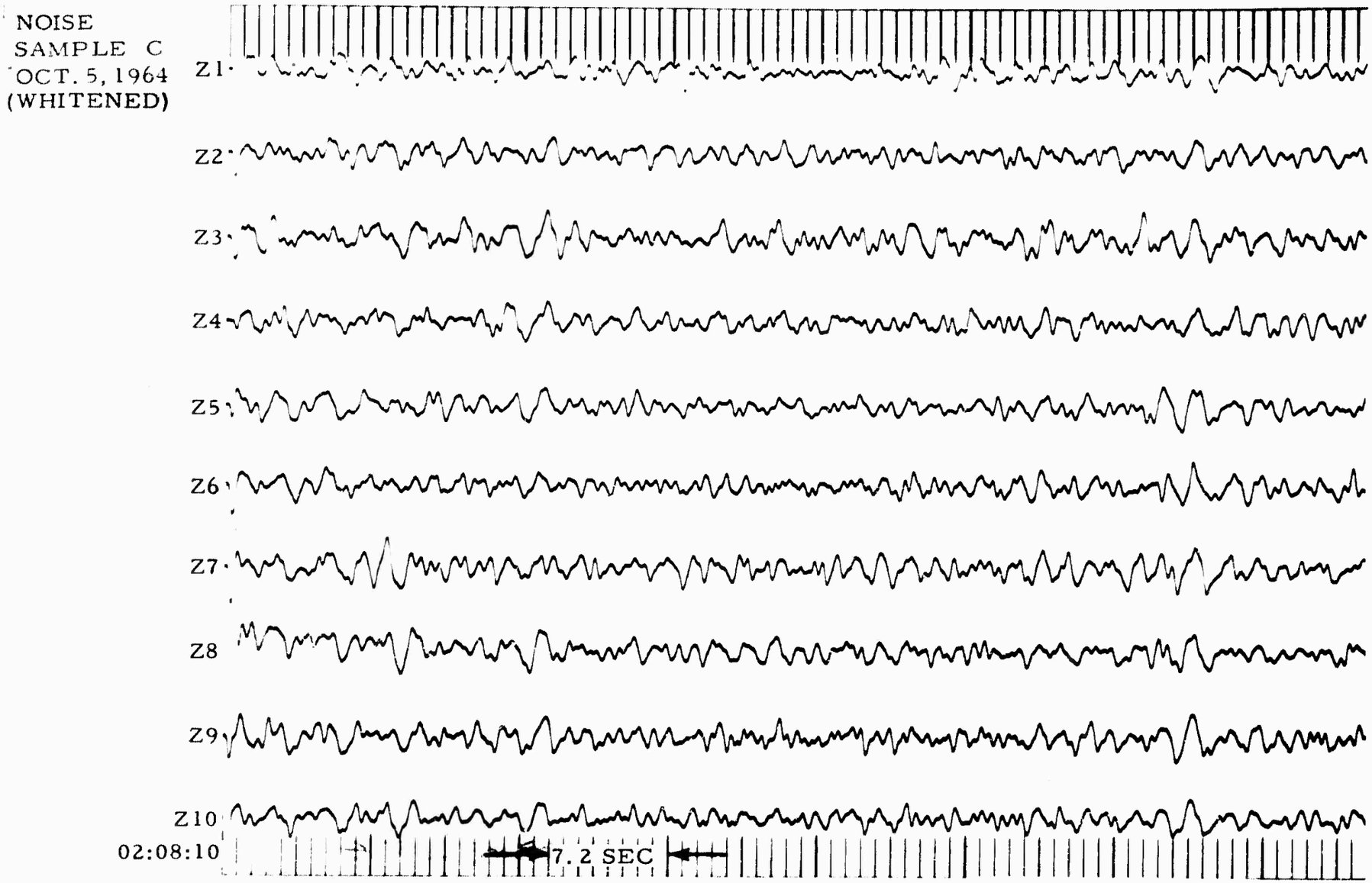

Figure A-5. A Short Portion of the Resampled and Whitened Surface Noise Sample C

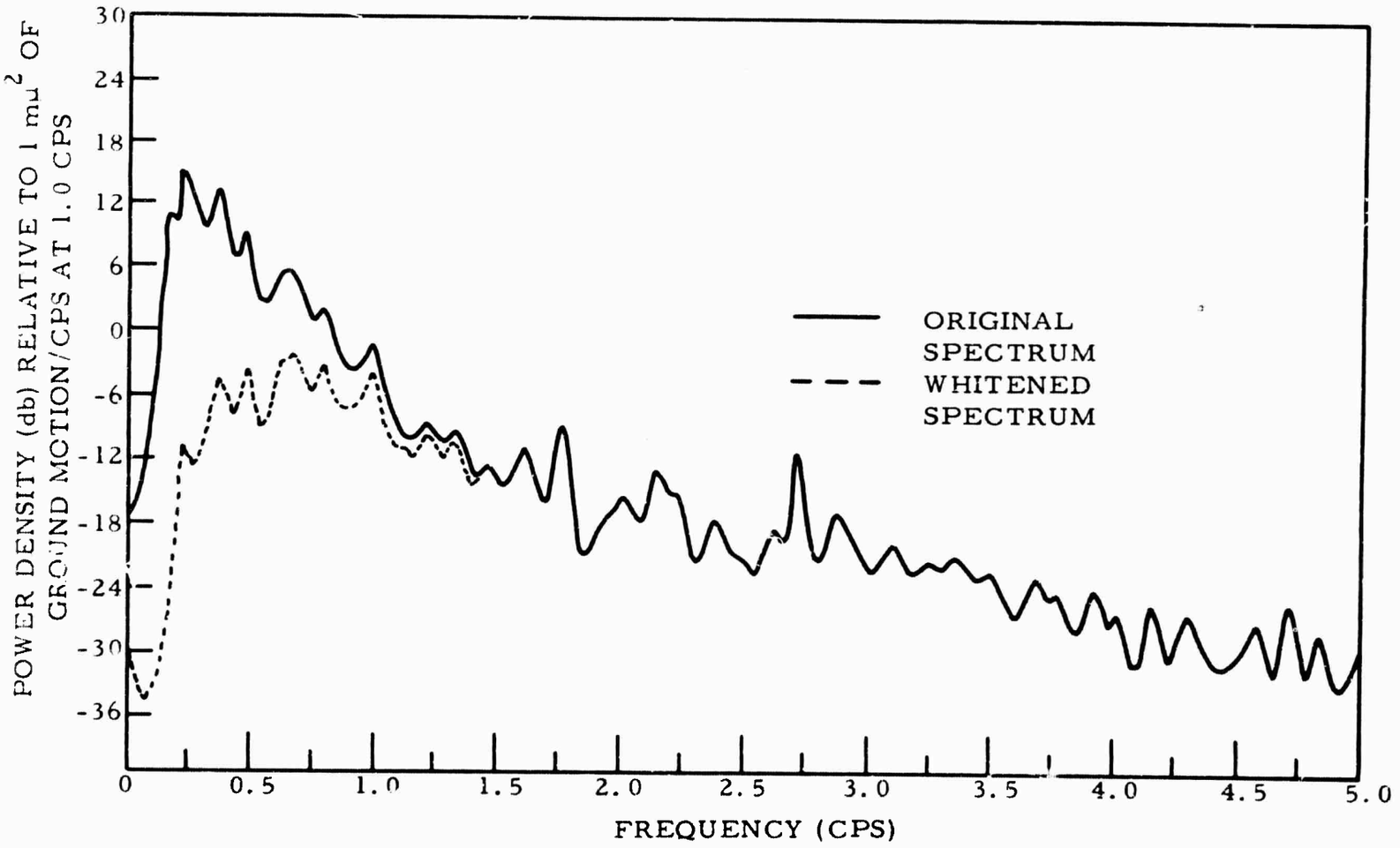

Figure A-6. Single-Channel Power Density Spectrum of Z-10 Surface, Noise Sample C

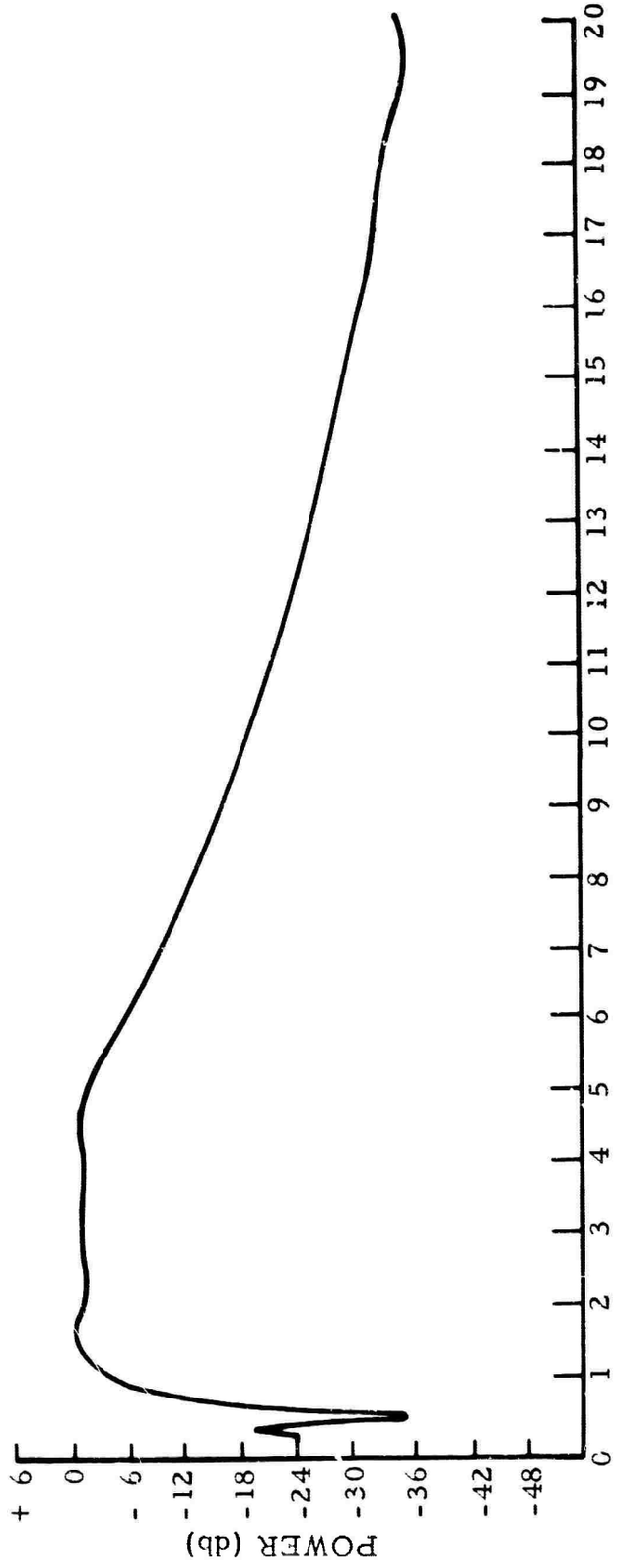

Figure A-7. Response of Whitening and Antialiasing Applied to Subsurface Data

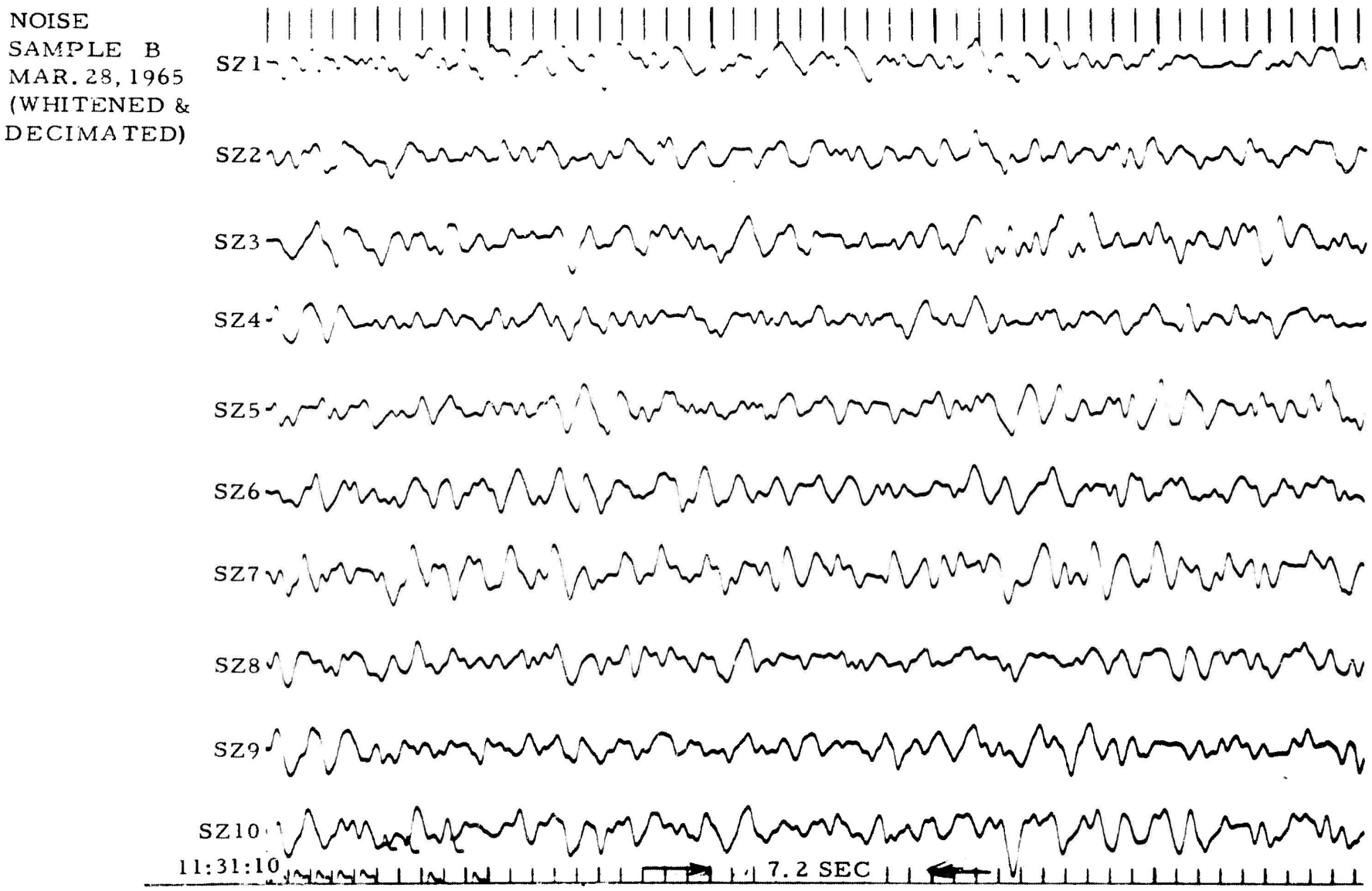

Figure A-8. A Short Portion of the Resampled and Whitened Subsurface Noise Sample B

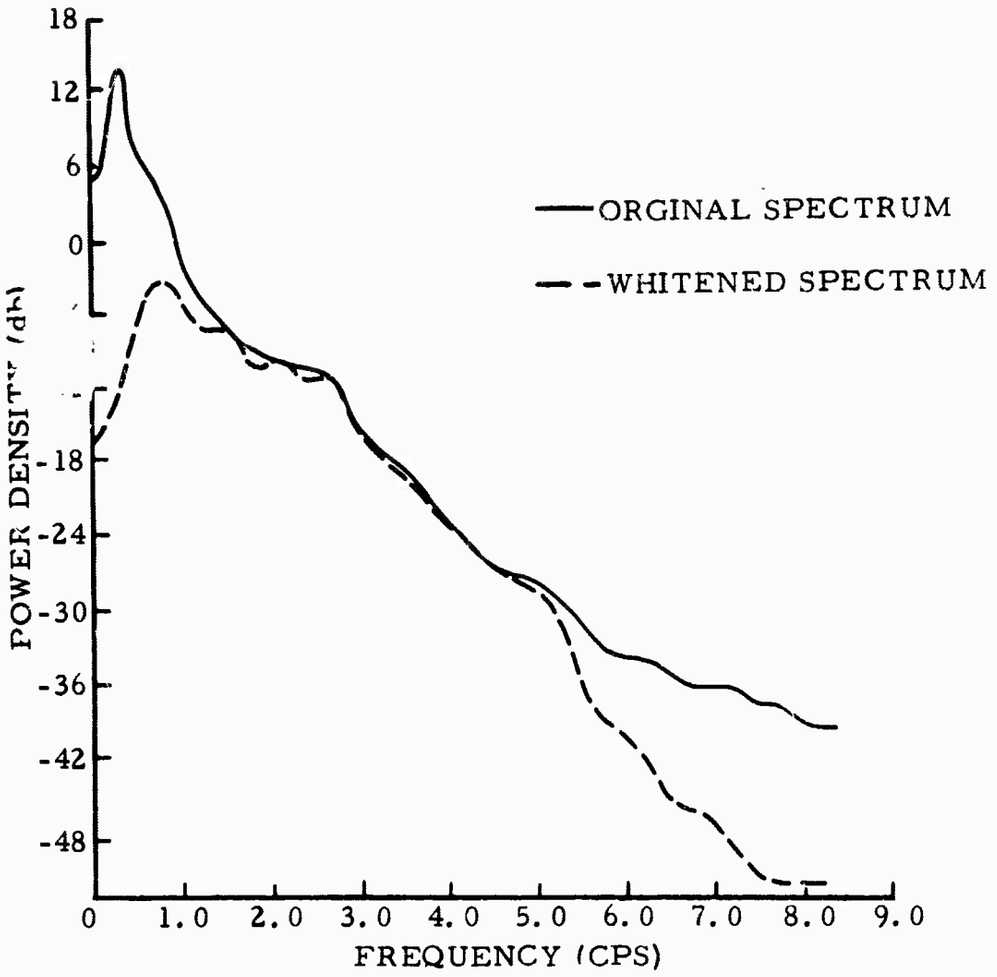

Figure A-9. Single-Channel Power Density Spectrum of SZ-5 for Subsurface Noise Sample B

Stacking or averaging the correlatio sets in this manner effectively results in a correlation matrix representation of the time-stationarity organized noise field. Such a noise model is necessary when used in developing filters which must be optimum on a long-time basis such as the filters used in an on-line processor.

The average correlation matrix for both the subsurface and surface noise fields has been displayed in a previous report.*

*Texas Instruments Incorporated, 1965, Noise Analysis for Uinta Basin Seismological Observatory, Sponsored by AFTAC, Oct. 15, p. IV-39.

APPENDIX B

UBO THEORETICAL NOISE AND SIGNAL MODELS

BLANK PAGE

APPENDIX B

UBO THEORETICAL NOISE AND SIGNAL MODELS

A. INTRODUCTION

This appendix details the development of the theoretical noise and signal models used in synthesis of the MCF systems discussed in the body of this report.

B. THE INFINITE-VELOCITY SIGNAL MODEL

The infinite-velocity signal model (commonly referred to as the IV signal model) is defined as a single-point region at $\vec{k} = 0$ in multi-dimensional wavenumber space. This model derives its name from the planar array application since, for a horizontal planar array, if $\vec{k} = 0$, then

$$\vec{V} = \frac{f}{k^2} \cdot \vec{k}$$

or $\vec{V}$ is infinite.

1. Formulation of the IV Model for a Planar Array (UBO MCF-1, -2, -6, and -8)

Formulation of the IV correlation matrix for a planar array is almost trivial. For infinite apparent horizontal velocity, the signal is detected in phase by all array instruments; thus,

$$\varphi_{ij}(\tau) = \varphi_{k\ell}(\tau) \qquad i, j, k, \ell = 1, 2 \cdots n$$

where n is the number of sensors. Alternately, this means that all correlations in the $\varphi_{ij}(\tau)$ correlation matrix are identical.

The procedure normally employed in forming this matrix is to use one autocorrelation function of the noise matrix as the $\varphi^{s}_{ij}(\tau)$, therefore insuring that

$$|\Phi^{s}_{ij}(f)| = |\Phi^{n}_{ij}(f)|$$

2. Formulation of the IV Model for Vertical or 3-Dimensional Arrays

Two approaches were used in synthesizing signal models for infinite apparent horizontal velocity signals. The first method, which involves

knowledge of the estimated signal arrival time with depth, was used in developing the model for UBO DG-1 through -4. The second approach, which involves a solution of Haskell's equations, was used in developing UBO IP-1 and -2.

a. UBO DG-1 through -4

The signal models used in developing UBO DG-1 through -4 were synthesized from knowledge of the signal arrival time with depth. *

Once these arrival times are known for a particular array configuration, $\vec{x}_i$, i = 1, 2, 3 . . . . N, formulation of the correlation matrix is accomplished by computing the crosspower spectra:

$$\Phi^{s}_{ij}(f) = s(f)\, e^{i2\pi f T_{ij}}$$

where: f = frequency

s(f) = prespecified signal autopower density spectra

$T_{ij} = T_i - T_j$

T_i = relative arrival times of the signal at sensor i

The corresponding time-domain correlation matrix is found by

$$\varphi^{s}_{ij}(\tau) = \int_{-\tau_m}^{\tau_m} \Phi_{ij}(f)\, e^{i2\pi f \tau} df \qquad \text{(B. 1)}$$

It is possible to compute the $\varphi^{s}_{ij}(\tau)$ directly in the time domain but, since the above method was used in developing the models used in this contract, the time-domain synthesis technique will be omitted.

b. UBO IP-1 and -2

The signal models used in developing UBO IP-1 and -2 were synthesized by first computing the signal spectra as a function of depth for white infinite-velocity signal. Haskell's equations were used in this frequency-domain solution. **

*Sax, R. L. and R. A. Hartenberger, 1964, Seismic Noise Prediction in the Center Well: June 2 (unpublished).

**Haskell, Norman A., 1962, Crustal reflection of plane P and SV waves: J. Geophysi. Res., v. 67, p. 4751.

The resulting complex solution is of the form $\Phi_i^s(f)$. The cross-and autopower spectra are found from

$$\Phi_{ii}^s(t) = \Phi_i^s(f) \cdot \Phi_i^{s}(f)$$

$$\Phi_{ij}^s(f) = \Phi_i^s(f) \cdot \Phi_j^{s*}(f)$$

where i represents the i^{th} sensor and the star represents the complex conjugate.

The corresponding time-domain correlation matrix is found from Equation (B.1).

C. ISOTROPIC SIGNAL AND NOISE MODELS

Three types of isotropic models were used in synthesizing signal and noise models for development of filters under this contract. These models are shown in Figure B-1 for a planar array at constant frequency f_c.

At this point, only models for planar arrays will be considered. As will be shown in subsection E. 1, the model for a multidimensional array or vertical array is quite easily derived from the correlation matrix of the planar array if only surface mode energy is considered, which is the case for all models developed under this contract.

1. Synthesis of Model I Correlation Matrix

The wavenumber (for constant frequency) representation of Model I is a solid disk of minimum velocity V_{min} and is symmetric about $\vec{k} = 0$.

The crosspower spectra for this model are given by*

$$\Phi_{ij}^s(f) = \frac{s(f)}{\pi f V_{min}} J_1 \left[\frac{2\pi f(\vec{x}_i - \vec{x}_j)}{V_{min}} \right]$$

where $s(f)$ = desired signal autopower value

J_1 = first-order Bessel function

$\vec{x}_i$ = vector location of i^{th} sensor

V_{min} = specified minimum velocity

---

*Texas Instruments Incorporated, 1961: Final Report Phase I VT/077, sponsored by AFTAC, Dec., p. 107.

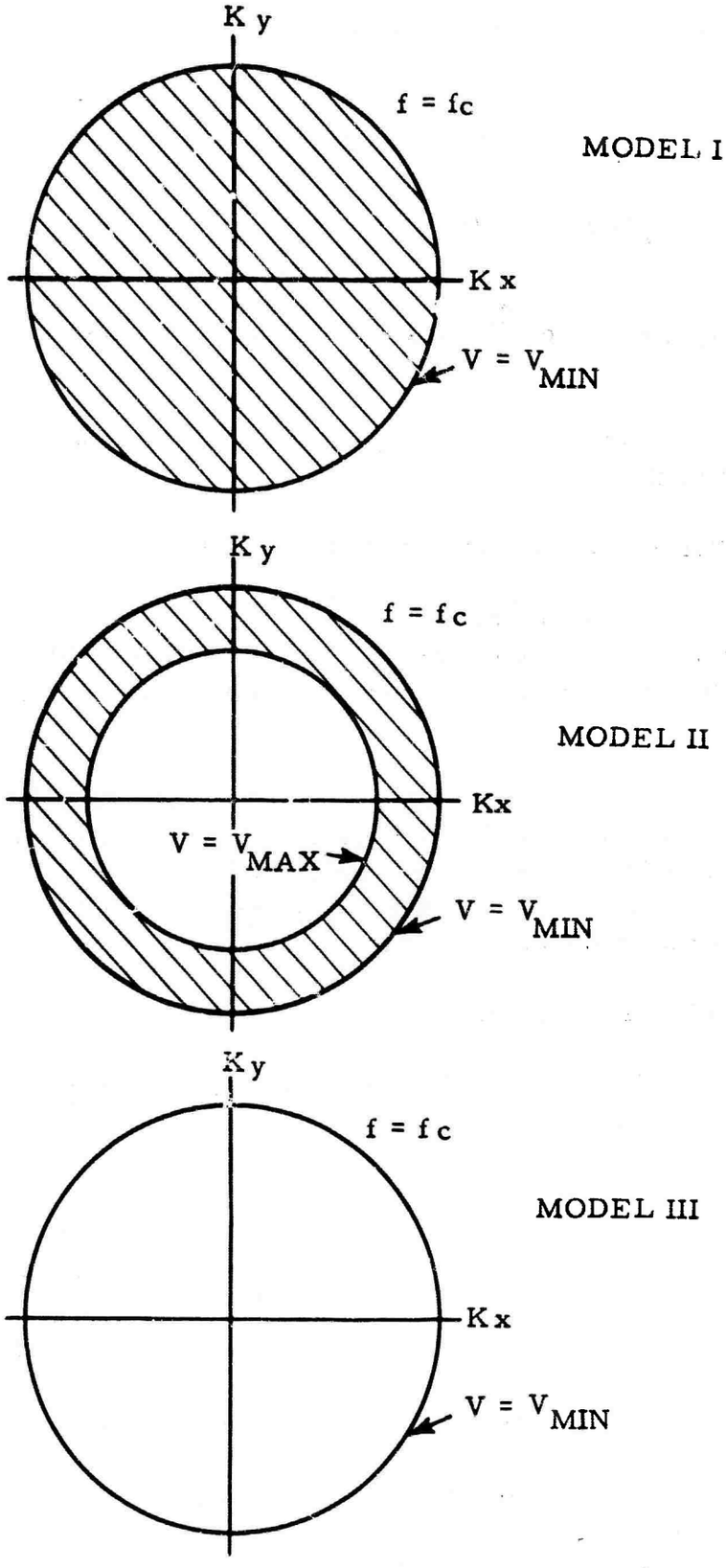

Figure B-1. Isotropic Signal and Noise Models at Frequency f_c for a Planar Array

The time-domain correlation matrix is obtained through the inverse Fourier transform [Equation (B.1)].

2. Synthesis of Model II Correlation Matrix

The wavenumber (for constant frequency) representation of Model II is an annaulus region of specified velocities V_{max} and V_{min} and is symmetric about $\vec{k} = 0$.

The crosspower spectra for this model are given by*

$$\Phi_{ij}^{s}(f) = \frac{s(f)}{\pi f\left(\frac{1}{V_{min}^2} - \frac{1}{V_{max}^2}\right)}\left[\frac{1}{V_{min}} \cdot J_1\left(\frac{2\pi f(\vec{x}_i - \vec{x}_j)}{V_{min}}\right) - \frac{1}{V_{max}} \cdot J_1\left(\frac{2\pi f(\vec{x}_i - \vec{x}_j)}{V_{max}}\right)\right]$$

The inverse Fourier transform [Equation (B.1)] is used to obtain the correlation matrix.

3. Synthesis of Model III Correlation Matrix

The wavenumber representation of Model III is a single circular line of velocity V_{min} with center at $\vec{k} = 0$.

The crosspower spectra for this model are given by**

$$\Phi_{ij}^{s}(f) = s(f)\, J_o\left[\frac{2\pi f(\vec{x}_i - \vec{x}_j)}{V_{min}}\right]$$

where J_o is the zero-order Bessel function.

The correlation matrix is obtained from the inverse Fourier transform [Equation (B.1)] of $\Phi_{ij}^{s}(f)$.

---

* Ibid, p. 107

**Ibid, p. 106

D. SIGNAL MODELS FOR UBO MCF-3, -4, -5, and -7

1. UBO MCF-3 and -7:

The signal designed for UBO MCF-3 and -7 was a Type I model (Figure B-1) where V_{min} = 8.1 km/sec (the approximate minimum teleseismic P-wave velocity) for all frequencies f where $0 \leq f \leq 6.94$ cps.

In developing this model,

$$s(f) = \Phi^{n}_{10*10}(f) \qquad 0 \leq f \leq 6.94$$

$$= 0 \qquad f > 6.94$$

where Φ^{n}_{10*10} was the autopower density spectra of the center seismometer noise correlation.

Figure B-2 presents a display of the resulting correlation matrix, and Figure B-3 is the 2-dimensional wavenumber spectral estimate of this signal model at f = 1.5 cps. This figure shows the signal region to lie between 0 and -3 db. The -3 db point will lie approximately on V_{min} if the model is properly designed.

2. UBO MCF-4

The signal model designed for UBO MCF-4 was a Type II model (Figure B-1) where V_{min} = 8.1 km/sec and V_{max} = 15.0 km/sec. s(f) was the same as that given for MCF-3 and -7 above.

Figure B-4 is the wavenumber spectral estimate of this model at f = 1.19 cps. This figure indicates that the signal area lies between 0 and -3 db. The 15.0-to-infinite-velocity region is unresolved due to the spectral window convolution with the true wavenumber spectrum.

3. UBO MCF-5

The signal model designed for UBO MCF-5 was a Type II model (Figure B-1) where V_{min} = 6.0 km/sec and V_{max} = 8.1 km/sec. s(f) was the same as that used in MCF-3 and -7 above.

Figure B-5 is the wavenumber spectral estimate of this signal model at 1.19 cps. The signal area is seen to lie in the 0 to -3 db

Text cont'd page B-11

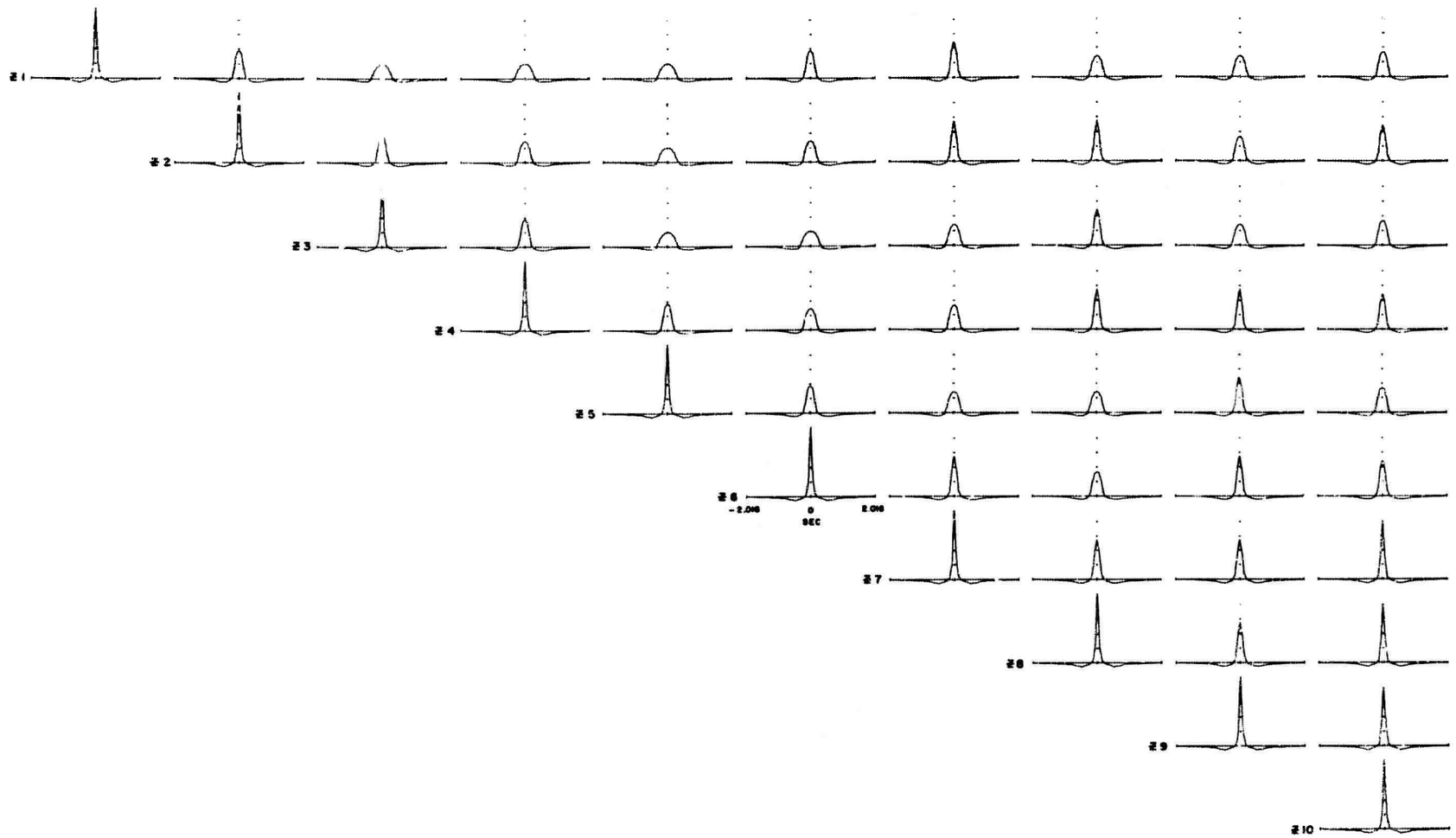

Figure B-2. Correlation Matrix for UBO Infinite Velocity to 8.1 Km/sec Signal Model

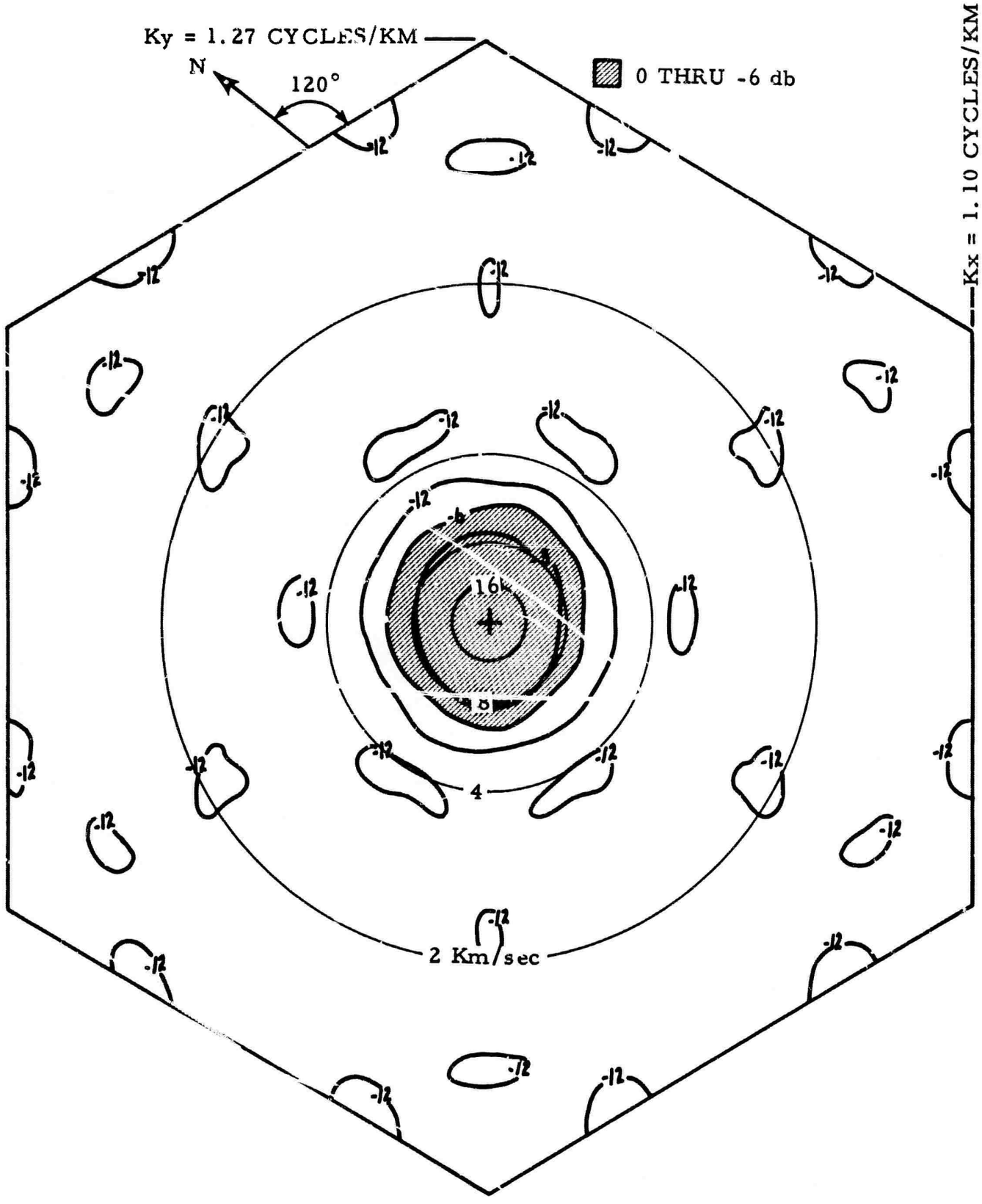

Figure B-3. Two-Dimensional Wavenumber Spectrum for UBO Infinite-Velocity-to-8.1 Km/sec Signal Model, f = 1.5 cps

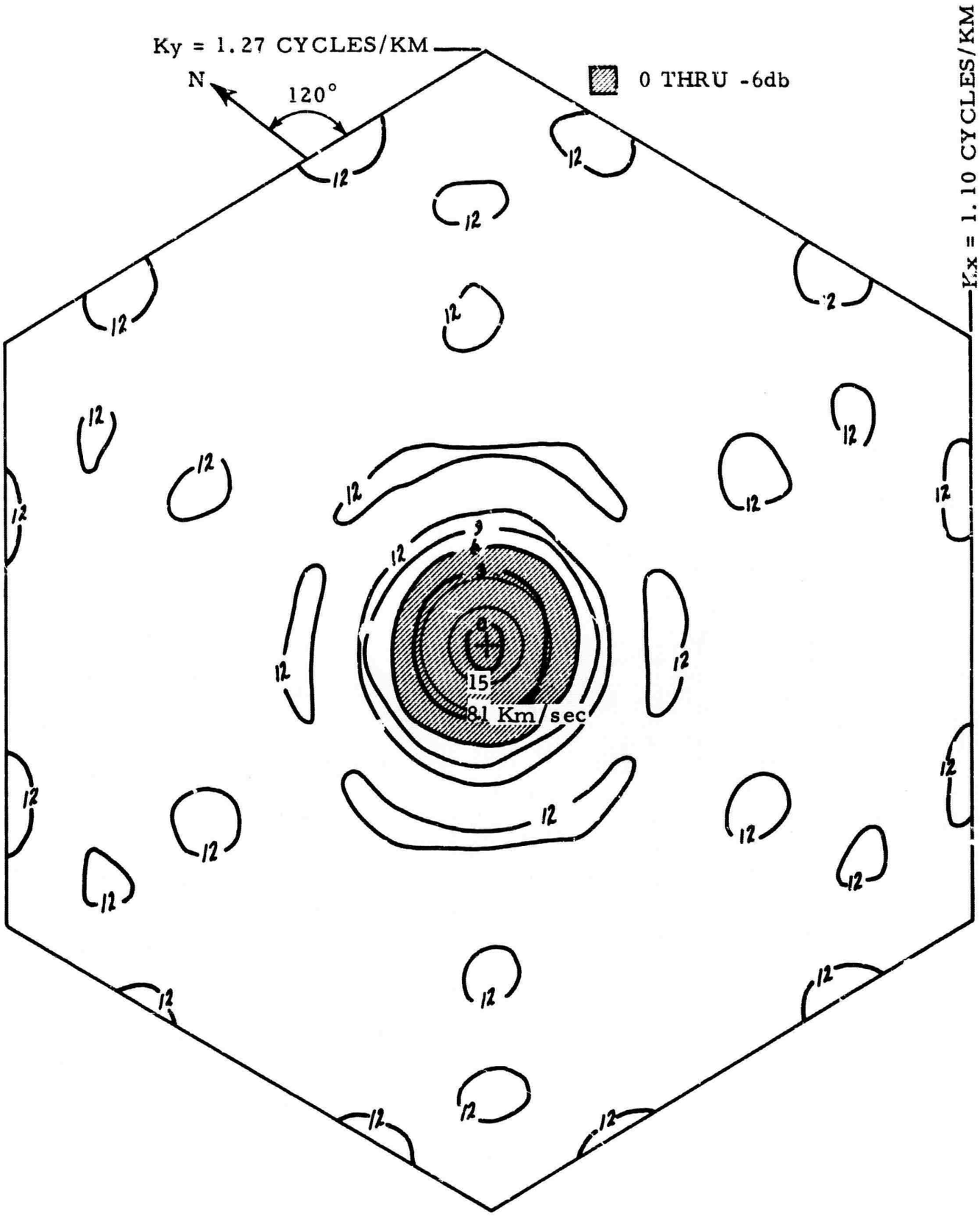

Figure B-4. Two-Dimensional Wavenumber Spectrum for UBO 15.0 to 8.1 Km/s Signal Model, f = 1.19 cps

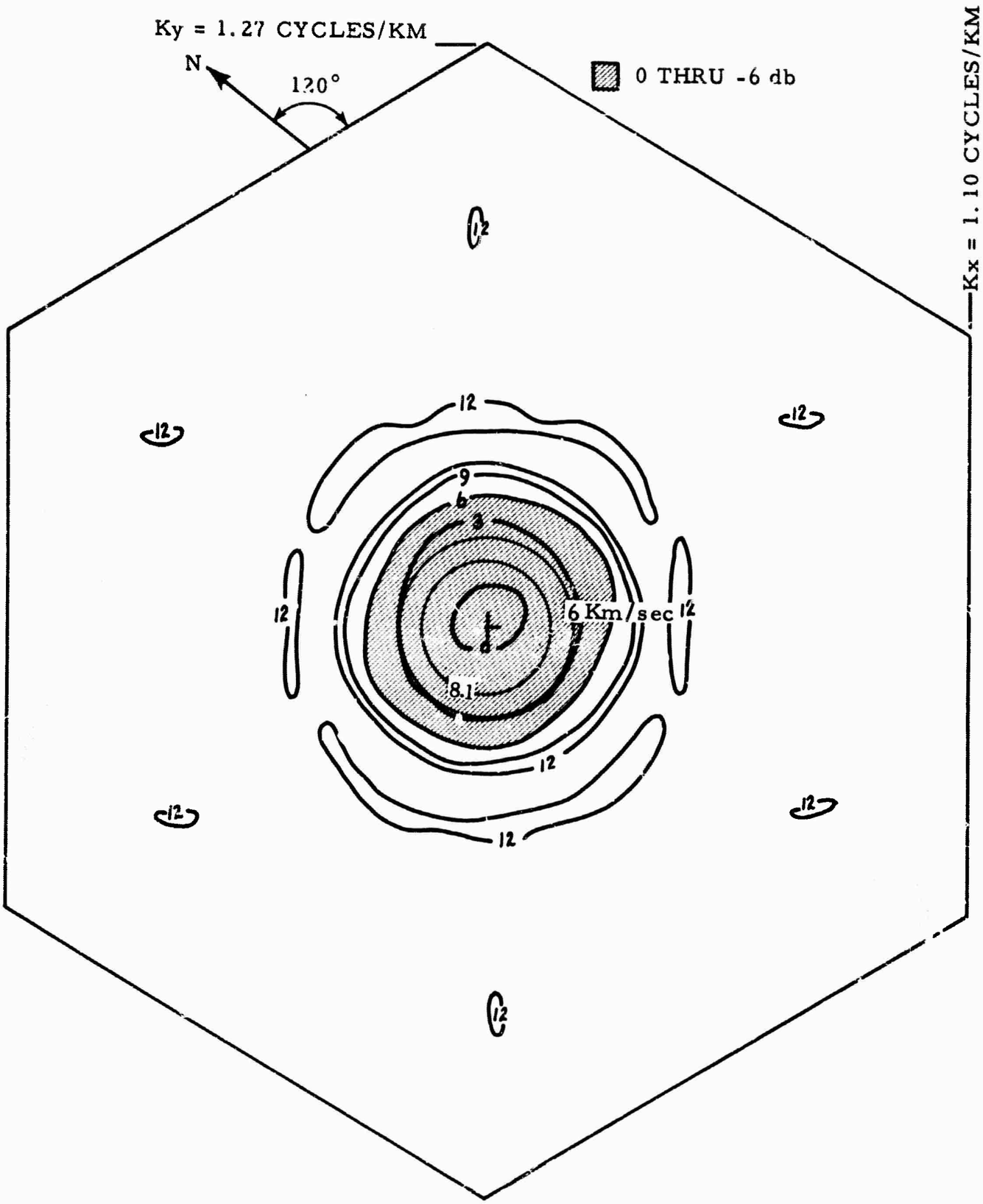

Figure B-5. Two-Dimensional Wavenumber Spectrum for UBO 8.1 to 6.0 Km/sec Signal Model, f = 1.19 cps

power range. The 8.1 to infinite-velocity region is unresolved as in the case of MCF-4.

E. MODELS FOR UBO IP-1

1. The Noise Model

The noise model for IP-1 consisted of surface mode energy only. For the 6-element vertical array, surface energy appears to propagate with infinite apparent vertical velocity, so the correlation set is easily derived from the correlation matrix of the planar array. The correlations for the vertical array will be given by

$$\varphi^{s}_{v_i * v_j} = \varphi^{s}_{10*10}$$

$$\varphi^{s}_{v_j * p_i} = \varphi^{s}_{10*p_i}$$

where the subscripts v and p are for the vertical and planar array, respectively; and subscripts i and j represent the sensors of the array. Subscript 10 indicates the center element of the subsurface planar array.

The correlation matrix for the subsurface planar array was constructed from Type III models using theoretical dispersion data to obtain the V_{min} as a function of frequency.* Fundamental first and second modes only were used in the following configuration:

- Fundamental Mode $0 \leq f \leq 2.0$
- First Mode $0.3 \leq f \leq 2.0$
- Second Mode $0.5 \leq f \leq 2.0$

The modes were equally weighted such that

$$\left| \Phi^{n}_{ij}(f) \right| = 1.0 \qquad 0 \leq f \leq 2.0$$

$$= 0 \qquad > 2.0$$

2. The Signal Model

The signal model was designed for IV signals as discussed in subsection B.2.

*Texas Instruments Incorporated, 1964: Array Research Semiannual Technical Report No. 2, sponsored by AFTAC, Nov. 15, p. I-34.

The signal spectrum was weighted the same as the noise spectrum, i.e.

$$| \Phi^{s}_{ij}(f) | = 1.0 \qquad 0 \le f \le 2.0$$

$$= 0 \qquad f > 2.0$$

F. MODELS FOR UBO IP-2

UBO IP-2 was designed for application to the 6-element deep-hole vertical array.

1. The Noise Model

The noise model was designed for surface-propagating noise which would appear as infinite-velocity energy to the vertical array. The correlation matrix for the noise, therefore, was an impulse function at $\tau = 0$ for all ij pairs. The impulse function was bandlimited for $0 \le f \le 2.0$ and

$$| \Phi^{n}_{ij}(f) | = 1.0 \qquad 0 \le f \le 2.0$$

$$= 0 \qquad f > 2.0$$

2. The Signal Model

The signal was defined for energy propagating with infinite apparent horizontal velocity and was developed according to subsection B.2 where

$$| \Phi^{s}_{ij}(f) | = 1.0 \qquad 0 \le f \le 2.0$$

$$= 0 \qquad f > 2.0$$

G. MODELS FOR UBO DG-1 THROUGH -4

Three models were developed for these filters:

(i) - noise model same as E-1
(ii) - signal model for uptraveling IV energy, same as developed in subsection B.2.a
(iii) - signal model for downtraveling energy which is the time reverse of (ii)

For each model,

$$| \Phi_{ij}(f) | = 1.0 \qquad 0 \le f \le 5.0$$

$$= 0 \qquad f > 5.0$$

The filters were developed using the following combinations:

Noise Model		Signal Model
DG-1	(i) + (iii)	(ii)
DG-2	(i) + (ii)	(iii)
DG-3	(i) + (iii)	(ii)
DG-4	(i) + (ii)	(iii)

Note: It is understood that the models for DG-1 and -2 differ from DG-3 and -4 since different sensor combinations were used.

APPENDIX C

METHOD OF RESISTOR APPROXIMATION AND LABORATORY TESTS

APPENDIX C

METHOD OF RESISTOR APPROXIMATION AND LABORATORY TESTS

Filter weights were converted to resistor values by the following equation:

$$R(\tau) = \frac{1}{A(\tau)} * SF$$

where

$R(\tau)$ = resistor values

$A(\tau)$ = filter weights

SF = scale factor chosen to cause all resistor values to fall in the range $10\ K \leq R(\tau) \leq 10M$

Then all $R(\tau)$ were compared with a Military Standard table of available resistor values, Table C-1, and the nearest value was chosen.

Delay line filters were fabricated and checked for system noise and frequency response characteristics. A bandlimited wavelet was input to a set of identical operational MAP filters located in front of the delay lines (point 1 in Figure C-1). Then, the outputs from these filters were input to each delay-line channel separately and the time-domain wavelets were recorded at each input-output pair (points 1, 2 and 3 in Figure C-1).

Ratio of the transforms of these wavelets was computed and plotted to give the frequency response of the individual filters.

Responses of the bandpass MAP filters were identical for all channels in both processors (within the plotting accuracy shown), and a representation is given in Figure C-2.

Plots of all frequency responses compared with their respective theoretical values were given in subsections VC and VIC.

Table C-1

MILITARY STANDARD 1% RESISTER VALUES

Resistance Tolerance
± 1 Percent

1.00	1.78	3.16	5.62
1.02	1.82	3.24	5.76
1.05	1.87	3.32	5.90
1.07	1.91	3.40	6.04
1.10	1.96	3.48	6.19
1.13	2.00	3.57	6.34
1.15	2.05	3.65	6.49
1.18	2.10	3.74	6.65
1.21	2.15	3.83	6.81
1.24	2.21	3.92	6.98
1.27	2.26	4.02	7.15
1.30	2.32	4.12	7.32
1.33	2.37	4.22	7.50
1.37	2.43	4.32	7.68
1.40	2.49	4.42	7.87
1.43	2.55	4.53	8.06
1.47	2.61	4.64	8.25
1.50	2.67	4.75	8.45
1.54	2.74	4.87	8.66
1.58	2.80	4.99	8.87
1.62	2.87	5.11	9.09
1.65	2.94	5.23	9.31
1.69	3.01	5.36	9.53
1.74	3.09	5.49	9.76

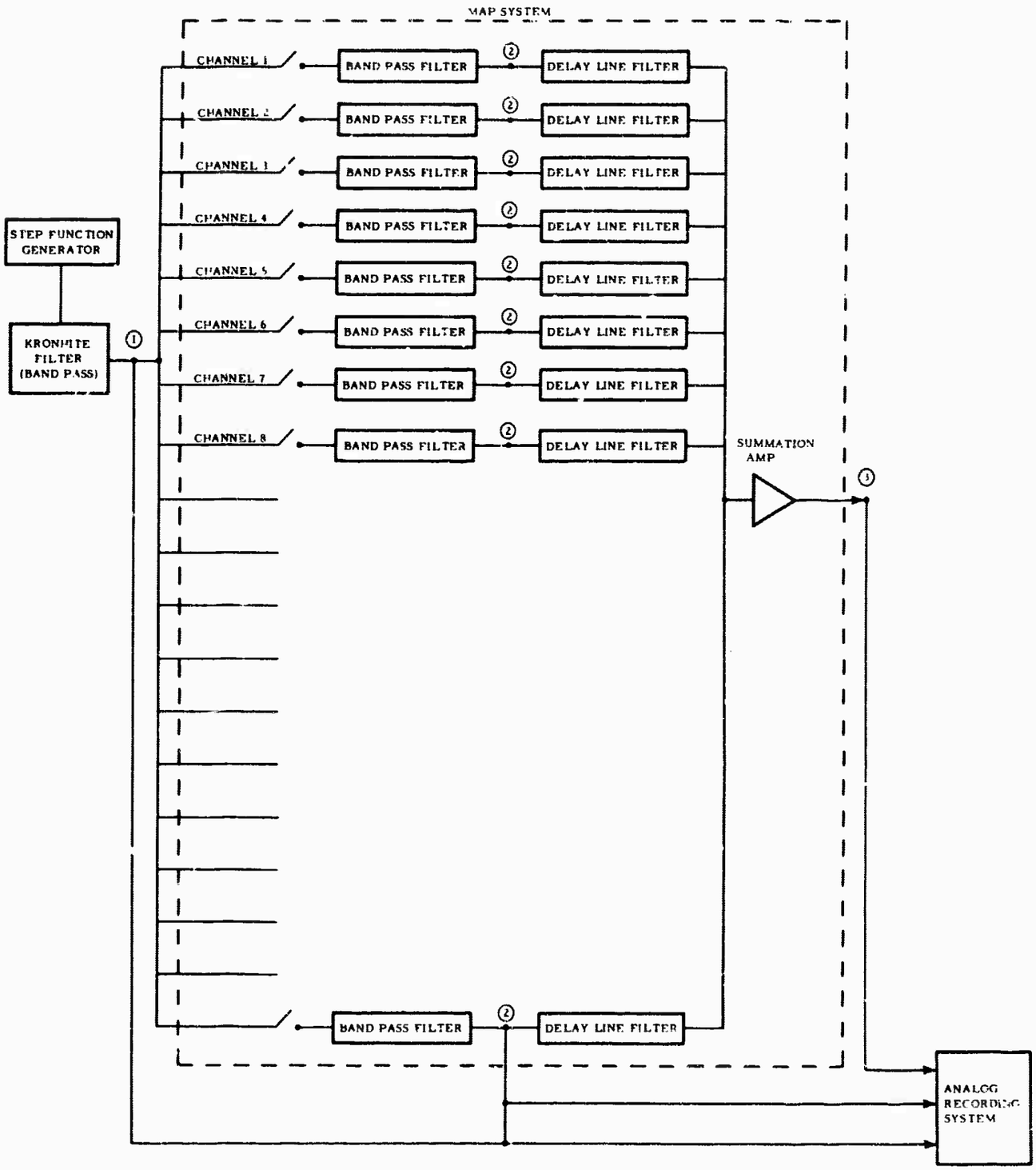

Figure C-1. Setup for Actual Frequency Response Determinations (1, 2 and 3 are points where measurements were taken)

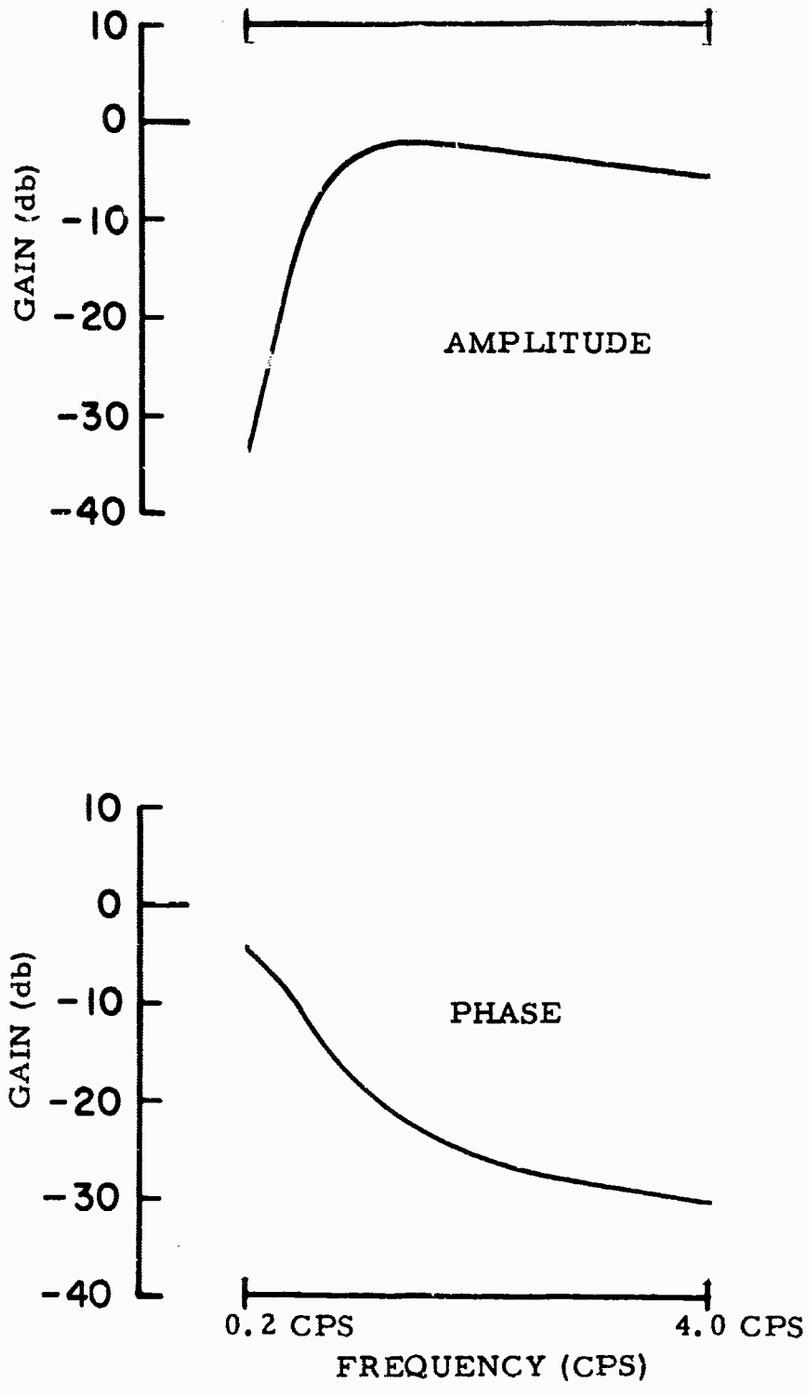

Figure C-2. Representative Frequency-Domain Transfer Function for MAP Bandpass Filters Located at the Input to All Delay Lines

APPENDIX D

SELECTED PROBLEMS

BLANK PAGE

APPENDIX D

SELECTED PROBLEMS

This appendix provides a discussion of two problems which arose during the development of the multichannel filters for the 10-channel processor (i. e. developed for the 10-element surface planar array).

A. EQUALIZATION PROBLEM

In the early stages of the contract period, the first multichannel filters developed were UBO MCF-1 and UBO MCF-3. The initial evaluation of these filters indicated that the filters were using gain inequality of the sensor outputs as a criteria for noise rejection. Briefly, this results because the measured noise matrix contained channel-to-channel gain differences which were caused by gain inequalities in the seismic recording system and by the variable properties of the noise field while the theoretical signal model was perfectly equalized between channels.

Such a system might work well in rejecting noise when the gain difference remains unchanged (which is unlikely). Nonequalized measured signals, when processed, possibly will be rejected also. This problem has been discussed in more detail in a previous report.*

The results that indicated MCF-1 and -3 were designing on-gain inequalities (Section V) are:

1. There is large signal-to-noise improvement at frequencies below 0.75 cps where the UBO array does not possess sufficient resolution to reject low-velocity noise on the basis of wavenumber component (e.g., at 0.25 cps, the array can resolve 1.87-km/sec energy)

2. The teleseismic signals processed with the filters were being attenuated slightly although the filters demonstrated flat, zero phase response

MCF-1 and -3 were redesigned and designated MCF-6 and -7 which used signal models that contained statistical gain fluctuation. The technique for adding the statistical gain fluctuation to the signal models has been presented in a previous report.** Basically, it involves multiplying the diagonal of the signal matrix by a constant.

---

*Texas Instruments Incorporated, 1964, Array Research, A re-evaluation of S/N Improvement for CPO using Local Noise: Spec Rpt 5, AFTAC, Dec. 15, p. 3.

**Texas Instruments Incorporated, 1964, Array Research Multichannel Filter Systems for Tonto Forest Observatory: Spec Rpt 3, AFTAC, Sept. 21, p. 3.

The redesigned MCF-6 and -7 were applied to the same noise samples used to evaluate MCF-1 and -3. A short portion of 3 of these noise samples both before and after filtering with MCF-6 is shown in Figures D-1, -2 and -3. The signal-to-noise improvement obtained through multichannel filtering and also through straight summation, plus the single-channel power density spectra for the multichannel filter output, the summation trace and the reference trace are shown in Figures D-4 through -6.

These figures indicate that by adding the statistical gain fluctuation to the signal model, MCF-6 no longer exhibits the large signal-to-noise improvement between frequencies of 0 to 0.75 cps. Additionally, the filter does not indicate improvement in the 0.75 to 5.0-cps frequency band comparable to that shown for MCF-1. The addition of gain fluctuation to the signal model did, therefore, eliminate one of the indicators on the gain equalization problem

A comparison of MCF-6 and MCF-1 then was made on the basis of wavenumber response, since measured signals processed by MCF-6 still were being slightly attenuated. The wavenumber response of the filters indicated, however, that MCF-1 appeared not to be designing on equalization criteria which would yield in effect an almost white wavenumber response, but was, in fact, using superdirectivity configuration to reject the very low-frequency, low-velocity noise. A discussion of superdirectivity is provided in Section V and has been presented in a previous report. *

It was, therefore, decided to use MCF-1 and -3 in the 10-channel processor (as opposed to MCF-6 and -7) since these filters did exhibit the large signal-to-noise improvement below 0.75 cps and were able to demonstrate, generally slightly better improvement relative to MCF-6 and -7 above 0.75 cps.

The important points to be derived from this analysis are:

- Filters designed using as a noise model the correlation matrix described in Appendix A did not exhibit a gain equalization problem.
- It was possible for a multichannel filter to assume a super-directivity configuration and demonstrate considerable improvement above a straight summation at low frequencies where the resolution of the array severely limited any type of simple processing.
- Addition of statistical gain fluctuation in this case restricted the noise-rejection capability of a multichannel filter system in the wideband (0 to 5.0 cps) sense.

---

* Texas Instruments Incorporated, 1964, Array Research, A re-evaluation of S/N Improvement for CPO using Local Noise: Spec Rpt 5, AFTAC, Dec. 15, p. 9.

Text cont'd page D-9

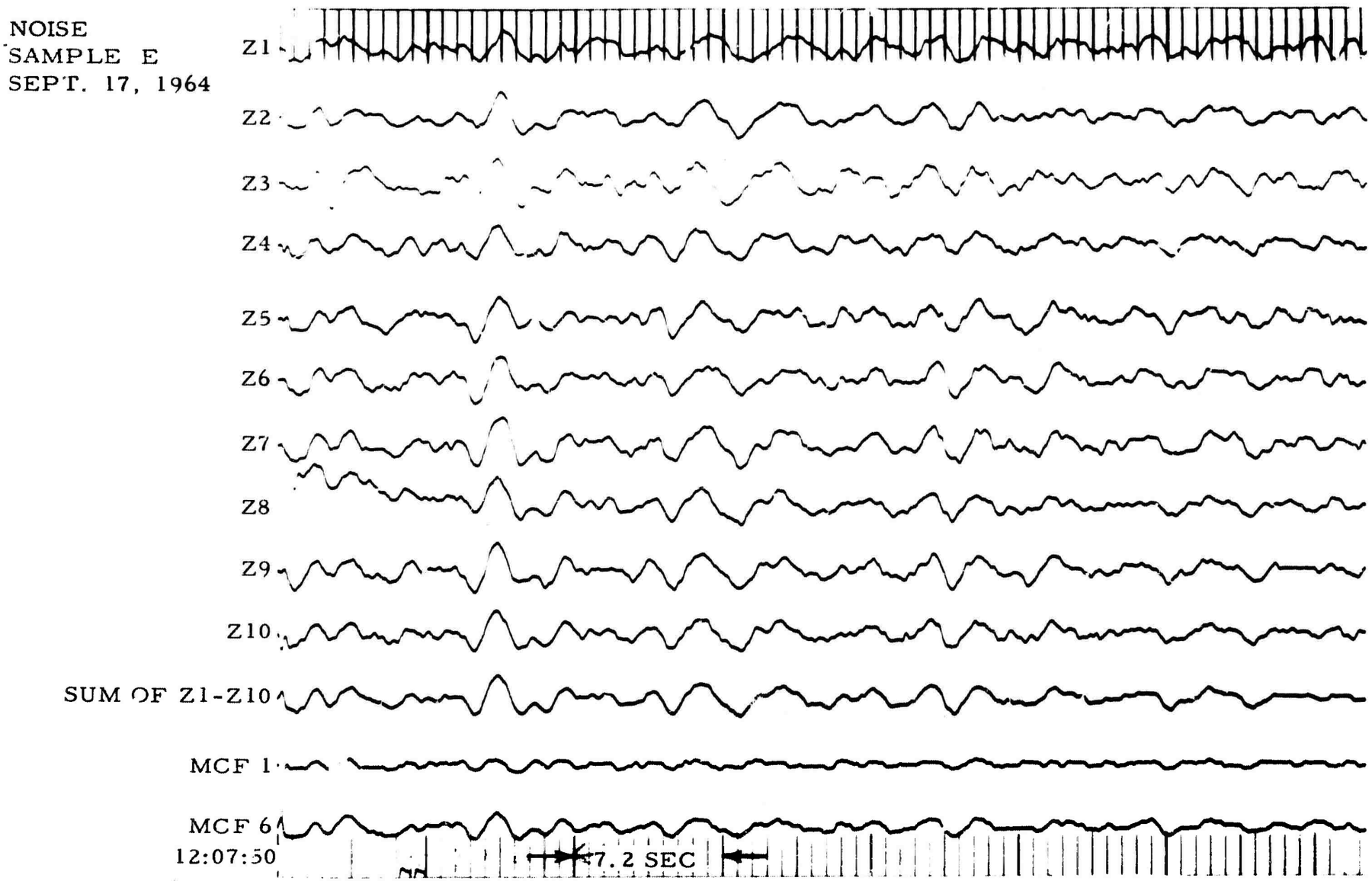

Figure D-1 A Short Portion of UBO Noise Sample E (Surface) Results of MCF-1 and -6

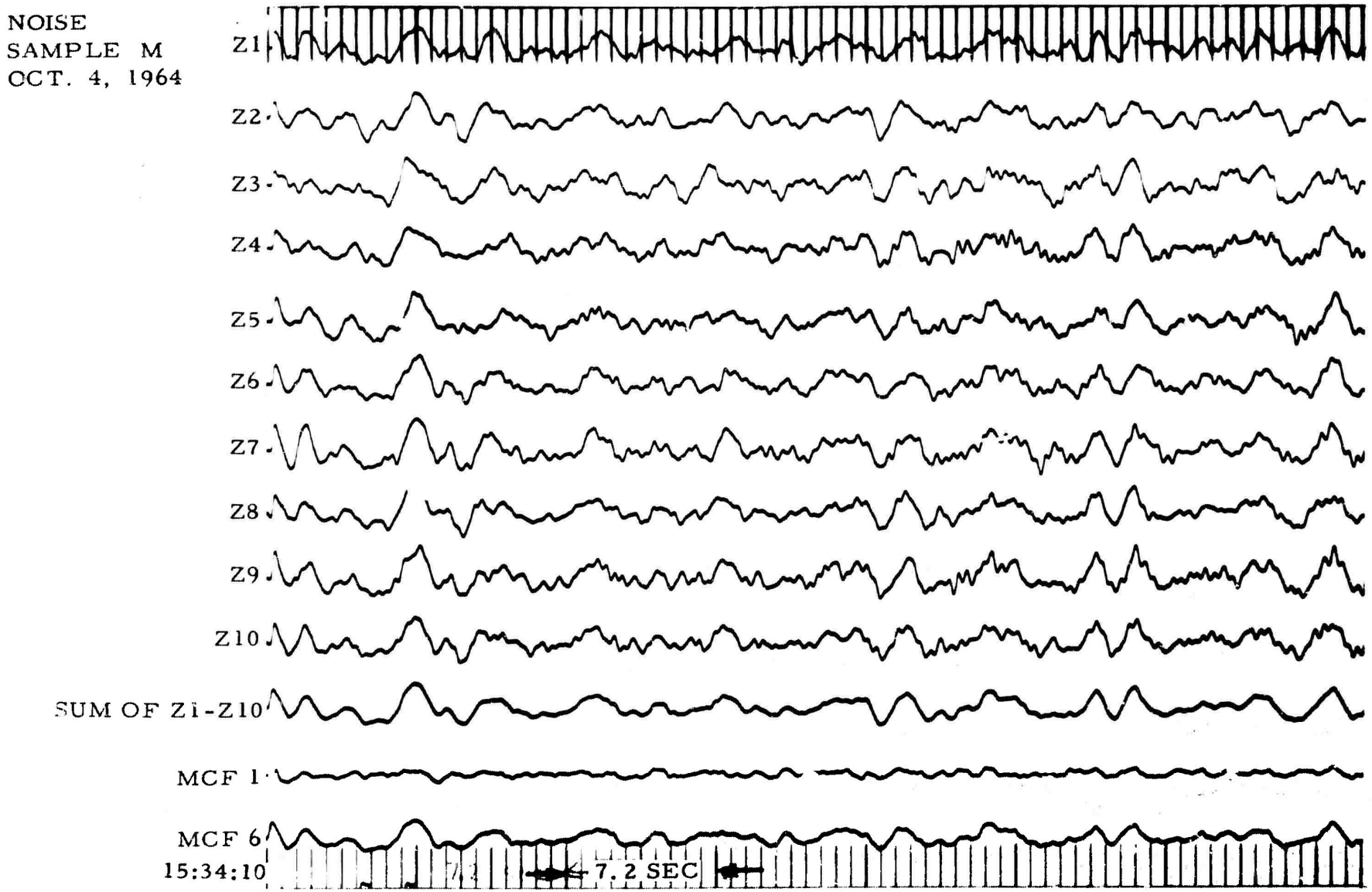

Figure D-2. A Short Portion of UBO Noise Sample M (Surface) Results of MCF-1 and -6

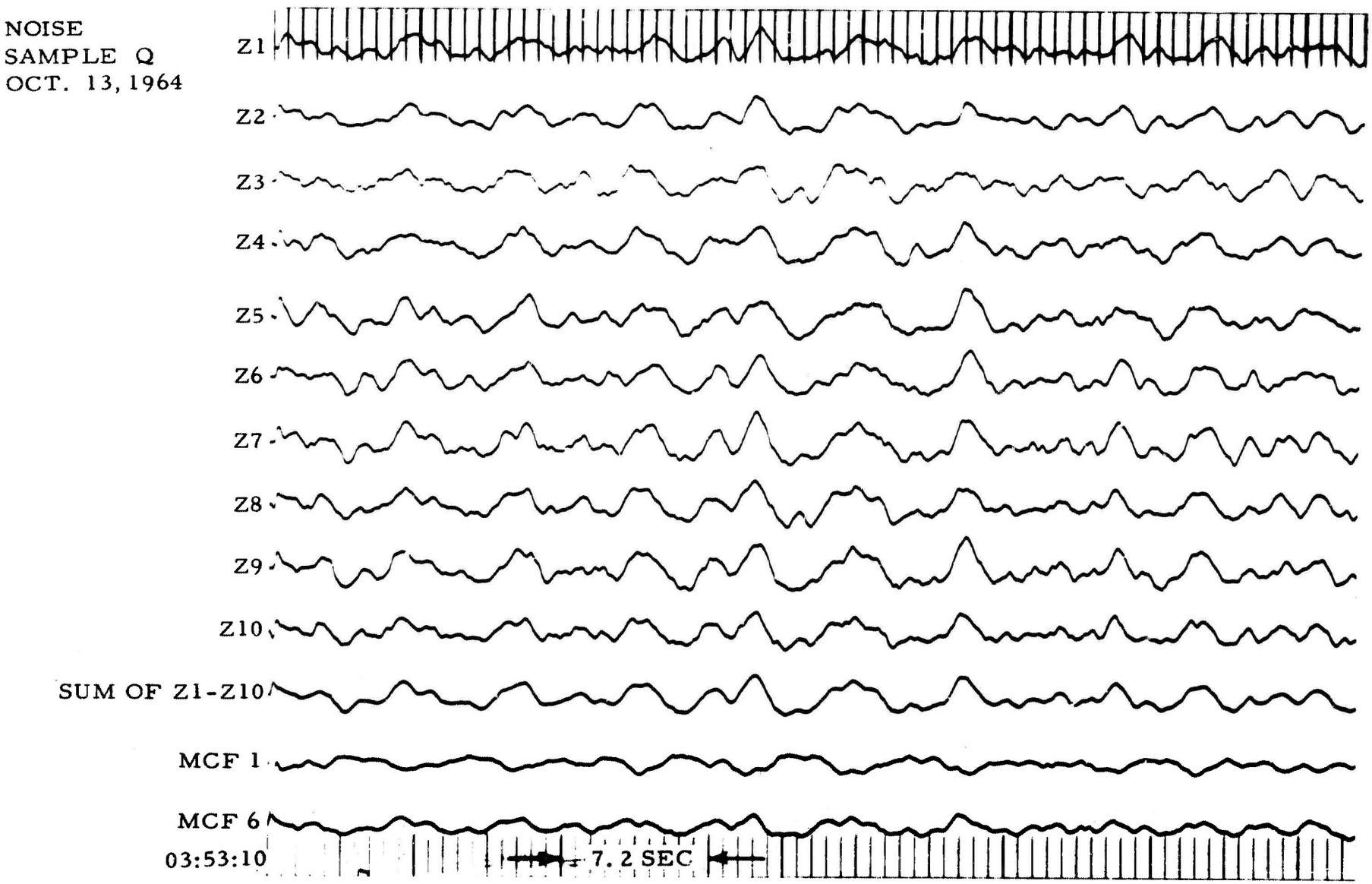

Figure D-3. A Short Portion of UBO Noise Sample Q (Surface) Results of MCF-1 and -6

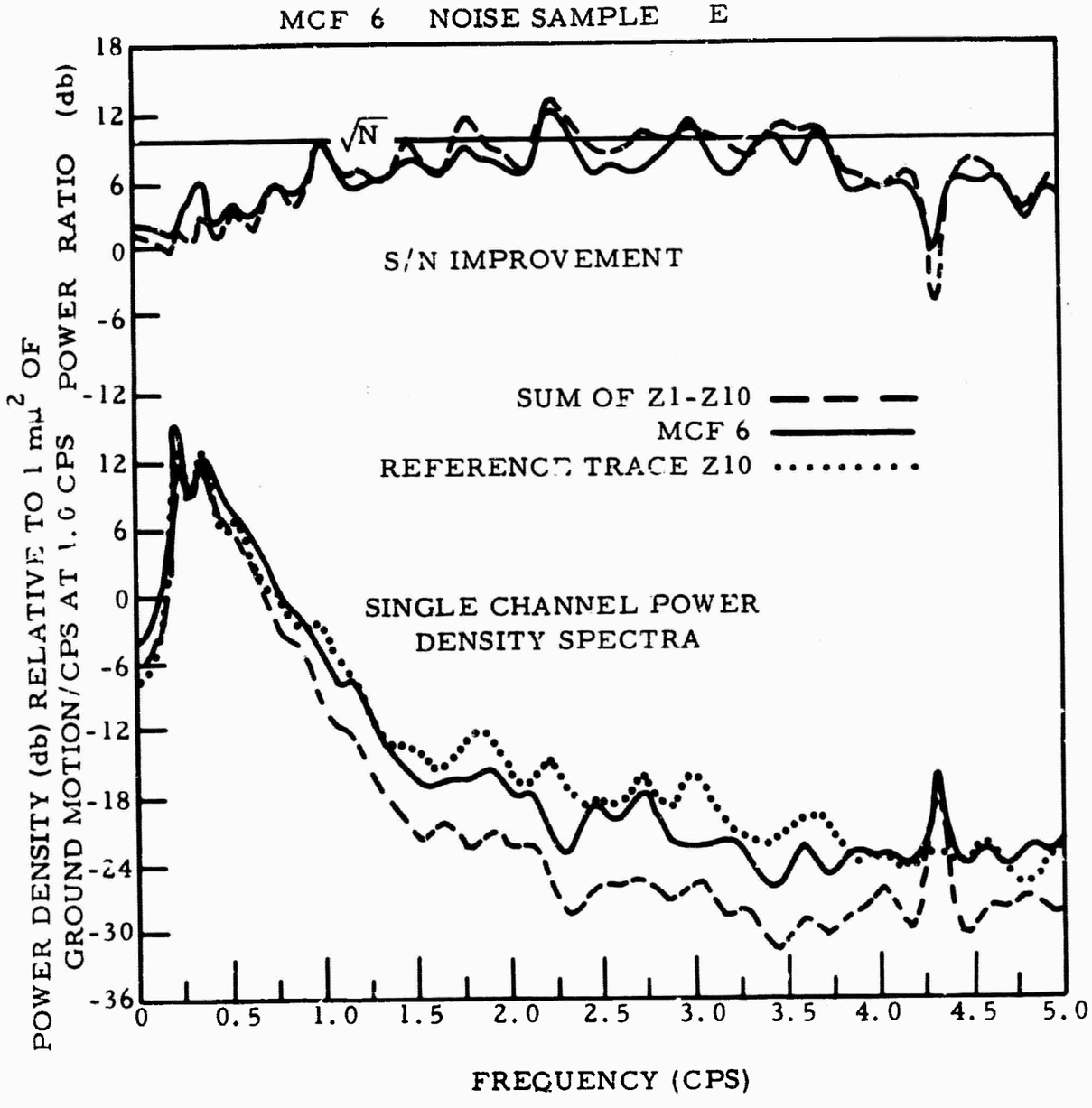

Figure D-4. S/N Improvement and Single-Channel Power Density Spectra for MCF-6 Noise Sample E

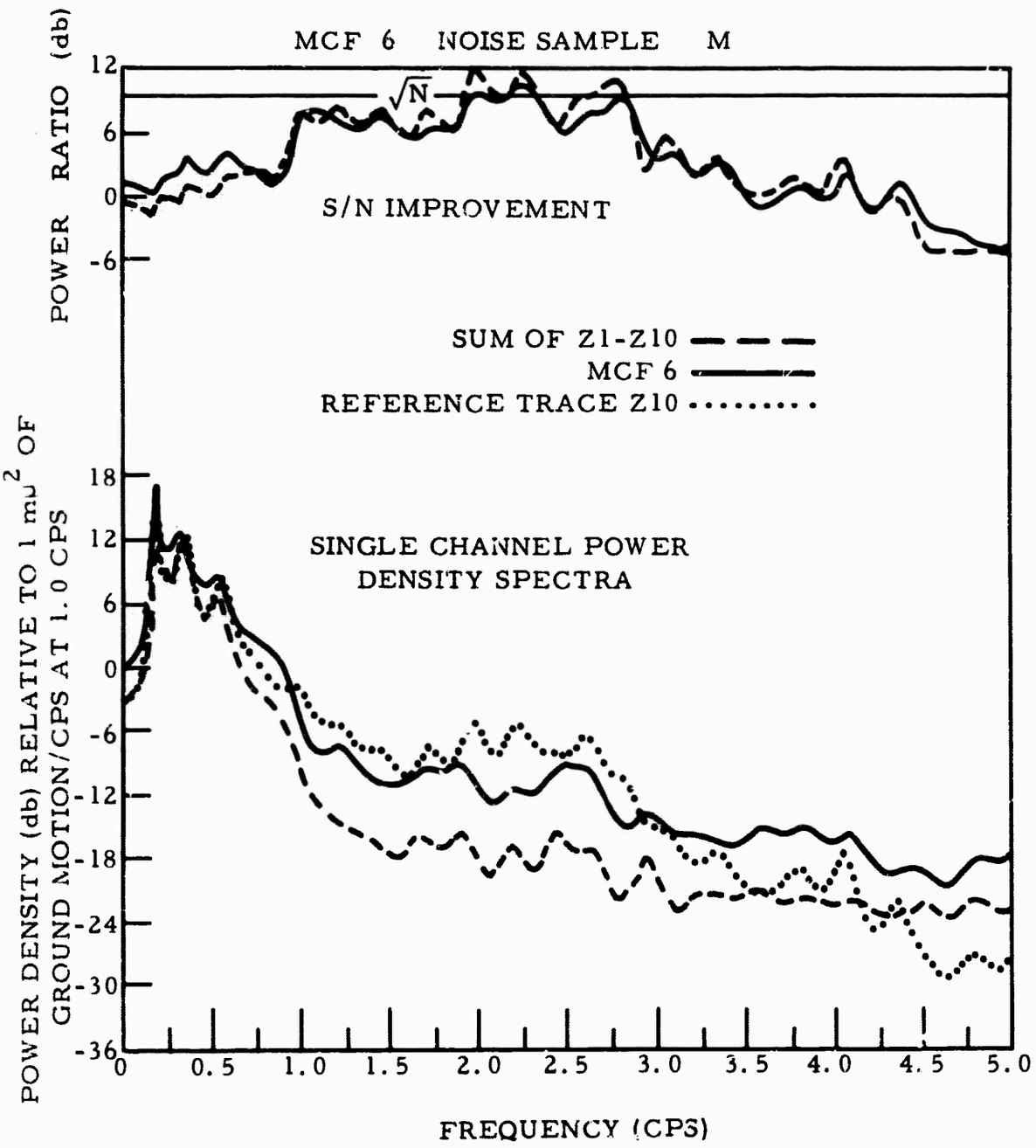

Figure D-5. S/N Improvement and Single-Channel Power Density Spectra for MCF-6 Noise Sample M

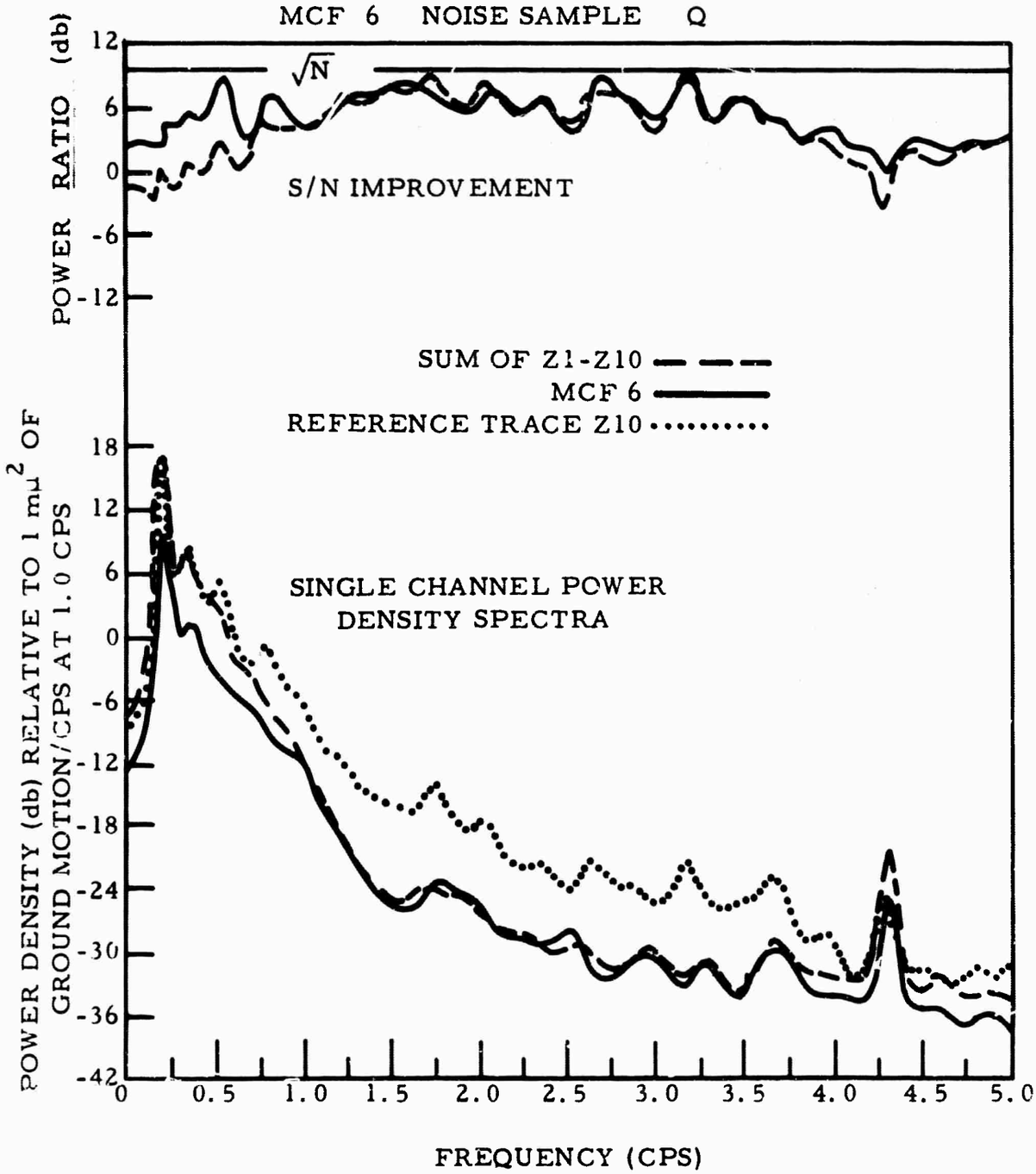

Figure D-6. S/N Improvement and Single-Channel Power Density Spectra for MCF-6 Noise Sample Q

B. ARRAY RESOLUTION

A second problem which arose during the initial stages of filter development under this contract was the capability of the array to resolve closely spaced noise and signal models in wavenumber space.

Initially, two multichannel filters designated UBO MCF-4 and UBO MCF-5 were designed which would velocity-partition signal energy in wavenumber space. The signal models are explained in more detail in Appendix B. Briefly, MCF-4 was developed using a signal model which defined the signal to be isotropic and to lie in the 15- to 8.1-km/sec region. MCF-5 defined the signal to be isotropic and to lie in the 8.1- to 6.0 km/sec region.

The 2- dimensional wavenumber response at 1.5 cps is shown in Figures D-7 and D-8 for MCF-4 and -5, respectively. Each of these filter responses indicates that the filter is unable to reject energy inside the maximum velocity range. It was shown in the UBO noise analysis* that high-velocity mantle P-wave energy does exist for this frequency, which indicates the filters should reject inside the maximum velocity range.

Since the array resolution is given by 1/d where d is the diameter of the array at a frequency of 1.5 cps, the array can resolve only 9-km/sec energy, which explains the inability of the filters to reject the high-velocity mantle P-wave noise while still retaining the ability to pass the given signal region.

*Texas Instruments Incorporated, 1965, Noise Analysis for Uinta Basin Seismological Observatory: AFTAC, Oct. 15, p. IV-36.

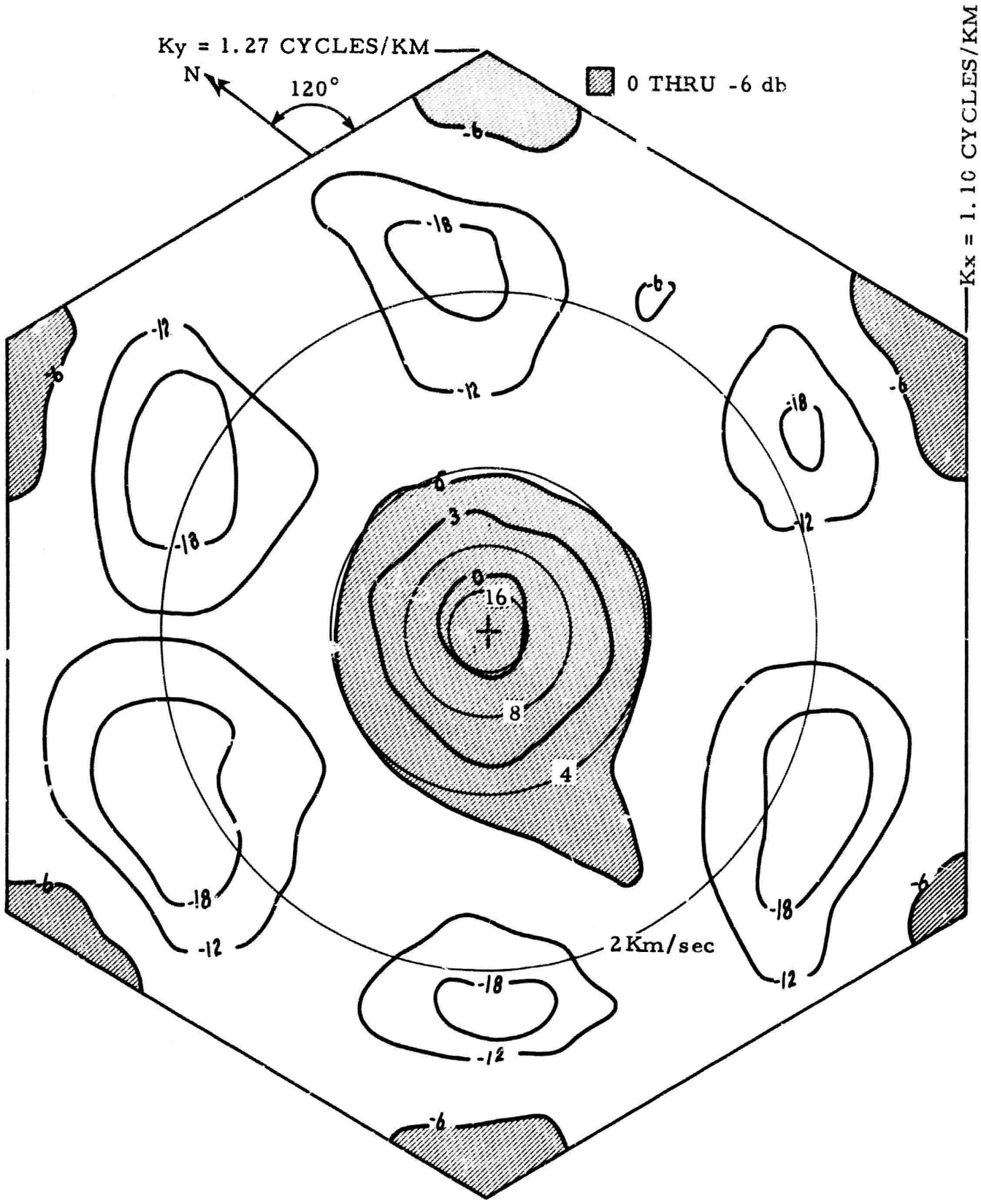

Figure D-7. Two-Dimensional Wavenumber Response UBO MCF-4, f=1.5 cps

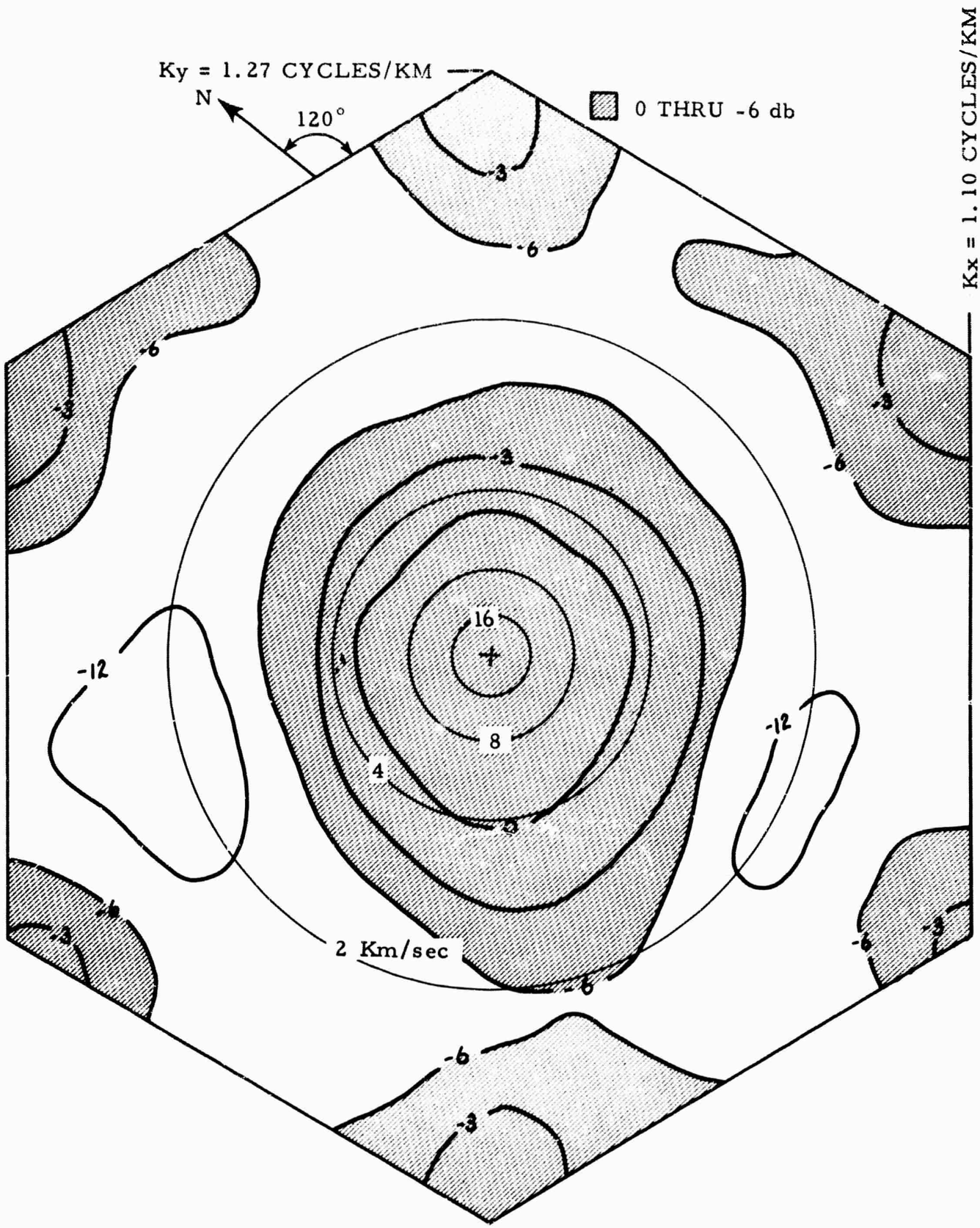

Figure D-8. Two-Dimensional Wavenumber Response UBO MCF-5, f=1.5 cps

APPENDIX E

UBO FILTER SYSTEM

APPENDIX E

UBO FILTER SYSTEM

This appendix outlines in tabular form the filters developed for the UBO signal and noise field. Included are optimum and beam-steer filters and also, those optimum filters which were developed but were not installed in the operational MAP.

Tables E-1 and E-2 outline the filter systems for the 10-channel and 19-channel system, respectively.

The reasons for providing this information in tabular form are two-fold: the tables will provide easy reference to the various filters during the reading of this report; the information will provide necessary data for station personnel interpreting the operational MAP output results.

Table

10-CHANNEL MAP FILTE L

IDENTIFICATION	MAP OUTPUT CHANNELS	INPUT CHANNELS	FILTER TYPE	SIG R
UBO MCF-1	1	Z1-10	Optimum	Infinit m S(f)/
UBO MCF-2	2	Z1-10	Optimum	Infinit m S(f)/ f ≥ 1 For f Decre mately
UBO MCF-3	3	Z1-10	Optimum	Infinit m KM/
UBO BS-1	4	Z1-10	Beam Steer	8.1 K te
UBO BS-2	5	Z1-10	Beam Steer	8.1 K te
UBO BS-3	6	Z1-10	Beam Steer	8.1 K te
UBO BS-4	7	Z1-10	Beam Steer	8.1 K te
UBO BS-5	8	Z1-10	Beam Steer	8.1 K te
UBO BS-6	9	Z1-10	Beam Steer	8.1 K te
UBO SS-1	10	Z1-10	Straight Sum.	Infinit S
UBO MCF-4*	N/A	Z1-10	Optimum	Isotro m KM/
UBO MCF-5*	N/A	Z1-10	Optimum	Isotro m KM/
UBO MCF-6*	N/A	Z1-10	Optimum	Infinit m Gain to S S(f)/
UBO MCF-7*	N/A	Z1-10	Optimum	Infinit m KM/ tuati Mode

*Developed but not installed in MAP.

A

Table E-1

L MAP FILTERS (SURFACE ARRAY)

	SIGNAL MODEL	NOISE MODEL	MAP DELAY FOR IMPULSE SIGNAL
m	Infinite Velocity S(f)/N(f) = 4.0	Measured Ambient Noise	1.0 sec Relative to Z-10
m	Infinite Velocity S(f)/N(f) = 2.75 f ≥ 1.0 cps For f < 1.0 cps S(f) Decreases at Approximately 18-db/octave	Measured Ambient Noise	1.0 sec Relative to Z-10
m	Infinite Velocity to 8.1 KM/sec, S(f)/N(f) = 4.0	Measured Ambient Noise	1.0 sec Relative to Z-10
teer	8.1 KM/sec 0° From N	N/A	1.0 sec Relative to Z-10
teer	8.1 KM/sec 60°E From N	N/A	1.0 sec Relative to Z-10
teer	8.1 KM/sec 120°E From N	N/A	1.0 sec Relative to Z-10
teer	8.1 KM/sec 180°E From N	N/A	1.0 sec Relative to Z-10
teer	8.1 KM/sec 240°E From N	N/A	1.0 sec Relative to Z-10
teer	8.1 KM/sec 300°E From N	N/A	1.0 sec Relative to Z-10
Sum.	Infinite Velocity	N/A	1.0 sec Relative to Z-10
m	Isotropic 15.0 to 8.1 KM/sec (S(f)/N(f) = 4.0	Measured Ambient Noise	N/A
m	Isotropic 8.1 to 6.0 KM/sec S(f)/N(f) = 4.0	Measured Ambient Noise	N/A
m	Infinite Velocity with Gain Fluctuation Added to Signal Model S(f)/N(f) = 4.0	Measured Ambient Noise	N/A
m	Infinite Velocity to 8.1 KM/sec with Gain Fluctuation Added to Signal Model S(f)/N(f) = 4.0	Measured Ambient Noise	N/A

Table

19-CHANNEL MAP FILTER

IDENTIFICATION	MAP OUTPUT CHANNELS	INPUT CHANNELS	FILTER TYPE	SIG
UBO MCF-8	1	SZ1-10	Optimum	Infinite S(f)/N
UBO IP-1	2	SZ1-10 on 4 Rings and 6 Vertical	Optimum	Infinite S(f)/N
UBO IP-2	3	6 Vertical	Optimum	Infinite S(f)/N
UBO DG-1	4	3 Vertical (4900, 6900, 8900 ft)	Optimum Deghost	Up-Tra Veloc
UBO DG-2	5	3 Vertical (4900, 6900, 8900 ft)	Optimum Deghost	Down-T Veloc
UBO DG-3	6	3 Vertical (3900, 5900, 7900 ft)	Optimum Deghost	Up-Tra Veloc
UBO DG-4	7	3 Vertical (3900, 5900, 7900 ft)	Optimum Deghost	Down-T Veloc
UBO BS-7	8	6 Vertical	Beam Steer	Uptrave Veloc
UBO BS-8	9	6 Vertical	Beam Steer	Up-Tra P-Wav
UBO BS-9	10	6 Vertical	Beam Steer	Up-Tra S-Wav
UBO BS-10	11	6 Vertical	Beam Steer	Down-T Veloc
UBO BS-11	12	6 Vertical	Beam Steer	Down-T P-Wav
UBO BS-12	13	6 Vertical	Beam Steer	Down-T S-Wav
UBO SS-2	14	6 Vertical	Straight Sum.	

NOTE: All velocities refer to apparent horizontal velocity.

A

Table E-2

ANNEL MAP FILTERS (SUB-SURFACE ARRAY)

FILTER TYPE	SIGNAL MODEL	NOISE MODEL	MAP RELAY FOR IMPULSE SIGNAL
Optimum	Infinite Velocity S(f)/N(f) = 4.0	Measured Ambient Noise	1.0 sec Relative to SZ-10
Optimum	Infinite Velocity S(f)/N(f) = 4.0	Theoretical Isotropic Surface-Mode Noise	1.0 sec Relative to SZ-10
Optimum	Infinite Velocity S(f)/N(f) = 4.0	Theoretical Isotropic Surface-Mode Noise	1.0 sec Relative to SZ-10
Optimum Deghost	Up-Traveling Infinite Velocity S(f)/N(f) = 4.0	Theoretical Isotropic Surface-Mode Noise and Down-Traveling Infinite Velocity Signal	1.55 sec Relative to SZ-10
Optimum Deghost	Down-Traveling Infinite Velocity S(f)/N(f) = 4.0	Theoretical Isotropic Surface-Mode Noise and Up-Traveling Infinite Velocity Signal	0.45 sec Relative to SZ-10
Optimum Deghost	Up-Traveling Infinite Velocity S(f)/N(f) = 4.0	Theoretical Isotropic Surface-Mode Noise and Down-traveling Infinite Velocity Signal	1.55 sec Relative to SZ-10
Optimum Deghost	Down-Traveling Infinite Velocity S(f)/N(f) = 4.0	Theoretical Isotropic Surface-Mode Noise and Up-Traveling Infinite Velocity Signal	0.45 sec Relative to SZ-10
Beam Steer	Uptraveling Infinite Velocity P-Waves	N/A	1.55 sec Relative to SZ-10
Beam Steer	Up-Traveling 8-KM/sec P-Waves	N/A	1.55 sec Relative to SZ-10
Beam Steer	Up-Traveling 8-KM/sec S-Waves	N/A	1.55 sec Relative to SZ-10
Beam Steer	Down-Traveling Infinite Velocity P-Waves	N/A	0.45 sec Relative to SZ-10
Beam Steer	Down-Traveling 8-KM/sec P-Waves	N/A	0.45 sec Relative to SZ-10
Beam Steer	Down-Traveling 8-KM/sec S-Waves	N/A	0.45 sec Relative to SZ-10
Straight Sum.	N/A	N/A	N/A

tal velocity.

B

UNCLASSIFIED

Security Classification

DOCUMENT CONTROL DATA - R&D

(Security classification of title, body of abstract and indexing annotation must be entered when the overall report is classified)

1. ORIGINATING ACTIVITY (Corporate author) Texas Instruments Incorporated P.O. Box 5621 Dallas, Texas 75222	2a. REPORT SECURITY CLASSIFICATION Unclassified 2b. GROUP

3. REPORT TITLE

Multiple Array Processors

4. DESCRIPTIVE NOTES (Type of report and inclusive dates)

Final Report, 1 October 1964 to 31 August 1964

5. AUTHOR(S) (Last name, first name, initial)

Edwards, James P. III

6. REPORT DATE	7a. TOTAL NO. OF PAGES	7b. NO. OF REFS
29 October 1965	153	11

8a. CONTRACT OR GRANT NO.	9a. ORIGINATOR'S REPORT NUMBER(S)
AF 33(657)-13904 b. PROJECT NO. c. VT/5052 d.	9b. OTHER REPORT NO(S) (Any other numbers that may be assigned this report)

10. AVAILABILITY/LIMITATION NOTICES

U.S. Government Agencies may obtain copies of this report directly from DDC. Other qualified users shall request through United States Air Force, AFTAC/VELA SEISMOLOGICAL CENTER, Washington, D.C. 20333

11. SUPPLEMENTARY NOTES	12. SPONSORING MILITARY ACTIVITY
Evaluation of MCF, Installation of two MAPS for UBO	Air Force Technical Application Center VELA Seismological Center Washington, D.C. 20333

13. ABSTRACT This report describes the synthesis and evaluation of multichannel filters for the Uinta Basin Seismological Observatory. The filters were designed for use in two on-line multiple array processors (MAP).

A 19-channel and a 10-channel multiple array processor were designed, fabricated and installed at the Uinta Basin Seismological Observatory.

The 19-channel processor was equipped with 7 multichannel filters and 6 beam-steer outputs. These filters were designed for operation on various configurations of the subsurface 3 dimensional system element array.

The 10-channel processor was equipped with 3 multichannel filters and 6 beam-steer outputs. All were designed for operation on the 10-element surface planar array.

DD FORM 1 JAN 64 1473

UNCLASSIFIED

Security Classification